

Contents of issue 4 vol. XLVI

- 411 PREFACE
- 413 A. BERTRAM, J. OLSCHESKI and R. SIEVERT, *Experimental and numerical investigations of thermal-mechanical behaviour of poly- and single-crystalline nickel-base superalloys*
- 431 A. BOKOTA, S. ISKIERKA, R. PARKITNY and B. RANIECKI, *Transient and residual stresses in progressive induction hardening of infinite solid cylinder*
- 449 A. FLOSS and V. ULBRICHT, *Elastic-plastic shells with finite deformations and contact treatment*
- 463 A. GANCZARSKI and J. SKRZYPEK, *Effect of initial prestressing on the optimal design of plates with respect to orthotropic brittle rupture*
- 485 L. GAUL and M. SCHANZ, *A viscoelastic boundary element formulation in time domain*
- 497 R. JOHN and H. BERGANDER, *Formulation of anisotropic equations by means of the theory of representations for tensor functions and the convective method of description*
- 505 M. S. KUCZMA and E. STEIN, *On nonconvex problems in the theory of plasticity*
- 531 D. LACHNER, H. LIPPMANN and L. S. TÓTH, *On Cosserat plasticity and plastic spin for isotropic materials*
- 541 T. ŁODYGOWSKI, P. PERZYNA, M. LENGNICK and E. STEIN, *Viscoplastic numerical analysis of dynamic plastic strain localization for a ductile material*
- 559 A. MEYERS, *On yield surface interpolation of prestrained ductile materials*
- 571 T. SADOWSKI, *Some remarks on modelling of semi-brittle ceramics by application of mesomechanics*
- 581 G. SZEFER, D. JASIŃSKA and J. W. SALAMON, *Concept of a singular surface in contact mechanics*

Polish Academy of Sciences

Institute of Fundamental Technological Research

Archives of Mechanics

Archiwum Mechaniki Stosowanej



volume 46

issue 4



Polish Scientific Publishers PWN

Warszawa 1994

ARCHIVES OF MECHANICS IS DEVOTED TO
Theory of elasticity and plasticity • Theory of nonclassical
continua • Physics of continuous media • Mechanics of
discrete media • Nonlinear mechanics • Rheology • Fluid
gas-mechanics • Rarefied gases • Thermodynamics

FOUNDERS

M. T. HUBER • W. NOWACKI • W. OLSZAK
W. WIERZBICKI

EDITORIAL ADVISORY COMMITTEE

W. SZCZEPIŃSKI—chairman • D. C. DRUCKER
W. FISZDON • P. GERMAIN • W. GUTKOWSKI
G. HERRMANN • J. RYCHLEWSKI
I. N. SNEDDON • G. SZEFER • Cz. WOŹNIAK
H. ZORSKI

EDITORIAL COMMITTEE

M. SOKOŁOWSKI—editor • A. BORKOWSKI
W. KOSIŃSKI • W. K. NOWACKI • M. NOWAK
P. PERZYNA • H. PETRYK • J. SOKÓŁ-SUPEL
Z. A. WALENTA • B. WIERZBICKA—secretary
S. ZAHORSKI

Copyright 1994 by Polska Akademia Nauk, Warszawa, Poland
Printed in Poland, Editorial Office: Świętokrzyska 21.
00-049 Warszawa (Poland)

Arkuszy wydawniczych 16,0. Arkuszy drukarskich 12,5 + wkł.
Papier offset, kl. III 80 g. B1. Oddano do składania w sierpniu 1994 r.
Druk ukończono w styczniu 1995 r.

Skład: *ArtGraph*, Warszawa, Okrężna 11 A
Druk i oprawa: Drukarnia Braci Grodzickich, Zabieniec, ul. Przelotowa 7

IV-th Polish-German Symposium on “Mechanics of Inelastic Solids and Structures”

Czarniejewo, September 13–17, 1993

THE ORIGINS OF Polish-German Symposia go back to early seventies. They are result of long lasting cooperation between Polish and German researchers in the field of Solid Mechanics. It became a custom to organize these Symposia every three years in turns in Poland and Germany. The VI Polish-German Symposium, which took place in Czarniejewo (historical complex) near Poznań has been generously sponsored by the Polish Committee of Scientific Research (KBN), and Deutsche Forschungsgemeinschaft (DFG). The co-chairman were Prof. Dr.-Ing. O. Bruhns from Ruhr-Universität Bochum (Germany), and Professors B. Raniecki and S. Kowalski from Center of Mechanics, IFTR, PAS (Poland).

The subject of Symposium covered the following fields: plastic anisotropy, optimisation of mechanical structures, localization and bifurcation, mechanics of granular materials, inclusions, porosity, damage, microstructural aspects of mechanical behaviour of solids, visco-plastic and visco-elastic behaviour of structures and materials, mechanics of phase transformations, superalloys and ceramics. Most of the papers presented at the Symposium were original.

The Editorial Committee of the Archives of Mechanics kindly offered possibility to publish some of the papers presented at this Symposium, those which had not been published in other journals. Because of the volume of one issue and organizational reasons, the present number contains conference papers which has already been revised and accepted for publication. The other papers will be published in the successive issues of the Journal.

B. Raniecki
(co-chairman)

A. Ziótkowski
(secretary)

Experimental and numerical investigations of thermal-mechanical behaviour of poly- and single-crystalline nickel-base superalloys

A. BERTRAM, J. OLSCHESKI and R. SIEVERT (BERLIN)

*Dedicated to Professor Dr.-Ing. F. G. Kollmann
on the occasion of his 60th birthday*

THE LIFE-TIME assessment of structural components operating at high temperatures, such as e.g. gas turbines, requires an accurate prediction of the inelastic material response by appropriate constitutive models. The present paper shows some inelastic properties of particle hardened nickel-base superalloys, which are used as turbine blade materials, and their modelling by Chaboche's viscoplastic model and an anisotropic three-dimensional viscoelastic model. The simulation possibilities are demonstrated for non-isothermal uni- and multiaxial cyclic behaviour of an isotropic material and for creep behaviour of a cubic single crystal in comparison with the experimental findings.

1. Introduction

AN ADVANCED design methodology of gas turbines requires the use of materials with high-temperature capabilities and, in addition, a realistic assessment of stresses and strains in the highly stressed parts of the system. Among the most highly stressed components, turbine blades are submitted to high temperature and thermal stress cycles combined with centrifugal loads. To achieve maximum performance, the inelastic material behaviour must be taken into account. In general, materials used in high-temperature applications, as e.g. nickel-base superalloys, exhibit both short-term plastic deformation, long-term creep deformation, and the interaction between them. The material inelasticity and the normal service conditions containing multiaxial, cyclic and non-isothermal loading histories represent a challenge for the predictive capabilities of the constitutive models in question. For that purpose, unified constitutive models have been developed in the past.

In the first part of this paper, the viscoplastic CHABOCHE model [1] has been applied to predict the material response of the nickel-base superalloy IN738LC, a polycrystalline cast alloy used as blade material for stationary gas turbines. The prediction capabilities of the model will be demonstrated with respect to non-proportional and non-isothermal loadings.

The second part of this paper deals with the description of isothermal creep behaviour of the single-crystalline superalloy CMSX6. The use of single crystals as turbine blade materials has the advantage of a higher thermodynamic efficiency because of a higher gas entry-temperature and a better corrosion resistance compared with similar polycrystalline materials. They are used mainly in flight engines. The disadvantage, from the theoretical point of view, is the greater complexity of the material behaviour because of the anisotropy which has to be modelled. We will present a three-dimensional constitutive model based on the tensor function approach which exhibits the cubic symmetry of the material. Furthermore, we will demonstrate the model capabilities to describe the crystal orientation-dependent creep behaviour of the material.

Part A. Description of isotropic behaviour at high temperature

2. Constitutive model and isothermal loading

2.1. Viscoplastic theories

Modelling of the inelastic behaviour of nickel-base superalloys is a complex task. These materials show complicated deformation phenomena due to the various strengthening mechanisms caused by second phase particles which are not well understood at present. For example, a typical response of superalloys is the non-monotonous variation of the yield strength with temperature as reported by POPE and EZZ [2]. Regarding the alloy IN 738 LC, this particular behaviour is shown in Fig. 1a. A further complexity arises from the history-dependence of the material behaviour which is obviously influenced by creep-fatigue interaction processes. Strain-rate dependent materials exhibit the phenomenon that the relaxation response is different if the relaxation process starts under the same applied stress, but from different points of a hysteresis loop (see, e.g. ROBINSON [3]).

There is a vast literature on inelastic constitutive models capable for high temperature applications. In particular, the state variable viscoplastic or unified theories, using only one inelastic strain component, have proved their suitability. The description of creep-fatigue interaction is based on coupling of the inelastic strain with hardening variables changing during the inelastic process. A literature survey on viscoplastic models with a special emphasis on the hardening rules used has been given by KREMPL [4]. An overview on the predictive capabilities of further models used in engineering practice can be found in [5].

A widely accepted representative of the class of unified models is the viscoplastic CHABOCHE model [1] which has been selected for the present investigation. A comparison of models with different flow rules, as e.g. those of BODNER–PARTOM [6] and CHABOCHE [1], has demonstrated (see OLSCHESKI *et al.* [7]) that the prediction behaviour of both models is very similar if the model calibration procedure is performed very carefully. Differences occur only if the direction of the inelastic deformation is of importance, such as in relaxation processes under multiaxial loading, see the example plotted in Fig. 2. There is experimental evidence that the direction of inelastic strain-rate is not determined by the stress deviator alone.

2.2. Isothermal uni- and multiaxial loading

The Chaboche model valid at isothermal conditions is given in Table 1. The material parameters are constitutive functions of temperature. The values of these functions have been determined for several temperatures by using isothermal uniaxial tests only. For this purpose the material parameters are divided into groups with respect to different ranges of hardening behaviour (e.g. primary and cyclic hardening) and determined by a stepwise optimization procedure based on the Levenberg–Marquardt algorithm [8]. Only simple strain-controlled tensils and cyclic tests, as well as monotonous creep tests have been used. The result of this calibration procedure with respect to IN 738 LC is shown in Table 2.

Table 1. Evolution equations of Chaboche's model for isothermal processes.**Hooke's law**

$$(2.1) \quad \mathbf{S} = \mathbf{C}(T)(\mathbf{E}_m - \mathbf{E}_i), \quad \mathbf{E}_m := \mathbf{E} - \mathbf{E}_{th}(T), \quad \mathbf{E}_{th} = \alpha(T)(T - T_0)\mathbf{1}.$$

Flow rule

$$(2.2) \quad \dot{\mathbf{E}}_i = \sqrt{\frac{3}{2}} \left\langle \frac{J_2(\mathbf{S}' - \mathbf{X}) - R_y}{K} \right\rangle^n \frac{\mathbf{S}' - \mathbf{X}}{\|\mathbf{S}' - \mathbf{X}\|},$$

$$\langle y \rangle := \begin{cases} y, & \text{if } y > 0 \\ 0, & \text{if } y \leq 0, \end{cases} \quad J_2(-) := \sqrt{\frac{3}{2}} \|(-)\|.$$

Hardening rules*isotropic*

$$(2.3) \quad \dot{R}_y = b(R_{y\infty} - R_y)\dot{p}, \quad \dot{p} = \sqrt{\frac{2}{3}} \|\dot{\mathbf{E}}_i\|, \quad R_y(t=0) = k,$$

kinematical

$$(2.4) \quad \dot{\mathbf{X}} = c \left(a \frac{\mathbf{S}' - \mathbf{X}}{J_2(\mathbf{S}' - \mathbf{X})} - \phi(p)\mathbf{X} \right) \dot{p} - d \left(\frac{J_2(\mathbf{X})}{a} \right) r \frac{\mathbf{X}}{J_2(\mathbf{X})},$$

$$\phi(p) = \phi_\infty - (\phi_\infty - 1)e^{-\omega p}.$$

E total strain tensor at small deformations, \mathbf{E}_{th} , \mathbf{E}_m , \mathbf{E}_i thermal, mechanical and inelastic strain tensor,**S**, \mathbf{S}' stress tensor and the deviator,**C** elastic stiffness tensor of 4th order,**X** internal stress tensor of induced anisotropy, $\|\cdot\|$ Euclidean norm, R_y isotropic internal stress, p accumulated inelastic strain.**Table 2. Material parameters of Chaboche's model for IN 738 LC.**

IN 738 LC	RT	450° C	600° C	750° C	850° C	950° C
E [MPa]	197 570.	188 550.	166 230.	152 450.	149 650.	139 370.
ν	0.33	0.33	0.33	0.33	0.33	0.33
K	111.	39.	84.	1166.	1150.	790.
n	8.6	10.	10.	5.9	7.7	6.8
k [MPa]	580.	460.	543.	330.	153.	79.
$R_{y\infty}$ [MPa]	439.	349.	554.	237.	0.	0.
b	17.	17.	13.	16.	317.	439.
a [MPa]	277.	234.	210.	319.	311.	188.
c	862.	1207.	724.	499.	201.	267.
ϕ_∞	0.47	0.36	0.46	0.73	1.	1.
ω	18.3	40.6	34.7	12.	(0.)	-
d [MPa/s]	0.	0.	$3.5 \cdot 10^{-3}$	$3.5 \cdot 10^{-3}$	$2.3 \cdot 10^{-2}$	$9 \cdot 10^{-2}$
r	-	(4.)	4.2	1.3	4.8	4.4

The material constants represent the typical temperature-dependence of the yield strength $R_{p(0.2)}$, Fig. 1a. At 750° C, IN 738 LC exhibits no strict monotonous strain-rate dependence as it is the case at 850° C and 950° C. At temperatures less than 600° C we have a quasi-strain-rate insensitivity. Therefore, relaxation tests instead of creep tests have been used in the calibration process at lower temperatures to check the remaining strain-rate dependence.

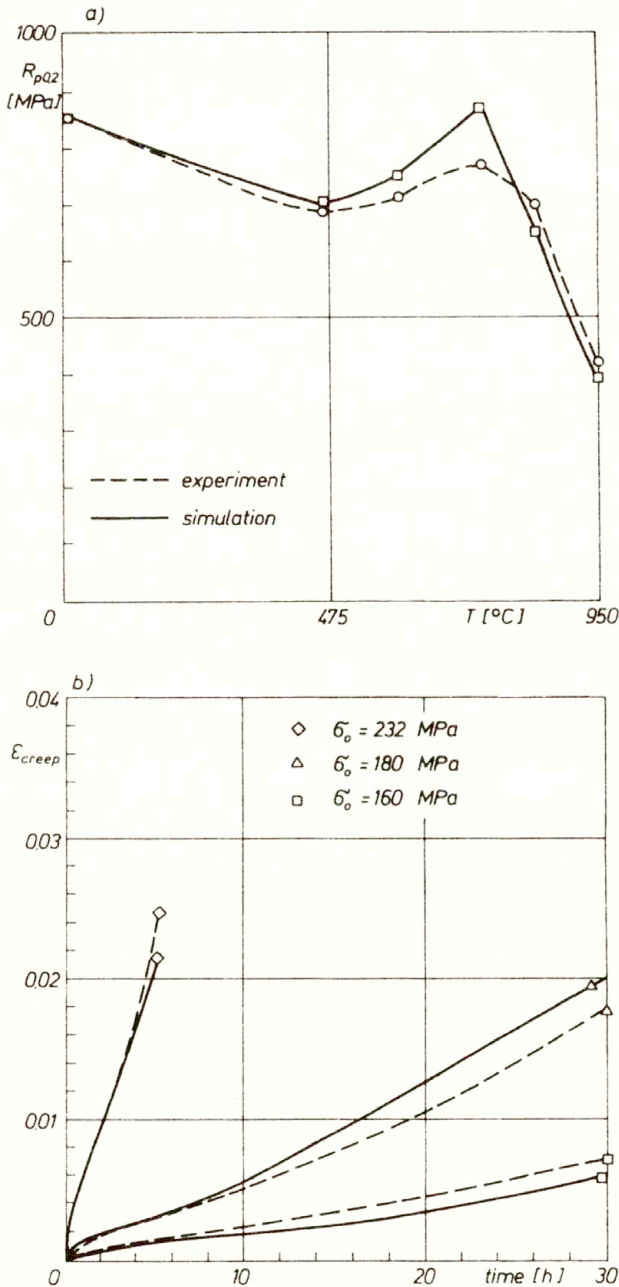


FIG. 1. Modelling of uniaxial behaviour: Temperature variation of the yield strength at $\dot{\epsilon} = 10^{-3}$ s a), creep behaviour at 950° C b).

Fig. 1b shows primary and secondary creep behaviour at 950° C. An increasing creep-rate at constant load is connected with a decreasing flow resistance. The varying creep-rate, as indicated in Fig. 1b, is predicted by the model on the basis of a competition between

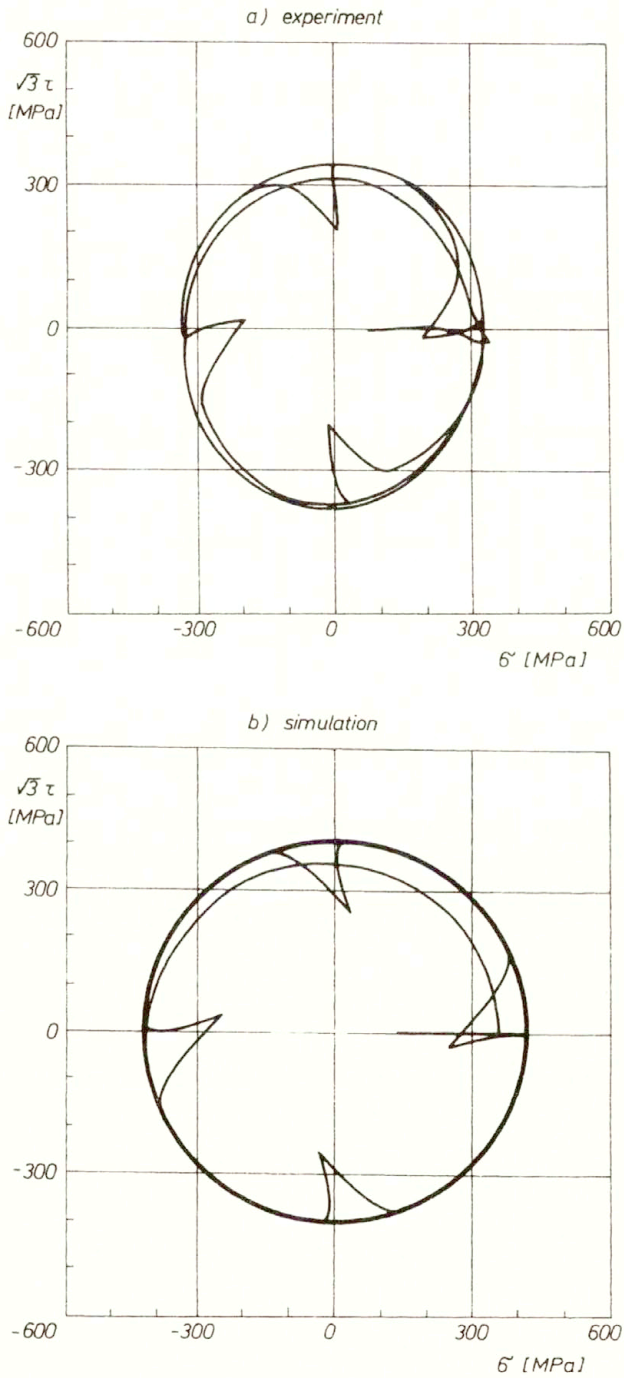


FIG. 2. Cyclic axial-torsional loading: Material response a) to a 90° out-of-phase straining with hold times at stress extrema (950°C , $\varepsilon_{\text{eq}} = 0.006$, $\dot{\varepsilon}_{\text{eq}} = 10^{-3}$ /s, $t_H = 120$ s) and its simulation b).

kinematical hardening and an isotropic softening which both converge to a certain limit but with different rates.

The behaviour of IN 738 LC under uniaxial cyclic loading at 850° C and 950° C is characterized by a stress saturation level which is reached after a few cycles, i.e. the material shows only a slight cyclic hardening. This observation leads to the values of the material parameters ϕ_∞ and ω of Table 2.

Figure 2 points out the multiaxial cyclic hardening behaviour at 950° C under a sinusoidal axial-torsional loading path where the axial and shear strain are controlled in 90° C — out-of-phase. This results in a circular strain path in the $\varepsilon - \gamma/\sqrt{3}$ plane. Hold times of strain were imposed at the peak stresses (ZIEBS *et al.* [9]). The material response in a saturated cycle, Fig. 2a, is simulated Chaboche's model which is calibrated to uniaxial behaviour only, Fig. 2b. As it is indicated in Fig. 2b, IN 738 LC exhibits no additional hardening under non-proportional cyclic loading either, at 950° C as well as at other temperatures. The same observation has been made for the isotropic particle hardened superalloy B1900+Hf (CHAN *et al.* [10]).

3. Non-isothermal loading

3.1. Model formulation

For isothermal loading, the rate equation of isotropic hardening, Eq. (2.3)₁, can be integrated to

$$(3.1) \quad R_y = \widehat{R}_y(p, T) := R_{y\infty}(T) - (R_{y\infty}(T) - k(T))e^{-b(T)p}.$$

As a generalization, this *finite state function* can be considered to be valid also in non-isothermal processes (BENALLAL and BEN CHEIKH [11], BHATTACHAR and STOUFFER [12]). Equivalent to Eq. (3.1) is the following incremental evolution equation:

$$(3.2) \quad \begin{aligned} \dot{R}_y &= \frac{\partial \widehat{R}_y}{\partial p} \dot{p} + \frac{\partial \widehat{R}_y}{\partial T} \dot{T}, \quad R_y(t=0) = k(T_0), \\ &= b(R_{y\infty} - R_y) \dot{p} + \frac{\partial \widehat{R}_y}{\partial T} \dot{T}. \end{aligned}$$

Obviously, the finite state function, Eq. (3.1), corresponds to a *temperature-rate term* in the rate equation (MORENO and JORDAN [13]).

Equation (3.2) contains two limiting cases: At the beginning of the process, $p = 0$, R_y is equal to the initial internal stress, $R_y = k$, and the \dot{T} — term reads (cf. SLAVIK and SEHITOGLU [14]):

$$(3.3) \quad \dot{R}_y = b(R_{y\infty} - R_y) \dot{p} + \frac{dk}{dT} \dot{T}.$$

In a saturated state, $p \rightarrow \infty$, the isotropic hardening variable $R := R_y - k$ has the evolution equation

$$(3.4) \quad \dot{R} = b(h - R) \dot{p} + \frac{dh}{dT} \dot{T}, \quad h(T) := R_{y\infty}(T) - k(T).$$

This form has been enlarged to consider additional hardening under non-proportional multiaxial loading (BENALLAL and BEN CHEIKH [15], MCDOWELL [16]). But the cycling hardening behaviour of high-temperature alloys with relatively high volume fraction of so-called γ' -particles ($> 40\%$, IN 738 LC, B1900+Hf) under in-phase and out-of-phase loading is essentially the same.

In general, one has to take into account static recovery in the evolution equation for isotropic hardening (CHABOCHE [17]). Such a static recovery term could be added to the rate equation (3.2). Static recovery of the internal back-stress, last term of Eq. (2.4)₁, has been considered to be able to simulate the creep behaviour of Fig. 1b, for example. Static recovery of the isotropic internal stress (elastic region) which is present especially at the beginning of the process, can be important for the description of the material behaviour at very low strain-rates ($\dot{\epsilon} < 10^{-7}/s$; cf. KREMPL [18]).

Calculations with a temperature-rate term in the kinematical hardening rule have not given any improvement of the simulation quality (cf. [19]). Therefore, only a \dot{T} -term in the isotropic hardening rule, Eq. (3.2), will be considered in the following section. The temperature functions of the material parameters are approximated by linear interpolation of the values obtained at certain temperatures, Table 2.

3.2. Non-isothermal uni- and multiaxial cyclic loading

Turbine blades are subjected to thermal-mechanical fatigue loading. Therefore it is necessary that the constitutive models should be able to predict non-isothermal stress-strain

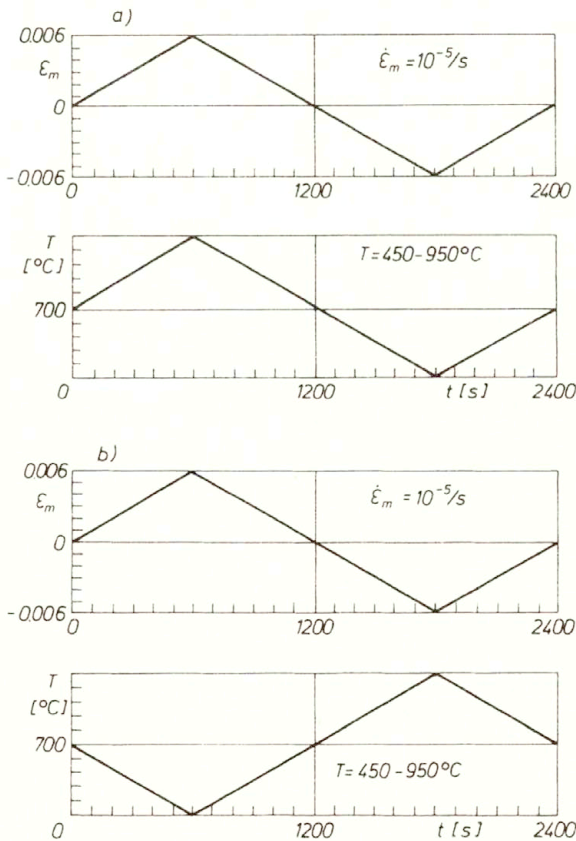


FIG. 3. Non-isothermal uniaxial cyclic loading; loading histories; in-phase a), out-of-phase b).

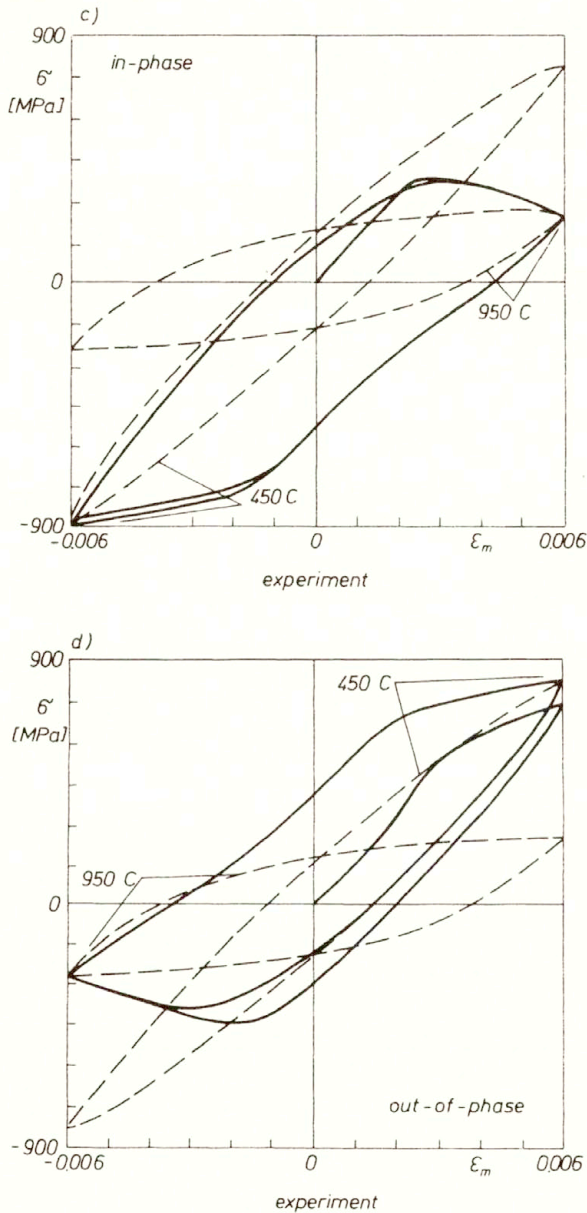


FIG. 3. Non-isothermal uniaxial cyclic loading: material response (c, d) $\dot{T} = 0.417^\circ \text{ C/s}$; solid lines represent non-isothermal and dashed lines — the isothermal behaviour.

behaviour of the material. Especially in cooled turbine blades, where strong temperature gradients are present, thermal stresses are an important load. Relevant to the stress is the mechanical part of strain. Hence, in the experiments the mechanical strain is controlled simultaneously with temperature. In the testing machine, the total strain is applied in

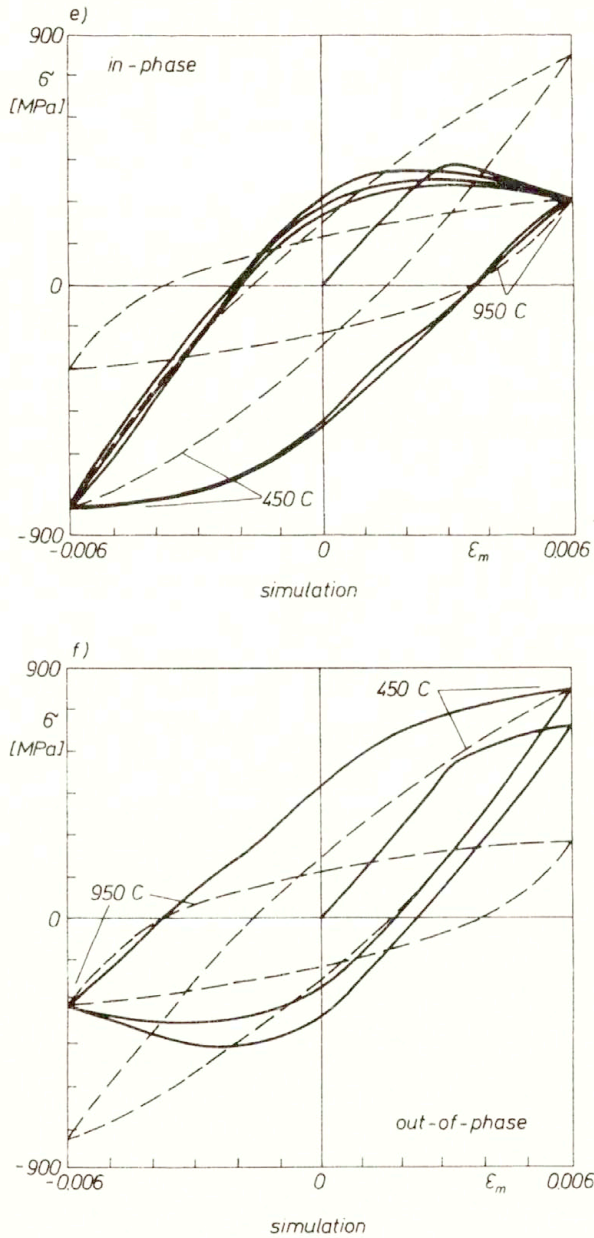
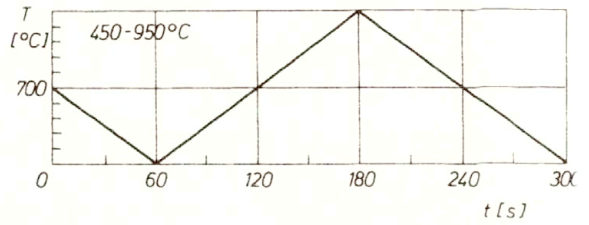
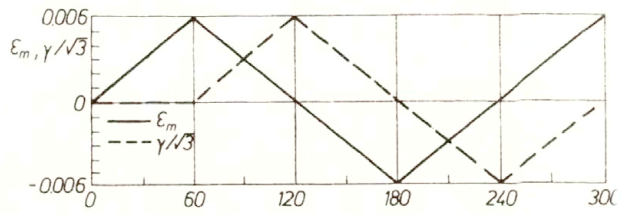
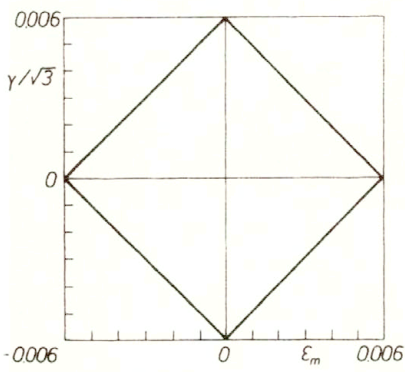
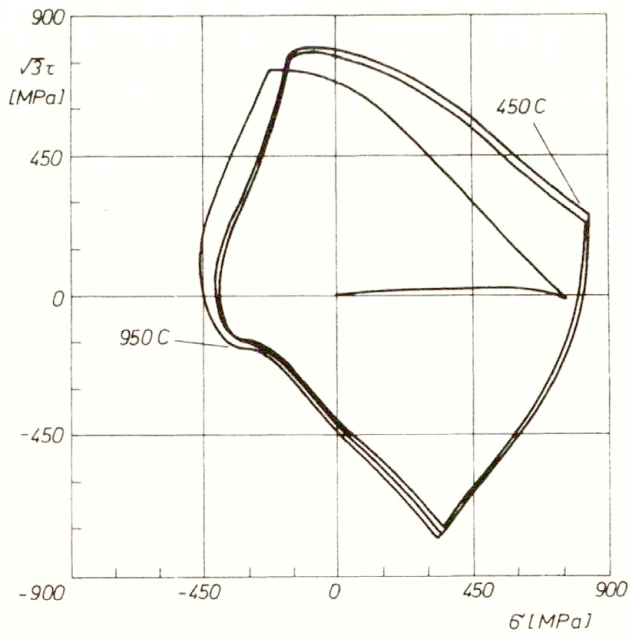


FIG. 3. Non-isothermal uniaxial cyclic loading: simulation (e, f) $\dot{T} = 0.417^\circ \text{C/s}$; solid lines represent non-isothermal and dashed lines — the isothermal behaviour.

such a way that the mechanical strain follows a given course in time, e.g. in-phase with temperature, Fig. 3a. At out-of-phase straining, Fig. 3b, the total strain does not have to be so large for compression and tension because of thermal expansion and shrinking, respectively.



a)



b) experiment

[Fig. 4.]

[422]

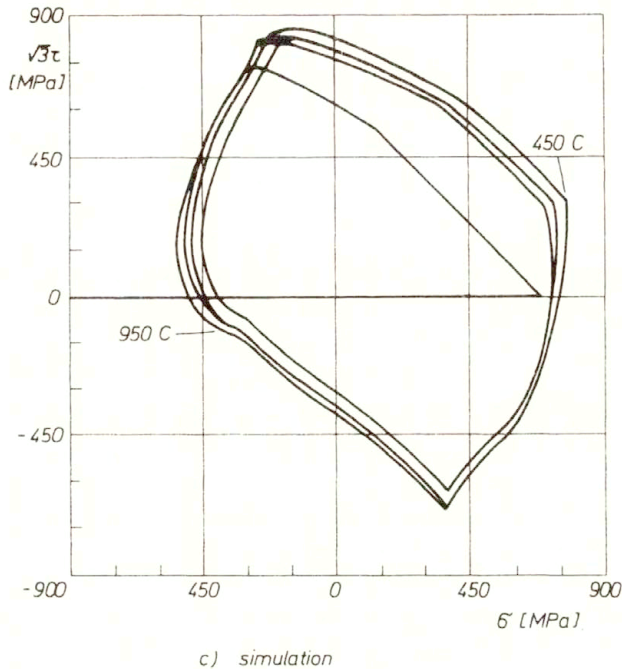


FIG. 4. Non-isothermal axial-torsional cyclic loading: Loading history a) $\dot{T} = 4.17^\circ \text{ C/s}$, material response b) and simulation c).

The material response measured in these uniaxial tests is shown in Figs. 3c,d. The full lines correspond to the non-isothermal cyclic loading in the temperature interval between 450 and 950° C. The dashed lines represent the material behaviour under isothermal cyclic straining at the maximum and minimum temperature of the non-isothermal cycle, respectively. The resulting stress levels at the strain amplitudes in both non-isothermal loadings are of the same order as those of the associated isothermal loadings. This leads to asymmetric hysteresis loops under non-isothermal conditions.

Predictions based on Chaboche's model with an additional temperature-rate term in the isotropic hardening rule, as already discussed in Sect. 3.1, Eq. (3.2), reproduce these phenomena, Figs. 3e,f. The material constants, see Table 2, are determined exclusively by isothermal uniaxial tests. Neglecting the temperature-rate term which characterizes hardening or softening induced by temperature changes, the prediction would not meet the isothermal stress amplitudes, especially at the low temperature amplitude, [19]. With the introduced temperature-rate term or, equivalently, with the finite state function, Eq. (3.1), the model reaches instantaneously the yield strength R_y corresponding to the actual temperature.

A more complex stress state results under non-isothermal multiaxial loading. An example is shown in Fig. 4. The thermal-mechanical loading history is plotted in Fig. 4a. The axial strain/shear strain path is of diamond shape. The temperature is applied under 180° out-of-phase with respect to the axial strain. Figure 4b shows the material response to the non-isothermal axial-torsional cyclic loading. The simulation of the material behaviour is given in Fig. 4c. The model prediction shows all the characteristic features of

the material response as there are the curvature of the stress-path which is due to the varying hardening and stress extrema which do not correspond to the strain extrema.

From the rheological point of view Chaboche's viscoplastic theory is a Bingham-type model (LEMAITRE and CHABOCHE [20]). At high temperature viscous effects (relaxation and creep) are more important. Therefore, anisotropic creep will be described by a Burgers-type model in the second part of this paper.

Part B. Description of cubic anisotropic behaviour at high temperature

4. Creep modelling

4.1. Constitutive theories for single crystals

For single crystals the situation is quite different from that for polycrystalline materials, as the creep behaviour depends highly on the orientation of the crystal within the specimen or structure. The times to rupture under monotonous creep conditions can differ from one orientation to another by an order of two decimal places. Therefore, any three-dimensional modelling must necessarily take into account the strong anisotropy of the behaviour.

In the literature basically two different methods are applied to model the three-dimensional creep behaviour of single crystals. One of them is to use the different classes of *slip systems* and to formulate uniaxial creep equations for them. The advantage is that these equations are much less complicated than the three-dimensional ones, and the assemblage of all slip systems assures a three-dimensional law that automatically secures the symmetry of the crystal. Interactions between the different slip systems seem to be important and enter solely due to the work-hardening law, namely by the cross-hardening parameters. The validity of this approach, however, is rather limited. In certain temperature regimes, the creep behaviour is dominated by diffusional creep, which has nothing to do with slip system mechanisms. For this reason slip system approaches turn out to be inadequate for creep modelling within these regimes [21, 22].

The other approach, which is favoured in the present paper, makes use of representations by *tensor functions*, which are well known from linear algebra. The problem of this approach, which is by no means trivial, lies mainly in the task of giving the resulting constants and variables a physical interpretation.

We will limit our considerations to the primary and secondary creep, excluding the tertiary creep phase, because little is known about three-dimensional anisotropic continuum damage. The uniaxial model, however, has been successfully enlarged by a Kachanov-type damage parameter, which also describes tertiary creep till rupture (see [23]).

4.2. Modelling by a viscoelastic differential equation

The starting point for the present approach is the uniaxial modelling of the monotonous primary and secondary creep behaviour under tensile loadings in the $[0\ 0\ 1]$ -orientation. This has been successfully done by means of a 4-parameter differential equation

$$(4.1) \quad \sigma'' + A_1 \sigma' + A_2 \sigma = A_3 \varepsilon'' + A_4 \varepsilon',$$

where the four coefficients $A_{1,2,3,4}$ depend solely on the stress σ , which is indeed constant

for creep tests. This dependence has been specified by means of a linear function

$$(4.2) \quad f(\sigma) = K_1 - K_2\sigma, \quad \text{with} \quad K_{1,2} > 0,$$

such that

$$\begin{aligned} A_1 &= A_{01}/f(\sigma), \\ A_2 &= A_{02}/f(\sigma)^2, \\ A_3 &= A_{03}, \\ A_4 &= A_{04}/f(\sigma), \end{aligned}$$

where the A_{0i} are material constants for isothermal processes. This form of dependence is equivalent to the introduction of an artificial time (see [23]). The applicability of this expression, however, is limited to a certain interval, where $f(\sigma)$ is positive. A more appropriate form of this dependence is

$$(4.3) \quad f(\sigma) = K_3 \exp(-K_4\sigma), \quad \text{with} \quad K_{3,4} > 0.$$

This function renders positive values in the whole (tension) stress regime.

The numerical integration of Eq. (4.1) can be easily done by introducing an internal variable and reducing the differential equation to a system of first order differential equations. Appropriate initial conditions for such variable result from its physical interpretation.

The three-dimensional generalization is a reinterpretation of Eq. (4.1) in the following way:

σ : the stress tensor \mathbf{S} ,

ε : the (infinitesimal) strain tensor \mathbf{E} ,

$A_{1,2,3,4}$: 4th rank tensors $\mathbf{A}_{1,2,3,4}$, fulfilling the cubic anisotropy conditions of the crystal.

The differential equation now reads

$$(4.4) \quad \mathbf{S}'' + \mathbf{A}_1 \mathbf{S}' + \mathbf{A}_2 \mathbf{S} = \mathbf{A}_3 \mathbf{E}'' + \mathbf{A}_4 \mathbf{E}'.$$

For the 4th rank tensors a complete cubic representation is known from linear algebra (see [24, 25, 26]) as a linear combination of 3 structural tensors

$$(4.5) \quad \mathbf{A}_i = \alpha_{i1} \mathbf{P}_1 + \alpha_{i2} \mathbf{P}_2 + \alpha_{i3} \mathbf{P}_3$$

given by

$$\begin{aligned} \mathbf{P}_1 &:= 1/3 \mathbf{I} \otimes \mathbf{I}, \\ \mathbf{P}_2 &:= \sum_{i=1}^3 \mathbf{e}_i \otimes \mathbf{e}_i \otimes \mathbf{e}_i \otimes \mathbf{e}_i - \mathbf{P}_1, \\ \mathbf{P}_3 &:= \mathbf{I} - \mathbf{P}_1 - \mathbf{P}_2, \end{aligned}$$

where \mathbf{e}_i denotes the lattice directors, \mathbf{I} the second rank identity, \mathbf{I} the fourth rank identity, and \otimes the tensorial product. α_{ij} are $4 \times 3 = 12$ (stress-dependent) material constants.

The stress dependence of these constants is assumed to be of an analogous form to Eq. (4.3). Instead of the (unique) tension stress in the uniaxial case, we need an expression for the stress intensity, which is invariant under cubic symmetry transformations. A complete integrity base for the specific symmetry group is given by the nine invariants (see [27])

$$\begin{aligned} J_1 &= \text{tr}(\mathbf{S}), \\ J_2 &= 1/2[\text{tr}^2(\mathbf{S}) + \text{tr}(\mathbf{S}^2)], \end{aligned}$$

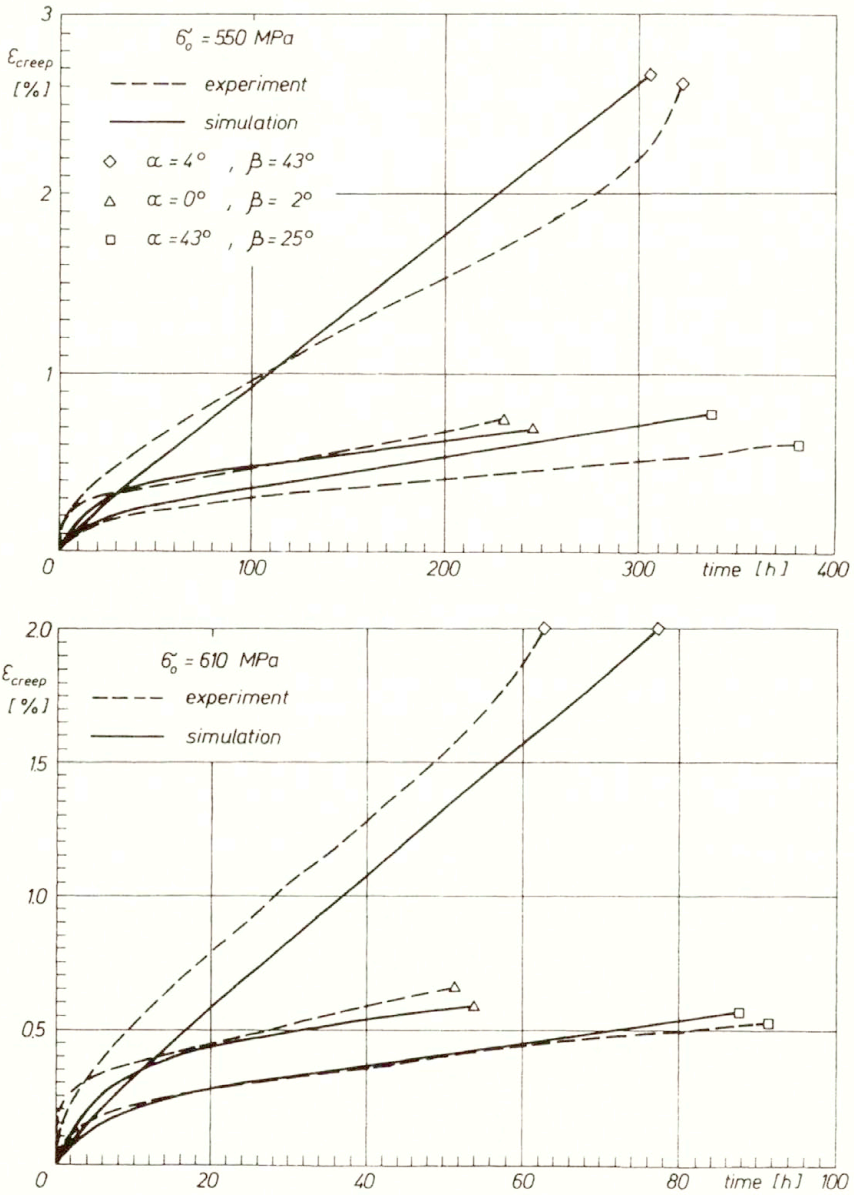


FIG. 5. Modelling of creep behaviour of a single crystal at different orientations, α and β are the first and second Eulerian angles.

$$J_3 = \det(\mathbf{S}),$$

$$J_4 = \sigma_{12}^2 + \sigma_{23}^2 + \sigma_{31}^2,$$

$$J_5 = \sigma_{12}\sigma_{23}\sigma_{31},$$

$$J_6 = (\sigma_{11} + \sigma_{22})\sigma_{12}^2 + (\sigma_{22} + \sigma_{33})\sigma_{23}^2 + (\sigma_{33} + \sigma_{11})\sigma_{31}^2,$$

$$\begin{aligned}
 J_7 &= \sigma_{12}^2 \sigma_{23}^2 + \sigma_{23}^2 \sigma_{31}^2 + \sigma_{31}^2 \sigma_{12}^2, \\
 J_8 &= \sigma_{11} \sigma_{12}^2 \sigma_{31}^2 + \sigma_{22} \sigma_{23}^2 \sigma_{12}^2 + \sigma_{33} \sigma_{31}^2 \sigma_{23}^2, \\
 J_9 &= \sigma_{11} \sigma_{22} \sigma_{12}^2 + \sigma_{22} \sigma_{33} \sigma_{23}^2 + \sigma_{33} \sigma_{11} \sigma_{31}^2.
 \end{aligned}$$

For our purposes the following ansatz-functions turned out to be appropriate:

$$(4.6) \quad f_i(\mathbf{S}) = K_{i1} \exp(-K_{i2} J_2 - K_{i3} J_4 - K_{i4} J_5 - K_{i5} J_6), \quad \text{with } K_{ij} > 0.$$

The number of the material constants can be reduced to 17 by assuming the inelastic incompressibility, as usual. The remaining set of material constants has been calibrated by the least square methods to tensile creep tests in different orientations. In Fig. 5 the results of an adjustment by a single set of parameters is shown for the single crystal superalloy CMSX6 at 760° C. The tests have been performed by Siemens-KWU. α and β are the first and second Eulerian angles, which determine the orientation of the crystal within the samples.

5. Conclusions

The inelastic deformation behaviour of particle hardened superalloys such as e.g. IN 738 LC has different microstructural origins dependent on both the temperature and the strain-rate applied. It was shown that phenomenological constitutive equations like those of the viscoplastic Chaboche model are able to simulate the inelastic response of this class of materials under uniaxial as well as multiaxial loadings. Furthermore, the need of an additional temperature-rate term in the evolution equation for isotropic hardening is established if non-isothermal loadings have to be considered. Even then, only isothermal uniaxial tests are, in the investigated loading range, necessary to calibrate the model.

The modelling of the primary and secondary creep behaviour of single crystals is based on a four-parameter differential equation with stress-dependent coefficients. The three-dimensional generalization uses representations of tensor functions performing the required material symmetries of a f.c.c. crystal. The orientation dependence of creep behaviour is reproduced by this model, as comparison with experiments shows.

Acknowledgements

The authors are grateful for the financial support of the Deutsche Forschungsgemeinschaft (DFG) within the Sonderforschungsbereich 339 of the Technical University Berlin. The contribution of Drs. J. MEERSMANN, J. ZIEBS and Mr. H.-J. KÜHN at the laboratory for mechanical testing (BAM-1.21) in performing the experimental work is gratefully acknowledged.

The single crystal part has been funded by Siemens-KWU within COST-Round II WP 501, which is gratefully acknowledged.

References

1. J.-L. CHABOCHE, *Viscoplastic constitutive equations for the description of cyclic anisotropic behaviour of metals*, Bull. de l'Academie des Sciences, Serie des Techniques, **25**, 33–42, 1977.
2. D.P. POPE and S.S. EZZ, *Mechanical properties of Ni₃Al and nickel-base alloys with high volume fraction of γ'* , Internat. Metals Reviews, **29**, 3, 136–167, 1984.

3. D.N. ROBINSON, *On thermo-mechanical testing in support of constitutive equation development for high-temperature application*, Lewis Research Center, NASA-CR 174879, 1985.
4. E. KREMPL, *Models of viscoplasticity, some comments on equilibrium (back) stress and drag stress*, *Acta Mech.*, **69**, 25–42, 1987.
5. O.T. BRUHNS *et al.*, *A comparative study of unified constitutive equations for modelling inelastic material behaviour*, [in:] Proc. Post-SMiRT Seminar No 5 on Inelastic Analysis, Fatigue and Life Prediction, Paris, 1993.
6. S.R. BODNER, *Review of a unified elastic-viscoplastic theory*, [in:] *Unified Constitutive Equations for Creep and Plasticity*, A.K. MILLER [Ed.], Elsevier Applied Science, 273–301, 1987.
7. J. OLSCHESKI, R. SIEVERT and A. BERTRAM, *A comparison of the predictive capabilities of two unified constitutive models at elevated temperatures*, [in:] *Constitutive Laws of Engineering Materials*, C.S. DESAI *et al.* [Eds.] ASME PRESS, 775–758, 1991.
8. J.J. MORE, *The Levenberg-Marquardt algorithm: implementation and theory* [in:] *Numerical Analysis*, G.A. WATSON [Ed.], *Lecture Notes in Mathematics* 630, A.D. DOLD, B. ECKMANN [Eds.], Springer-Verlag, Berlin, 105–116, 1978.
9. J. ZIEBS, J. MEERSMANN and H.-J. KÜHN, *Effects of proportional and non-proportional straining sequences on hardening/softening behavior of IN 738 LC at elevated temperatures* [in:] *Multiaxial Plasticity*, A. BENALLAL *et al.* [Eds.], MECAMAT'92, Laboratoire de Mécanique et Technologie, Cachan-France, 224–255, 1992.
10. K.S. CHAN, U.S. LINDHOLM, S.R. BODNER and A. NAGY, *High temperature inelastic deformation of the B1900+Hf alloy under multiaxial loading: theory and experiment*, *J. Engng. Mat. Technology*, **112**, 7–14, 1990.
11. A. BENALLAL and A. BEN CHEIKH, *Constitutive equations for anisothermal elasto-viscoplasticity* [in:] *Constitutive Laws for Engineering Materials*, C.S. DESAI *et al.* [Eds.], 667–674, 1987.
12. V.S. BHATTACHAR and D.C. STOUFFER, *Constitutive equations for the thermomechanical response of Rene'80: Part I, 2*, *J. Engng. Mat. Technology*, **115**, 351–364, 1993.
13. V. MORENO and E.H. JORDAN, *Prediction of material thermomechanical response with a unified viscoplastic constitutive model*, *Int. J. Plasticity*, **2**, 223–245, 1986.
14. D. SLAVIK and H.A. SEHITOGLU, *A constitutive model for high temperature loading: Part I, II* [in:] *Thermal Stress, Material Deformation and Thermo-Mechanical Fatigue*, H. SEHITOGLU, S.Y. ZAMRIK [Eds.] ASME, PVP-123, 65–83, 1987.
15. A. BENALLAL and A. BEN CHEIKH, *Damage and rupture of viscoplastic structures under anisothermal cyclic loadings*, [in:] *High Temperature Fracture Mechanisms and Mechanics*, EGF6, P. BENSUSSAN [Ed.] MEP, 227–247, 1990.
16. D.L. MCDOWELL, *A nonlinear kinematic hardening theory for cyclic thermo-plasticity and thermoviscoplasticity*, *Int. J. Plasticity*, **8**, 695–728, 1992.
17. J.-L. CHABOCHE, *Thermodynamically based viscoplastic constitutive equations: theory versus experiment*, [in:] *High Temperature Constitutive Modeling — Theory and Application*, A.D. FREED, K.P. WALKER [Eds.], ASME, MD-Vol. 26, AMD-Vol. 121, 207–226, 1991.
18. E. KREMPL, *Isotropic viscoplasticity theory based on overstress for small strain*, presented at the 6th Polish-German Symposium on Mechanics on Inelastic Solids and Structures, Czerniejewo, Poland, 1993.
19. R. SIEVERT, C. HAFTAOGU and J. OLSCHESKI, *Verifizierung und Weiterentwicklung von zwei viskoplastischen Stoffmodellen für Teilchen-härtende Nickelbasis-Legierungen auf der Grundlage ein- und mehrachsiger thermisch-mechanischer Versuche* [in:] *Forschungsbericht 1990–1992 des Sfb 339*, TU Berlin, 407–443, 1993.
20. J. LEMAITRE and J.-L. CHABOCHE, *Mechanics of solid materials*, Cambridge University Press, 1990.
21. R.A. MACKAY and R.D. MAIER, *The influence of orientation on the stress rupture properties of nickel-base superalloy single crystals*, *Metall. Trans.*, **13A**, 1747–1754, 1982.
22. D.J. SHAH, *Orientation dependence of creep behavior of single crystal γ' (Ni₃Al)*, *Scripta Metallurgica*, **17**, 8, 997–1002, 1983.
23. A. BERTRAM, J. OLSCHESKI, M. ZELEWSKI and R. SIEVERT, *Anisotropic creep modeling for f.c.c. single crystals* [in:] *Creep in Structures*, IUTAM Symposium Cracow/Poland 1990, M. ŻYCZKOWSKI [Ed.], Springer-Verlag, Berlin, 1991.
24. A. BERTRAM, J. OLSCHESKI, R. SIEVERT and M. ZELEWSKI, *Constitutive modeling of the creep behaviour of single crystals with applications to notched specimens* [in:] *Constitutive Laws for Engineering Materials*, C.S. DESAI *et al.* [Eds.], ASME Press, New York 1991.
25. A. BERTRAM and J. OLSCHESKI, *Formulation of anisotropic linear viscoelastic constitutive laws by a projection method* [in:] *High Temperature Constitutive Modeling — Theory and Application*, A. FREED, K.P. WALKER

- [Eds.], ASME, MD-Vol. 26, AMD-Vol., 121, 129–137, 1991.
26. A. BERTRAM and J. OLSCHESKI, *Zur Formulierung anisotroper linearer anelastischer Stoffgleichungen mit Hilfe einer Projektionsmethode*, ZAMM, **73**, 4–5, T401-T403, 1993.
 27. G.F. SMITH and E. KIRAL, *Integrity bases for N symmetric second-order tensors — the crystal classes*, Rend. Circ. Mat. Palermo II, Ser. **18**, 5–22, 1959.

BUNDESANSTALT FÜR MATERIALFORSCHUNG AND — PRÜFUNG (BAM) BERLIN, GERMANY.

Received January 3, 1994.

Transient and residual stresses in progressive induction hardening of infinite solid cylinder

A. BOKOTA, S. ISKIERKA, R. PARKITNY (CZĘSTOCHOWA)
and B. RANIECKI (WARSZAWA)

A MODEL OF NUMERICAL simulation of progressive induction hardening has been presented in the paper. In the model the coupling of electromagnetic, thermal field, phase transformations field and stress field are considered. The electromagnetic field has been calculated from Maxwell's equations taking into consideration variation of conductivity and permeability of the material during the process. The power losses (from eddy currents) result in changing of thermal field in the conducting materials which is described by Fourier–Kirchhoff equation. The thermal field in the hardened element is also affected by heat exchange with surroundings, mainly through the cooling medium. The fractions of phases created during the phase transformations have been calculated by means of TTT-heating diagram and TTT-cooling diagram. The instant and residual stresses have been determined on the basis of the thermoplasticity theory with isotropic hardening by the finite element method. The numerical calculations have been made for a steel axi-symmetrical element hardened by the induction progressive method.

List of symbols

- \mathbf{D} deviator of stress tensor [MPa],
- \mathbf{E} tensor of material constants [MPa],
- \mathbf{e}^e tensor of elastic strains,
- \mathbf{e} tensor of total strains,
- \mathbf{e}^θ tensor of dilatational strains,
- \mathbf{e}^p tensor of plastic strains,
- \mathbf{K} matrix of stiffness,
- \mathbf{R} vector of external loads [MN],
- \mathbf{T} tensor of stresses [MPa],
- t_\star^α the known stress vector on Γ [MPa],
- \mathbf{U} vector of displacements [m],
- Y actual level of effective stress [MPa],
- Y_θ thermal softening modulus [MPa/K],
- α heat transfer coefficient [W/(m²K)],
- $\alpha_A, \alpha_B, \alpha_M, \alpha_P$ coefficients of linear thermal dilatation for austenite, bainite, martensite and pearlite, respectively,
- $\gamma_A, \gamma_B, \gamma_M, \gamma_P$ coefficients of phase transformations of austenite into bainite, austenite into martensite and austenite into pearlite, respectively,
- $\eta_A, \eta_B, \eta_M, \eta_P$ phase contents of austenite, bainite, martensite and pearlite, respectively,
- κ hardening modulus [MPa],
- ε_{ef}^p effective plastic strain,
- ρ_{cef} effective thermal capacity [J/(m³K)],
- ∇_α covariant differential operator,
- ∂_α partial differential operator,
- λ thermal conductivity coefficient [W/(mK)],
- ρ density [kg/m³],
- x^α Euler coordinates [m],
- $\varphi_i(x^\alpha)$ base or approximating function,
- Φ matrix of corresponding derivatives of approximating function,

- ϕ the vector of approximating or base functions,
- Θ_0 temperature of surroundings [K],
- \cdot internal complete product of tensor,
- \circ internal non-complete product of tensor,
- $(\dot{}) = \frac{d()}{dt}$ time derivative.

1. Introduction

THE MATHEMATICAL description of the induction hardening process is complex, as it concerns the electromagnetic, thermal and mechanical phenomena occurring in the bodies which, in the process of induction heating followed by cooling, undergo phase transformations. Due to the complexity of the model, very few papers have appeared dealing generally with the induction hardening process, especially with the progressive one.

The papers by T. INOUE, B. RANIECKI [10], B. RANIECKI [18], B. HINDENWALL [7], A. J. FLETCHER, R. F. PRICE [6] and T. INOUE, S. NAGAKI, T. KISHINO, M. MONKAWY [9] deal with the stress states resulting from non-uniform and non-free change of specific volume, with regard to the phase transformations at the cooling process. The available empirical data or formulas by M. AVRAMI [1] and by D. P. KOISTINEN and R. E. MARGURGER [14] have been used there. Also certain concepts of general approach to the kinetics of phase transformations have been included in the papers [9, 21, 22]. The mathematical model of induction hardening presented in the papers by W. SEIDEL and H. UETZ [19] and by G. ORTH [17] merely allows to determine the distribution of the electromagnetic field and thermal field in the hardened element. In the paper by M. MELANDER [16] the problem of induction hardening is treated in a general way.

The mathematical model of induction hardening that accounts for the mutual correlation of the electromagnetic field and the thermal field, the influence of the thermal field on the phase transformations and the effect of thermal field and phase transformations on the stress states have been developed and presented in this paper. The electromagnetic field distribution has been determined on the basis of the Maxwell equations, whereas the temperature field has been calculated on the grounds of the Fourier–Kirchhoff equation. The phase transformations during the process of heating and cooling have been determined on the grounds of the TTT diagrams. The calculated fractions of phases and the thermal field have been used for determining the stress states. The calculations account for the changes in the thermomechanical parameters of the material. They depend on the phase content and the thermal field. Residual stresses have been calculated on the basis of non-isothermic plastic flow model with linear-isotropic strain hardening. The exemplary calculations have been made by means of the finite element method for an axi-symmetrical bar hardened by induction progressive method.

2. Electromagnetic field in conducting medium

The electromagnetic field is determined by Maxwell's equations,

$$(2.1) \quad \begin{aligned} \operatorname{rot} \mathbf{H} &= \gamma \mathbf{E} + \frac{\partial \mathbf{D}}{\partial t}, & \operatorname{rot} \mathbf{E} &= -\frac{\partial \mathbf{B}}{\partial t}, \\ \operatorname{div} \mathbf{D} &= \rho, & \operatorname{div} \mathbf{B} &= 0. \end{aligned}$$

The equations are supplemented by constitutive relations:

$$(2.2) \quad \mathbf{B} = \mu\mathbf{H}, \quad \mathbf{D} = \varepsilon\mathbf{E}.$$

Assuming a steady-state process and considering the displacement current density to be negligible for line frequency, the magnetic vector potential in two-dimensional or axi-symmetrical geometries is given by the equation [4, 8]

$$(2.3) \quad \left(\operatorname{div} \frac{1}{\mu} \operatorname{grad} \right) \underline{\mathbf{A}} - j\omega\gamma\underline{\mathbf{A}} = -\underline{\mathbf{J}}_S,$$

where $\underline{\mathbf{A}}$ is magnetic vector potential (complex r.m.s. value, in the further part of the paper underlining which denotes a complex value will be omitted), ω , γ , μ and j are the angular frequency, conductivity, magnetic permeability, and complex operator, respectively, $\underline{\mathbf{J}}_S$ is the time-harmonic source current density vector (complex r.m.s. value).

In the case of a long straight conductor or a ring-shaped conductor, the integro-differential finite element formulation replaces Eq. (2.3) (containing two unknown quantities: magnetic vector potential and source current density vector) by the integro-differential equation containing only the unknown magnetic vector potential and the measurable total current in the conductor [15] (Fig. 1).

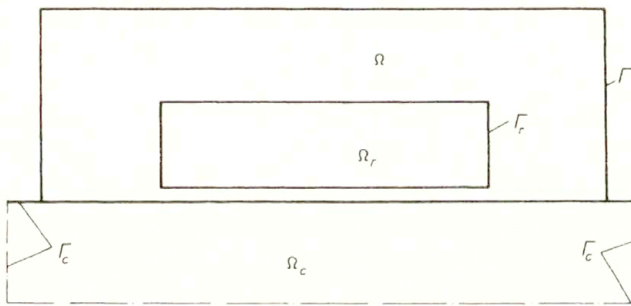


FIG. 1. General scheme of the investigated region.

On the basis of Ampère law we can write:

$$(2.4) \quad I = \iint_{\Omega_r} J_S d\Omega - j\omega\gamma \iint_{\Omega_r} A d\Omega,$$

where $A (A = |\underline{\mathbf{A}}|, A = A_\varphi(r, z))$ is the component of vector $\underline{\mathbf{A}}$, and the integration is carried out over the cross-section of the conductor.

The known value of the source current density can be determined directly from the equation

$$(2.5) \quad J_S = \frac{I}{\Delta} + j\frac{\omega\gamma}{\Delta} \iint_{\Omega_r} A d\Omega,$$

where Δ is the equivalent conductor cross-sectional area. The source current density J_S is constant over the cross-sectional surface of the straight conductor.

By substitution of J_S from Eq. (2.5) into the right-hand side of Eq. (2.1) we obtain an integro-differential equation containing only the unknown quantity, i.e. the magnetic

vector potential A [8, 15]

$$(2.6) \quad \left(\operatorname{div} \frac{1}{\mu} \operatorname{grad} \right) A - j\omega\gamma A + j\frac{\omega\gamma}{\Delta} \iint_{\Omega_r} A d\Omega = -\frac{I}{\Delta}.$$

In the system of cylindrical coordinates (r, z) (for the axi-symmetrical case), Eq. (2.6) assumes the form

$$(2.7) \quad \frac{1}{\mu} \left(\nabla^2 A - \frac{A}{r^2} \right) - j\omega\gamma A + j\frac{\omega\gamma}{\Delta} \iint_{\Omega_r} A d\Omega = -\frac{I}{\Delta}.$$

For the axi-symmetrical system the area Δ is determined by the relationship [15];

$$(2.8) \quad \Delta/r = \iint_{\Omega_r} \frac{1}{r'} dr' dz$$

and the quantity rJ_S is constant in any plane ($\theta = \text{const}$) of the conductor cross-section, which results from the assumption that the electric current has only one component θ .

The application of Bubnov–Galerkin method [23] to Eq. (2.7) with a certain basic function (φ) , $(\varphi \in H^1)$ selected in the area Ω gives the basic equation in the form:

$$(2.9) \quad \iint_{\Omega} \left(\nabla A \cdot \nabla \phi + \frac{A}{r^2} \phi + j\omega\mu\gamma A \phi - j\frac{\omega\mu\gamma}{\Delta} \iint_{\Omega_r} A \phi d\Omega - \frac{\mu I}{\Delta} \phi \right) d\Omega = \oint_{\Gamma} \frac{\partial A}{\partial n} \phi d\Gamma.$$

The problem above has been solved by the finite element method with discretization of the examined region into first order tetragonal elements and infinite elements [2].

In the case considered (the ring and the surrounding space, Fig. 1), we have to do with an unbounded region. One of the methods of solving such a problem consists in combining the methods of finite elements and infinite elements. The idea lies in the fact that the region of interest (with sources, heterogeneity and anisotropy of the medium) is discretized into finite elements, whereas the remaining part of the region (far away from the investigated place) is modelled by infinite elements, where the interpolating functions fulfil the differential equation at infinity.

After discretization of the considered finite region into first order tetragonal finite elements, and of the infinite region — into infinite elements, the sought function (A) is approximated by the so-called nodal functions belonging to the elements, i.e.:

$$(2.10) \quad A(x^\alpha) = A_i \varphi_i(x^\alpha), \quad A_{i,\alpha}(x^\alpha) = A_i \varphi_{i,\alpha}(x^\alpha).$$

After substitution of Eq. (2.10) into Eq. (2.9) one obtains the system of equations in the form:

$$(2.11) \quad \sum_i^{N^e} \iint_{\Omega^e} \left(\nabla A \cdot \nabla \varphi_i + \frac{A}{r^2} \varphi_i + j\omega\mu\gamma A \varphi_i - \left(j\frac{\omega\mu\gamma}{\Delta} \iint_{\Omega_r} A d\Omega \right) \varphi_i - \frac{\mu I}{\Delta} \varphi_i \right) d\Omega = \sum_i^{N^b} \oint_{\Gamma^e} \frac{\partial A}{\partial n} \varphi_i d\Gamma,$$

where the region Ω under considerations is divided into N^e finite elements, which implies N^b boundary elements.

The infinite element of Lagrange type [2] has been applied in the paper. Basic functions of infinite elements have been assumed on the grounds of basic functions of the finite elements. The introduction of modifications related to the use of finite elements into the computer programs is easy to carry out. Moreover, the method allows us to keep symmetry and the bandwidth of the coefficient matrix.

The solution of Eq. (2.11) enables us to determine directly the distribution of currents ($\gamma \mathbf{E}$) and magnetic induction (\mathbf{B}) and, indirectly, of power loss density (\dot{Q}) which in strong magnetic fields ($H > 3000\text{A/m}$) (regardless of the magnetic hysteresis) is [8]:

$$(2.12) \quad \dot{Q} = \omega^2 \gamma A A^*.$$

The power loss density (\dot{Q}) results in changing thermal field in conducting materials, which is described by Fourier–Kirchhoff equation.

3. Thermal field

In solid bodies the thermal field is described by the Fourier–Kirchhoff equation:

$$(3.1) \quad \nabla \cdot (\lambda \nabla \Theta) - (\rho c_{\text{ef}}) \frac{\partial \Theta}{\partial t} - (\rho c_{\text{ef}}) \nabla \Theta \cdot \mathbf{v} = -\dot{Q},$$

where c_{ef} is the effective thermal capacity ($c_{\text{ef}} = c_{\text{ef}}(\Theta)$), λ is thermal conductivity coefficient ($\lambda = \lambda(\Theta)$) and ρ is density.

Using the Bubnov–Galerkin method [3, 23] in Eq. (3.1) for the basic function (ϕ) one obtains in the region Ω_c (Fig. 1):

$$(3.2) \quad \int_{\Omega_c} \left(\lambda \partial_\alpha \Theta \partial_\alpha \phi + (\rho c_{\text{ef}}) \frac{\partial \Theta}{\partial t} \phi + (\rho c_{\text{ef}}) \partial_\alpha \Theta v_\alpha \phi - \dot{Q} \phi \right) d\Omega = \int_{\Gamma_c} \lambda \partial_\alpha \Theta \phi n_\alpha d\Gamma - \int_{\Gamma_c} (q + \alpha(\Theta - \Theta_0)) \phi d\Gamma,$$

where (ϕ) is the base function, $q = \lambda \partial_\alpha \Theta n_\alpha$ is the flux for Γ_c , and n_α is the vector normal to Γ_c .

After the discretization of the region under consideration by finite elements, the sought function (Θ) is approximated by the so-called nodal functions belonging to the elements, i.e.:

$$(3.3) \quad \Theta(x^\alpha) = \Theta_i \varphi_i(x^\alpha), \quad \Theta_{,\alpha}(x^\alpha) = \Theta_i \varphi_{i,\alpha}(x^\alpha).$$

The solution $\Theta = \Theta(x^\alpha, t)$ is assumed in the form

$$(3.4) \quad \Theta(x^\alpha, t) = \phi_i(x^\alpha) \Theta_i(t).$$

By substitution of the boundary conditions one obtains:

$$(3.5) \quad \int_{\Omega_c} \left(\lambda \partial_\alpha \Theta \partial_\alpha \phi + (\rho c_{\text{ef}}) \frac{\partial \Theta}{\partial t} \phi + (\rho c_{\text{ef}}) \partial_\alpha \Theta v_\alpha \phi - \dot{Q} \phi \right) d\Omega + \int_{\Gamma_c} \alpha \Theta \phi d\Gamma = \int_{\Gamma_c} \alpha \Theta_0 \phi d\Gamma.$$

The region Ω_c under considerations is divided into N_c^e finite elements, which implies N_c^b boundary elements, and by substituting Eqs. (3.3) to Eq. (3.5) one obtains

$$(3.6) \quad \sum_i^{N_c^e} \int_{\Omega_c^e} \left((\lambda_i \partial_\alpha \phi_j \partial_\alpha \phi_i + (\rho c_{ef}) \partial_\alpha \phi_j v_\alpha \phi_i) \Theta_j + (\rho c_{ef}) \phi_j \frac{\partial \Theta_j}{\partial t} \phi_i \right) d\Omega \\ + \sum_i^{N_c^b} \int_{\Gamma_c^e} \alpha_i \phi_j \phi_i \Theta_j d\Gamma = \sum_i^{N_c^e} \int_{\Omega_c^e} \dot{Q} \phi_i d\Omega + \sum_i^{N_c^b} \int_{\Gamma_c^e} \alpha_i \phi_j \phi_i \Theta_j d\Gamma.$$

The region under consideration has been divided into tetragonal elements with bilinear base functions and approximating functions.

Since the temperature in the mesh nodes is time-dependent (cf. Eq. (3.2)), a certain approximation after a period of time in a certain time space I is assumed. The system of Eqs. (3.6) can be written in the form:

$$(3.7) \quad \mathbb{H}\mathbb{T}^s = \mathbb{D},$$

where

$$(3.8) \quad \mathbb{H} = \vartheta \mathbb{K} + \mathbb{M} + \vartheta \mathbb{B}, \quad \mathbb{D} = (\mathbb{M} - (1 - \vartheta)(\mathbb{K} - \mathbb{B}))\mathbb{T}^{s-1} + \mathbb{B}\mathbb{T}_0^s + \mathbb{O}, \quad \mathbb{T} = \mathbb{T}(\Theta_j), \\ \mathbb{K} = \mathbb{K}(K_{ij}), \quad K_{ij} = \int_{\Omega_c} (\lambda_i \partial_\alpha \varphi_j \partial_\alpha \varphi_i) d\Omega, \\ \mathbb{M} = \mathbb{M}(M_{ij}), \quad M_{ij} = \frac{1}{\Delta t} \int_{\Omega_c} (\rho c_{ef}) \varphi_j \varphi_i d\Omega + \int_{\Omega_c} (\rho c_{ef}) \partial_\alpha \varphi_j v_\alpha \varphi_i d\Omega, \\ (3.9) \quad \mathbb{B} = \mathbb{B}(B_{ij}), \quad B_{ij} = \int_{\Gamma_c} \alpha_i \varphi_i \varphi_j d\Gamma, \\ \mathbb{O} = \mathbb{O}(O_i), \quad O_i = \int_{\Omega_c} \dot{Q} \varphi_i d\Omega,$$

$\Delta t = t^s - t^{s-1}$ is finite increment of time t .

In the solution it is assumed that $\vartheta = 2/3$ (Crank Nicholson scheme [23]).

For the calculation of Eqs. (3.9), the Gauss–Legendre numerical integration method has been used. The solution of Eq. (3.7) yields the sought temperatures in the nodes of the mesh assumed ($\Theta_j = \Theta_j(t)$), at the time $t = s\Delta t$.

4. Numerical simulation of phase transformations in carbon steels

Phase transformations of heating and cooling of carbon steels take place generally in the states of nonequilibrium, i.e. in time periods much shorter than those required for equilibrium transformations. Transformations in the process of cooling are dependent upon the cooling rate and, in the particular case of isothermal transformations, on the temperature and transformation time. The schematic TTT-diagram for steels with content 0.9% wtC has been presented in [24] (Fig. 2 and 3). Volume fractions of the transformed phases are determined by Avrami expression [1, 7]:

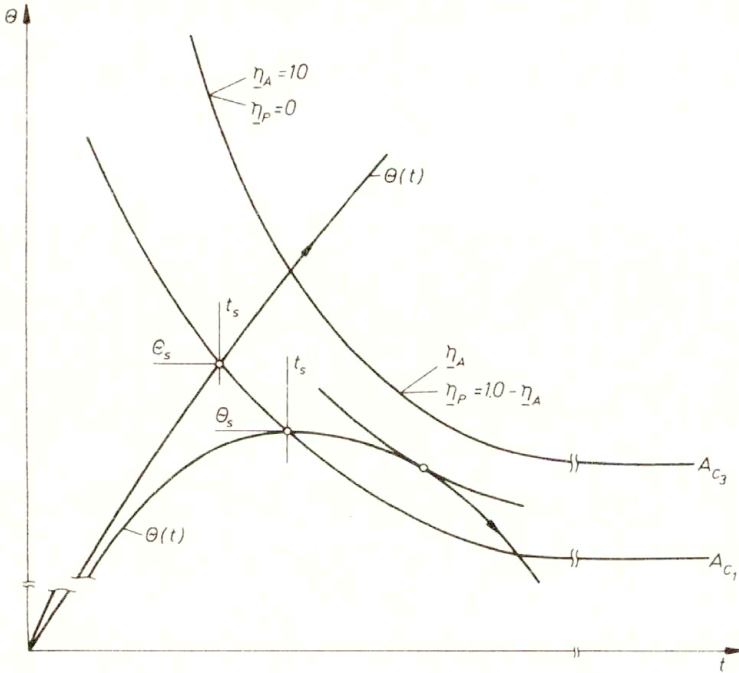


FIG. 2. TTT-heating graph for a carbon steel.

$$\begin{aligned}
 \eta_A(\theta, t) &= 1 - \exp(-b(\theta)t^{n(\theta)}), \\
 \eta_P(\theta, t) &= \eta_A(1 - \exp(-b(\theta)t^{n(\theta)})), \\
 \eta_B(\theta, t) &= \eta_A(1 - \eta_P)(1 - \exp(-b(\theta)t^{n(\theta)})),
 \end{aligned}
 \tag{4.1}$$

in which t is time, whereas $b(\theta)$ and $n(\theta)$ are constants defined by

$$n(\theta) = \frac{\ln\left(\frac{\ln(1 - \eta_f)}{\ln(1 - \eta_s)}\right)}{\ln\left(\frac{t_s}{t_f}\right)}, \quad b(\theta) = \frac{-\ln(1 - \eta_s)}{(t_s)^{n(\theta)}}.
 \tag{4.2}$$

Here $\eta_A, \eta_B, \eta_P (\sum \eta_i = 1)$ are, respectively, the volume fractions of austenite, bainite and pearlite. It is assumed that $\eta_A = 1, \eta_s = 0.01, \eta_f = 0.99$, whereas $t_s = t_s(\theta)$ and $t_f = t_f(\theta)$ are the time of the start and the end of the transformation, respectively:

The volume fraction of martensite is determined on the basis of Koistinen's and Marburger's equations [10, 14] for $\theta < M_s$ (Fig. 3):

$$\eta_M = \eta_A(1 - \eta_B - \eta_P)(1 - \exp(-0.011(M_s - \theta))).
 \tag{4.3}$$

The increment of isotropic strain resulting from the temperature and phase transformations has been determined by considering all possible cases of cooling, i.e.:

a) heating:

$$d\epsilon^{\Theta h} = \begin{cases} \alpha_P d\theta, & \text{for } t < t_s, \\ \eta_A \alpha_A d\theta - \gamma_A d\eta_A + \eta_P \alpha_P d\theta, & \text{for } t \in \langle t_s, t_f \rangle, \\ \alpha_A d\theta, & \text{for } t > t_f, \end{cases}
 \tag{4.4}$$

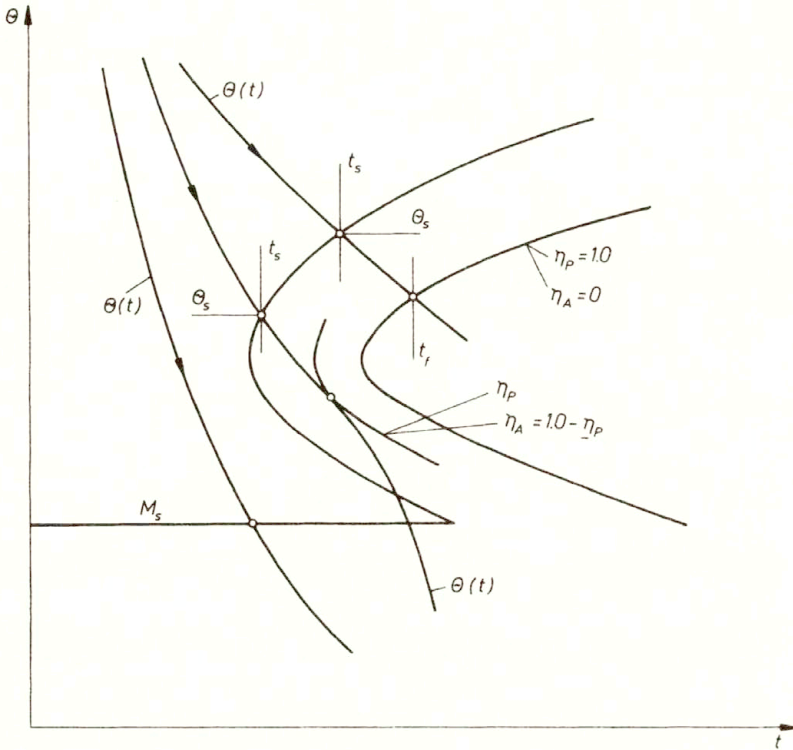


FIG. 3. TTT-cooling graph for a carbon steel.

where $\eta_P = 1 - \eta_A$;

b) cooling:

$$(4.5) \quad de^{\Theta h} = \begin{cases} \eta_A \alpha_A d\Theta + \eta_P \alpha_P d\Theta, & \text{for } t < t_s, \\ \eta_A \alpha_A d\Theta + \eta_B \alpha_B d\Theta + \gamma_B d\eta_B + \eta_P \alpha_P d\Theta + \gamma_P d\eta_P, & \text{for } t \in \langle t_s, t_f \rangle, \\ \eta_A \alpha_A d\Theta + \eta_B \alpha_B d\Theta + \eta_M \alpha_M d\Theta + \gamma_M d\eta_M + \eta_P \alpha_P d\Theta, & \text{for } t \geq t_s^M, \end{cases}$$

where

$$\eta_A = 1 - \eta_B - \eta_P - \eta_M, \quad \alpha_A = \alpha_A(\Theta), \quad \alpha_B = \alpha_B(\Theta), \quad \alpha_M = \alpha_M(\Theta), \\ \alpha_P = \alpha_P(\Theta)$$

are coefficients of linear thermal expansion for austenite, bainite, martensite and pearlite, respectively, $\gamma_B = \gamma_B(\Theta)$, $\gamma_M = \gamma_M(\Theta)$, $\gamma_P = \gamma_P(\Theta)$ are coefficients of phase transformations of austenite into bainite, austenite into martensite and austenite into pearlite, respectively.

In order to confirm the correctness of the assumed model of phase transformations, dilatometric tests on simulator of heat cycles for steel of chemical composition, 0.89% C, 0.30% Mn, 0.29% Si, 0.014% P, 0.012% S have been performed. Very good compatibility of results obtained from the dilatation calculations by means of expressions (4.4)–(4.5) confirms the correctness of the model assumed (Fig. 4). For the dilatation calculations

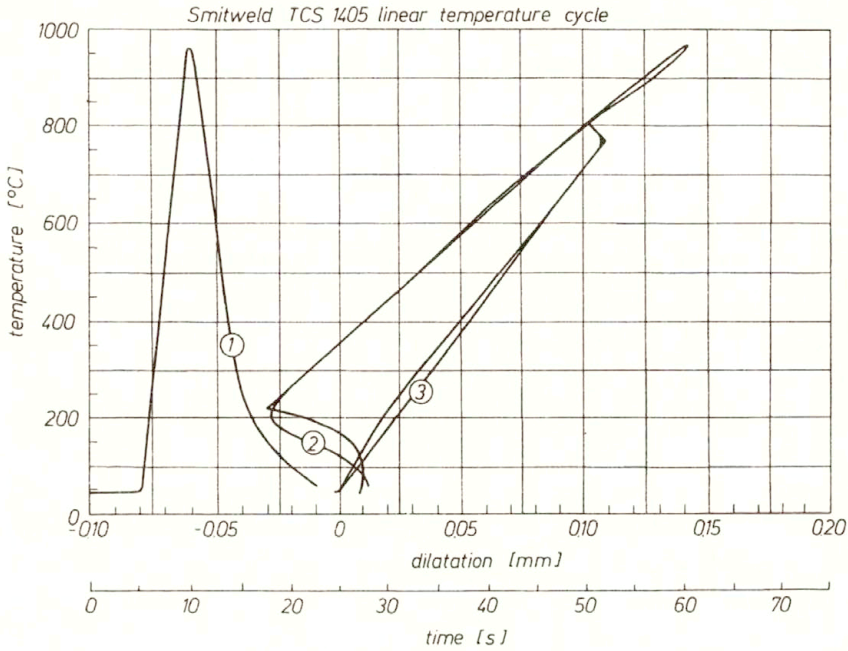


FIG. 4. Temperature (1) and dilatometric curves obtained from dilatometric tests (2) and calculations (3).

the value of coefficients of linear expansion ($\alpha_{(t)}$) and volume change ($\gamma_{(t)}$) have been obtained from dilatometric test. They are as follows:

$$\alpha_A = 21 \cdot 10^{-6}, \quad \alpha_B = \alpha_M = \alpha_P = 13.8 \cdot 10^{-6} [1/K], \quad \gamma_B = \gamma_P = 0.0012, \\ \gamma_M = 0.0084.$$

5. Mathematical model of elasto-plastic states in hardening steel elements

The constitutive relations for elastic range of strain are assumed in the classical form:

$$(5.1) \quad \dot{\mathbf{T}} = \mathbf{E} \circ \dot{\mathbf{e}}^e + \dot{\mathbf{E}} \circ \mathbf{e}^e, \quad \mathbf{e}^e = \mathbf{e} - \mathbf{e}^p - \mathbf{e}^\Theta,$$

where $\mathbf{T} = \mathbf{T}(\sigma^{\alpha\beta})$ is the tensor of stresses, $\mathbf{E} = \mathbf{E}(E^{\alpha\beta\gamma\mu}(\Theta))$ is the tensor of material constants, $\mathbf{e}^e = \mathbf{e}(\varepsilon_{\alpha\beta}^e)$ is the tensor of elastic strains, $\mathbf{e} = \mathbf{e}(\varepsilon_{\alpha\beta})$ is the tensor of total strains ($\mathbf{e} = \frac{1}{2}(\nabla \mathbf{u} + \nabla \mathbf{u}^T)$), $\mathbf{e}^\Theta = \mathbf{e}(\varepsilon_{\alpha\beta}^{\Theta H})$ is the tensor of dilatational strains and $\mathbf{e}^p = \mathbf{e}(\varepsilon_{\alpha\beta}^p)$ is the tensor of plastic strains.

The equilibrium equations are expressed in terms of stress rates (disregarding the mass forces)

$$(5.2) \quad \nabla_\beta \dot{\sigma}^{\alpha\beta} = 0, \quad \dot{\sigma}^{\alpha\beta} = \dot{\sigma}^{\beta\alpha}, \quad \dot{\sigma}^{\alpha\beta} n_\beta = \dot{i}^\alpha,$$

where \dot{i}^α is the rate of surface tractions on the Γ_c (Fig. 1).

The authors have assumed the model of non-isothermal plastic flow in which the plastic strain rate $\dot{\mathbf{e}}^p$ is expressed by relationship [12, 13, 20]:

$$(5.3) \quad \dot{\mathbf{e}}^p = \lambda \frac{\partial \mathbf{f}}{\partial \mathbf{T}}, \quad \dot{f} = 0, \quad f = 0,$$

where f is the yield function.

In what follows we shall use the Huber–Mises yield condition and the model of isotropic hardening. Thus,

$$(5.4) \quad f = \left(\frac{3}{2} \mathbf{D} \cdot \mathbf{D} \right)^{1/2} - Y(\Theta, \varepsilon_{\text{ef}}^p) = 0,$$

where \mathbf{D} is the deviator of stress tensor, $\varepsilon_{\text{ef}}^p$ is effective plastic strain ($\varepsilon_{\text{ef}}^p = (2(\dot{\mathbf{e}}^p \cdot \dot{\mathbf{e}}^p)/3)^{1/2}$) and $Y = Y(\Theta, \eta, \varepsilon_{\text{ef}}^p)$ is the actual level of effective stress ($D_{\text{ef}} = (3(\mathbf{D} \cdot \mathbf{D})/2)^{1/2}$) corresponding to point lying on the simple (uniaxial) tension (or compression) curve.

Using the consistency equation $\dot{f} = 0$ one gets the following expression for the multiplier $\dot{\lambda}$ (cf. [3, 12, 13, 20])

$$(5.5) \quad \dot{\lambda} = 2Y \frac{3\mathbf{D} \cdot \dot{\mathbf{T}}^* - 2Y Y_{\Theta} \dot{\Theta}}{9\mathbf{D} \circ \mathbf{E} \circ \mathbf{D} + 4Y^2 \kappa},$$

where

$$\dot{\mathbf{T}}^* = \mathbf{E} \circ (\dot{\mathbf{e}} - \dot{\mathbf{e}}^{\ominus}) + \mathbf{E} \circ \mathbf{e}^e, \quad \kappa = \partial Y / \partial \varepsilon_{\text{ef}}^p, \quad Y_{\Theta} = \partial Y / \partial \Theta.$$

This problem has been solved by the finite element method.

By applying the Bubnov–Galerkin method for equilibrium equations (5.2), one obtains

$$(5.6) \quad \int_{\Omega_c} \sigma^{\alpha\beta} \partial_{\beta} \varphi d\Omega = \int_{\Gamma_c} i_{*}^{\alpha} \varphi d\Gamma,$$

where i_{*}^{α} is the known stress vector on Γ_c .

After substituting constitutive relations (5.1) (specified for axially-symmetrical problem) into (5.6) and discretizing the region considered by means of finite elements, where the unknown functions (\mathbf{u} and \mathbf{v}) are approximated by the so-called nodal functions assigned to elements [3, 12, 23]

$$(5.7) \quad \mathbf{u}(x^{\alpha}) = \mathbf{u}_i \varphi_i(x^{\alpha}), \quad \mathbf{u}_{,\alpha}(x^{\alpha}) = \mathbf{u}_i \varphi_{i,\alpha}(x^{\alpha}),$$

one gets the system of equations in the form:

$$(5.8) \quad \mathbf{K}\dot{\mathbf{U}} = \dot{\mathbf{R}} + \sum_{e=1}^{N^e} \left(\int_{\Omega_c^e} \Phi \circ \mathbf{E} \circ \dot{\mathbf{e}}^{\ominus} d\Omega + \int_{\Omega_c^e} \Phi^T \circ \mathbf{E} \circ \sum_i \delta^i \dot{\mathbf{e}}^p d\Omega + \int_{\Omega_c^e} \Phi \circ \dot{\mathbf{E}} \circ \mathbf{e}^e d\Omega \right),$$

where \mathbf{U} is the vector of displacements, \mathbf{R} is the vector of external loads, \mathbf{K} is the matrix of stiffness, Φ is the matrix of corresponding derivatives of the approximating function, ϕ , ($\phi = \phi(\varphi, \alpha)$) and φ is the vector of approximating functions (cf. (3.4)).

The solution of system of Eqs. (5.8) yields the displacement rates resulting from the increment of thermal and mechanical loads and phase transformations, namely the stress tensor $\dot{\mathbf{T}}^{\ominus p}$. The problem has been solved by means of the implicit scheme, and the total stresses at this stage of solution are equal to

$$(5.9) \quad \mathbf{T}^{\ominus p}(t + \Delta t) = (1 - \vartheta) \mathbf{T}^{\ominus p}(t) + \vartheta \left(\mathbf{T}^{\ominus p}(t) + \left(\dot{\mathbf{T}}^{\ominus}(\Delta t) + \sum_{k=1}^{i-1} \delta^i \dot{\mathbf{T}}_k^p(\Delta t) \right) \Delta t \right).$$

Parameter ϑ has been assumed to be equal to 0.5. In this solution the modified Newton–Raphson algorithm [12, 20] is used.

6. Calculation example

The exemplary calculations have been made for a hardened shaft made of steel of the chemical composition identical to that of the dilatometric sample. The longitudinal section of the system under consideration is presented in Fig. 5.

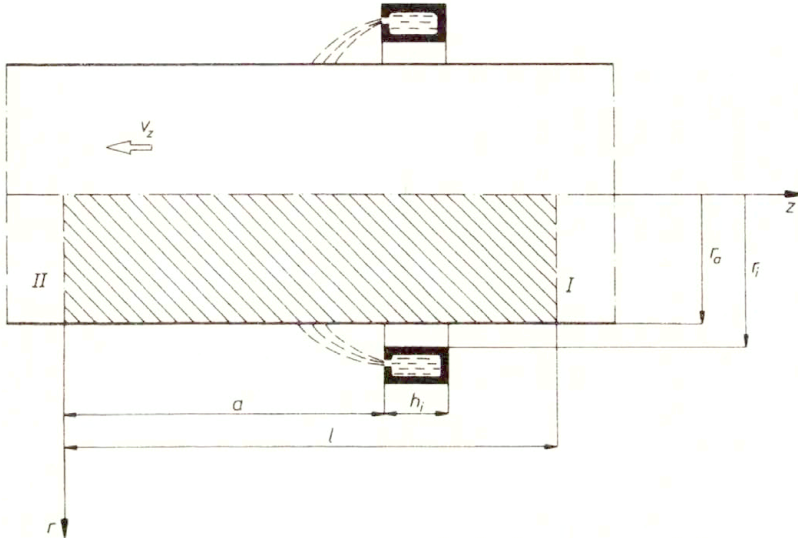


FIG. 5. Longitudinal section of the investigated region.

The following boundary conditions are assumed:

For the electromagnetic field:

- $A = 0$ on the symmetry axis,
- $A = 0$ for $y \rightarrow \infty$ or $r \rightarrow \infty$.

For the thermal field:

- $\lambda \frac{\partial \Theta}{\partial r} = -\alpha(\Theta - \Theta_0)$ on the external surface of the bar,
 $\alpha = \alpha_0(\Theta - \Theta_0)^{1/3}$,
- $\frac{\partial \Theta}{\partial r} = 0$ on the axis of symmetry,
- $\Theta = \Theta_0$ on the surface I,
- $\frac{\partial \Theta}{\partial z} = 0$ on the surface II.

For the stress field:

- zero stress vector on the external surface of the object has been assumed.

The following parameters have been assumed in the calculations

$$a = 0.098, \quad h_i = 0.012, \quad l = 0.160, \quad r_a = 0.0225, \quad r_i = 0.025 \text{ [m]}, \\ f = 10000 \text{ [Hz]}, \quad v = 0.004 \text{ [m/s]}, \quad \alpha_0 = 800 \text{ [W/(m}^2\text{K}^{4/3})], \quad \Theta_0 = 300 \text{ [K]}.$$

Specific heat, electrical and thermal conductivity of the steel are the functions of temperature which have been determined according to [11, 24]. Young's modulus and hardening modulus are the functions of temperature and structural contents which have been determined according to the suggestions by MELANDER [11, 16].

The power density distribution has been obtained from Eq. (2.12) by solving the Eq. (2.11). It made it possible to calculate the thermal field of the bar on the basis of Eq. (3.1) (Fig. 6).

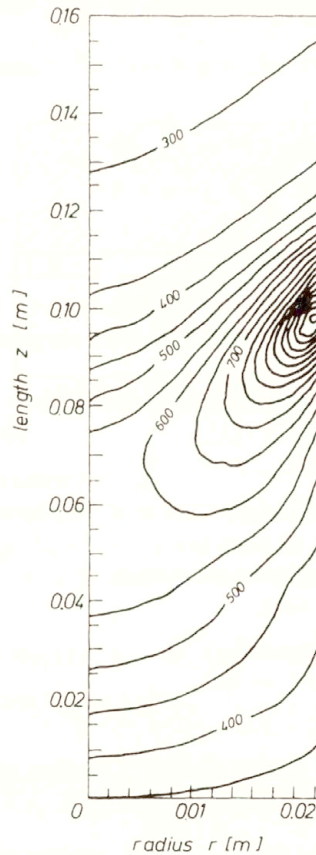


FIG. 6. Temperature field in hardened bar.

The kinetics of the austenite-martensite transformation for the bar area is shown in Fig. 7. The calculation of kinetics of austenite-pearlite and austenite-martensite transformations in the cooling process have been made only for the area where the pearlite-austenite transformation had occurred earlier. The final phase content after hardening is presented in Fig. 8. A portion of the bar (slice) contained between two parallel planes perpendicular to the z -axis have been considered in the stress calculation. It has been assumed that at fixed time the temperature changes only along the radius ($\theta = \theta(r)$). The obtained solution fulfils the conditions of the plane strain state with the force normal to the z -axis direction equal to zero. The calculations of the effect of martensite contents upon the yield point have also been made.

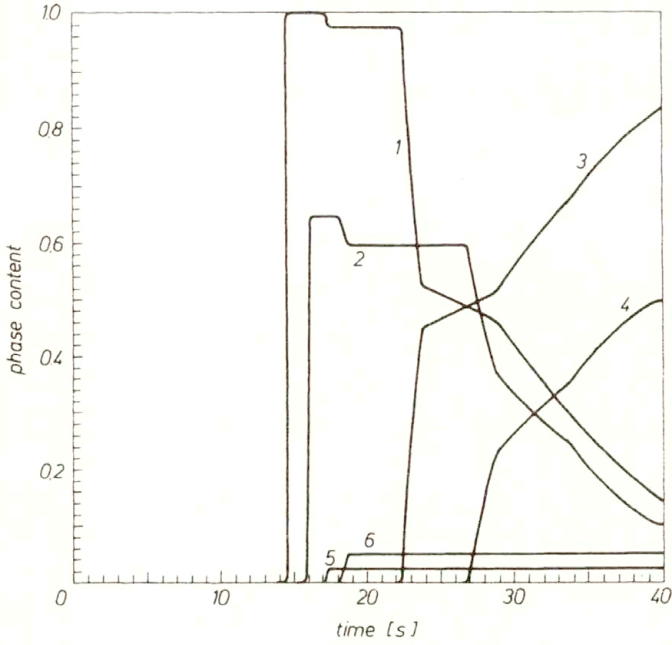


FIG. 7. Kinetics of phase transformation during the progressive induction hardening process. 1 — austenite — on surface, 2 — austenite — depth = 3 mm, 3 — martensite — on surface, 4 — martensite — depth = 3 mm, 5 — pearlite + bainite — on surface, 6 — pearlite + bainite — depth = 3 mm.

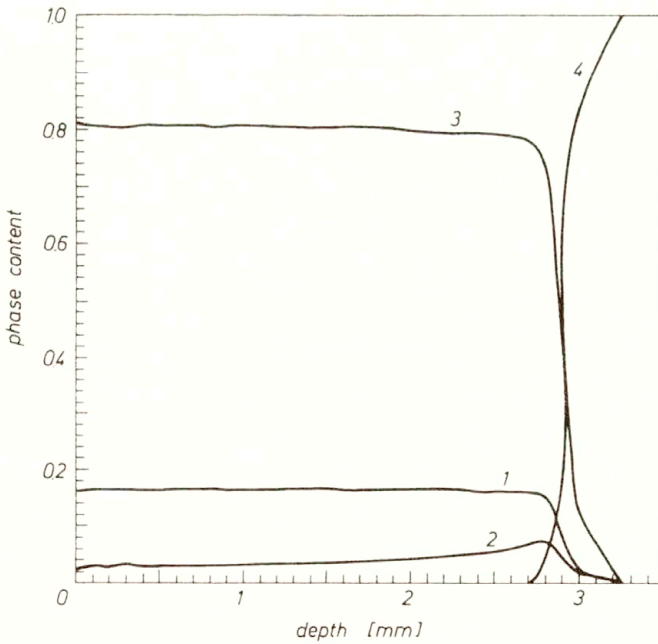
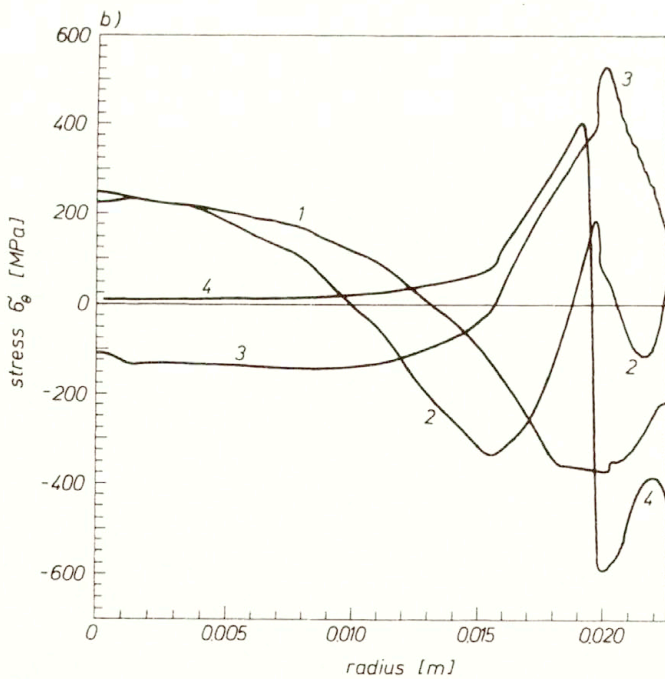
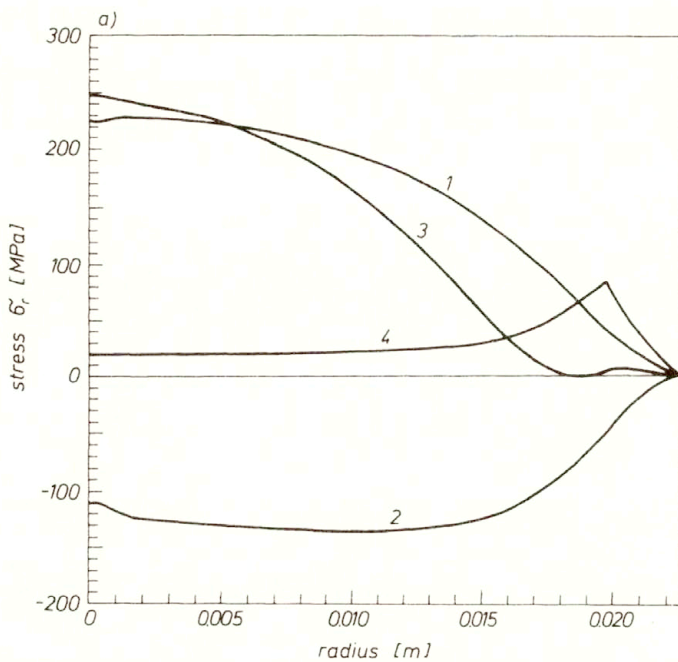


FIG. 8. Volume fractions of particular phase after hardening process. 1 — retained austenite, 2 — pearlite + bainite, 3 — martensite, 4 — non-transformed pearlite.



[Fig. 9.]

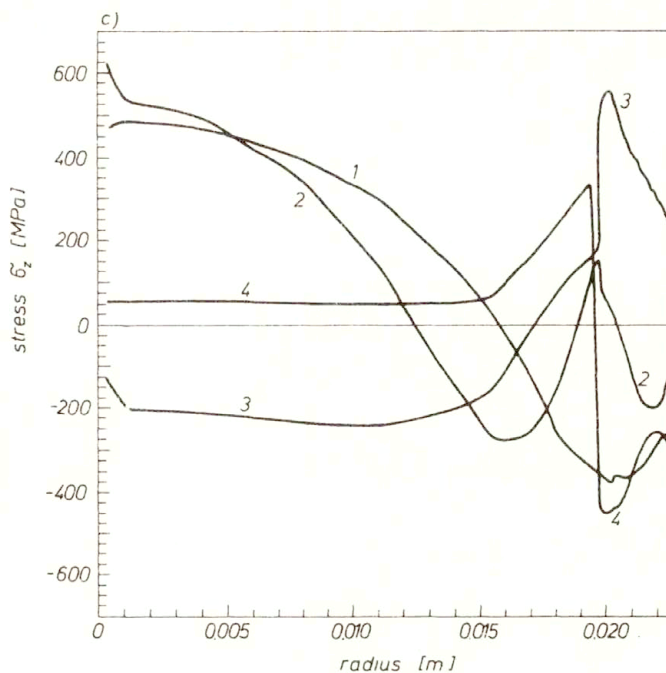


FIG. 9. Kinetics of stress components during the hardening process. a) σ_r component: 1 — $z = 0.128$ m, 2 — $z = 0.120$ m, 3 — $z = 0.100$ m, 4 — $z = 0.000$ m; b) σ_ϕ component: 1 — $z = 0.128$ m, 2 — $z = 0.120$ m, 3 — $z = 0.100$ m, 4 — $z = 0.000$ m; c) σ_z component: 1 — $z = 0.128$ m, 2 — $z = 0.120$ m, 3 — $z = 0.100$ m, 4 — $z = 0.000$ m.

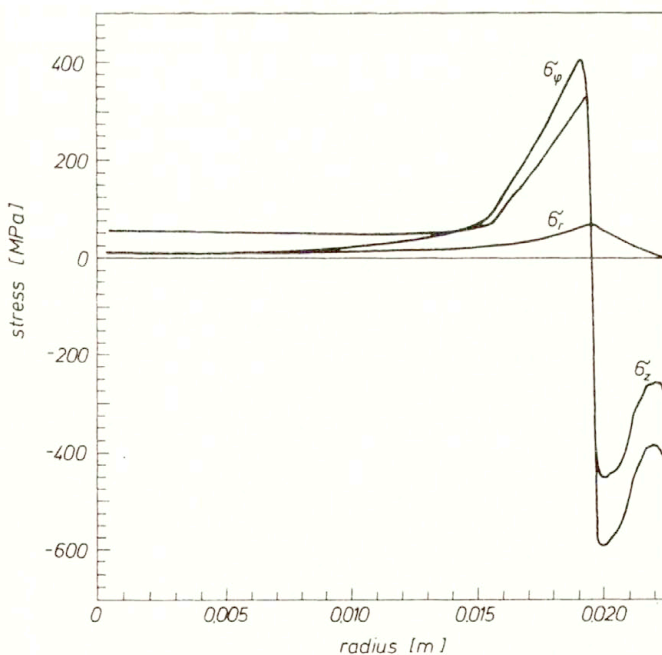


FIG. 10. Residual stresses after the hardening process.

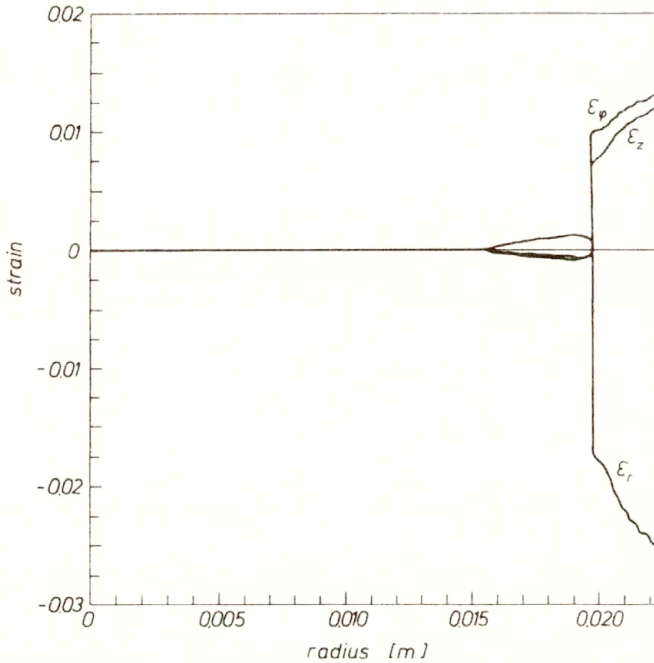


FIG. 11. Residual strains after the hardening process.

The obtained numerical simulation results of stresses and strains are presented in Figs. 9–11. The transient and residual stresses calculated on the basis of the proposed model have been presented as functions of the radius in Figs. 9 and 10. The plastic strains have been presented in Fig. 11.

7. Conclusions

The model has been presented taking into account the coupling of electromagnetic and thermal field, and the influence of thermal field and phase transformations on the stresses, thus enabling the calculation of the thermal fields, the volume fractions of the particular phases, instantaneous and residual stress states and hardening zones in the process of progressive induction hardening of steel elements.

The correctness of the assumed model of phase transformations has been confirmed by dilatometric test, leading to a very good compatibility of results. The result of the induction hardening process is the material hardening and a desirable distribution of residual stresses in the hardened zone.

Acknowledgement

The paper is supported by the Research Committee, KBN Project No 3 1014 91 91 on „Thermomechanics of damage and phase transformation in materials”.

References

1. M. AVRAMI, *Kinetics of phase change*, J. Chemical Phys., I., 7, 1103–1112, Dec. 1939; II. 8, 212–224, Feb. 1940; III. 9, 117–184, Feb. 1941.
2. P. BETTESS, *More on infinite elements*, Int. J. for Num. Meth. in Engng., 15, 1613–1626, 1980.
3. A. BOKOTA, S. ISKIERKA and R. PARKITNY, *Computer simulation of surface induction hardening of steel cylindrical components*, I.I.T.T. Congress, Oct. 7–8, Paris 1991; Technology Transfer Series, A. NIKU-LARI [Ed.], pp. 141–146, 1991.
4. Y. DEASALOS, J. GIUSTI and R. LOMBRY, *Contraintes de trempe superficielle par induction H.F. dans un barreau cylindrique*, Rev. Gen. Therm., No 284–285, 673–679, 1985.
5. A.J. FLETCHER, *Thermal stress and strain generation in heat treatment*, Elsevier, London 1989.
6. A.J. FLETCHER and R.F. PRICE, *Generation of thermal stress and strain during quenching of low-alloy steel plates*, Metals Technology, 427–446, Nov. 1981.
7. B. HINDENWALL, *Prediction of residual stresses created during quenching. Especially the quench response in carburized steel*, Linköping Studies in Science and Technology, Dissertation No 39, Linköping 1979.
8. S.R.H. HOOLE, *Computer-aided analysis and design of electromagnetic devices*, Elsevier, New York, Amsterdam, London 1989.
9. T. INOUE, S. NAGAKI, T. KISHINO and M. MONKAWA, *Description of transformation kinetics, heat conduction and elastic-plastic stress in the course of quenching and tempering of some steels*, Ingenieur-Archiv, 50, 315–327, 1981.
10. T. INOUE and B. RANIECKI, *Determination of thermal-hardening stress in steels by use of thermoplasticity theory*, J. Mech. and Phys. of Solids, 26, 3, 187–212, 1978.
11. B. JANSSON, M. ROLFSON, A. THUVANDER, A. MELANDER and C. WULLIMANN, *Calculation of microstructure and hardness of hot-rolled bars*, Materials Science and Technology, 7, 118–127, Feb. 1991.
12. M. KLEIBER and T. NIEZGODA, *Numerical analysis of thermo-elasto-plastic problems*, Engng. Trans., 36, 4, 645–660, 1988.
13. M. KLEIBER and B. RANIECKI, *Elastic-plastic materials at finite strains*, In: Plasticity Today. Modelling, Methods and Applications, A. SAWCZUK and G. BINACCHI [Eds.], Elsevier, pp. 3–46, 1985.
14. D.P. KOISTINEN and R.E. MARBURGER, *A general equation prescribing the extent of the austenite-martensite transformation in pure iron-carbon alloys and plain carbon steels*, Acta Metallurgica, 7, 59–60, 1959.
15. A. KONRAD, *Integrodifferential finite element formulation of two-dimensional steady-state skin effect problems*, IEEE Trans. on Mag., MAG-18, 1, 284–292, 1982.
16. M.A. MELANDER, *Computational and experimental investigation of induction and laser hardening*, Linköping Studies in Science and Technology, Dissertation No 124, Linköping 1985.
17. G. ORTH, *Berechnung des Temperaturfeldes bei der induktiven Vorschubhärtung und Vorausbestimmung der Härte*, Elektrowärme International, 46, B4, 180–188, August 1988.
18. B. RANIECKI, *Thermodynamic reference model for elastic-plastic solids undergoing phase transformations*, Arch. Mech., 43, 2–3, 343–376, 1991.
19. W. SEIDEL and H. UETZ, *Rechnerische Vorausbestimmung des Härteergebnisses bei der Induktionshärtung*, Harterei-Technische Mitteilungen, 37, 5, 211–262, Sept.ct. 1982.
20. M.D. SNYDER and K.J. BATHE, *A solution procedure for thermo-elastic-plastic and creep problems*, Nuclear Engng. and Design, 64, 49–80, 1981.
21. K. TANAKA, R. IWASAKI and S. NAGAKI, *On T-T and C-C-T diagrams of steels: a phenomenological approach to transformation kinetics*, Ingenieur-Archiv, 54, 81–90, 1984.
22. K. TANAKA, R. IWASAKI and Y. SATO, *Analysis of transformation superelastic deformation in pure iron*, Ingenieur-Archiv, 54, 309–320, 1984.
23. R. WAIT and A.R. MITCHELL, *Finite element analysis and applications*, J. Wiley and sons, Chichester 1985.
24. *Characteristics of steel. Tool steels* [in Polish], Silesia, Katowice 1987.

CZEŹOCHOWA UNIVERSITY OF TECHNOLOGY
INSTITUTE OF MECHANICS AND MACHINE DESIGN, CZEŹOCHOWA.

CZEŹOCHOWA UNIVERSITY OF TECHNOLOGY
ELECTRICAL DEPARTMENT, CZEŹOCHOWA
and
POLISH ACADEMY OF SCIENCES
INSTITUTE OF FUNDAMENTAL TECHNOLOGICAL RESEARCH.

Received January 3, 1994.

Elastic-plastic shells with finite deformations and contact treatment

A. FLOSS and V. ULBRICHT (DRESDEN)

THE PRESENTED theory of shells is developed from the basic equations of the theory of continua in material description. The basic equations are set up in a rate form, in accordance with the constitutive theory. The constitutive equations are expressed in form of a linear tensor relation between the Truesdell stress rate and deformation rate, with related equations of evolution. The variational principle of the shell in a rate form is presented. As a consequence of the included contact problem, additional requirements concerning the solution and the virtual velocities of the variational principle arise. The penalty method is applied to the treatment of the contact problem. The penalty term is set up in a rate form, the rate of the contact load is determined as a function of the velocities of the shell and the body in contact. The applicability of this theory is illustrated by a one-dimensional field problem of shells of revolution.

1. Introduction

THE PRESENTED THEORY is developed from the basic equations of the theory of continua in material description. The basic equations are set up in a rate form in accordance with the constitutive theory. The constitutive equations are expressed in the form of a linear tensor relation between the Truesdell stress rate and the deformation rate, with related evolutionary equations. The kinematics of the considered shell continuum is based on a deformation model characterized by the normal hypothesis. The variational principle of the shell in a rate form is presented.

As a consequence of the included contact problem, additional requirements concerning the solution and the virtual velocities of the variational principle arise. The penalty method is applied to the treatment of the contact problem. The penalty term is set up in a rate form, the rate of the contact load is determined as a function of the velocities of the shell and the body in contact. The applicability of this theory is illustrated by the one-dimensional field problem of shells of revolution.

2. Basic equations

In the material description, the independent variables are the time-independent parameters Θ^λ of the material particles in a convective coordinate system and the time t . The shape of the parametric lines, the base vector system and the metric depend on space and time.

All variables are referred to the base vectors of the actual configuration

$$(2.1) \quad \mathbf{g}_\lambda = \frac{\partial \mathbf{x}}{\partial \Theta^\lambda} = \mathbf{x}_{,\lambda} = \mathbf{g}_\lambda(\Theta^\mu, t), \quad \lambda = 1, 2, 3,$$

where

$$(2.2) \quad \mathbf{x} = x^k(\theta^\lambda, t)\mathbf{e}_k$$

is the position vector of the material particle of time t . This includes the reference configuration $\overset{\circ}{\mathbf{x}}$ of time $t = 0$, which is only needed for the definition of the displacement vector

$$(2.3) \quad \mathbf{u} = \mathbf{x} - \overset{\circ}{\mathbf{x}} = \mathbf{u}(\Theta^\lambda, t)$$

and the strain tensor

$$(2.4) \quad \varepsilon_{\lambda\mu} = \frac{1}{2}(u_{\lambda|\mu} + u_{\mu|\lambda} - u_{\nu|\lambda}u^\nu{}_{|\mu}).$$

The velocity vector is the material time derivative of the position vector

$$(2.5) \quad \boldsymbol{\nu} = \dot{\mathbf{u}} = \frac{D}{Dt}(u^\lambda \mathbf{g}_\lambda) = \dot{\mathbf{x}}.$$

In the material description, there are linear relations, first between the rate of deformation and the gradient of the velocity, and second — between the rate of deformation and the strain rate:

$$(2.6) \quad d_{\lambda\mu} = \frac{1}{2}(\nu_{\mu|\lambda} + \nu_{\lambda|\mu}) = \dot{\varepsilon}_{\lambda\mu}.$$

For the rate formulation of the field problem, the equations of equilibrium in the rate form

$$(2.7) \quad \dot{G}^{\lambda\mu} = t^{\lambda\mu}{}_{|\lambda} - \nu^\kappa{}_{|\kappa} \sigma^{\lambda\mu}{}_{|\lambda} + \sigma^{\lambda\kappa} \nu^{\mu}{}_{|\kappa\lambda} + \rho(\dot{f}^\mu - \nu^\kappa{}_{|\kappa} f^\mu) = 0 \quad \text{in } V$$

are needed, where $\sigma^{\lambda\mu}$ is the Cauchy stress tensor, and $t^{\lambda\mu}$ is the Truesdell stress rate.

Combining the equations of equilibrium written in rate form with the virtual velocity $\delta\nu$ we obtain the variational principle in a rate form

$$(2.8) \quad \delta II_i - \delta II_a = 0,$$

with

$$\delta II_i = \int_V (t^{\lambda\mu} \delta d_{\lambda\mu} + \sigma^{\lambda\kappa} g^{\mu\nu} \nu_{\nu|\kappa} \delta \nu_{\mu|\lambda}) dV$$

and

$$\delta II_a = \int_{O_p} \frac{D}{Dt}(\mathbf{p} dA) \delta \nu + \int_V \rho \dot{\mathbf{f}} \delta \nu dV.$$

The term δII_i characterizes the deformation behaviour of the continuum, and the term δII_a is due to the surface forces \mathbf{p} and the body forces \mathbf{f} .

The constitutive equations are introduced in the form of a linear tensor relation between the Truesdell stress rate and the rate of deformation, with related equations of evolution for the set of internal state variables [1]:

$$(2.9) \quad \begin{aligned} t^{\kappa\lambda} &= C^{\kappa\lambda\mu\nu} d_{\mu\nu} + s^{\kappa\lambda}, & s^{\kappa\lambda} &= s_T^{\kappa\lambda} \dot{T} + s_R^{\kappa\lambda}, \\ \dot{h}_{(i)} &= B_{(i)}^{\mu\nu} d_{\mu\nu} + e_{(i)}, & e_{(i)} &= e_{T(i)} \dot{T} + e_{R(i)}, \quad i = 1, \dots, N. \end{aligned}$$

The tensors $C^{\kappa\lambda\mu\nu}$ and $B_{(i)}^{\mu\nu}$ describe time-independent, that is elastic as well as elastic-plastic material behaviour, $s_T^{\kappa\lambda}$ and $e_{T(i)}$ take into account the dependence of temperature, and $s_R^{\kappa\lambda}$ and $e_{R(i)}$ — such rheological effects as viscoelasticity and viscoplasticity.

If the symmetry conditions

$$(2.10) \quad C^{\kappa\lambda\mu\nu} = C^{\mu\nu\kappa\lambda}$$

are satisfied, the potential

$$(2.11) \quad \Pi_D^* = \frac{1}{2} C^{\kappa\lambda\mu\nu} d_{\kappa\lambda} d_{\mu\nu} + s^{\kappa\lambda} d_{\kappa\lambda}$$

exists and we can formulate a potential for the internal parts of the variational principle

$$(2.12) \quad \delta \Pi_i = \delta(\Pi_f), \quad \Pi_f = \int_V \left(\Pi_D^* + \frac{1}{2} \sigma^{\lambda\kappa} g^{\mu\nu} \nu_\mu |_{\lambda} \nu_\nu |_{\kappa} \right) dV.$$

3. Shell theory

The kinematics of the considered shell continuum is based on a deformation model characterized by the normal hypothesis. The kinematic relations are a special case of the general assumptions of continuum mechanics.

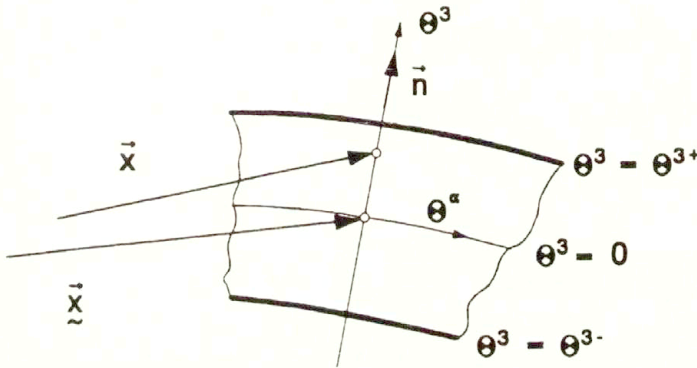


FIG. 1. Position vector of the shell continuum.

The position vector (Fig. 1) is assumed in the form

$$(3.1) \quad \mathbf{x} = \underline{\mathbf{x}}(\Theta^\alpha, t) + \Theta^3 h(\Theta^\alpha, t) \mathbf{n}(\Theta^\alpha, t) = \underline{\mathbf{x}}(\Theta^\lambda, t),$$

where $\underline{\mathbf{x}}$ is the position vector of the reference surface, \mathbf{n} is the normal vector and h is the shell thickness.

The base vectors and the normal vector of the shell are given by

$$(3.2) \quad \mathbf{a}_{\alpha} = \underline{\mathbf{x}}_{,\alpha} \quad \text{and} \quad \mathbf{n} = \frac{\mathbf{a}_1 \times \mathbf{a}_2}{|\mathbf{a}_1 \times \mathbf{a}_2|} = \frac{1}{\sqrt{a}} (\mathbf{a}_1 \times \mathbf{a}_2).$$

The time derivative of the position vector (3.1) yields the velocity vector

$$(3.3) \quad \mathbf{v} = \underline{\mathbf{v}} + \Theta^3 h \left(\boldsymbol{\omega} + \frac{\dot{h}}{h} \mathbf{n} \right).$$

The kinematical variables of the shell theory are the rate of displacement $\underline{\mathbf{v}}$ of the reference surface and the velocity $\boldsymbol{\omega}$ of the normal vector.

As a consequence of the normal hypothesis, we get the following kinematic constraint for $\underline{\mathbf{v}}$ and $\boldsymbol{\omega}$:

$$(3.4) \quad \frac{D}{Dt} (\mathbf{a}_\alpha \mathbf{n}) = 0 = \underline{\mathbf{v}}_{,\alpha} \mathbf{n} + \mathbf{a}_{\alpha} \boldsymbol{\omega} = \nu_3 |_{\alpha} + \omega_\alpha.$$

In rate of deformation, inessential terms in the derivative of the shell thickness are neglected:

$$(3.5) \quad \begin{aligned} d_{\alpha\beta} &= \frac{1}{2}(S_{\alpha}^{\gamma}\delta_{\beta}^{\delta} + S_{\beta}^{\gamma}\delta_{\alpha}^{\delta})(d_{\gamma\delta} + \Theta^3 d_{\gamma\delta}), \\ d_{\alpha 3} &= 0, \quad d_{33} = \dot{h}h, \end{aligned}$$

with

$$d_{\gamma\delta} = \mathbf{a}_{\gamma}\underline{\nu}_{,\delta} = \underline{\nu}_{\gamma}\|_{\delta} - \nu_3 b_{\gamma\delta}, \quad d_{\gamma\delta} = h\mathbf{a}_{\gamma}\boldsymbol{\omega}_{,\delta},$$

and

$$S_{\alpha}^{\beta} = \delta_{\alpha}^{\beta} - \Theta^3 h b_{\alpha}^{\beta}.$$

Variables $d_{\alpha\beta}$ and $d_{\gamma\delta}$ are the first and the second deformation rates of the shell continuum.

The variational principle in the rate form for the shell results from the variational principle of the continuum (2.8), by integrating over Θ^3 and eliminating the static variables, which are not admissible in a two-dimensional theory [2]:

$$(3.6) \quad \begin{aligned} \delta\Pi_i + \delta\Pi_n - \delta\Pi_a &= 0, \\ \delta\Pi_i &= \int_M \left\{ \dot{\mathbf{n}}^{\alpha\beta}\delta d_{\beta\alpha} + \dot{\mathbf{m}}^{\alpha\beta}\delta d_{\beta\alpha} + q^{\alpha}(\omega^{\beta}\delta\underline{\nu}_{\beta}\|_{\alpha} + \underline{\nu}_{\beta}\|_{\alpha}\delta\omega^{\beta}) \right. \\ &\quad \left. + n^{\alpha\gamma}\underline{\nu}_3\|_{\gamma}\delta\underline{\nu}_3\|_{\alpha} + m^{\gamma\delta}b_{\delta\gamma}h\omega^{\alpha}\delta\omega_{\alpha} + m^{\alpha\gamma}b_{\alpha}^{\beta}\underline{\nu}_3\|_{\gamma}\delta\omega_{\beta} \right\} dA, \\ \delta\Pi_a &= \int_M \left\{ \frac{1}{\sqrt{a}} \frac{D}{Dt}(\sqrt{a}\mathbf{P})\delta\underline{\nu} + \frac{1}{\sqrt{a}} \frac{D}{Dt}(\sqrt{a}h\mathbf{S})\delta\boldsymbol{\omega} \right\} dA \\ &\quad + \int_C \left\{ \frac{1}{\sqrt{c}} \frac{D}{Dt}(\sqrt{c}\mathbf{N})\delta\underline{\nu} + \frac{1}{\sqrt{c}} \frac{D}{Dt}(\sqrt{c}h\mathbf{M})\delta\boldsymbol{\omega} \right\} ds. \end{aligned}$$

The stress resultants $n^{\alpha\beta}$ and $m^{\alpha\beta}$ and their objective time derivatives $\dot{\mathbf{n}}^{\alpha\beta}$ and $\dot{\mathbf{m}}^{\alpha\beta}$ are defined by

$$(3.7) \quad n^{\alpha\beta} = \int_{-\Theta^{3-}}^{\Theta^{3+}} \sqrt{\frac{g}{a}} \sigma^{\alpha\gamma} S_{\gamma}^{\beta} d\Theta^3, \quad m^{\alpha\beta} = \int_{-\Theta^{3-}}^{\Theta^{3+}} \sqrt{\frac{g}{a}} \sigma^{\alpha\gamma} S_{\gamma}^{\beta} \Theta^3 d\Theta^3$$

and

$$(3.8) \quad \begin{aligned} \dot{\mathbf{n}}^{\alpha\beta} &= \frac{1}{\sqrt{a}} \frac{D}{Dt}(\sqrt{a}n^{\alpha\beta}) + n^{\alpha\gamma}a^{\delta\beta}d_{\delta\gamma}, \\ \dot{\mathbf{m}}^{\alpha\beta} &= \frac{1}{h\sqrt{a}} \frac{D}{Dt}(h\sqrt{a}m^{\alpha\beta}) + m^{\alpha\gamma}a^{\delta\beta}d_{\delta\gamma}. \end{aligned}$$

\mathbf{P} and \mathbf{S} are the force and moment per unit area of the reference surface, and \mathbf{N} and \mathbf{M} are the boundary force and moment per unit of length of the boundary C .

The kinematic constraint (3.4) due to the normal hypothesis is introduced to the variational principle in the form of a subsidiary condition

$$(3.9) \quad \Pi_n = \int_M \dot{q}^{\alpha}(\underline{\nu}_3\|_{\alpha} + \omega_{\alpha}) dA,$$

where the variable

$$\dot{q}^\alpha = \frac{1}{\sqrt{a}} \frac{D}{Dt} (\sqrt{a} q^\alpha)$$

plays the role of a Lagrangian multiplier.

The constitutive relations between the stress resultants in rate form (3.8) and the deformation rate (3.5) of the shell are obtained from the constitutive equations of the continuum (2.9) by introducing the kinematic assumptions of the shell and integrating over the shell thickness

$$(3.10) \quad \begin{aligned} \dot{n}^{\alpha\beta} &= A_{(0)}^{\alpha\beta\gamma\delta} d_0^{\delta\gamma} + A_{(1)}^{\alpha\beta\gamma\delta} d_1^{\delta\gamma} + D_{(0)}^{\alpha\beta}, \\ \dot{m}^{\alpha\beta} &= A_{(1)}^{\alpha\beta\gamma\delta} d_0^{\delta\gamma} + A_{(2)}^{\alpha\beta\gamma\delta} d_1^{\delta\gamma} + D_{(1)}^{\alpha\beta}, \end{aligned}$$

with

$$(3.11) \quad A_{(i)}^{\alpha\beta\gamma\delta} = \int_{-\Theta^{3-}}^{\Theta^{3+}} \sqrt{\frac{g}{a}} (\tilde{C}^{\alpha\varepsilon\zeta\gamma} S_\varepsilon^\beta S_\zeta^\delta + \sigma^{\alpha\gamma} a^{\delta\beta}) (\Theta^3)^i d\Theta^3, \quad i = 0, 1, 2$$

and

$$D_{(i)}^{\alpha\beta} = \int_{-\Theta^{3-}}^{\Theta^{3+}} \sqrt{\frac{g}{a}} S_\gamma^\beta \tilde{\sigma}^{\alpha\gamma} (\Theta^3)^i d\Theta^3, \quad i = 0, 1.$$

The condition of plane stress is included.

If the material of the shell allows to create a potential, we can also formulate a potential for the shell continuum,

$$(3.12) \quad \begin{aligned} \Phi &= \frac{1}{2} A_{(0)}^{\alpha\beta\gamma\delta} d_0^{\beta\alpha} d_0^{\delta\gamma} + A_{(1)}^{\alpha\beta\gamma\delta} d_0^{\beta\alpha} d_1^{\delta\gamma} \\ &\quad + \frac{1}{2} A_{(2)}^{\alpha\beta\gamma\delta} d_1^{\beta\alpha} d_1^{\delta\gamma} + D_{(0)}^{\alpha\beta} d_{\beta\alpha} + D_{(1)}^{\alpha\beta} d_{\beta\alpha}. \end{aligned}$$

4. Formulation of the contact problem

The contact of the shell with a rigid body can be characterized by the condition of non-penetration

$$(4.1) \quad \varepsilon = \hat{\mathbf{n}}(\mathbf{x} - \hat{\mathbf{x}}) \geq \mathbf{0},$$

where $\hat{\mathbf{n}}$ is the normal vector and $\hat{\mathbf{x}}$ — the position vector of the surface of the contact body (Fig. 2). This condition leads to a kinematical constraint, that restricts the displacement to the direction normal to the contact surface.

If you use the penalty procedure to solve the contact problem, the contact condition is satisfied approximately. The contact load vector

$$(4.2) \quad \hat{\mathbf{P}} = k[-\varepsilon]_+(\hat{\mathbf{n}}\mathbf{n}) = \hat{P}\mathbf{n} \quad \text{with} \quad [-\varepsilon]_+ = \max(0, \cdot)$$

is determined as a function of the depth of penetration of the shell into the contact body and of the penalty factor k . It is assumed that the contact load acts along the normal to the shell.

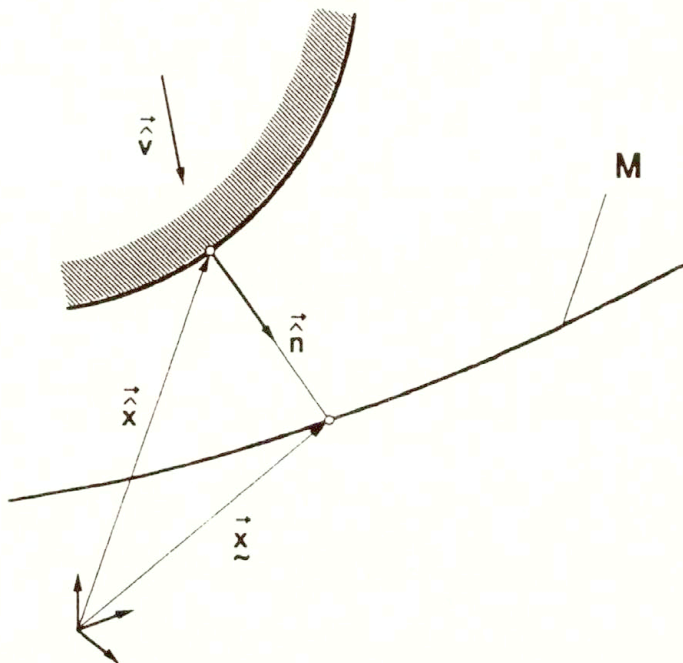


FIG. 2. Shell and contact body.

Combination of the objective time derivative of the contact load vector with the virtual velocity $\delta \underline{\nu}$ yields the variational formulation of the penalty term in the rate form [3]

$$(4.3) \quad \delta \Pi_k = - \int_M \frac{1}{\sqrt{a}} \frac{D}{Dt} (\sqrt{a} \hat{\mathbf{P}}) \delta \underline{\nu} dA = - \int_M \left[\left(\frac{\dot{\sqrt{a}}}{\sqrt{a}} \mathbf{n} + \boldsymbol{\omega} \right) \hat{\mathbf{P}} + \dot{\hat{\mathbf{P}}} \mathbf{n} \right] \delta \underline{\nu} dA,$$

with

$$\dot{\hat{\mathbf{P}}} = k \{ -[-\text{sign}(\varepsilon)]_+ [(\underline{\nu} - \hat{\nu}) \hat{\mathbf{n}}] (\hat{\mathbf{n}} \mathbf{n}) + [-\varepsilon]_+ (\hat{\mathbf{n}} \boldsymbol{\omega}) \},$$

where the change of the contact load $\dot{\hat{\mathbf{P}}}$ is a function of the velocities of the shell and the contact body.

The friction between the shell and the contact body leads to an additional contact load that acts in the tangential plane of the shell. Contrary to the contact load acting in the normal direction, the friction load is not a result of a geometrical constraint but of the interaction between two surfaces. For the shells of revolution (Sec. 5), the friction is taken into account as an additional external load.

5. Shells of revolution

The kinematic relations are set up in a rigid cylindrical coordinate system (Fig. 3).

The kinematic variables are the velocities

$$(5.1) \quad \underline{\nu} = [\nu^r, \nu^y, \chi]^T \quad \text{with} \quad \nu^r = \dot{r}, \quad \nu^y = \dot{y}, \quad \chi = \dot{\varphi}.$$

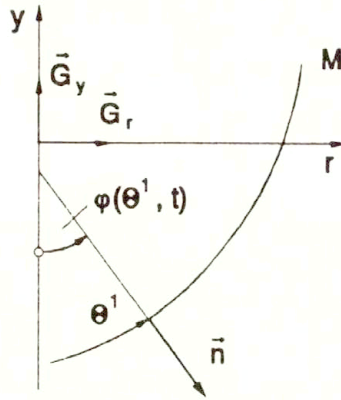


FIG. 3. Cylindrical coordinate system.

After specifying the kinematic terms for the one-dimensional problem and integrating in the peripheral circumferential direction, the variational principle for the shell continuum (3.6) has the following form:

$$(5.2) \quad \delta(\Pi_{iR}) - \delta\Pi_{aR} = 0$$

with

$$\begin{aligned} \Pi_{iR} &= \int_L \{U_p(\underline{\nu}, \underline{\nu}_{,1}) + U_g(\underline{\nu}, \underline{\nu}_{,1}) + \dot{q}^1(\underline{\nu}_{,1}^T \underline{c}_1 + \underline{\nu}^T \underline{c}_2)\} d\Theta^1, \\ U_p &= \frac{1}{2} \underline{\nu}_{,1}^T \underline{A}_1 \underline{\nu}_{,1} + \underline{\nu}^T \underline{A}_2 \underline{\nu}_{,1} + \frac{1}{2} \underline{\nu}^T \underline{A}_3 \underline{\nu} + \underline{\nu}_{,1}^T \underline{a}_1 + \underline{\nu}^T \underline{a}_2, \\ U_g &= \frac{1}{2} \underline{\nu}_{,1}^T \underline{H} \underline{\nu}_{,1} + \underline{\nu}^T \underline{Q} \underline{\nu}_{,1} + \frac{1}{2} \underline{\nu}^T \underline{M} \underline{\nu}, \end{aligned}$$

and

$$\begin{aligned} \delta\Pi_{aR} &= \int_L \{\delta U_a(\underline{\nu}, \underline{\nu}_{,1}) + \delta U_k(\underline{\nu}, \underline{\nu}_{,1})\} d\Theta^1 + \sum_{i=1}^2 \{\delta \underline{\nu}^T (\underline{M}_c \underline{\nu} + \underline{T} \dot{\underline{n}}_s)\}, \\ \delta U_a &= \delta \underline{\nu}^T (\underline{Q}_p \underline{\nu}_{,1} + \underline{M}_p \underline{\nu} + \underline{T} \dot{\underline{p}}_s), \\ \delta U_k &= \delta \underline{\nu}^T (\underline{Q}_k \underline{\nu}_{,1} + \underline{M}_k \underline{\nu} + \underline{T} \dot{\underline{p}}_k). \end{aligned}$$

The expression Π_{iR} is a potential that described the deformation behaviour, where U_p represents the physical nonlinearity and U_g the geometrical nonlinearity.

The part $\delta\Pi_{aR}$ of the variational principle, that comes from the external loads, additionally contains the term of contact loads δU_k , where the change of contact load is given as a function of the velocities of the shell and the contact body

$$\dot{\underline{p}}_k = [\dot{\underline{P}}_n, \dot{\underline{P}}_t, 0]^T = \underline{D}_k(\underline{\nu} - \underline{\nu}_k) + \underline{k}_k.$$

Using the Hamilton principle, the variational principle of the shell of revolution leads to

a one-dimensional linear boundary value problem for the rates

$$(5.4) \quad \begin{aligned} \underline{k} &= \tilde{A}_1 \underline{\nu}_{,1} + \tilde{A}_2^T \underline{\nu} + \underline{a}_1 + \dot{q}^1 \underline{c}_1, \\ \underline{k}_{,1} &= (\tilde{A}_2 - \tilde{Q}_p) \underline{\nu}_{,1} + (\tilde{A}_3 - \tilde{M}_p - D_k) \underline{\nu} + \underline{a}_2 + \dot{q}^1 \underline{c}_2 - \underline{T} \dot{p}_s + D_k \underline{\nu}_k - \underline{k}_k, \\ 0 &= \underline{c}_1^T \underline{\nu}_{,1} + \underline{c}_2^T \underline{\nu}. \end{aligned}$$

After elimination of the Lagrangian multiplier \dot{q}^1 and rearranging, we obtain the following canonical system of differential equations

$$(5.5) \quad \underline{\dot{y}}_{,1} = \underline{B}(\underline{z}) \underline{\dot{y}} + \underline{b}(\underline{z})$$

with

$$\underline{\dot{y}} = [\underline{\nu}^T, \underline{k}^T]^T = \underline{\dot{y}}(\Theta^1, t), \quad \underline{z} = \underline{z}(\Theta^1, t)$$

and

$$\underline{B} = \begin{bmatrix} \underline{B}_1 & \underline{B}_2 \\ \underline{B}_3 & \underline{B}_4 \end{bmatrix}, \quad \underline{b} = \begin{bmatrix} \underline{b}_1 \\ \underline{b}_2 \end{bmatrix}.$$

This system must be solved for a given state of the shell state \underline{z} at time t .

The linear boundary value problem is embedded in the nonlinear initial value problem

$$(5.6) \quad \underline{\dot{z}} = \underline{C}(\underline{z}) \underline{\dot{y}} + \underline{c}, \quad \underline{z}(t_0) = \underline{z}_0.$$

The solution yields the shell state variables \underline{z} as functions of t .

6. Treatment of the contact problem including friction

In accordance with the incremental formulation of the variational principle, one has to determine the rates of contact loads \hat{P}_n and \hat{P}_t in (5.3) for the current contact state.

If we assume the contact body having the velocity

$$(6.1) \quad \hat{\underline{\nu}} = \hat{\nu}^r \mathbf{G}_r + \hat{\nu}^y \mathbf{G}_y,$$

we obtain for the velocity of the shell (relative to the contact body), in the normal direction of the contact surface $\hat{\mathbf{n}}$ (see Fig. 4)

$$(6.2) \quad \psi = (\underline{\nu} - \hat{\underline{\nu}}) \hat{\mathbf{n}} = (\nu^r - \hat{\nu}^r) \sin \hat{\varphi} - (\nu^y - \hat{\nu}^y) \cos \hat{\varphi}.$$

The condition

$$(6.3) \quad \psi < 0$$

characterizes the loading process and yields the rate of the contact load

$$(6.4) \quad \hat{P}_n = -k \psi (\hat{\mathbf{n}} \mathbf{n}) = -k \psi \cos(\hat{\varphi} - \varphi).$$

Coulomb's friction law is used in combination with a stick-slip model (see Fig. 5). If the tangential component of the velocity between the contact body and the shell

$$(6.5) \quad \nu = (\underline{\nu} - \hat{\underline{\nu}}) \mathbf{t} = (\nu^r - \hat{\nu}^r) \cos \varphi + (\nu^y - \hat{\nu}^y) \sin \varphi$$

is less than the limit of the sliding velocity

$$(6.6) \quad |\nu| < \nu_{\min},$$

then we suppose adhesion. In this case the rate of the contact load in tangential direction is

$$(6.7) \quad \hat{P}_t = -k [(\underline{\nu} - \hat{\underline{\nu}}) \hat{\mathbf{t}}] (\hat{\mathbf{t}} \mathbf{t}) = -k [(\nu^r - \hat{\nu}^r) \cos \hat{\varphi} + (\nu^y - \hat{\nu}^y) \sin \hat{\varphi}] \cos(\hat{\varphi} - \varphi).$$

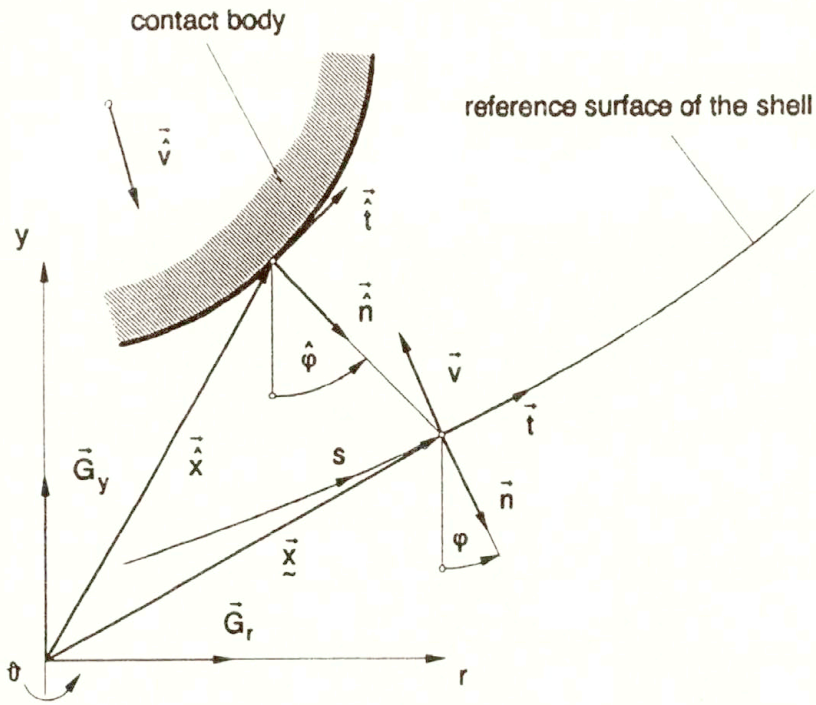


FIG. 4. Contact of the shell of revolution.

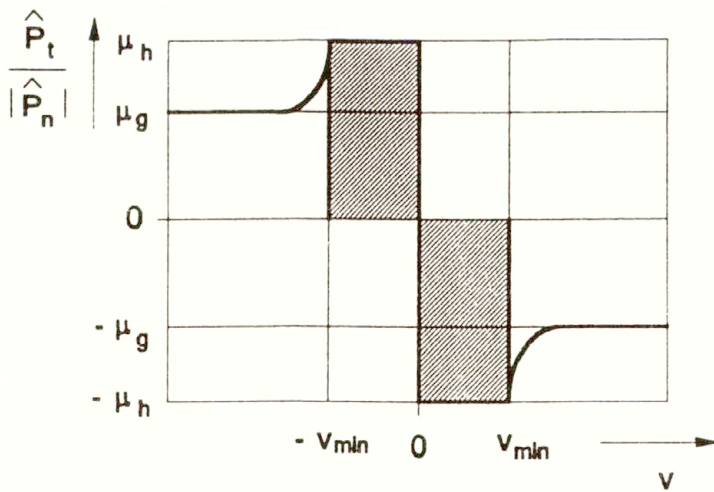


FIG. 5. Friction model.

The transition from sticking to sliding is characterized by the condition

$$(6.8) \quad |\hat{P}_t| > \mu_h |\hat{P}_n|.$$

In this case the friction load will be reduced to the sliding level, which is defined by the

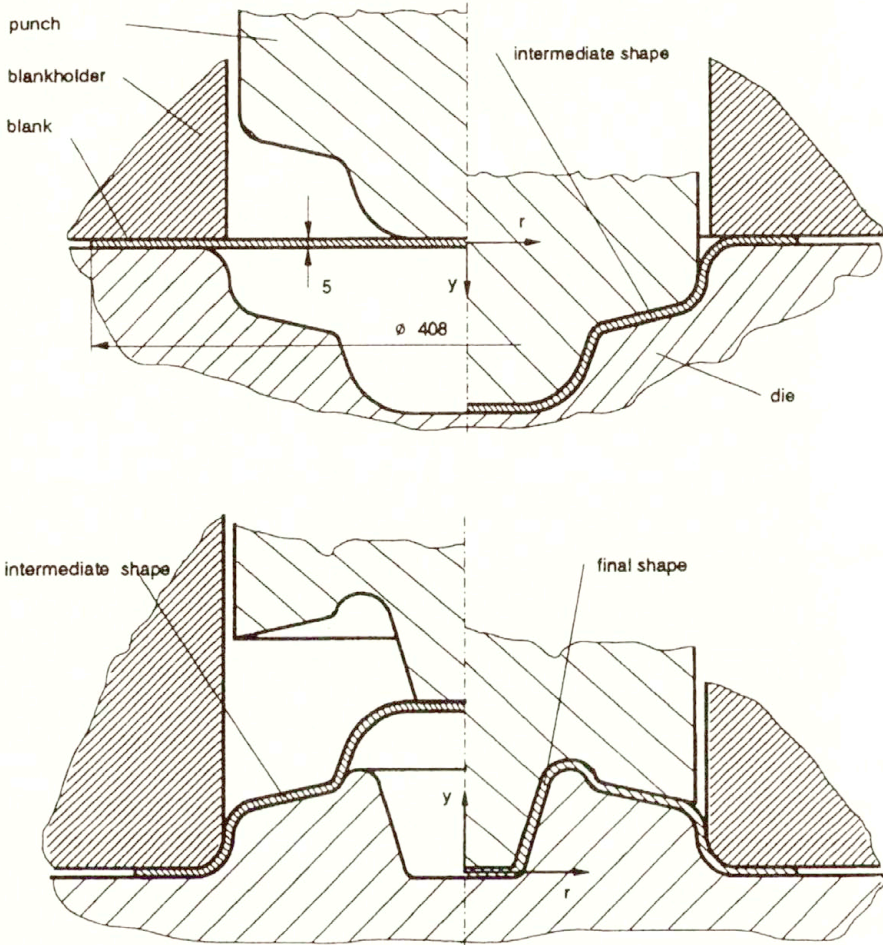


FIG. 6. Deep drawing simulation—tool geometry, material properties and contact parameters

material properties

- material
 - Young's modulus
 - Poisson's ratio
 - isotropic hardening function
- $$\sigma_F = \sigma_{F0} \left\{ 1 + \frac{c_0}{c_2} [(\varepsilon_v^{pl} + c_1)^{c_2} - c_2^{c_2}] \right\}$$

Deep drawing steel
 $E = 2.1 \cdot 10^5$ MPa
 $\nu = 0.3$
 $\sigma_{F0} = 220$ MPa
 $c_0 = 0.4475, c_1 = 10^{-6}, c_2 = 0.43$

contact parameters

- penalty factor
- contact tolerance
- velocity of the punch
- Coulomb's friction
 - sliding friction coefficient
 - sticking friction coefficient
 - blankholder pressure (constant)

$k = 10^4$ MPa/mm
 $\varepsilon_a = 0.2$ mm
 $v_p = 1$ mm/s
 $\mu_g = 0.04$
 $\mu_h = 0.06$
 $p_N = 1$ MPa

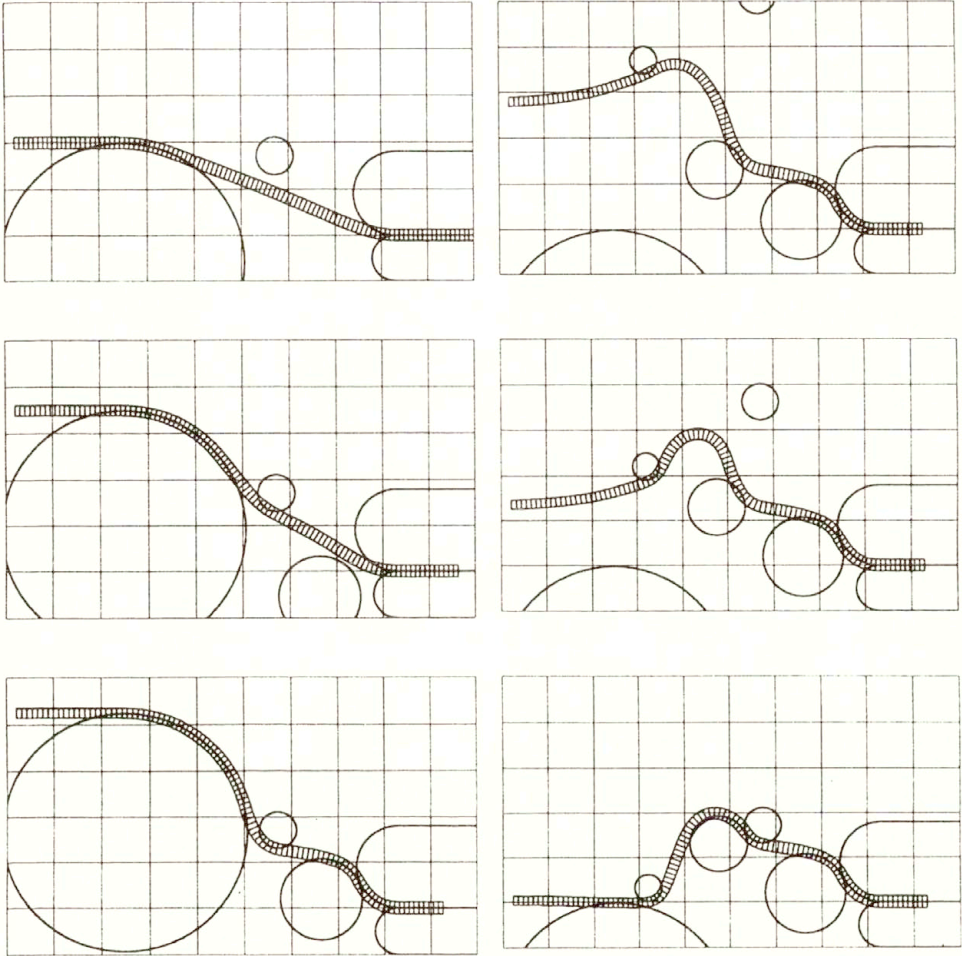


FIG. 7. Deep drawing simulation — the shell and the contact geometry in different phases of the deep drawing process.

friction coefficient μ_g within the time-step Δt

$$(6.9) \quad \hat{P}_t = \frac{1}{\Delta t} [\mu_g \text{sign}(\hat{P}_t) |\hat{P}_n| - \hat{P}_t].$$

If the condition

$$(6.10) \quad |\nu| \geq \nu_{\min}$$

is satisfied, we have sliding friction. Then the rate of the contact load is calculated from the formula

$$(6.11) \quad \hat{P}_t = \mu_g \text{sign}(\nu) k \psi - \frac{1}{\Delta t} [\mu_g \text{sign}(\nu) |\hat{P}_n| + \hat{P}_t].$$

The condition

$$(6.12) \quad \psi > 0$$

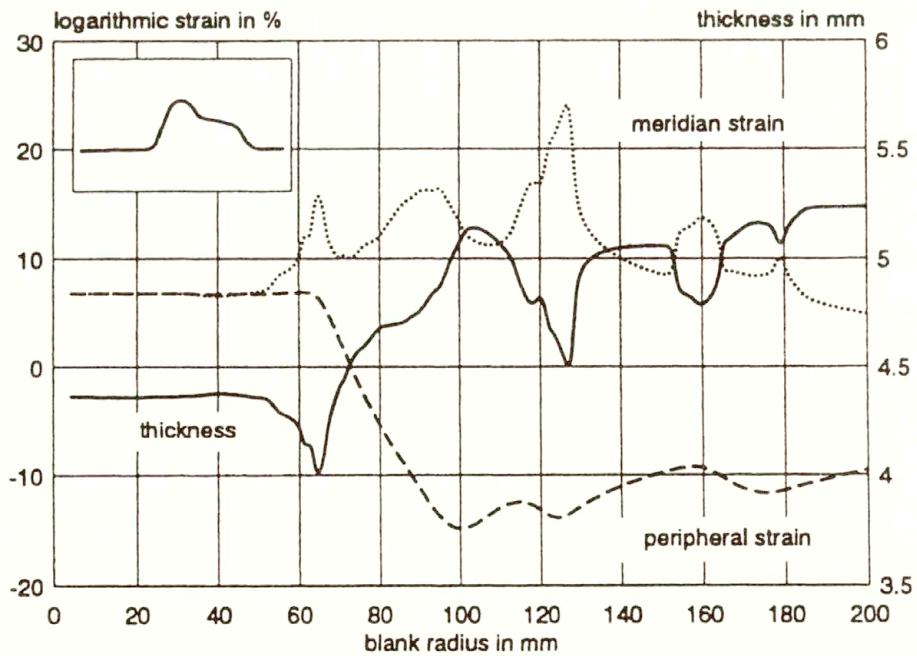
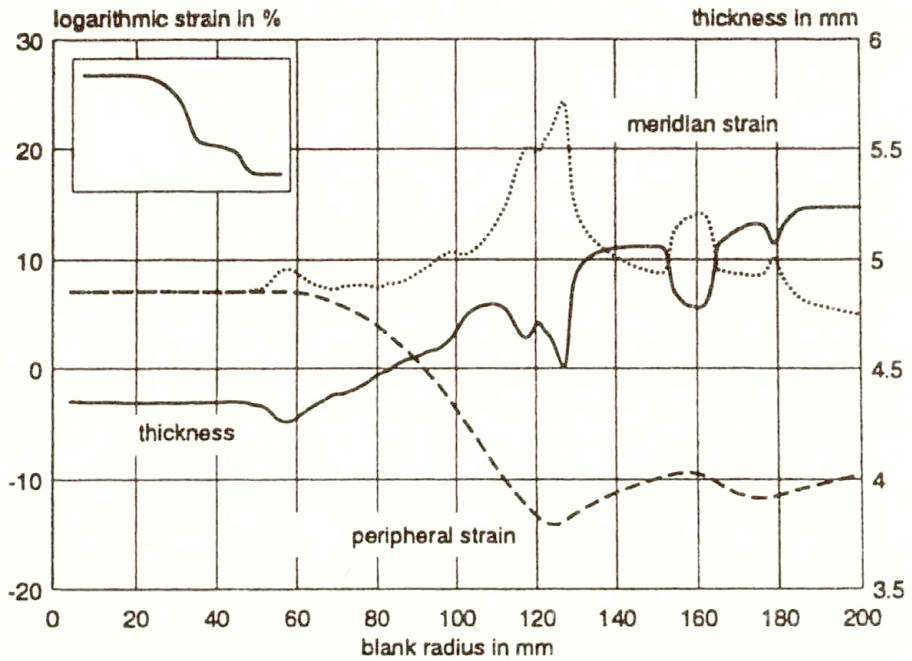


FIG. 8. Deep drawing simulation — meridional strain, peripheral strain and distribution of thickness of the intermediate shape and of the final shape.

describes the process of unloading. As long as the shell point is leaving the contact domain, the contact loads will be removed:

$$(6.13) \quad \dot{\hat{P}}_n = -\frac{\psi}{\varepsilon} \hat{P}_n, \quad \dot{\hat{P}}_t = -\frac{\psi}{\varepsilon} \hat{P}_t.$$

7. Example

The presented example was calculated by means of a program which is based on the transmission matrix procedure. The numerical calculation starts from the integration of (3.11) for a given shell state by using an integration procedure that takes into account the discontinuity of the elastic-plastic material behaviour. The fourth-order Runge–Kutta formula, in combination with a transmission matrix procedure, is applied for the solution of the linear boundary value problem (5.5). The nonlinear initial value problem (5.6) is solved by the second-order Runge–Kutta formula. A detailed description of the applied algorithms is given in [3]. Additional comparisons of the program with benchmark tests [4, 5], experiments and numerical solutions based on other theories [6, 7] are published in [3].

The example demonstrates the simulation of a deep drawing process with intermediate shape. Figure 6 shows the principle of the manufacturing process, the material properties and the contact parameters. Elastic-plastic material with isotropic hardening is assumed. The friction between the tool and the sheet metal is taken into account. In the domain of the blank-holder an additional pressure is assumed.

Figure 7 shows the discretized model of the shell and the contact geometry in different phases of the deep drawing process. The results are shown in Fig. 8. The diagrams represent the calculated meridional strain, the peripheral strain and the distribution of the thickness as functions of the original distance from the punch center of the intermediate shape and of the final shape.

References

1. H. BERGANDER, *Deformationsgesetze der Standardform in konvektiver Metrik*, Techn. Mech., **8**, 31–40, 1987.
2. V. ULBRICHT, *Physikalisch und geometrisch nichtlineare Schalentheorie in konvektiver Metrik*, Habilitation, TU, Dresden 1986.
3. A. FLOSS, *Geometrisch und physikalisch nichtlineare Rotationschalen in materialer Beschreibung unter Berücksichtigung des Kontaktproblems*, Dissertation, TU, Dresden 1994.
4. J.K. LEE, R. WAGONER and E. NAKAMACHI, *A benchmark test for sheet forming analysis*, Ohio State University, Columbus, Ohio 43210, Report ERCINSH, 1990.
5. M.J. SARAN, *Numerical and experimental investigations of deep drawing of metal sheets*, ASME J. Engng. for Industry, **112**, 272–277, 1990.
6. G. LANDGRAF, *Umformung doppelt gekrümmter Flächen*, Tagung Festkörpermechanik, Fachbuchverlag Leipzig, Band BXLII, 1–10, 1988.
7. M. SELIG, *Numerische Simulation von rotationssymmetrischen Blechumformprozessen unter Verwendung der Deformationstheorie*, Workshop numerische Methoden der Plastomechanik, Universität Hannover, 1992.

TECHNISCHE UNIVERSITÄT DRESDEN
INSTITUT FÜR FESTKÖRPERMECHANIK, DRESDEN, GERMANY.

Received January 31 1994.

Effect of initial prestressing on the optimal design of plates with respect to orthotropic brittle rupture

A. GANCZARSKI and J. SKRZYPEK (KRAKÓW)

THE AIM of the present paper is the analysis of effect of initial prestressing on the optimal design of axisymmetric plates of uniform creep strength or plates optimal with respect to lifetime, which are subject to combined loadings. In problems of optimization formulated above not only thickness of a structure but also parameters of prestressing are decision variables as well. Assuming the time hardening theory associated with the Kachanov orthotropic brittle rupture hypothesis as the constitutive relationships for creep, two types of coupling are discussed: when orthotropic damage induces or not induces anisotropic creep in initially isotropic material. The simplified von Kármán theory of thin axisymmetric plates has been extended to viscoelasticity.

1. Introduction

WHEN OPTIMIZATION of structures under creep conditions is formulated, three typical global optimization problems may be distinguished (cf. ŻYCZKOWSKI [17]):

- 1) minimization of volume when loading and lifetime are prescribed,
- 2) maximization of loading when volume and lifetime are prescribed,
- 3) maximization of lifetime when volume and loading are prescribed.

The lifetime of structure τ_r (global condition), in most cases, is not given in the explicit form but results from the condition of the initiation of first macrocracks $\inf \psi_k(x_j, \tau_r) = 0$ (local damage condition), where ψ_k denotes components of Kachanov-type continuity function. Therefore, first two formulations are inconvenient from the viewpoint of practical applications (they both require the shooting method). In consequence, third approach to be the most convenient, particularly, when the condition of constant volume is built into the shape correction procedure.

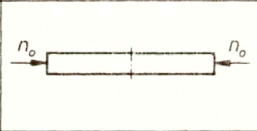

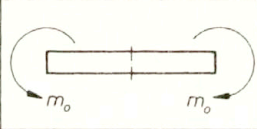
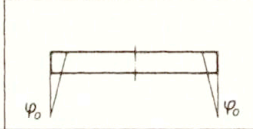
Apart from classification based on the global criterion presented above, one may introduce another one, based on the local criterion. Generally, the local criterion applied for elastic problems leads to the solutions of uniform strength, and analogously, in the case of optimization under creep conditions, it yields solutions of uniform creep strength. In consequence, three local approaches to uniform creep strength may be formulated:

- 1) when loading and lifetime are prescribed,
- 2) when volume and lifetime are prescribed,
- 3) when loading and volume are prescribed.

The aim of the present paper is the analysis of mechanisms of brittle damage and the design of prestressed axisymmetric plates of uniform creep strength (third local formulation) or optimal design of plates with respect to lifetime or volume (third or first global formulations), which are subject to combined loadings. When problems of optimization are formulated, not only the thickness of a structure but parameters of prestressing are considered as decision variables as well. Therefore it is important to distinguish precisely the behaviour of prestressing, which is varying in time, from other loadings, which are constant and may appear as the equality constraints. The nature of the prestressing, which is

considered as the excitation imposed on the structure, also requires explanations. Generally, one has to distinguish between the internal and external excitations. The prestressing fibres in reinforced concrete is an example for the first case, whereas the cylindrical shell prestressed by external circumferential cable — the second. In both cases discussed, the excitations may have the nature of forces or distortions. Typical examples of excitations, such as the radial prestressing force n_0 or the displacement Δ , and the radial prestressing moment m_0 or the angle of support φ_0 , for membrane and bending states, respectively, are illustrated in Tabl. 1.

Table 1. Boundary excitations in axisymmetric plates.

		boundary excitations	
		force - type	displacement - type
state	membrane		
	bending		
coupling $\mathcal{F}(n_0, m_0, \Delta, \varphi_0) = 0$			

Apart from the order of the theory, which may include or not the coupling between the membrane and bending effects, both the membrane and bending states may additionally be coupled by the boundary conditions. Generally, such a coupling can be described by a function dependent on the excitation parameters:

$$(1.1) \quad \mathfrak{J}(n_0, m_0, \Delta, \varphi_0) = 0.$$

From practical point of view, only a few particular representations of the function \mathfrak{J} make sense. These cases are as follows:

1. Uncoupling, when the function \mathfrak{J} depends only on one of the arguments:

$$(1.2) \quad \mathfrak{J}(n_0) = 0, \quad \text{or} \quad \mathfrak{J}(m_0) = 0, \quad \text{or} \quad \mathfrak{J}(\Delta) = 0, \quad \text{or} \quad \mathfrak{J}(\varphi_0) = 0.$$

2. Unilateral coupling of membrane and bending states, when function \mathfrak{J} may be solved with respect to one of its arguments:

$$(1.3) \quad m_0 = j(n_0), \quad \text{or} \quad \varphi_0 = j(\Delta).$$

3. Bilateral coupling, when function \mathfrak{J} implicitly depends on more than one argument:

$$(1.4) \quad \mathfrak{J}(\Delta, \varphi_0) = 0.$$

Structures of uniform creep strength are usually found in an iterative way. Corrections of both the thickness and the prestressing parameters are introduced until the local Kachanov-type damage condition $\psi_k(x_j, \tau_r)$ (the objective function) is satisfied at each point x_j , under additional equality constraint of constant volume (the third local

formulation). In general, structures of uniform creep strength are not optimal with respect to lifetime $\tau_r \rightarrow \max$, taken as the objective function. From the practical point of view, structures of uniform creep strength (the objective function) when lifetime is prescribed (the equality constraint) might be more promising. Therefore appropriate numerical procedures, which allow for optimal design with respect to lifetime (the first local formulation), are also enclosed. Formulation of optimality conditions for structures of uniform creep strength, and a proposal of the numerical procedure for maximization of lifetime, are also the aim of the present paper (the global formulation). Comparison of both the local and the global formulations is a basis of practical recommendation for engineers.

Assuming the time hardening hypothesis and the orthotropic damage growth rule as the constitutive equations for creep and creep rupture, one may classify the damage mechanisms, which may appear in plates when the boundary conditions and external loadings are prescribed. The second step is the optimal control of damage mechanisms, where not only the classical shape optimization but also optimization of the prestressing have been taken into account.

Both the thickness and the prestressing optimization problems have allowed us to increase significantly the lifetime (τ_j). The postcritical phase associated with the propagation of damage zones has not been considered ($\tau_I < \tau \leq \tau_{II}$).

2. Formulation of the problem and basic equations

2.1. Basic equations for axisymmetric plates under axisymmetric loadings

Let us consider axisymmetric sandwich plate of a variable thickness of working layers g_s and a variable core depth $h_s - g_s$, loaded by the external pressure (cf. Fig. 1).

Introducing the cylindrical coordinate system centered in the middle of the plate, we assume that

- loadings are reduced to the midsurface,
- displacements of the midsurface are small as compared to the plate thickness, but the geometry changes are taken into account (the second order theory),
- segments which are straight and normal to the midsurface before deformation remain straight and normal after deformation, and their lengths do not change (the Love–Kirchhoff hypothesis),
- total strains, which are small, are decomposed into the elastic and the creep components $\varepsilon_{r/\theta}^{\pm} = \varepsilon_{r/\theta}^{e\pm} + \varepsilon_{r/\theta}^{c\pm}$ and the elastic components satisfy the Hooke law,
- the plate is subject to plane stress state,
- the thickness of the plate depends only in the radial coordinate r .

Let us apply the general mixed approach, where the equation of membrane state is written by means of the Airy function, whereas the equation of bending state — by the appropriate deflection function (cf. TIMOSHENKO [15], GANCZARSKI and SKRZYPEK [7], also GANCZARSKI [8]). To this end we introduce the Fourier expansions of displacements

$$w(r, \theta) = f(r) \cos k\theta, \text{ and the following definition of the Airy function } n_r = \frac{1}{r} \frac{dF}{dr},$$

$$n_\theta = \frac{d^2 F}{dr^2}. \text{ Hence}$$

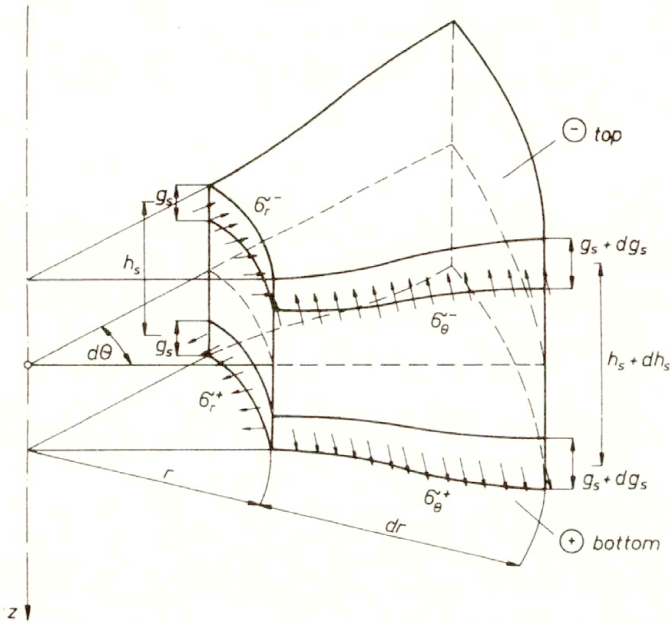


FIG. 1. Axisymmetric sandwich plate of variable thickness loaded by an external pressure.

for $\tau = 0$

$$\begin{aligned}
 & \frac{1}{B_s} \Delta_r^2 F + \frac{d}{dr} \left(\frac{1}{B_s} \right) \left(2 \frac{d^3 F}{dr^3} + \frac{2 - \nu}{r} \frac{d^2 F}{dr^2} - \frac{1}{r^2} \frac{dF}{dr} \right) \\
 & \quad + \frac{d^2}{dr^2} \left(\frac{1}{B_s} \right) \left(\frac{d^2 F}{dr^2} - \frac{\nu}{r} \frac{dF}{dr} \right) = 0, \\
 (2.1) \quad & \mathcal{D}_s \Delta_r^2 f + \frac{d\mathcal{D}_s}{dr} \left(2 \frac{d^3 f}{dr^3} + \frac{2 + \nu}{r} \frac{d^2 f}{dr^2} - \frac{1 + 2k^2}{r^2} \frac{df}{dr} + 3 \frac{k^2}{r^3} f \right) + \frac{d^2 \mathcal{D}_s}{dr^2} \\
 & \quad \times \left(\frac{d^2 f}{dr^2} + \frac{\nu}{r} \frac{df}{dr} - \nu \frac{k^2}{r^2} f \right) - \frac{1}{r} \frac{dF}{dr} \frac{d^2 f}{dr^2} - \frac{d^2 F}{dr^2} \left(\frac{1}{r} \frac{df}{dr} - \frac{k^2}{r^2} f \right) - q_z = 0;
 \end{aligned}$$

for $\tau \geq 0$

$$\begin{aligned}
 & \frac{1}{B_s} \Delta_r^2 \dot{F} + \frac{d}{dr} \left(\frac{1}{B_s} \right) \left(2 \frac{d^3 \dot{F}}{dr^3} + \frac{2 - \nu}{r} \frac{d^2 \dot{F}}{dr^2} - \frac{1}{r^2} \frac{d\dot{F}}{dr} \right) \\
 & \quad + \frac{d^2}{dr^2} \left(\frac{1}{B_s} \right) \left(\frac{d^2 \dot{F}}{dr^2} - \frac{\nu}{r} \frac{d\dot{F}}{dr} \right) = -\Delta_r \left(\frac{\dot{n}_\theta^c - \nu \dot{n}_r^c}{B_s} \right) - \frac{1 + \nu}{r} \frac{d}{dr} \left(\frac{\dot{n}_\theta^c - \dot{n}_r^c}{B_s} \right), \\
 (2.2) \quad & \mathcal{D}_s \Delta_r^2 \dot{f} + \frac{d\mathcal{D}_s}{dr} \left(2 \frac{d^3 \dot{f}}{dr^3} + \frac{2 + \nu}{r} \frac{d^2 \dot{f}}{dr^2} - \frac{1 + 2k^2}{r^2} \frac{d\dot{f}}{dr} + 3 \frac{k^2}{r^3} \dot{f} \right) \\
 & \quad + \frac{d^2 \mathcal{D}_s}{dr^2} \left(\frac{d^2 \dot{f}}{dr^2} + \frac{\nu}{r} \frac{d\dot{f}}{dr} - \nu \frac{k^2}{r^2} \dot{f} \right) - \left(\frac{1}{r} \frac{dF}{dr} \frac{d^2 \dot{f}}{dr^2} \right) - \left[\frac{d^2 F}{dr^2} \left(\frac{1}{r} \frac{d\dot{f}}{dr} - \frac{k^2}{r^2} \dot{f} \right) \right] \\
 & \quad = -\frac{d^2 \dot{m}_r^c}{dr^2} - \frac{1}{r} \frac{d(2\dot{m}_r^c - \dot{m}_\theta^c)}{dr} + \frac{k^2}{r^2} \dot{m}_\theta^c,
 \end{aligned}$$

where the operators independent of circumferential coordinate take the forms:

$$(2.3) \quad \begin{aligned} \Delta_{r..} &= \frac{d^2..}{dr^2} + \frac{1}{r} \frac{d..}{dr} - \frac{k^2}{r^2} \dots \\ \Delta_{r..}^2 &= \frac{d^4..}{dr^4} + \frac{2}{r} \frac{d^3..}{dr^3} - \frac{1+2k^2}{r^2} \frac{d^2..}{dr^2} + \frac{1+2k^2}{r^3} \frac{d..}{dr} + \frac{k^2(k^2-4)}{r^4} \dots \end{aligned}$$

Symbol $k = 0, 1, \dots, N$ denotes the number of half-waves, and decides whether the deformation is symmetric or nonsymmetric. For numerical examples only the fundamental mode ($k = 0$) was allowed for, due to the symmetry considered.

Introduction of the sandwich section is very convenient from the numerical point of view, namely, the plate section may be treated as the double point substitutive section and, hence, the process of integration of stresses along the thickness is reduced to summing them up. Definitions associated with the sandwich section require appropriate extension of the classical definitions, namely:

Love–Kirchhoff hypothesis

$$(2.4) \quad \varepsilon_{r/\theta}^{\pm} = \pm \kappa_{r/\theta} \frac{h_s}{2} + \lambda_{r/\theta},$$

constitutive equations (cf. PENNY and MARRIOTT [12])

$$(2.5) \quad \sigma_{r/\theta}^{\pm} = \frac{E}{1-\nu^2} \left[\pm (\kappa_{r/\theta} + \nu \kappa_{\theta/r}) \frac{h_s}{2} + (\lambda_{r/\theta} + \nu \lambda_{\theta/r}) - (\varepsilon_{r/\theta}^{c\pm} + \nu \varepsilon_{\theta/r}^{c\pm}) \right],$$

definitions of generalized inelastic forces

$$(2.6) \quad \begin{aligned} n_{r/\theta}^c &= \frac{B_s}{2} [\varepsilon_{r/\theta}^{c+} + \varepsilon_{r/\theta}^{c-} + \nu (\varepsilon_{\theta/r}^{c+} + \varepsilon_{\theta/r}^{c-})], \\ m_{r/\theta}^c &= \frac{D_s}{h_s} [\varepsilon_{r/\theta}^{c+} - \varepsilon_{r/\theta}^{c-} + \nu (\varepsilon_{\theta/r}^{c+} - \varepsilon_{\theta/r}^{c-})], \end{aligned}$$

and, finally, the membrane and the bending stiffnesses (cf. ARMAND [1]):

$$(2.7) \quad D_s = \frac{E h_s^2 g_s}{2(1-\nu^2)}, \quad B_s = 2 \frac{E g_s}{(1-\nu^2)}.$$

In the above definitions h_s and g_s denote the core depth and the working layers thickness of the substitutive sandwich section (Fig. 2), superscripts \pm correspond to bottom or top layers, superscript c denotes creep components, subscripts r/θ denote radial and circumferential components, whereas dots stand for time derivatives of the corresponding quantities.

The derived systems of equations (2.1), (2.2) are the unilaterally coupled Kármán systems extended to the case of visco-elastic plate of variable thickness. In the classical Kármán formulation, the full coupling of the equations of membrane and bending states occurs (cf. KÁRMÁN [10], also FUNG [2]), when additional nonlinear terms associated with Gaussian curvature appear in the equation of bending state (the third order theory). The unilateral coupling of the systems (2.1), (2.2) allows us to consider the equation of membrane state independently. In the next step, the stress function is inserted into the equation of bending state to yield the deflection function.

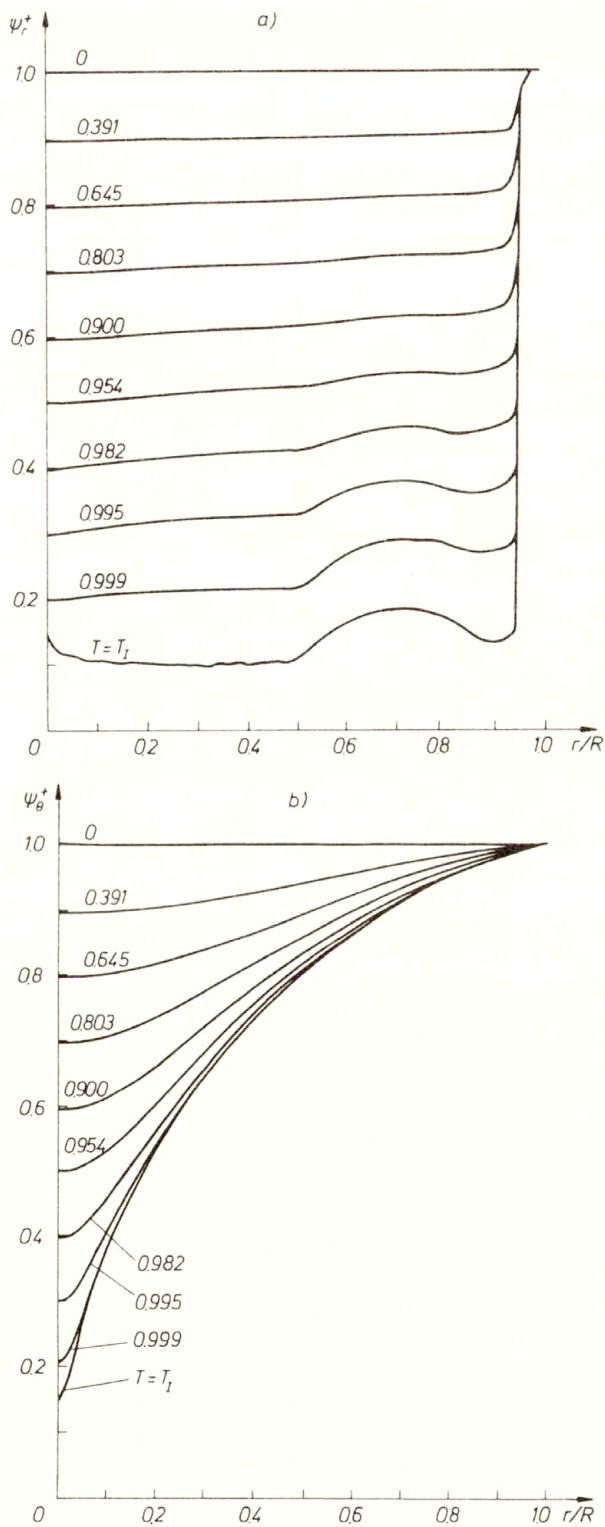


FIG. 2. Evolution of continuity functions: a) radial ψ_r^+ , b) circumferential ψ_θ^+ , in nonprestressed plate of partially uniform creep strength.

2.2. Constitutive equations for creep

All the previously derived formulae are not complete since the constitutive equations have not been specified. In this section the physical equations are given in the form of general orthotropic relationships for the substitutive sandwich section.

We assume the similarity of deviators based on the flow theory for initially isotropic materials:

$$(2.8) \quad \dot{\varepsilon}_{kl}^{c\pm} = \frac{3}{2} \frac{\dot{\varepsilon}_i^{c\pm}}{\sigma_i^{\pm}} s_{kl}^{\pm}, \quad k, l = r, \theta,$$

and the time-hardening hypothesis associated with the Kachanov–Rabotnov orthotropic brittle rupture law (cf. KACHANOV [9], GANCZARSKI and SKRZYPEK [3, 4, 6, 7], also GANCZARSKI [5, 8]).

$$(2.9) \quad \dot{\varepsilon}_i^{c\pm} = (\sigma_i^{\text{net}\pm})^m \mathbf{f}(\tau), \quad \dot{\psi}_k^{\pm} = -C_k \left\langle \frac{\sigma_k^{\pm}}{\psi_k^{\pm}} \right\rangle^{n_k}, \quad k = r, \theta,$$

where $\mathbf{f}(\tau)$ is a given time function, $\langle \rangle$ denote McAuley brackets, and the intensities of the stress, the net stress (with the effect of deterioration taken into account), and the strain rates are defined by the following formulae:

$$(2.10) \quad \sigma_i^{\pm} = \sqrt{\frac{3}{2} s_{kl}^{\pm} s_{kl}^{\pm}}, \quad \sigma_i^{\text{net}\pm} = \sqrt{\left(\frac{\sigma_r^{\pm}}{\psi_r^{\pm}} \right)^2 + \left(\frac{\sigma_{\theta}^{\pm}}{\psi_{\theta}^{\pm}} \right)^2 - \frac{\sigma_r^{\pm} \sigma_{\theta}^{\pm}}{\psi_r^{\pm} \psi_{\theta}^{\pm}}}, \\ \dot{\varepsilon}_i^{\pm} = \sqrt{\frac{2}{3} \dot{\varepsilon}_{kl}^{\pm} \dot{\varepsilon}_{kl}^{\pm}}.$$

Finally, for the plane stress and incompressibility of creep we find

$$(2.11) \quad \dot{\varepsilon}_{r/\theta}^{c\pm} = \frac{(\sigma_i^{\text{net}\pm})^m}{\sigma_i^{\pm}} \left(\sigma_{r/\theta}^{\pm} - \frac{\sigma_{\theta/r}^{\pm}}{2} \right) \mathbf{f}(\tau), \quad \dot{\varepsilon}_z^{c\pm} = -(\dot{\varepsilon}_r^{c\pm} + \dot{\varepsilon}_{\theta}^{c\pm}).$$

In the above formulation, the isotropic creep law is coupled with the orthotropic damage law. This means that creep process is governed by the isotropic flow rule (2.8), in spite of the orthotropic nature of the damage growth (2.9). The last one affects only the time-hardening hypothesis (2.9), where the stress intensity σ_i^{\pm} is replaced by the net-stress intensity $\sigma_i^{\text{net}\pm}$ (2.10) (the weak coupling). This simplified approach is justified only in case of proportional loadings. In general, when nonproportional loadings are allowed for, the orthotropic deterioration process may result in the modified orthotropic flow rule, where s_{kl}^{\pm} and $\sigma_i^{\text{net}\pm}$ appear instead of σ_{kl}^{\pm} and σ_i^{\pm} (the strong coupling). Hence, instead of (2.8) we obtain

$$(2.12) \quad \dot{\varepsilon}_{kl}^{c\pm} = \frac{3}{2} \frac{\dot{\varepsilon}_i^{c\pm}}{\sigma_i^{\text{net}\pm}} s_{kl}^{\text{net}\pm}, \quad s_{kl}^{\text{net}\pm} = \frac{\sigma_{r/\theta}^{\pm}}{\psi_{r/\theta}^{\pm}} - \frac{1}{2} \frac{\sigma_{\theta/r}^{\pm}}{\psi_{\theta/r}^{\pm}},$$

where $\dot{\varepsilon}_{kl}^{c\pm}$ is given by Eq. (2.9). Equation (2.9) contains the independent material constants C_k, n_k (the material orthotropy), and the independent principal components of the continuity function ψ_k . Since the data concerning the material orthotropy for creep rupture are not available at present, in the next applications we consider the case of material isotropy $C_r = C_{\theta} = C$, and $n_r = n_{\theta} = n$, but admitting the independent

evolution of macrocracks in both principal directions ψ_r, ψ_θ . An example of comparison of the general (2.12) or the simplified flow rule (2.8), when orthotropic damage induces or not induces anisotropic creep in the initially isotropic material, is discussed. No additional effect of the material deterioration process on the membrane or bending stiffnesses is taken into account. In other words, the elastic stiffnesses are held constant throughout the creep process considered.

The numerical examples are presented for the plates made of the ASTM 321 stainless steel: $E = 1.77 \times 10^5$ MPa, $\sigma_0 = 1.18 \times 10^2$ MPa, $\nu = 0.3$, $R = 0.5$ m, $h_s = 0.025$ m, $g_s = 0.005$ m, $q_z = 118$ kPa; the temperature-dependent (783 K) material constants for creep rupture are (cf. ODQVIST [11]): $C = 2.13 \times 10^{-42}$ Pa $^{-n}$ /s, $n = 3.9$, $m = 5.6$, whereas material constants for the prestressing ring made of ASTM 310 stainless steel are as follows: $E_* = E$, $\nu_* = \nu$, $A = 2g_s \times 2g_s = 4g_s^2$. The elastic prestressing ring is thin enough to satisfy the following relationship combining the displacement and the radial force: $u_* = n_0 R^2 / E_* A_*$, where E_* , A_* and u_* are the Young modulus of the ring, the area of the cross section, and the displacement, respectively.

2.3. Initial, boundary and continuity conditions

Two boundary problems are considered:

- A simply supported plate prestressed by the elastic ring, imposed with the initial fit D , which produces the initial radial force n_0 ($D \stackrel{\text{def}}{=} R_{\text{ring}} - R_{\text{plate}}$ denotes the difference of initial radii of the ring and plate, but some changes of the prestressing force n_0 result from the creep-damage process in the plate):

$$(2.13) \quad \begin{array}{ll} \text{for } \tau = 0 & \text{for } \tau > 0 \\ n_r(0) = n_\theta(0), & \dot{n}_r(0) = \dot{n}_\theta(0), \\ n_r(R) = -n_0, & \dot{n}_r(R)d\tau = dn_0, \\ D = \frac{R}{2G}[n_\theta(R) - \nu n_r(R)] - u_*, & dD = \frac{R}{2G}[\dot{n}_\theta(R) - \nu \dot{n}_r(R)]d\tau - du_* = 0, \\ m_r(R) = 0, & \dot{m}_r(R)d\tau = 0, \\ \varphi(0) = 0, & \dot{\varphi}(0) = 0, \\ f(R) = 0, & \dot{f}(R) = 0. \end{array}$$

- A clamped plate prestressed by the elastic ring, imposed with the initial fit D , which produces the initial radial forces n_0 :

$$(2.14) \quad \begin{array}{ll} \text{for } \tau = 0 & \text{for } \tau > 0 \\ n_r(0) = n_\theta(0), & \dot{n}_r(0) = \dot{n}_\theta(0), \\ n_r(R) = -n_0, & \dot{n}_r(R)d\tau = dn_0, \\ D = \frac{R}{2G}[n_\theta(R) - \nu n_r(R)] - u_*, & dD = \frac{R}{2G}[\dot{n}_\theta(R) - \nu \dot{n}_r(R)]d\tau - du_* = 0, \\ \varphi(0) = 0, & \dot{\varphi}(0) = 0, \\ \varphi(R) = 0, & \dot{\varphi}(R) = 0, \\ f(R) = 0, & \dot{f}(R) = 0, \end{array}$$

where $\varphi = -df/dr$ is the angular deflection of the plate, n_0 is the peripheral prestressing force, and u_* the peripheral radial displacement.

In both cases under consideration the prestressing problem might be classified as the mixed-type force-distortions, since neither the force nor the boundary displacement are explicitly given, but are results of interaction between the plate and the elastic ring. The stiffnesses of both elements eventually produce the response of the structure to the initial prestressing imposed.

2.4. Numerical algorithm for creep problem

Numerical algorithm for creep problem will be formulated in the most general case of the prestressed plate, of variable thicknesses of both the working layers and the core, which is subject to brittle creep rupture described by the orthotropic damage law. Problems of the plate under pure bending, or of the plate of constant thickness, appear as particular cases. Numerical procedure begins when the elastic solution is known. Assuming the shape of the structure in nodal points $[g_s, h_s]_j$, loadings, prestressing parameters and distortions $[n_0, e, m, \varphi_0]$, the continuity functions $[\psi_{r/\theta}^\pm]_j \equiv 1$ at the instant of time $\tau = 0$, we obtain the elastic solution by means of the Finite Difference Method (the Gauss elimination procedure applied to the matrix composed of five bands). First, the equation of membrane state is solved and the distribution of Airy function is found $[F]_j$. Then, the equation of bending state is solved providing the displacements $[f]_j$. When the displacements $[f]_j$ are known, the vector of elastic state $[u^e, \lambda_{r/\theta}^e, \varphi^e, k_{r/\theta}^e, \varepsilon_{r/\theta/z}^{e\pm}, \sigma_{r/\theta}^{e\pm}, n_{r/\theta}^e, m_{r/\theta}^e]_j$ is determined. Then the program enters the creep loop, which requires the vector of stress intensities, continuity functions and strain rates $[\sigma_i^\pm, \sigma_i^{net\pm}, \psi_{r/\theta}^\pm, \dot{\varepsilon}_{r/\theta/z}^{c\pm}]_j$. In consequence, when the right-hand sides of the equation systems $[\dot{n}_{r/\theta}^c, \dot{m}_{r/\theta}^c]_j$ are known, rates of change of both the Airy function $[\dot{F}]_j$ and displacements $[\dot{f}]_j$ vectors are found, and finally rates of the vector of state can be found $[\dot{u}, \dot{\lambda}_{r/\theta}, \dot{\varphi}, \dot{k}_{r/\theta}, \dot{\varepsilon}_{r/\theta/z}^\pm, \dot{\sigma}_{r/\theta}^\pm, \dot{n}_{r/\theta}, \dot{m}_{r/\theta}]_j$. In the next time step, applying the Runge–Kutta II method, the „new” vector of state is computed, and the program jumps at the beginning of the creep loop. Numerical procedure is repeated until the lowest value of the continuity functions reaches a certain level, and then the program quits the loop via the conditional statement.

The problem of a proper choice of both the spatial and the time steps, applied in integral procedures, requires some explanations. Magnitudes of both steps have been experimentally chosen. Number of the nodal points along the radius of the structure which does not influence the lifetime (the spatial step) is equal to 50. In case of the time step, it is necessary to introduce the variable step in order to be assured of the rates of continuity functions at the appropriate level 0.002–0.006. The time step is increasing during the primary creep, it does not change during the secondary creep, and is decreasing when the creep process enters the tertiary phase.

2.4. Optimality criteria, auxiliary conditions and decision variables

2.4.1. Optimality criteria

2.4.1.1. *Structures of uniform creep strength.* Structures of the uniform creep strength must satisfy the following local condition:

$$(2.15) \quad C(n+1) \int_0^{\tau_l} [\sigma_{\text{red}}(r_j, \tau)]^n d\tau = 1,$$

for all points $r_j \in \mathbf{v}$, or at least, along appropriate lines or surfaces to produce a rupture mechanism (cf. ŻYCZKOWSKI [17]). In case when the condition (2.15) is simultaneously fulfilled at all points of the structure, first macrocracks appear simultaneously everywhere, which defines “the structures of uniform creep strength with respect to brittle rupture”. Despite the fact that the condition of simultaneous damage may be satisfied for only one fibre of the uniform bending section (or for one working layer of the sandwich section), ŻYCZKOWSKI [17] suggests to use the term “the structures of uniform creep strength”, though “the structures of uniform creep strength in broader sense” seems to be more adequate in this case. On the other hand, assuming the orthotropic damage law and the sandwich section model, the structures of uniform creep strength fulfil the condition

$$(2.16) \quad \inf\{\psi_{r/\theta}^{\pm}(r_j)\} = 0, \quad r_j \in \mathbf{v}.$$

2.4.1.2. Structures optimal with respect to lifetime τ_l . In some particular cases, dependent of the nature of loadings and the mode of support (prestressed plate of constant thickness), it is not possible to achieve the uniform creep strength in the broader sense. Therefore, the optimization problem must be formulated on the basis of global condition:

$$(2.17) \quad \tau_l \rightarrow \max, \quad \mathbf{v} = \text{const},$$

or when a dual formulation is used:

$$(2.18) \quad \mathbf{v} \rightarrow \min, \quad \tau_l = \text{const}.$$

2.4.2. Constraints. The optimality criteria formulated above require appropriate constraints, which may take the following form:

A. Inequality constraints

- Strength constraints — the Huber–Mises–Hencky condition for nominal stress intensity:

$$(2.19) \quad \sqrt{(\sigma_r^{\pm})^2 - \sigma_r^{\pm} \sigma_{\theta}^{\pm} + (\sigma_{\theta}^{\pm})^2} \leq \sigma_0 / \mathbf{x},$$

where \mathbf{x} denotes a safety factor. The effect of material deterioration on σ_0 is not taken into account.

- Initial stability constraints — the elastic stability condition:

$$(2.20) \quad n_0 \ll n_E,$$

where n_E denotes the basic Eulerian force (a possibility of creep buckling has not been included into the analysis).

- The prestressing constraint of the maximal eccentricity e , such that the prestressing ring does not exceed the half-thickness of the structure

$$(2.21) \quad e_{\max} \leq h/2.$$

- The geometric constraint of the minimal thickness for the sandwich section, excluding a possibility of intersection of working layers:

$$(2.22) \quad h_s \geq h_{s_{\min}} = g_s.$$

B. Equality constraints

- The condition of constant volume:

$$(2.23) \quad \mathbf{v} = 2\pi \int_0^R [\alpha(h_s - g_s) + 2\beta g_s] r \, dr = \text{const},$$

$$\delta \mathbf{v} = 2\pi \int_0^R [\alpha(\delta h_s - \delta g_s) + 2\beta \delta g_s] r \, dr = 0,$$

where α, β are arbitrary weight factors for the core and layers materials, or

- The condition of constant lifetime:

$$(2.23') \quad \tau_I = \text{const}.$$

- The condition of constant surface loadings:

$$(2.24) \quad q_z = \text{const}.$$

2.4.3. Decision variables. Decision variables create appropriate vectors of control variables, defined as follows:

- For the membrane-type prestressing [n_0 or $\Delta, g_s(r), h_s(r)$], where n_0 is the initial prestressing force, Δ is the initial membrane distortion, and $g_s(r), h_s(r)$ are distributions of thicknesses of working layers and the core of the sandwich section;

- For the bending-type prestressing [m_0 or $\varphi_0, g_s(r), h_s(r)$], where m_0, φ_0 are the prestressing radial moment and the initial bending distortion.

2.5. Optimization methods

According to the previously presented optimality criteria, three numerical procedures of optimization have been suggested, all based on the iterative corrections of the vector of decision variables.

1. When the first procedure of optimization with respect to uniform creep strength under constant loadings and constant volume of a structure is used, increments of decision variables are chosen proportionally to the levels of continuity function (cf. GANCZARSKI [5, 8]):

$$(2.25) \quad \Delta g_{s_j} = \mathcal{P}_1 \Delta \psi_j - \Delta g_m, \quad \Delta h_{s_j} = \mathcal{P}_2 \Delta \psi_j - \Delta h_m, \quad \Delta \psi_j = 1 - \inf(\psi_{r/\theta}^\pm)_j,$$

where the average corrections $\Delta g_m, \Delta h_m$ must satisfy the constant volume condition

$$(2.26) \quad \Delta g_m = \frac{\sum_j \mathcal{P}_1 \Delta \psi_j x_j}{\sum_j x_j}, \quad \Delta h_m = \frac{\sum_j \mathcal{P}_2 \Delta \psi_j x_j}{\sum_j x_j},$$

whereas the step factors $\mathcal{P}_1, \mathcal{P}_2$ should be chosen experimentally. When the most general approach is used, thicknesses of the working layers g_s , and the core h_s , may be changed independently, but in this paper the proportional changes are assumed when $\zeta = g_s/h_s = 1/5$, and $\mathcal{P}_1 = \mathcal{P}_2 = \mathcal{P}$ is held such that the working layers to core depth ratio of the section is fixed and, in consequence, only one independent decision variable remains. The process of damage equalization is continued until the following condition is fulfilled:

$$(2.27) \quad \inf(\psi_{r/\theta}^\pm)_j \leq \text{EPSI} \cong 0 \quad \forall j.$$

2. When the procedure of optimization with respect to uniform creep strength under constant loading and prescribed lifetime τ_I is applied, a modification of the strategy

discussed above is proposed. At each optimization step k the volume is subsequently decreased according to the modified shape corrections:

$$(2.28) \quad \Delta g_{s_j} = \zeta \Delta h_{s_j} = -\mathcal{P}[\max(\Delta \psi_j) - \Delta \psi_j],$$

when $\tau_{1k} \geq \tau_1$, else the shape corrections are governed by (2.25) under the constant volume until the condition $\tau_{1k} = \tau_1$ is fulfilled.

3. Numerical procedure applied in case of optimization with respect to maximal lifetime τ_1 differs slightly from the approaches presented above as far as the global nature of the objective function is concerned. It starts from a vector of decision variables, for instance when the shape of constant thickness and parameters of prestressing equal to zero are presumed, and at the end of the creep process, the shape corrections are imposed under constant volume, according to the rule (2.25) as long as the global condition $\tau_{1k} > \tau_{1k-1}$ holds and the stability (2.18) and the geometric (2.19) constraints are satisfied. Then the procedure is stopped, since further thickness corrections (2.25) result in reducing the lifetime.

The first and second procedures suggested are essentially relevant to the concept of the full damage design method. This method leads to exact solutions optimal with respect to maximal lifetime when the following requirements are satisfied:

- a) structure is statically determinate,
- b) single loadings are applied,
- c) the geometry changes are neglected.

If the above assumptions are violated, the uniform creep strength solution occurs to be only an approximate "optimal solution". An exact one may be obtained when more rigorous optimization approaches are used. This kind of design method has been earlier used by ŚWISTERSKI *et al.* [14], when the optimal shape of a column with geometry changes taken into account has been sought in order to minimize the volume, when the time to rupture was fixed. The authors have concluded that some corrections of thickness superimposed on the shape of uniform creep strength may improve the solution, as far as time to rupture is concerned. However, SKRZYPEK and EGNER [13] proved that the disk of uniform creep strength under steady loadings (not prestressed) is the optimal one in the sense of the lifetime. On the other hand, the disk of partially uniform creep strength (with active lower geometric constraint) under unsteady loadings (prestressed) is not optimal, because appropriate additional corrections of thickness may lead to certain (practically negligible) increase of the lifetime. Therefore, the second assumption restricting the loadings to single ones, seems to be not essential, because in [13], the authors have considered structures under combined loadings.

3. Effect of the orthotropic deterioration process on the creep process

As it was previously mentioned, essential differences between the isotropic (2.8) and the orthotropic (2.9) formulations of the flow rule may appear only in case of a nonproportional path of loading. To support this hypothesis, some additional tests have been done. Namely, two plates of different support conditions: simply supported or clamped, have been considered (cf. Table 2). Moreover, all attempts of approximate estimation of the quotient $s_{kl}^{\text{net}}/\sigma_i^{\text{net}}$ show that terms associated with the damage mutually reduce. In case of the simple supported plate, both components of continuity parameters and stresses are approximately equal $\psi_r \cong \psi_\theta$, and $\sigma_r \cong \sigma_\theta$ at the central region of the plate, whereas

Table 2. Comparison of lifetime with respect to flow rule: isotropic or orthotropic.

Type of flow rule	support conditions	Lifetime
isotropic $\dot{\varepsilon}_{kl}^c = \frac{3}{2} \frac{\varepsilon_t^c}{\sigma_t} s_{kl}$	simply supported	$\tau_1 = 13.25$
orthotropic $\dot{\varepsilon}_{kl}^c = \frac{3}{2} \frac{\varepsilon_t^c}{\sigma_t^{\text{net}}} s_{kl}^{\text{net}}$	simply supported	$\tau_1 = 13.21$
isotropic $\dot{\varepsilon}_{kl}^c = \frac{3}{2} \frac{\varepsilon_t^c}{\sigma_t} s_{kl}$	clamped	$\tau_1 = 78.75$
orthotropic $\dot{\varepsilon}_{kl}^c = \frac{3}{2} \frac{\varepsilon_t^c}{\sigma_t^{\text{net}}} s_{kl}^{\text{net}}$	clamped	$\tau_1 = 78.97$

in the case of the clamped plate $0 \leftarrow \psi_r \ll \psi_\theta \cong 1$ and $|\sigma_r| \gg |\sigma_\theta|$ are observed at the clamped section of the plate. In both cases the effect of orthotropic damage on the isotropic or orthotropic creep is practically negligible (Table 2).

Therefore, the isotropic formulation of the creep flow rule (weak coupling between the deterioration and creep) is used for further analysis.

4. Examples

4.1. Plates of variable core depth of uniform creep strength or/and optimal with respect to lifetime under constant volume

4.1.1. Simply supported plates prestressed by the elastic ring. When the core depth of the plate is subject to optimization $h_s = \text{var}$, the terms associated with derivatives of membrane stiffness in Eqs. (2.1), (2.2) are omitted. Thus, the following mixed optimization problems are formulated:

- Either the distribution of core depth $h_s(r)$, and the parameter of initial prestressing n_0 are sought for under the constant volume constraint, such that the uniform creep strength (2.14) is achieved:

$$(4.1) \quad \inf\{\psi_{r/\theta}^\pm(h_s(r_j), n_0)\} = 0, \quad \forall r_j.$$

- Or, in case when the above criterion can not be fulfilled, the vector of decision variables which maximizes the lifetime (2.15), under the elastic stability (2.18), the constant volume (2.21), and the lower geometric (2.20) constraints, is sought

$$(4.2) \quad \tau_1(h_s(r_j), n_0) \rightarrow \max.$$

Starting from the solution obtained for nonprestressed plate ($n_0 = 0$), it is easily visible that almost the whole bottom working layer suffers damage with respect to the radial component of continuity function $\psi_r^\pm \cong 0$, except for a narrow zone where the geometric constraint is active (cf. Fig. 2). Therefore the plate is classified as the structure of partially uniform creep strength.

The improvement of the plate lifetime, compared to the plate of constant thickness, versus the initial prestressing force n_0 , is presented in Fig. 3. It is easy to notice that, at the beginning, the increase of the initial prestressing force causes the lifetime to grow. The lifetime reaches the maximum at point *C* where the force is $n_0/\sigma_0 R = -2.5 \times 10^{-3}$, and then it starts to decrease. Further attempts increase of prestressing ($n_0/\sigma R < -3.2 \times$

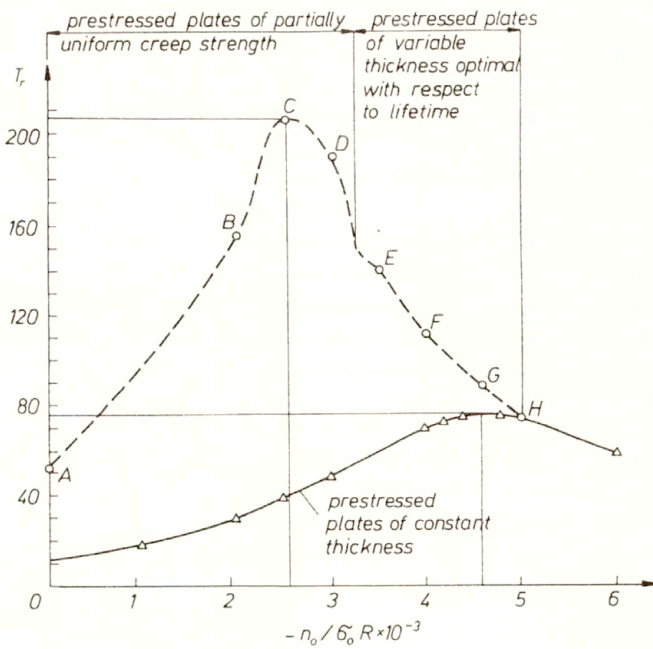


FIG. 3. Influence of initial prestressing force $n_0/\sigma_0 R$ on lifetime of simply supported plates optimally designed with respect to either uniform creep strength or maximal time to rupture (results for prestressed plates of constant thickness cf. GANCZARSKI and SKRZYPEK [6]).

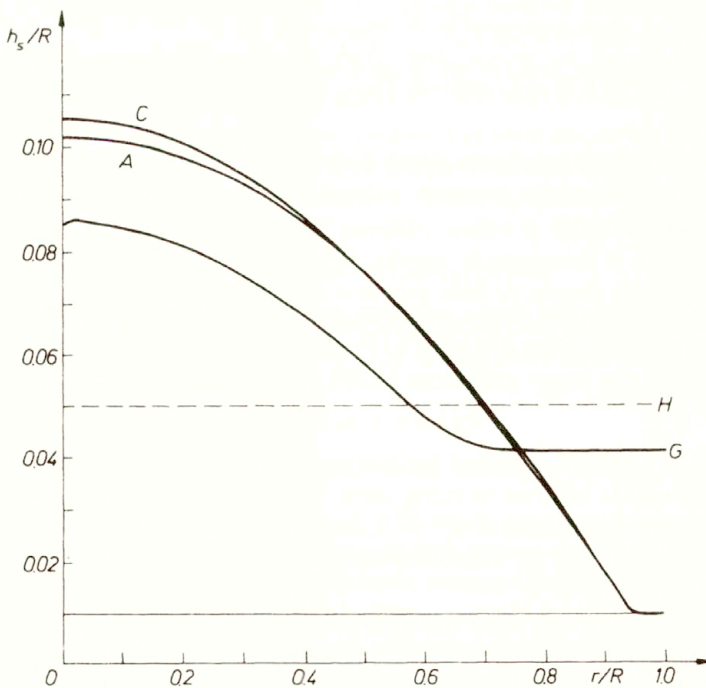


FIG. 4. Profiles of simply supported plates optimally designed with respect to either uniform creep strength or maximal time to rupture.

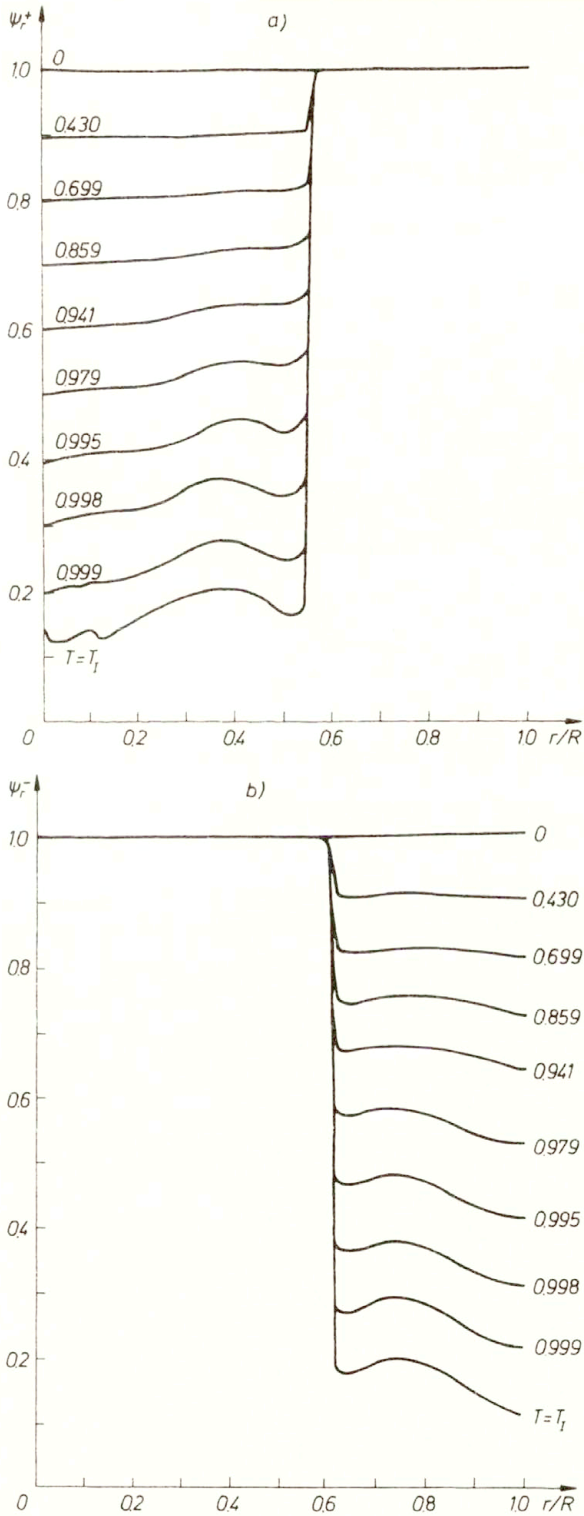


FIG. 5. Evolution of continuity functions for working layers: a) bottom ψ_r^+ , b) top ψ_r^- , in nonprestressed plate of partially uniform creep strength.

10^{-3}) leads to the optimization range where the criterion of maximum lifetime becomes predominant. Optimal profiles of the plate which correspond to selected points from Fig. 3 are shown in Fig. 4.

When the initial prestressing increases, the zones of constant thickness become thicker and broader. Finally, at point *H*, the zone of constant thickness is extended over the whole plate, and further thickness optimization becomes impossible.

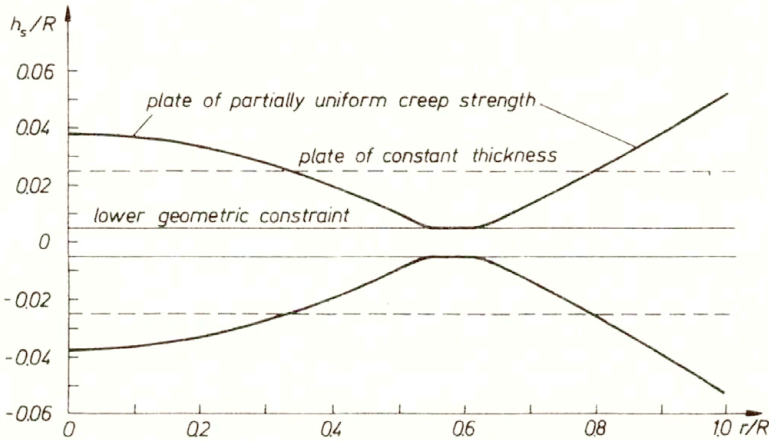


FIG. 6. Nonprestressed plate of partially uniform creep strength.

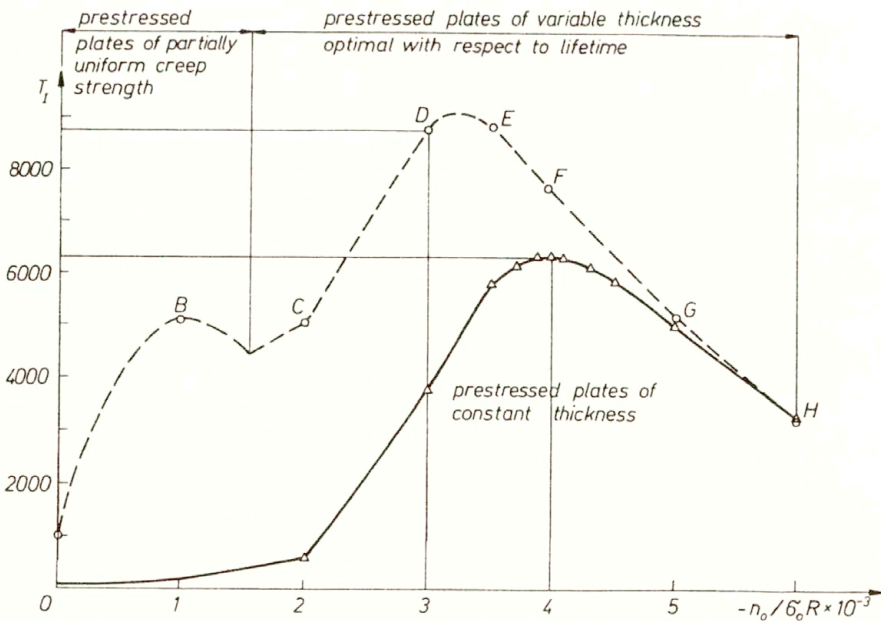


FIG. 7. Influence of initial prestressing force $n_0/\sigma_0 R$ on lifetime of clamped plates optimally designed with respect to either uniform creep strength or maximal time to rupture (results for prestressed plates of constant thickness cf. GANCZARSKI [8]).

4.1.2. Clamped plates prestressed by the elastic ring. Let us consider a clamped plate. It is easy to predict that two damage zones with respect to the radial component of the continuity function ψ_r , one in the top ψ_r^- and other in the bottom ψ_r^+ working layers, are produced. Typical evolution of continuity functions ψ_r^\pm for nonprestressed plate ($n_0 = 0$) has been shown in Fig. 5. The bottom $\psi_r^+ \cong 0$ and the top $\psi_r^- \cong 0$ damage zones are separated by a narrow zone where the geometric constraint is active. The optimal candy-shape plate of partially uniform creep strength is shown in Fig. 6. In case when both the thickness and the initial prestressing are subject to optimization, the lifetimes of optimal plates compared to the plates of constant thickness have been presented in Fig. 7. The solution is quantitatively similar to the one obtained for the simply supported plate, as far as a shift of the lifetime maximum towards lower magnitudes of initial forces when compared to the plate of constant thickness is observed. However, the range of initial prestressing where the structure should be optimized with respect to maximal lifetime is broader, the maximum maximum of the lifetime is found for $n_{0\text{opt}}/\sigma_0 R = -3.0 \times 10^{-3}$. The corresponding optimal profiles, approaching the shape of constant thickness when the magnitude of prestressing increases, are presented in Fig. 8.

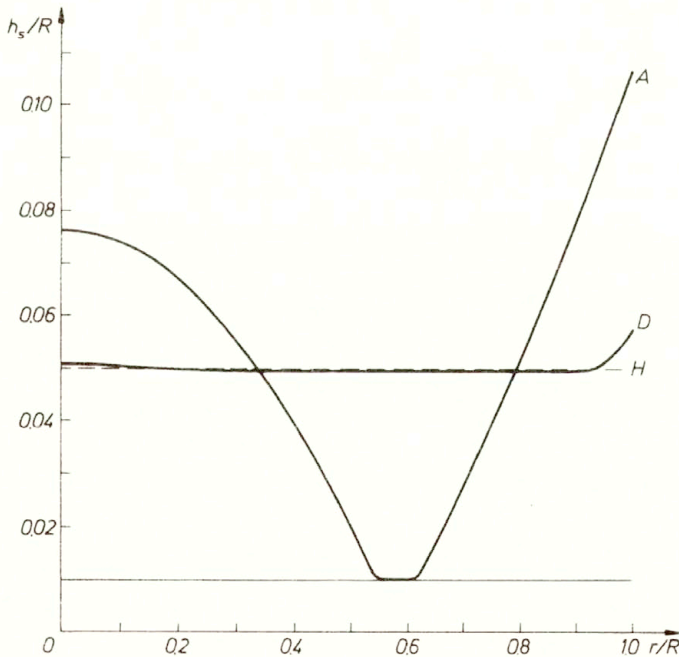


FIG. 8. Profiles of initially prestressed clamped plates optimally designed with respect to either uniform creep strength or maximal time to rupture.

4.2. Plates of variable core depth of uniform creep strength under constant lifetime

The case of design with respect to the uniform creep strength when the lifetime is prescribed, despite some numerical difficulties associated with necessity of using the shooting method, is important for practical applications. It allows us to reduce the volume of struc-

ture, which usually is the aim of optimal design. This subsection deals with optimization of a nonprestressed ($n_0 = 0$) simply supported plate, which has been described by Eqs. (2.1) and (2.2). The optimization problem, based on the local criterion 1, is formulated as follows: the distribution of the core $h_s(r)$, under prescribed lifetime and the geometric constraint (2.20), is sought for, such that the uniform creep strength is satisfied (2.14). The optimal shape of partially uniform creep strength, with the peripheral zone of active geometric constraint is shown in Fig. 9. Volume of the optimal plate has been reduced to 45% compared to the plate of constant thickness.

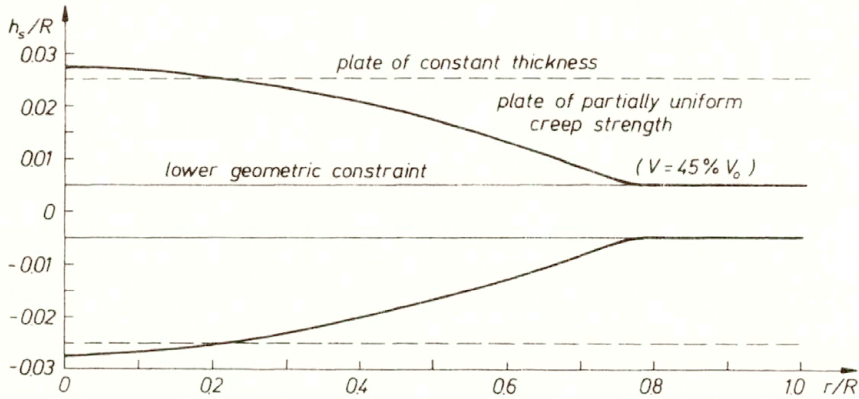


FIG. 9. Nonprestressed plate optimally designed with respect to uniform creep strength under prescribed lifetime (volume reduced to 45%).

4.3. Plates of uniform creep strength of variable thicknesses of both the core and working layers

All solutions shown so far, have dealt with plates of a variable core depth but constant thickness working layers ($g_s = \text{const}$). Hence the possibility of optimization with respect to membrane stiffness B_s has not been taken into account. This factor may lead to certain elongation of the lifetime, but the bending stiffness turned out to be predominant. Let us estimate the percentage of increase of the lifetime in case of optimization with respect to both parameters of sandwich section (g_s, h_s), to support the statement that the influence of working thickness layer variations on the lifetime is not too large, and significantly elongates the computer time. The nonprestressed simply supported plate, described by mixed formulation of system of equations (2.1), (2.2), is analyzed. In general, thicknesses of the core and working layers may change independently, but here the proportional variations of them $\zeta = g_s/h_s = 1/5$ have been assumed. This assumption not only allows to analyze one independent decision variable instead of two, for instance h_s , but also guarantees the constant ratio of working layers thickness to core depth. On the other hand, this assumption makes the lower geometric constraint (2.20) always passive, because thickness of working layers is changed proportionally to the thickness of the core, and working layers will never be in contact. Nevertheless, optimization of the core depth distribution $h_s(r)$, and simultaneously of the working layers thickness $g_s = \zeta \times h_s$, leads to structures of uniform creep strength (2.14) only when the constraint of constant volume (2.21) is applied. Additional troubles, when the problem formulated above is solved, deal

with a singularity of radial stress in the supported section of the plate. To overcome this problem, the de l'Hospital principle may successfully be used, because when the thickness approaches zero $h_s \rightarrow 0$, the infinite radial curvature $\kappa_r \rightarrow \infty$ is reached. The above inconvenience has been avoided by arbitrarily assumed minimum thickness constraint $h_s \geq h_{s0}/50$, where h_{s0} is the uniform plate core depth, and by the de l'Hospital principle associated with the backwards computed finite differences. The optimal shape of uniform creep strength, versus the profile of a jump-like variable thickness, is shown in Fig. 10 (cf. GANCZARSKI [5], also GANCZARSKI and SKRZYPEK [7]). At the instant of rupture, the whole bottom working layer is subject to damage with respect to radial continuity function $\psi_r^+ \cong 0$.

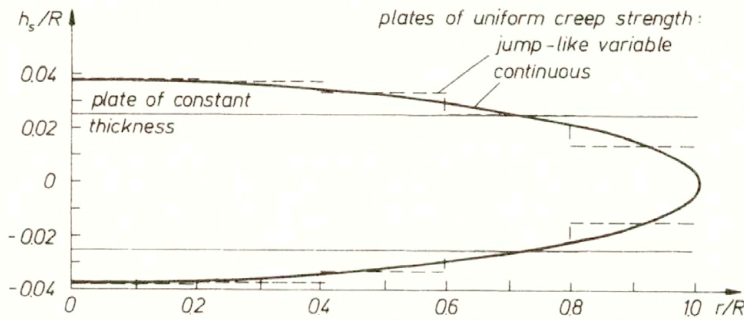


FIG. 10. Plates of uniform creep strength of jump-like variable and continuous thicknesses (case of variable thickness of both the working layers and the core).

Conclusions

1. Simultaneous thickness and prestressing optimization allow us to enhance significantly the lifetime, for both considered cases, simply supported or clamped, unless the magnitude of initial prestressing, which corresponds to the longest lifetime, $n_{0opt}/\sigma_0 R = -4.6 \times 10^{-3}$ in case of simply supported or $n_{0opt}/\sigma_0 R = -5.0 \times 10^{-3}$ in case of clamped plate, respectively, is exceeded.

2. Over-prestressing of the plate ($n_{0opt}/\sigma_0 R = -5.0 \times 10^{-3}$ in case of simply supported and $n_{0opt}/\sigma_0 R = -6.0 \times 10^{-3}$ in case of clamped plate) makes further thickness design impossible since structures of uniform thickness become optimal.

3. Simultaneous design of both the distribution of working layers thickness and the core depth (under constant ratio $\zeta = 1 : 5$ held) additionally enhances the lifetime, but the computation time highly increases.

4. Design with respect to the uniform creep strength when the lifetime is prescribed, furnishes the optimal profiles with enlarged zone of active lower geometric constraint, and it allows to reduce significantly the volume of the structure (up to 45%).

A general comparison of the lifetime for all considered cases of plates optimally prestressed or designed is presented in Tabl. 3.

Table 3. Comparison of the lifetimes for optimally prestressed or/and designed plates.

mode of support	reference plate $h_{s0}, n_0 = 0$	design variables		
		$h_{s\text{opt}}, n_0 = 0$ u.c.s.	$g_s/h_s = \zeta_{\text{opt}}, n_0 = 0$ u.c.s.	$h_{s\text{opt}}, n_{0\text{opt}}$ u.c.s.
simply supported	τ_1^s	3.94 τ_1^s (p.A-Fig.3)	6.19 τ_1^s (Fig.10)	15.84 τ_1^s (p.C-Fig.3)
clamped	$\tau_1^c = 5.97\tau_1^s$	u.c.s.	—	$\tau_1 \rightarrow \max$
		2.22 τ_1^c (p.A-Fig.7)		18.52 τ_1^c (p.D-Fig.7)

5. Summary

In the present paper, a wide class of boundary and prestressing problems is presented. The general equations of thin axisymmetric plates of variable thickness under the membrane-bending state is extended to the case of unsteady creep, with the material deterioration taken into account. The problem is written in the mixed form, the Airy and displacement functions being used. Two formulations of coupling between the deterioration and the creep processes are considered. Despite the damage process governed by the orthotropic law, the initially isotropic material is subject to either the isotropic creep (the scalar coupling between the deterioration and creep), or the orthotropic creep process (the tensorial-type coupling). It is shown that numerical differences between these two formulations are practically negligible when the proportional loadings are concerned. The appropriate joint numerical algorithm, based on the Finite Difference Method with respect to radial coordinate and the Runge–Kutta II with respect to time-steps, is used. The built-in optimization unit, which allows us to choose one of three optimization criteria: uniform creep strength when either the volume or lifetime are prescribed (the local approaches), or optimization with respect to maximal lifetime (the global approach), are used.

Acknowledgments

The authors want to express their appreciation to Professor M. ŻYCKOWSKI of the Cracow University of Technology who provided us with substantial suggestions concerning the formulation of coupling between the orthotropic rupture process and the modified creep flow rule (Sec. 3). Additionally, special appreciations are offered to Professor P. GUMBERT of Technical University of Berlin, and to Professor Z. MRÓZ of the Polish Academy of Sciences who provided us with many useful critical comments on the subject of this paper which influenced the final text. The paper was supported by the grant KBN-PB/233/D4/93/03.

References

1. J.L. ARMAND, *Applications of the theory of optimal control of distributed-parameter system to structural optimization*, NASA Report CR-2044, 1972.
2. Y.C. FUNG, *Foundations of solid mechanics* [Polish transl.], PWN, Warszawa, Chapter 16, 493–494, 1969.
3. A. GANCZARSKI and J. SKRZYPEK, *On optimal design of disks with respect to creep rupture*, Proc. IUTAM Symp. Creep in Struct., Springer Verlag, M. ŻYCKOWSKI [Ed.], 571–577, 1991.

4. A. GANCZARSKI and J. SKRZYPEK, *Optimal shape of prestressed disks against brittle rupture under unsteady creep conditions*, Structural Optimization, **4**, 47–54, 1992.
5. A. GANCZARSKI, *Optimal axially-symmetric plates subject to brittle creep rupture*, ZAMM, Z. angew. Math. Mech., **72**, 6, 543–546, 1992.
6. A. GANCZARSKI and J. SKRZYPEK, *Brittle rupture mechanisms of axisymmetric plates subject to creep under surface and thermal loadings*, Trans. 12-th Intern. Conf. on Structural Mechanics in Reactor Technology, Elsevier K.F. KUSSMAUL [Ed.], vol. L, 263–268, 1993.
7. A. GANCZARSKI and J. SKRZYPEK, *Axisymmetric plates optimally designed against brittle rupture*, Proc. The World Congress on Optimal Design of Structural Systems in Rio de Janeiro, vol. 1, 197–204, 1993.
8. A. GANCZARSKI, *Analysis of brittle damage and optimal design of prestressed axisymmetric structures in creep conditions under combined loadings*, PhD Thesis, Cracow University of Technology, 1993.
9. L.M. KACHANOV, *Introduction to continuum damage mechanics*, Martinus Nijhoff Publishers, Dordrecht, Boston, Lancaster 1986.
10. T. von KÁRMÁN, *Festigkeitsprobleme im Maschinenbau*, Encyklopadie der mathematischen Wissenschaften, Bd. IV, Vol. 4, Sect. 27, 349, 1910.
11. F.K.G. ODOVIST, *Mathematical theory of creep and creep rupture*, Oxford Mathematical Monographs, Clarendon Press, 1966.
12. R.K. PENNY, D.L. MARRIOTT, *Design for creep*, Maidenhead, McGraw Hill, Berkshire, England, 1971.
13. J. SKRZYPEK and W. EGNER, *On the optimality of disks of uniform creep strength against brittle rupture*, Engng. Opt., **21**, 4, 243–264, 1993.
14. W. ŚWISTERSKI, A. WRÓBLEWSKI and M. ŻYCZKOWSKI, *Geometrically non-linear eccentrically compressed columns of uniform creep strength vs optimal columns*, Int. J. Non-linear Mechanics, **18**, 4, 287–296, 1983.
15. S. TIMOSHENKO and J.N. GOODIER, *Theory of elasticity*, McGraw-Hill Book Company, Inc., 1951.
16. M. ŻYCZKOWSKI, *Optimal structural design under creep conditions*, Appl. Mech. Rev., **41**, 11, 453–461, 1988.
17. M. ŻYCZKOWSKI, *Recent advances in optimal structural design of shells*, Eur. J. Mech., A/Solids, 11, Special issue, 5–24, 1992.

CRACOW UNIVERSITY OF TECHNOLOGY, KRAKÓW.

Received January 21, 1994.

A viscoelastic boundary element formulation in time domain

*Dedicated to Professor Dr.-Ing. F. G. Kollmann
on the occasion of his 60th birthday*

L. GAUL (STUTTGART) and M. SCHANZ (HAMBURG)

THE BOUNDARY ELEMENT METHOD (BEM) provides a powerful tool for the calculation of elastodynamic response in the frequency and time domain. Field equations of motion and corresponding boundary and initial conditions are written in the form of integral equations. Other than in domain methods only the boundary is discretized. The boundary data often are of primary interest because they govern the transfer dynamics of the members and the energy radiation into the surrounding medium. Formulations of BEM currently include conventional viscoelastic constitutive equations in the frequency domain. In the present paper viscoelastic behaviour is implemented in a time domain approach as well. The constitutive equations are generalized by taking into account time derivatives of fractional orders. Previous paper of the authors on this subject was based on generation of a viscoelastic fundamental solution in the time domain. The present approach uses an analytical integration of the boundary integral equation in a time step. Viscoelastic constitutive properties are introduced by means of the elastic-viscoplastic correspondence principle and the Laplace transformation. The transient response is obtained by inverse transformation. Wave propagation in a 3-D viscoelastic continuum is studied numerically.

1. Introduction

THE CALCULATION of transient behaviour of 3 – D continua by boundary element formulations in the time domain is currently restricted to elastic solids. Viscoelastic solids are treated effectively by BEM in the frequency domain. Calculation of transient response via the frequency domain requires the inverse Fourier transform. Since the frequency response is known in a limited frequency range, truncation effects appear. On the other hand, direct calculation of viscoelastic solids in time domain requires the knowledge of viscoelastic fundamental solutions.

Such a solution can be obtained by means of an elastic-viscoelastic correspondence principle. In [7] the fundamental elastic solution has been transformed in the Laplace domain and then the elastic-viscoelastic correspondence principle has been adopted. For a simple rheological material model, an analytical inverse Laplace transformation is given. This leads to the viscoelastic fundamental solution in the time domain.

For the implementation of this viscoelastic fundamental solution in a 3 – D time domain BEM program it is advantageous to perform the time integration analytically in a time step. This has been carried out successfully in [11], but it leads to a very complicated series solution. An alternative approach to obtain a viscoelastic boundary integral formulation in time domain is presented by the authors in [6]. Generalization of this approach for constitutive equations with better curve fitting properties of the measured data is the aim of the present paper.

2. Constitutive equation

Decomposition of the stress tensor σ_{ij} into the hydrostatic part $\sigma_{kk}\delta_{ij}/3$ and the

deviatoric part s_{ij} yields

$$(2.1) \quad \sigma_{ij} = \frac{1}{3}\sigma_{kk}\delta_{ij} + s_{ij}, \quad \text{where} \quad s_{ii} = 0.$$

The corresponding decomposition holds for the strain tensor ε_{ij}

$$(2.2) \quad \varepsilon_{ij} = \frac{1}{3}\varepsilon_{kk}\delta_{ij} + e_{ij}, \quad \text{where} \quad e_{ii} = 0.$$

Two independent sets of constitutive equations for viscoelastic materials exist after this decomposition

$$(2.3) \quad \sum_{k=0}^N p'_k \frac{d^k}{dt^k} s_{ij} = \sum_{k=0}^M q'_k \frac{d^k}{dt^k} e_{ij}, \quad \sum_{k=0}^N p''_k \frac{d^k}{dt^k} \sigma_{ii} = \sum_{k=0}^M q''_k \frac{d^k}{dt^k} \varepsilon_{ii}.$$

More flexibility in fitting the measured data in a large frequency range is obtained by replacing the integer order time derivatives by the fractional order time derivatives [5].

The derivative of fractional order α is defined by

$$(2.4) \quad \frac{d^\alpha x(t)}{dt^\alpha} = \frac{1}{\Gamma(1-\alpha)} \frac{d}{dt} \int_0^t \frac{x(t-\tau)}{\tau^\alpha} d\tau, \quad 0 \leq \alpha < 1$$

with the Gamma function $\Gamma(1-\alpha) = \int_0^\infty e^{-x} x^{-\alpha} dx$ as the inverse operation of the fractional integration attributed to RIEMANN and LIOUVILLE [12]. A different definition based on generalized finite differences is given by GRÜNWARD [9]

$$(2.5) \quad \frac{d^\alpha x(t)}{dt^\alpha} = \lim_{N \rightarrow \infty} \left\{ \left(\frac{t}{N} \right)^{-\alpha} \sum_{j=0}^{N-1} \frac{\Gamma(j-\alpha)}{\Gamma(-\alpha)\Gamma(j+1)} x \left[t \left(1 - \frac{j}{N} \right) \right] \right\}.$$

This discrete definition is more convenient in constitutive equations solved by time stepping algorithms, and it can be shown to be equivalent to the definition in Eq. (2.4). The fractional derivative in Eqs. (2.4), (2.5) appear to be complicated in the time domain. However, the Laplace transform for vanishing initial conditions reveals the useful result

$$(2.6) \quad \mathcal{L} \left\{ \frac{d^\alpha x(t)}{dt^\alpha} \right\} = s^\alpha \mathcal{L} \{ x(t) \},$$

where s is the Laplace variable.

With the definitions (2.4) and (2.5), the generalized viscoelastic constitutive equations are given by

$$(2.7) \quad \sum_{k=0}^N p'_k \frac{d^{\alpha_k}}{dt^{\alpha_k}} s_{ij} = \sum_{k=0}^M q'_k \frac{d^{\alpha_k}}{dt^{\alpha_k}} e_{ij}, \quad \sum_{k=0}^N p''_k \frac{d^{\alpha_k}}{dt^{\alpha_k}} \sigma_{ii} = \sum_{k=0}^M q''_k \frac{d^{\alpha_k}}{dt^{\alpha_k}} \varepsilon_{ii}.$$

For $N = M = 1$ and integer time derivatives, the corresponding rheological model is given in Fig. 1 with two springs and a viscous dashpot. It shows one of the two possible

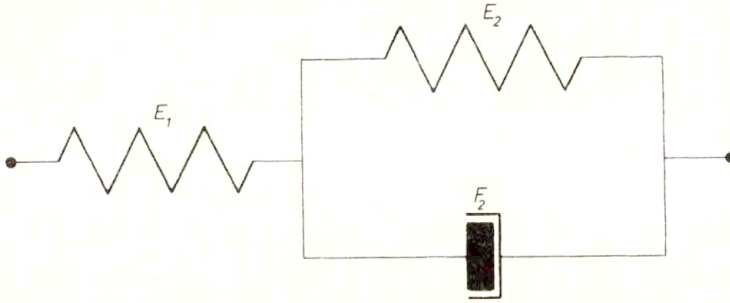


FIG. 1. Three parameter model.

representations of a uniaxial stress-strain equation

$$(2.8) \quad p \frac{d}{dt} \sigma + \sigma = E \left(\varepsilon + q \frac{d}{dt} \varepsilon \right),$$

with

$$(2.9) \quad p = \frac{F_2}{E_1 + E_2}, \quad E = \frac{E_1 E_2}{E_1 + E_2}, \quad q = \frac{F_2}{E_2}.$$

Application of fractional derivatives in the model leads to the generalized model with 5 parameters,

$$(2.10) \quad p \frac{d^\alpha}{dt^\alpha} \sigma + \sigma = E \left(\varepsilon + q \frac{d^\beta}{dt^\beta} \varepsilon \right).$$

The Second Law of Thermodynamics requires that [2]

$$(2.11) \quad \begin{aligned} E &\geq 0, & q &> p, \\ q &\geq 0, & \alpha &= \beta, \\ p &> 0. \end{aligned}$$

These constraints ensure nonnegative energy dissipation.

If the same damping mechanisms are assumed in the hydrostatic and deviatoric stress-strain states, the corresponding 3 – D constitutive equations are obtained by replacing the uniaxial stress and strain with the hydrostatic and the deviatoric states.

A powerful tool for calculating the viscoelastic behaviour from a known elastic response is the elastic-viscoelastic correspondence principle. According to this principle [4], the viscoelastic solution is calculated from the analytical elastic solution by replacing the elastic moduli in the Fourier or Laplace transformed domain with the transformed response functions of the viscoelastic material model. The viscoelastic solution is then obtained by inverse transformation.

For the above mentioned generalized three-parameter model the elastic-viscoelastic correspondence is given by

$$(2.12) \quad 3K \rightarrow 3K \frac{1 + q_K s^{\alpha_K}}{1 + p_K s^{\alpha_K}}, \quad 2G \rightarrow 2G \frac{1 + q_G s^{\alpha_G}}{1 + p_G s^{\alpha_G}},$$

where K is the elastic bulk modulus and G the elastic shear modulus. In Eq. (2.12) the transformation property (2.6) has been used.

3. Elastic BE-formulation

For completeness, let us recall the boundary integral equation of elastodynamics in the time domain [1]. The Lamé field equations of a homogeneous isotropic elastic domain Ω with boundary Γ are given by

$$(3.1) \quad (c_1^2 - c_2^2)u_{i,ij} + c_2^2 u_{j,ii} + b_j = \ddot{u}_j,$$

with displacement coordinate $u_j(x, t)$ and wave speeds

$$(3.2) \quad c_1^2 = \frac{K + \frac{4}{3}G}{\rho}, \quad c_2^2 = \frac{G}{\rho},$$

where ρ denotes the mass density. The corresponding traction and displacement boundary conditions are

$$(3.3) \quad \begin{aligned} t_{(n)i}(\mathbf{x}, t) &= \sigma_{ik}n_k = p_i(\mathbf{x}, t) & \mathbf{x} \in \Gamma_t, \\ u_i(\mathbf{x}, t) &= q_i(\mathbf{x}, t) & \mathbf{x} \in \Gamma_u, \end{aligned}$$

and the initial conditions are

$$(3.4) \quad \begin{aligned} u_i(\mathbf{x}, 0) &= u_{0i}(\mathbf{x}), \\ u_i(\mathbf{x}, 0) &= v_{0i}(\mathbf{x}), \mathbf{x} \in \Omega. \end{aligned}$$

The 3-D Stokes fundamental displacement tensor of the Lamé Equation (3.1) in an unbounded space, excited by the volume force $b_j(\mathbf{x}, \xi, t, \tau) = \delta(t - \tau)\delta(\mathbf{x} - \xi)e_j$ is given by (e.g. ERINGEN and SUHUBI [3])

$$(3.5) \quad \begin{aligned} \tilde{u}_{ij}(\mathbf{x}, \xi, t, \tau) &= \frac{1}{4\pi\rho} \left\{ \frac{t - \tau}{r^2} \left(\frac{3r_i r_j}{r^3} - \frac{\delta_{ij}}{r} \right) \left[H \left(t - \tau - \frac{r}{c_1} \right) - H \left(t - \tau - \frac{r}{c_2} \right) \right] \right. \\ &\quad \left. + \frac{r_i r_j}{r^3} \left[\frac{1}{c_1^2} \delta \left(t - \tau - \frac{r}{c_1} \right) - \frac{1}{c_2^2} \delta \left(t - \tau - \frac{r}{c_2} \right) \right] + \frac{\delta_{ij}}{rc_2^2} \delta \left(t - \tau - \frac{r}{c_2} \right) \right\}, \end{aligned}$$

where $r = \sqrt{r_i r_i}$, $r_i = x_i - \xi_i$ is the Euclidean distance between the field point \mathbf{x} and the load point ξ . Capital H denotes the unit step function, and δ the Dirac distribution. The corresponding fundamental stress vector components are obtained by substituting (3.5) into the constitutive equation and adopting Cauchy's stress formula with the outward normal n_k

$$(3.6) \quad \tilde{t}_{(n)ij} = \sigma_{ik}n_k = \rho(c_1^2 - 2c_2^2)\tilde{u}_{j m, m} \delta_{ik}n_k + \rho c_2^2(\tilde{u}_{ji, k}n_k + \tilde{u}_{jk, i}n_k).$$

The dynamic extension of Betti's reciprocal work theorem [8] combines two states of displacements and tractions, $(\tilde{u}_{ij}, \tilde{t}_{(n)ij})$ and $(u_j, t_{(n)j})$ respectively, and leads to the boundary integral equation

$$(3.7) \quad \begin{aligned} c_{ij}(\xi)u_j(\xi, t) &= \int_{\Gamma} [t_{(n)i}(\mathbf{x}, \tau) * \tilde{u}_{ij}(\mathbf{x}, \xi, t, \tau) - \tilde{t}_{(n)ij}(\mathbf{x}, \xi, t, \tau) * u_i(\mathbf{x}, \tau)]d\Gamma \\ &\quad + \int_{\Omega} \rho \{ b_i(\mathbf{x}, \tau) * \tilde{u}_{ij}(\mathbf{x}, \xi, t, \tau) + v_{0i}(\mathbf{x}) \cdot \tilde{u}_{ij}(\mathbf{x}, t) + u_{0i}(\mathbf{x}) \cdot \tilde{u}_{ij}(\mathbf{x}, t) \}d\Omega, \end{aligned}$$

where $c_{ij} = \delta_{ij}/2$ for a smooth boundary. The boundary integral is defined in the sense of a Cauchy principal value. The asterisk $*$ denotes the convolution with respect to time and is defined by

$$(3.8) \quad \Phi * \Psi = \begin{cases} 0, & t < 0, \\ \int_0^t \Phi(t - \tau)\Psi(\tau)d\tau, & t \geq 0. \end{cases}$$

The integral equation (3.7) will be reduced to an integral equation with boundary integrals only if the volume forces b_i and the initial conditions vanish. Discretization of the boundary integral equation in space and time leads to the boundary element formulation. Only the time discretization by introducing n equal steps Δt is discussed here. The simplest nontrivial choice ensuring that no terms of the fundamental stress vector such as derivatives of the Dirac distribution drop out in the boundary integral equation are linear shape functions for the displacements u_i and constant shape functions for the tractions $t_{(n)i}$ in time domain

$$(3.9) \quad u_i(\mathbf{x}, \tau) = \left(U_{il}^{m-1} \frac{t_m - \tau}{\Delta t} + U_{il}^m \frac{\tau - t_{m-1}}{\Delta t} \right) \eta_l(\mathbf{x}),$$

$$(3.10) \quad t_{(n)i}(\mathbf{x}, \tau) = \mathbf{1} \cdot T_{il}^m \cdot \mu_l(\mathbf{x}).$$

The spatial shape functions are denoted by $\eta_l(\mathbf{x})$ and $\mu_l(\mathbf{x})$. The nodal values are U_{il}^m, T_{il}^m for the corresponding boundary element Γ_l at time $t_m = m\Delta t$. Substitution of Eqs. (3.9), (3.10) reduces the boundary integral (3.7) to

$$(3.11) \quad \int_0^t \int_{\Gamma} [t_{(n)i}(\mathbf{x}, \tau) \cdot \tilde{u}_{ij}(\mathbf{x}, \xi, t - \tau) - \tilde{t}_{(n)ij}(\mathbf{x}, \xi, t - \tau) \cdot u_i(\mathbf{x}, \tau)] d\Gamma d\tau \\ = \sum_l \sum_{m=1}^n \int_{\Gamma_l} \int_{t_{m-1}}^{t_m} \left[\tilde{u}_{ij}(\mathbf{x}, \xi, t - \tau) \cdot \mathbf{1} \cdot \mu(\mathbf{x}) \cdot T_{il}^m \right. \\ \left. - \tilde{t}_{(n)ij}(\mathbf{x}, \xi, t - \tau) \cdot \eta_l(\mathbf{x}) \cdot \left(\frac{\tau}{\Delta t} (U_{il}^m - U_{il}^{m-1}) + U_{il}^{m-1} \frac{t_m}{\Delta t} - U_{il}^m \frac{t_{m-1}}{\Delta t} \right) \right] d\tau d\Gamma.$$

Analytical time integration of Eq. (3.11) can be carried out because of the time dependence of the Dirac and Heaviside functions. This integration leads to piecewise defined functions [15]. For the sake of brevity, the integration is indicated only for the first term on the right-hand side of Eq. (3.11)

$$(3.12) \quad \int_{t_{m-1}}^{t_m} \tilde{u}_{ij}(\mathbf{x}, \xi, t - \tau) d\tau \\ = \frac{1}{4\pi \varrho} \begin{cases} 0, & t < t_{m-1} + \frac{r}{c_1}, \\ f_0(r) \frac{1}{2} \left[(t - t_{m-1})^2 - \left(\frac{r}{c_1} \right)^2 \right] + f_1(r) \frac{1}{c_1^2}, & t_{m-1} + \frac{r}{c_1} < t < t_m + \frac{r}{c_1}, \\ f_0(r) \left[tt_m - tt_{m-1} - \frac{t_m^2}{2} + \frac{t_{m-1}^2}{2} \right], & t_m + \frac{r}{c_1} < t < t_{m-1} + \frac{r}{c_2}, \\ f_0(r) \left[tt_m - \frac{t_m^2}{2} - \frac{t^2}{2} + \frac{1}{2} \left(\frac{r}{c_2} \right)^2 \right] + f_2(r) \frac{1}{c_2^2}, & t_{m-1} + \frac{r}{c_2} < t < t_m + \frac{r}{c_2}, \\ 0 & t_m + \frac{r}{c_2} < t, \end{cases}$$

with the abbreviations depending only on spatial coordinates

$$\begin{aligned}
 f_0(r) &= \frac{3r_i r_j}{r^5} - \frac{\delta_{ij}}{r^3}, \\
 f_1(r) &= \frac{r_i r_j}{r^3}, \\
 f_2(r) &= \frac{\delta_{ij}}{r} - \frac{r_i r_j}{r^3}.
 \end{aligned}$$

The time intervals are valid only for the time step $\Delta t < [(r/c_2) - (r/c_1)]$. By substituting $t_m = m\Delta t, t_{m-1} = (m - 1)\Delta t$ and $t = n\Delta t$ in Eq. (3.12) it can be seen, that the functions depend on the difference $(n - m)$. This implies that the functions in (3.11) depend only on the difference between the observation and the excitation time. After time and space discretization with point collocation, a system of algebraic equations [15] is obtained

$$(3.13) \quad [0.5\mathbf{I} + \mathbf{T}] \mathbf{u} + \sum_{m=1}^{n-1} \mathbf{T}^{(n-m+1)(m)} \mathbf{u} = \sum_{m=1}^n \mathbf{U}^{(n-m+1)(m)} \mathbf{t},$$

where \mathbf{I} is the identity matrix, $\mathbf{T}^{(m)}$ and $\mathbf{U}^{(m)}$ are the influence matrices of stresses and displacements at the time step m . The vectors $\mathbf{u}^{(m)}$ and $\mathbf{t}^{(m)}$ contain all the nodal displacements and tractions of the time step m .

4. Viscoelastic BE-formulation

In order to obtain a viscoelastic boundary integral formulation from the elastic formulation (3.13), the elastic-viscoelastic correspondence principle (2.12) is applied. This requires the Laplace transformation of (3.13). The matrices in (3.13) consist of the functions (3.12) and the fundamental solutions of the tractions for all points ξ , after time integration. For the sake of brevity the procedure of deducing a viscoelastic formulation is explained for the integral (3.12) only.

The one-sided Laplace transformation

$$(4.1) \quad \mathcal{L}(f) = F(s) = \int_0^\infty f(t)e^{-st} dt, \quad f(t) = \frac{1}{2\pi i} \int_{x-i\infty}^{x+i\infty} F(s)e^{st} ds, \quad t > 0$$

leads to the transformation of the first term on the right-hand side of Eq. (3.11),

$$\begin{aligned}
 (4.2) \quad & \int_0^\infty \sum_{m=1}^n \int_{t_{m-1}}^{t_m} \tilde{u}_{ij}(\mathbf{x}, \xi, t - \tau) d\tau e^{-st} dt \\
 &= \frac{1}{4\pi \rho} \sum_{m=1}^n \left\{ \int_{t_{m-1} + \frac{r}{c_1}}^{t_m + \frac{r}{c_1}} \left[f_0(r) \frac{1}{2} \left((t - t_{m-1})^2 - \left(\frac{r}{c_1} \right)^2 \right) + f_1(r) \right] e^{-st} dt \right. \\
 & \quad + \int_{t_m + \frac{r}{c_1}}^{t_{m-1} + \frac{r}{c_2}} f_0(r) \left(tt_m - tt_{m-1} - \frac{t_m^2}{2} + \frac{t_{m-1}^2}{2} \right) e^{-st} dt \\
 & \quad \left. + \int_{t_{m-1} + \frac{r}{c_2}}^{t_m + \frac{r}{c_2}} \left[f_0(r) \left(tt_m - \frac{t_m^2}{2} - \frac{t^2}{2} + \frac{1}{2} \left(\frac{r}{c_2} \right)^2 \right) + f_2(r) \right] e^{-st} dt \right\}.
 \end{aligned}$$

After integrating over the time interval of (4.2), the elastic constants are replaced by the viscoelastic impact response functions. The elastic bulk and shear moduli appear only in the compression wave speed c_1 and the shear wave speed c_2 . Thus the corresponding viscoelastic expressions

$$(4.3) \quad \begin{aligned} c_{1v}^2 &= \frac{1}{\varrho} \left(K \frac{1 + q_K s^{\alpha_K}}{1 + p_K s^{\alpha_K}} + \frac{4}{3} G \frac{1 + q_G s^{\alpha_G}}{1 + p_G s^{\alpha_G}} \right), \\ c_{2v}^2 &= \frac{1}{\varrho} G \frac{1 + q_G s^{\alpha_G}}{1 + p_G s^{\alpha_G}}, \end{aligned}$$

are inserted in the integrated Eq. (4.2). After Laplace transformation this leads to

$$(4.4) \quad \begin{aligned} &\mathcal{L} \left(\sum_{m=1}^n \int_{t_{m-1}}^{t_m} \tilde{u}_{ij}(\mathbf{x}, \xi, t - \tau) d\tau \right) \\ &= \frac{1}{4\pi\varrho} \sum_{m=1}^n (e^{-st_{m-1}} - e^{st_m}) \left\{ f_0(r) \frac{1}{s^2} \left[\left(\frac{r}{c_{1v}} \right) e^{-\frac{r}{c_{1v}}s} - \left(\frac{r}{c_{2v}} \right) e^{-\frac{r}{c_{2v}}s} \right] \right. \\ &\quad \left. + f_1(r) \frac{1}{s} e^{-\frac{r}{c_{1v}}s} + f_2(r) \frac{1}{s} e^{-\frac{r}{c_{2v}}s} \right\}. \end{aligned}$$

Causality of the solution implies that no response is present prior to the arrival of the waves. This physical requirement is assumed for the numerical inversion of Eq. (4.4). The correspondence relation

$$(4.5) \quad F(s)e^{-st_{m-1}} - F(s)e^{-st_m} \bullet \rightarrow f(t - t_{m-1})H(t - t_{m-1}) - f(t - t_m)H(t - t_m)$$

is taken into account as well. The inverse transformation of (4.4) leads therefore to a function defined piecewise in the time ranges of Eq. (3.12). The inversion is carried out numerically by the method of Talbot [16].

5. Numerical example

The propagation of waves in a 3 - D continuum has been calculated by the present boundary element formulation in the time domain. The problem geometry and the associated boundary discretization are shown in Fig. 2.

Linear shape functions in space have been used. The free end is excited by a pressure jump according to a unit step function $H(t)$. The opposite end is fixed at the nodes. The time step size Δt has been chosen close to the time it takes for the viscoelastic compression wave to travel across the largest element.

The viscoelastic material data of a corning glass at 550°C are used (Fig. 2) in this example.

Figure 3 shows the longitudinal displacement in the center of the free end cross-section as a function of time for several values of the damping parameter q in the constitutive equation (2.8).

Wave reflections at the fixed and the free end appear. The viscoelastic wave speed of the compressional wave front is given by

$$(5.1) \quad c_{1v}^2 = \frac{1}{\varrho} \left(K \frac{q_K}{p_K} + \frac{4}{3} G \frac{q_G}{p_G} \right).$$

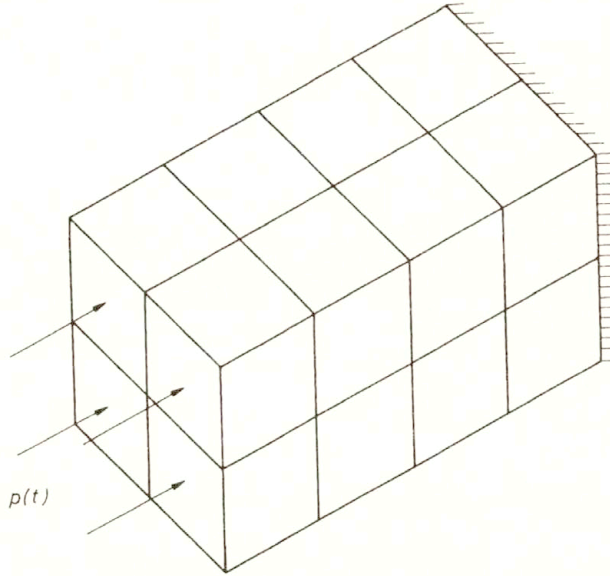


FIG. 2. Step function excitation of a 3-D rod by $p(t) = H(t) \text{ N/m}^2$. Geometric data: length = 4 m, height = 2 m, width = 2 m. Material data: $E = 2.075 \cdot 10^9 \frac{\text{N}}{\text{m}^2}$, $\nu = 0.25$, $\rho = 1000 \frac{\text{kg}}{\text{m}^3}$, $p_K = p_G = 3.5 \text{ sec}^{0.635}$, $\alpha_K = \alpha_G = 0.635$, $q_K = q_G = q \text{ sec}^{0.635}$.

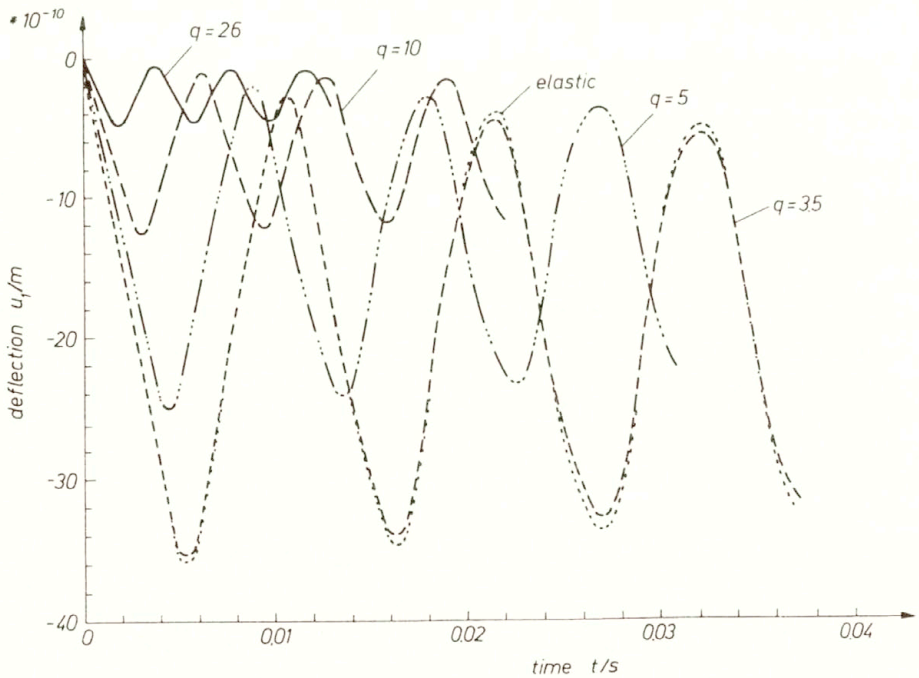
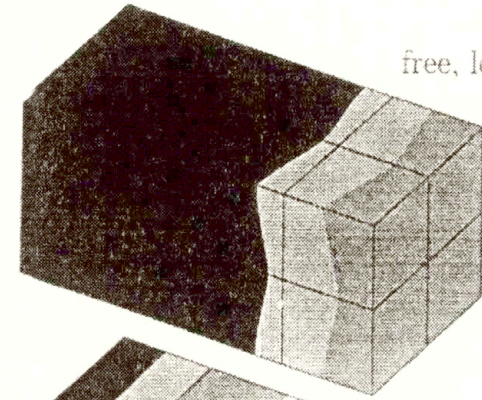


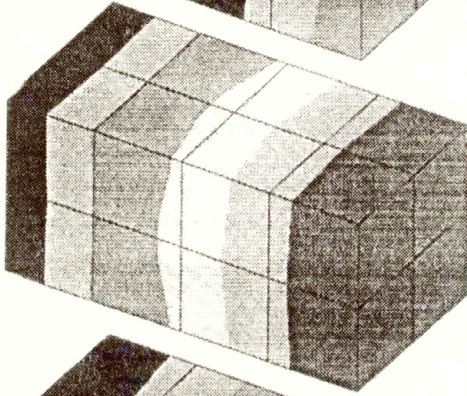
FIG. 3. Longitudinal displacement response in the middle of loaded cross-section.

fixed end

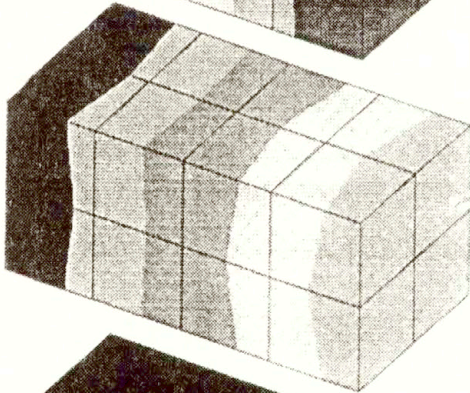
free, loaded end



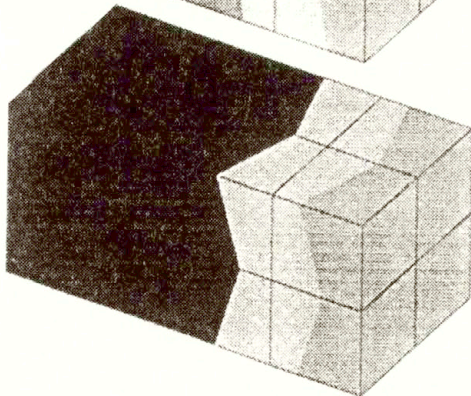
$i\Delta t = 2$



$i\Delta t = 5$



$i\Delta t = 13$



$i\Delta t = 15$



FIG. 4. Displacement fields of transient wave propagation at different time steps.

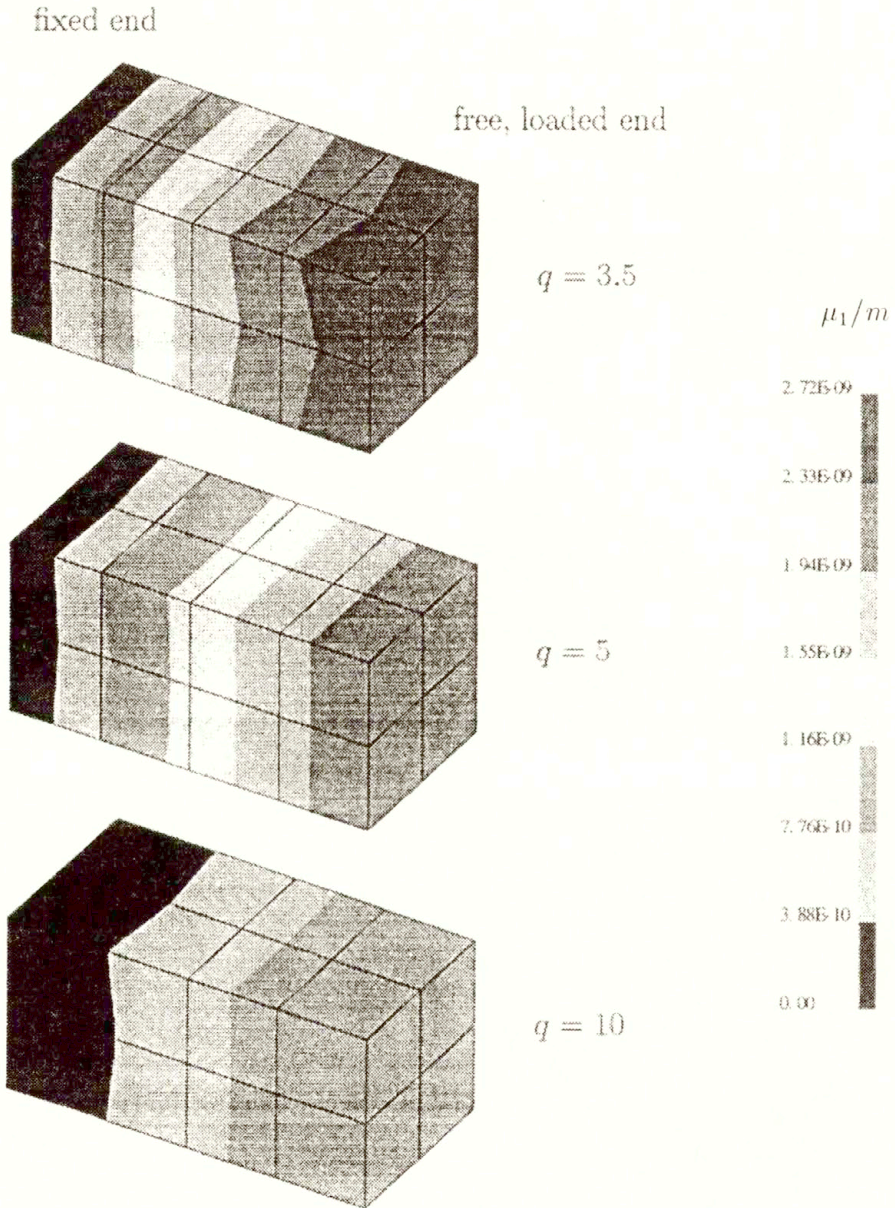


FIG. 5. Influence of variable damping coefficient in displacement field at a fixed time.

Increasing damping parameters q stiffen the solid and increase the wave speed. Shorter travel times show up in Fig. 3 and the stiffening leads also to smaller deflections. The displacement field of transient wave propagation at several time steps $i\Delta t$ is shown in Fig. 4. The wave starts to propagate at the left-hand side after loading in the first picture ($i\Delta t = 2$), between the second ($i\Delta t = 5$) and third picture ($i\Delta t = 13$) it is reflected at the fixed end of the bar. In the fourth picture ($i\Delta t = 15$) the wave has nearly reached

the free end of the bar. Compared with the analytical solution of the $1 - D$ rod [13], numerical damping is indicated in the $3 - D$ solution by amplitude decay. Instability due to the improper choice of time steps below the critical value in the elastic case is much less significant in the viscoelastic case [14]. The wave forms for fixed time step but for different damping coefficients q are shown in Fig. 5. As a result of stiffening by the viscous influence, a faster propagation of the wave front is detected.

6. Conclusions

So far published BEM formulations in elastodynamics calculate viscoelastic solids via the Laplace or Fourier transform domain. The elastic moduli are replaced by the corresponding viscoelastic moduli. The calculation of transient response in time domain requires inverse transformation [10] which is associated with truncation effects when the solution (e.g. in the frequency domain) is known in a limited frequency range only. To avoid this problem, the BEM formulation in time domain is derived in the present paper, which converts the elastic formulation to a viscoelastic one. It turned out to be advantageous to perform the conversion after integration over a time step Δt rather than to replace the elastic by viscoelastic one fundamental solution. The conversion is carried out by applying the elastic-viscoplastic correspondence principle in the Laplace domain. The inverse transformation is performed numerically and thus it allows to take general constitutive equations into account, including those with fractional time derivatives. The wave propagation in a viscoelastic rod is calculated by the BEM in the time domain. The material behaviour is described by a rheological three-parameter model which has been generalized by introducing two fractional time derivatives.

Acknowledgement

The subject of the paper is related to a research project on the BEM. Support by the Deutsche Forschungsgemeinschaft (DFG) is gratefully acknowledged.

References

1. H. ANTES, *Anwendungen der Methode der Randelemente in der Elastodynamik und der Fluidodynamik*, Mathematische Methoden in der Technik 9, B.G. Teubner, Stuttgart 1988.
2. R.L. BAGLEY and P.J. TORVIK, *On the fractional calculus model of viscoelastic behaviour*, J. Rheology, **30**, 1, 133–155, 1986.
3. A.C. ÉGINGEN and E.S. SUHUBI, *Elastodynamics*, Vol. II, Academic Press, New York, San Francisco, London 1975.
4. W. FLUGGE, *Viscoelasticity*, Springer-Verlag, New York, Heidelberg, Berlin 1975.
5. L. GAUL, P. KLEIN and S. KEMPFLE, *Damping description involving fractional operators*, Mechanical Systems and Signal Processing, **5**, 2, 81–88, 1991.
6. L. GAUL and M. SCHANZ, *BEM formulation in time domain for viscoelastic media based on analytical time integration*, Proc. 14th Boundary Element International Conference, vol. II, 223–234, Sevilla, Spain 1992.
7. L. GAUL, M. SCHANZ and C. FIEDLER, *Viscoelastic formulations of BEM in time and frequency domain*, Engng. Analysis with Boundary Elements, **10**, 137–141, 1992.
8. D. GRAFFI, *Über den Reziprozitätssatz in der Dynamik elastischer Körper*, Ingenieur Archiv, **22**, 45–46, 1954.
9. A.K. GRÜNWARD, *Ueber „begrenzte“ Derivationen und deren Anwendung*, Zeitschrift f. Mathematik u. Physik, **12**, 441–480, 1967.
10. P. KLEIN, *Zur Beschreibung der dynamischen Wechselwirkung von Fundamentstrukturen mit dem viskoelastischen Baugrund durch dreidimensionale Randelementformulierungen*, Bericht aus dem Institut für Mechanik, Universität der Bundeswehr, Hamburg, January 1990.

11. W.-D. MEIER, *Untersuchung zur analytischen Zeitintegration der Randintegralgleichung für ein viskoelastisches 3-D Kontinuum*, Institut für Mechanik, Fachbereich Maschinenbau, Studienarbeit, Universität der Bundeswehr, Hamburg 1992.
12. K.B. OLDHAM and J. SPANIER, *The fractional calculus*, Academic Press, New York, London 1974.
13. M. SCHANZ and L. GAUL, *Implementation of viscoelastic behaviour in a time domain boundary element formulation*, Appl. Mech. Rev., **46**, (11, Part 2), 41–46, 1993.
14. M. SCHANZ, L. GAUL and H. ANTES, *Numerical damping and instability of a 3-D BEM time-stepping algorithm*, [in:] Extended Abstracts of IABEM 93, Braunschweig 1993.
15. B. STEINFELD, *Numerische Berechnung dreidimensionaler Kontaktprobleme Bauwerk-Boden mittels zeitabhängiger Randintegralgleichungen der Elastodynamik*, Tech. Wiss. Mitteilungen Nr. 93–1, Ruhr-Universität, Bochum 1993.
16. A. TALBOT, *The accurate numerical inversion of Laplace transforms*, J. Inst. of Mathematics and its Applications, **23**, 97–120, 1979.

INSTITUTE A OF MECHANICS
UNIVERSITY OF STUTTGART, STUTTGART
and
INSTITUTE OF MECHANICS
UNIVERSITY OF THE FEDERAL ARMED FORCES, HAMBURG, GERMANY.

Received November 26, 1993.

Formulation of anisotropic equations by means of the theory of representations for tensor functions and the convective method of description

R. JOHN (DRESDEN) and H. BERGANDER (RADEBEUL)

THE PAPER is aimed at the derivation of constitutive equations of large elastic-plastic deformations of anisotropic materials. The constitutive theory of Y.F. Dafalias is discussed. Application of convective coordinates to the theory is presented leading to the final form of the constitutive equations.

1. Introduction

NUMERICAL METHODS in solid-state mechanics have gained general acceptance. The existing programs facilitate the calculation of physical and geometrical nonlinearities. In order to analyse the deformation behaviour and the corresponding stress distribution, extensive universal software has been developed. The constitutive equations have to determine the relations between the stresses and the strains.

The numerical programs, which are developed in the Department of Solid-State Mechanics of the T.U. in Dresden, are used to simulate geometrical nonlinearities. Because of some advantages in the formulation of mechanical relations, the material or convective method of description is used in our department. But the material subprograms have too many restrictions concerning the calculation of physical nonlinear problems.

The aim of this theoretical study is the development of constitutive equations for large elastoplastic deformations in the case of anisotropic material behaviour. The convective coordinates will be used.

First, the constitutive theory established by Y.F. DAFALIAS [1] will be analysed. In the second part, a short presentation of the convective way of description will be given. And in the last part, the final form of the constitutive equations will be presented.

2. Constitutive theory by Y. F. Dafalias

2.1. Special features

A constitutive theory for large elastoplastic deformations and anisotropic material behaviour was published by Y. F. DAFALIAS in 1987 [1]. Let us present three characteristic features of that theory.

1. All values which are used to describe the material behaviour, are collected in the concept of structure variables. Using this form for the derivation of the constitutive relations, it is possible to employ the theory of representation for tensor functions.

2. The question of non-uniqueness of the unstressed configurations is answered by the introduction of three different unstressed configurations. It is shown that the same result is obtained, independently of the choice of the relaxed configuration.

3. The basic line of thought is the distinction between the kinematics of the continuum and the kinematics of the underlying substructure, which was established by MANDEL in 1971 [2]. The spin of the substructure is defined as the difference between the material spin and the plastic spin. All rates of the kinematic variables must be expressed in terms involving the corotation with the substructural spin.

2.2. Structure variables

The introduction of structure variables in the constitutive relations is necessary for the description of the anisotropic material behaviour. The tensorial structure variables **S** can be either purely orientational or can be “evolving” tensors (with variable eigenvalues and eigenvectors). They are tensors of arbitrary order. Examples of structure variables are unit vectors or specific tensors, such as the back-stress tensor. A collection of the corresponding material behaviour is given in Table 1. The substructure is defined by the tensorial structure variables, but the spin of the substructure is in general not equal to the spin of these tensors.

Table 1. Structural tensors and the corresponding material behavior.

S	material behavior
scalar-valued or isotropic tensor	isotropic
$S_{\text{initial}} = \mathbf{0}$ and $S_{\text{subsequently}} \neq \mathbf{0}$ (S is an evolving tensor)	isotropic in reference to its initial unstressed configuration anisotropic with respect to subsequent relaxed configurations
all S have purely orientational character	initial symmetries persist in reference to subsequent unstressed configurations
S purely and non-purely orientational tensors	there are initial and evolving anisotropies

2.3. Definition of the unstressed configurations

There are three different unstressed configurations. By integration of the substructural spin it is possible to obtain a director-vector triad in each of these configurations. The orientation of this triad is expressed by the orthogonal tensor β . The definitions of the unstressed configurations are given in the Table 2. The configuration k_i was used by MANDEL [2]. Dafalias emphasises that, with respect to the decomposition of the rates of deformation and the spins, the configuration k_0 leads to clear relations.

Table 2. Definitions of the unstressed configurations.

	k_u	unstressed configurations	
		k_0	k_i
feature	arbitrary orientation	$F^e = V$	fixed orientation in reference to a global system
$F = F^e F^p$	$VR_u^e R_u^p U$ $F^e F^p$	$VR^{ep} U$ VP	$VR_i^e R_i^p U$ $F_i^e F_i^p$
rotation of the substructure	β_u	β	$\beta_i = I$
F_s	$VR_u^e \beta_u$ $F^e \beta_u$	$V\beta$	VR_i^e F_i^e
	$\beta_u \neq R_u^p$	$\beta \neq R^{ep}$	$\beta_i \neq R_i^p$

2.4. Application of the theory on the representation for isotropic tensor functions

Consider an anisotropic material represented by the constitutive relation

$$(2.1) \quad \sigma = f(\epsilon) \Rightarrow \sigma = f(\epsilon, \xi_i).$$

The second order tensor σ is a function of the second order tensor ϵ . The anisotropy results in a variation of σ with the orientation of ϵ with respect to the material. In order to specify these orientations, it is possible to introduce i material tensors ξ_i .

The principle of isotropy of space requires, that an arbitrary transformation \mathbf{Q} of the orthogonal group \mathbf{O} , applied to both the material and ϵ , should produce the same orthogonal transformation of σ

$$(2.2) \quad \forall \mathbf{Q} \in \mathbf{O} : f(\bar{\epsilon}, \bar{\xi}_i) = \bar{f}(\epsilon, \xi_i) \quad \bar{\epsilon} = \mathbf{Q}\epsilon\mathbf{Q}^T, \quad \bar{\xi}_i = \mathbf{Q}\xi_i\mathbf{Q}^T \quad \text{and} \quad \bar{f} = \mathbf{Q}f\mathbf{Q}^T.$$

This means that σ is an isotropic function with respect to ϵ and the material tensors ξ_i . Consider now the invariance group \mathbf{S} of the additional material tensors ξ_i

$$(2.3) \quad \bar{\xi}_i = \xi_i, \quad \mathbf{Q} \in \mathbf{S} \subset \mathbf{O}.$$

Using this relation we obtain

$$(2.4) \quad \forall \mathbf{Q} \in \mathbf{S} \subset \mathbf{O} : f(\bar{\epsilon}, \bar{\xi}_i) = \bar{f}(\epsilon, \xi_i),$$

where σ is an anisotropic function with respect to ϵ . The type of anisotropy is specified by the invariance group of the material tensors ξ_i . Table 3 shows the effect of different additional material tensors. The theory of representation for isotropic tensor functions ([3, 4 and 5]) is a powerful tool for the development of anisotropic constitutive equations.

Table 3. The effect of different additional material tensors.

additional arguments	invariance group	material characteristic
$\mathbf{v}_1, \mathbf{v}_2, \mathbf{v}_3$	\mathbf{I}	anisotropic
$\mathbf{M}_1 = \mathbf{v}_1 \otimes \mathbf{v}_1, \mathbf{M}_2 = \mathbf{v}_2 \otimes \mathbf{v}_2,$ $\mathbf{M}_3 = \mathbf{v}_3 \otimes \mathbf{v}_3$	$\mathbf{I}, \mathbf{R}_1, \mathbf{R}_2, \mathbf{R}_3$	orthotropic
$\mathbf{M}_3 = \mathbf{v}_3 \otimes \mathbf{v}_3$	$\mathbf{I}, \mathbf{R}_1, \mathbf{R}_2, \mathbf{R}_3$ rotations about \mathbf{v}_3	transverse isotropy

2.5. Constitutive law

In the sequel our attention will be focussed on the unstressed configuration k_u , since this is the most general one and suitable for the description in convective coordinates. The elastic relations are developed with respect to the unstressed configuration k_u .

ψ is the complementary free energy per unit mass, and Π is the stress tensor referred to the unstressed configuration. The equation

$$(2.5) \quad \mathbf{E}^e = \rho_u \frac{\partial \bar{\psi}}{\partial \Pi}$$

defines the elastic relation at k_u . By calculating the time derivative of (2.5) (use of the same corotational rates) and by transformation to the current configuration, one obtains the relation for the elastic rate of deformation

$$(2.6) \quad \mathbf{D}^e = \mathbf{D}^r + \mathbf{D}^c = \mathcal{L}^{-1} : \overset{\square}{\sigma} + \langle \lambda \rangle \mathbf{N}^c.$$

\mathbf{D}^r and \mathbf{D}^e represent the incrementally reversible and the elastoplastic coupling or damage components of \mathbf{D}^e at k . \mathcal{L} is the incrementally elastic modulus, $\overset{\square}{\sigma}$ the corodeformational rate and $\langle \lambda \rangle$ the loading index.

The yield criterion at the current configuration is given by

$$(2.7) \quad f(\sigma, \mathbf{s}) = 0, \quad \mathbf{N}^n = \left(\frac{\partial f}{\partial \sigma} \right)_{\mathbf{s}}$$

(it does not define a fixed yield surface in the stress space for given values of \mathbf{s} , because the \mathbf{s} change together with σ , due to elastic embedding). \mathbf{N}^n is the symmetric stress gradient with respect to the yield criterion. The rates of plastic deformation, the plastic spin and the corotational rates for the structure variables have the following form:

$$(2.8) \quad \begin{aligned} \mathbf{D}^p &= \langle \lambda \rangle \mathbf{N}^p(\Pi, \mathbf{S} \text{ in } k_u), \\ \mathbf{W}^p &= \langle \lambda \rangle \mathbf{\Omega}^p(\Pi, \mathbf{S} \text{ in } k_u), \\ \overset{\Delta}{\mathbf{S}} &= \langle \lambda \rangle \bar{\mathbf{S}}(\Pi, \mathbf{S} \text{ in } k_u). \end{aligned}$$

The specification of the loading index is possible by using the consistency condition

$$(2.9) \quad \mathbf{N}^n : \overset{*}{\sigma} + \frac{\partial f}{\partial \mathbf{s}} \cdot \overset{*}{\mathbf{s}} = 0.$$

The equations

$$(2.10) \quad \overset{\vee}{\sigma} = \Lambda : \mathbf{D}$$

and

$$(2.11) \quad \Lambda = \mathcal{L} - \bar{h}(\lambda) \frac{(\mathcal{L} : \mathbf{N}') \otimes (\mathbf{N} : \mathcal{L})}{H + \mathbf{N} : \mathcal{L} : \mathbf{N}^p + \mathbf{N}^n : \mathcal{L} : \mathbf{N}^c}$$

represent the final form of the constitutive relations. The basic structure of the elastoplastic moduli (2.11) is equal to that for small deformations. The loading direction is diverging from \mathbf{N}^n to \mathbf{N} .

3. Convective method of description

In the development of constitutive laws different ways of description are possible. In this paper the convective way of description [6] is preferred.

The coordinate values are firmly attached to the particle, so that the coordinate lines move along with the progressing deformation. The convective method of description is characterized by a time-dependent system of base vectors and by time-dependent metrics. It connects the material description with Eulerian tensors.

4. Constitutive equations in convective coordinates

4.1. Kinematics

The values Θ^μ characterize the material particle. The material line segment with respect to the reference, the current and the unstressed configuration is given by

$$\begin{aligned}
 d\mathbf{X} &= \mathbf{X}_{,\mu}d\Theta^\mu = \mathbf{G}_\mu d\Theta^\mu, \\
 d\mathbf{x} &= \mathbf{x}_{,\mu}d\Theta^\mu = \mathbf{g}_\mu d\Theta^\mu, \\
 d\mathbf{p} &= \mathbf{p}_{,\mu}d\Theta^\mu = \boldsymbol{\gamma}_\mu d\Theta^\mu.
 \end{aligned}
 \tag{4.1}$$

The multiplicative decomposition of the deformation gradient,

$$\begin{aligned}
 \mathbf{F} &= \mathbf{F}^e \mathbf{F}^p = \mathbf{V} \mathbf{R}^e \mathbf{R}^p \mathbf{U} = \delta^\mu{}_\nu \mathbf{g}_\mu \mathbf{G}^\nu, \\
 \mathbf{F}^e &= \delta^\mu{}_\nu \mathbf{g}_\mu \boldsymbol{\gamma}^\nu = V^{\mu\kappa} g_{\kappa\lambda} R^{e\lambda}{}_\nu \mathbf{g}_\mu \boldsymbol{\gamma}^\nu, \\
 \mathbf{F}^p &= \delta^\mu{}_\nu \boldsymbol{\gamma}_\mu \mathbf{G}^\nu = R^{p\mu}{}_\kappa G^{\kappa\lambda} U_{\lambda\nu} \boldsymbol{\gamma}_\mu \mathbf{G}^\nu,
 \end{aligned}
 \tag{4.2}$$

establishes the relations for the material line segment in different configurations. The rate of deformation \mathbf{L} is defined by

$$\mathbf{L} = \dot{\mathbf{F}}\mathbf{F}^{-1} = \dot{\mathbf{F}}^e \mathbf{F}^{e-1} + \mathbf{F}^e \dot{\mathbf{F}}^p \mathbf{F}^{p-1} \mathbf{F}^{e-1} = g_{\mu\kappa} L^\kappa{}_\nu \mathbf{g}^\mu \mathbf{g}^\nu.
 \tag{4.3}$$

Using the corotational rates, the relations

$$\begin{aligned}
 \mathbf{D}^e &= \left(\overset{\Delta}{\mathbf{F}}^e \mathbf{F}^{e-1} \right)_s, \\
 D_{\mu\nu}^e &= \frac{1}{2} (g_{\mu\kappa} L^\kappa{}_\nu - g_{\mu\kappa} P^\kappa{}_\nu + g_{\mu\kappa} \omega^{\kappa\lambda} \gamma_{\lambda\nu} \\
 &\quad + g_{\nu\kappa} L^\kappa{}_\mu - g_{\nu\kappa} P^\kappa{}_\mu + g_{\nu\kappa} \omega^{\kappa\lambda} \gamma_{\lambda\mu}),
 \end{aligned}
 \tag{4.4}$$

$$\begin{aligned}
 \mathbf{D}^p &= \left(\mathbf{F}^e \overset{\Delta}{\mathbf{F}}^p \mathbf{F}^{p-1} \mathbf{F}^{e-1} \right)_s, \\
 D_{\mu\nu}^p &= \frac{1}{2} (g_{\mu\kappa} P^\kappa{}_\nu - g_{\mu\kappa} \omega^{\kappa\lambda} \gamma_{\lambda\nu} + g_{\nu\kappa} P^\kappa{}_\mu - g_{\nu\kappa} \omega^{\kappa\lambda} \gamma_{\lambda\mu}),
 \end{aligned}
 \tag{4.5}$$

with $\dot{\mathbf{p}} = \dot{\mathbf{F}}^p \mathbf{F}^{p-1} \mathbf{p} = \mathbf{P} \mathbf{p}$ and $\boldsymbol{\omega} = \dot{\beta} \beta^{-1}$ represent the elastic and plastic rate of deformation. The elastic transformation of the structure variables

$$\begin{aligned}
 \mathbf{A} &= \det(\mathbf{F}^e)^w \mathbf{F}^{e-1} \mathbf{a} \mathbf{F}^{e-T}, \\
 A^{\mu\nu} &= \left(\frac{\sqrt{g}}{\sqrt{\gamma}} \right)^w a^{\mu\nu},
 \end{aligned}
 \tag{4.6}$$

and their increments from the unstressed to the current configuration

$$\begin{aligned}
 \overset{\Delta}{\mathbf{A}} &= \det(\mathbf{F}^e)^w \mathbf{E}^{e-1} \overset{\square}{\mathbf{a}} \mathbf{F}^{e-T}, \\
 &= \boldsymbol{\beta} (\boldsymbol{\beta}^T \mathbf{A} \boldsymbol{\beta})^\bullet \boldsymbol{\beta}^T, \\
 &= \dot{\mathbf{A}} + \mathbf{A} \boldsymbol{\omega} - \boldsymbol{\omega} \mathbf{A}
 \end{aligned}
 \tag{4.7}$$

characterize the elastic embedding. \mathbf{A} stands for a tensor of order two. The exponent w depends on the physical meaning of the structure variable (is it connected with a material line segment or not). If the stress $\boldsymbol{\sigma}$ varies in the current configuration without causing any plastic deformation, the \mathbf{F}^e varies due to the elastic deformation change. However, due to its elastic embedding, \mathbf{a} will vary in such a way that \mathbf{A} will remain constant.

In convective coordinates the transformations of the variables will differ by a scalar

factor only,

$$(4.8) \quad \begin{aligned} \hat{\Delta} A^{\mu\nu} &= \dot{A}^{\mu\nu} + P^\mu{}_\kappa A^{\kappa\nu} + A^{\mu\kappa} P^\nu{}_\kappa + A^{\mu\kappa} \gamma_{\kappa\lambda} \omega^{\lambda\nu} - \omega^{\mu\kappa} \gamma_{\kappa\lambda} A^{\lambda\nu}, \\ \hat{\Delta} A^{\mu\nu} &= \left(\frac{\sqrt{g}}{\sqrt{\gamma}} \right)^w \square a^{\mu\nu}. \end{aligned}$$

4.2. Kinetics

The coordinates of the elastic strain tensor are determined by

$$(4.9) \quad E_{\mu\nu}^e = \rho_u \frac{\partial \bar{\psi}(II^{\kappa\lambda}, S^{\rho\dots\vartheta})}{\partial II^{\mu\nu}}.$$

Equation (4.9) yields the corotational rate for the elastic strain

$$(4.10) \quad \begin{aligned} \hat{E}_{\mu\nu}^e &= \hat{E}_{\mu\nu}^r + \hat{E}_{\mu\nu}^c, \\ &= \mathcal{L}_{\mu\nu\kappa\lambda}^{u-1} \hat{II}^{\lambda\kappa} + \langle \lambda \rangle N_{\mu\nu}^{cu}, \end{aligned}$$

with respect to the unstressed configuration k_u . Transformation to the current configuration leads to the coordinates of the elastic rate of deformation

$$(4.11) \quad \begin{aligned} D_{\mu\nu} &= D_{\mu\nu}^r + D_{\mu\nu}^c, \\ &= \mathcal{L}_{\mu\nu\kappa\lambda}^{-1} \square \sigma^{\lambda\kappa} + \langle \lambda \rangle N_{\mu\nu}^c. \end{aligned}$$

The relation between the representations of the elastic moduli in different configurations is given by the formula

$$(4.12) \quad \mathcal{L}^{\mu\nu\kappa\lambda} = \frac{\sqrt{\gamma}}{\sqrt{g}} \mathcal{L}^{u\mu\nu\kappa\lambda}.$$

The coordinates of the elasto-plastic coupling term are in both configurations the same,

$$(4.13) \quad N_{\mu\nu}^c = N_{\mu\nu}^{cu}.$$

$N_{\mu\nu}^c$ depend on the corotational rates of the structure variables. The coordinates for the corodeformational rate $\square \sigma^{\mu\nu}$

$$(4.14) \quad \square \sigma^{\mu\nu} = \sigma^{\mu\nu} (L^\kappa{}_\kappa + P^\kappa{}_\kappa + \omega^{\kappa\lambda} \gamma_{\lambda\kappa}),$$

which take into account the corotation with the substructure and the elastic embedding, contain the coordinates of the substructural spin and the metric of the unstressed configuration. To analyse the whole problem it is necessary to define the coordinates of the plastic rate of deformation and the plastic spin

$$(4.15) \quad \begin{aligned} \hat{\Delta} S^{\mu\dots\xi} &= \langle \lambda \rangle \bar{S}^{\mu\dots\xi}(II^{\kappa\lambda}, S^{\rho\dots\vartheta} \text{ at } k_u), \\ D_{\mu\nu}^p &= \langle \lambda \rangle N_{\mu\nu}^p(II^{\kappa\lambda}, S^{\rho\dots\vartheta} \text{ at } k_u), \\ W_{\mu\nu}^p &= \langle \lambda \rangle \Omega_{\mu\nu}^p(II^{\kappa\lambda}, S^{\rho\dots\vartheta} \text{ at } k_u). \end{aligned}$$

With the yield criterion in the current configuration

$$(4.16) \quad f(\sigma^{\mu\nu}, s^{\rho\dots\vartheta}) = 0, \quad N_{\mu\nu}^n = \left(\frac{\partial f}{\partial \sigma^{\mu\nu}} \right)_s$$

and the consistency condition of the yield criterion it is possible to determine the loading index λ

$$(4.17) \quad \lambda = \frac{N_{\mu\nu} \mathcal{L}^{\nu\mu\kappa\lambda} D_{\lambda\kappa}}{H + N_{\mu\nu} \mathcal{L}^{\nu\mu\kappa\lambda} N_{\lambda\kappa}^p + N_{\mu\nu}^n \mathcal{L}^{\nu\mu\kappa\lambda} N_{\lambda\kappa}^c},$$

$$H = -\frac{\partial f}{\partial s^{\rho\dots\vartheta}} \bar{s}^{\rho\dots\vartheta}.$$

The final form of the constitutive law is given by

$$(4.18) \quad \overset{\vee}{\sigma}^{\mu\nu} = A^{\mu\nu\kappa\lambda} D_{\lambda\kappa},$$

$$A^{\mu\nu\kappa\lambda} = \mathcal{L}^{\mu\nu\kappa\lambda} - \bar{h}(\lambda) \frac{\mathcal{L}^{\mu\nu\eta\xi} N_{\xi\eta}^i N_{\vartheta\rho} N_{\rho\sigma} \mathcal{L}^{\rho\vartheta\kappa\lambda}}{H + N_{\eta\xi} \mathcal{L}^{\xi\eta\delta\zeta} N_{\zeta\delta}^p + N_{\eta\xi}^n \mathcal{L}^{\xi\eta\delta\zeta} N_{\zeta\delta}^c}.$$

In relation (4.18) the term $\overset{\vee}{\sigma}^{\mu\nu}$ denote the coordinates of Truesdell’s stress-rate

$$(4.19) \quad \overset{\vee}{\sigma}^{\mu\nu} = \dot{\sigma}^{\mu\nu} + \sigma^{\mu\nu} L_{\kappa}^{\kappa}.$$

The following relations hold for the expressions of the second part of Eq. (4.18)

$$(4.20) \quad N_{\mu\nu} = N_{\mu\nu}^n - Z^{n\lambda\kappa} \mathcal{L}_{\kappa\lambda\mu\nu}^{-1},$$

$$N_{\mu\nu}^i = N_{\mu\nu}^p + N_{\mu\nu}^c - \mathcal{L}_{\mu\nu\kappa\lambda}^{-1} Z^{p\lambda\kappa},$$

$$\bar{h}(\lambda) = 0 \quad \text{for } \lambda \leq 0,$$

with

$$(4.21) \quad Z^{p\mu\nu} = -(\sigma^{\mu\kappa} N_{\kappa\lambda}^p g^{\lambda\nu} + g^{\mu\kappa} N_{\kappa\lambda}^p \sigma^{\lambda\nu}) + (\sigma^{\mu\kappa} \Omega_{\kappa\lambda}^p g^{\lambda\nu} - g^{\mu\kappa} \Omega_{\kappa\lambda}^p \sigma^{\lambda\nu} + N_{\kappa\lambda}^p g^{\lambda\kappa} \sigma^{\mu\nu}),$$

$$\Gamma^{\mu\nu} = -(\sigma^{\mu\kappa} N_{\kappa\lambda}^n g^{\lambda\nu} + g^{\mu\kappa} N_{\kappa\lambda}^n \sigma^{\lambda\nu}) + N_{\kappa\lambda}^n \sigma^{\lambda\kappa} g^{\mu\nu} + \Gamma^{\mu\nu},$$

$$\Gamma^{\mu\nu} = -\left(s^{\kappa\dots\mu} \frac{\partial f}{\partial s^{\kappa\dots\lambda}} g^{\lambda\nu} + g^{\mu\kappa} \frac{\partial f}{\partial s^{\kappa\dots\lambda}} s^{\nu\dots\lambda} \right) + w \frac{\partial f}{\partial s^{\kappa\dots\lambda}} s^{\kappa\dots\lambda} g^{\mu\nu}.$$

Now the constitutive relations are complete. Further studies are necessary to apply these relations written in convective coordinates to various types of materials.

References

1. Y.F. DAFALIAS, *Issues on the constitutive formulation at large elastoplastic deformations, Part 1. Kinematics, Part 2. Kinetics*, Acta Mechanica, **69**, 119–138, 1987; **73**, 121–146, 1988.
2. J. MANDEL, *Plasticité classique et viscoplasticité*, Courses and Lectures, 97, Intern. Center for Mechanical Sciences, Springer, Udine-Wien-New York 1971.
3. C.-C. WANG, *A new representation theorem for isotropic functions: an answer to Professor G.F. Smith’s criticism of my papers on representations for isotropic functions*, Arch. Rational Mech. Anal., **36**, 166–223, 1970.
4. J. P. BOEHLER, *A simple derivation of representations for non-polynomial constitutive equations in some cases of anisotropy*, ZAMM, **59**, 157–167, 1979.

5. J. P. BOEHLER [Ed.], *Applications of tensor functions in solid mechanics*, Courses and Lectures, 292, Springer Verlag, 1987.
6. H. BERGANDER, *Deformationsgesetze der Standardform in konvektiver Metrik*, Technische Mechanik, **8**, 31–40, 1987.

INSTITUTE FOR SOLID-STATE MECHANICS
TU DRESDEN, GERMANY.

Received January 31, 1994.

On nonconvex problems in the theory of plasticity

M. S. KUCZMA^(*) and E. STEIN (HANNOVER)

THIS PAPER presents a brief review of published results of experimental studies in which nonconvex yield surfaces were obtained and results of micromechanical investigations of the elastic-plastic behaviour of metal matrix composites. For such a class of nonconvex problems a variational inequality formulation is proposed. The variational inequality expresses the general, intrinsic features of the elastic-plastic deformation process and may be interpreted as a weak formulation of the loading/unloading criteria of the flow theory of plasticity. This formulation covers the case where the yield function is nonconvex and which can be defined as a non-smooth multisurface yield function in Koiter's sense. The proposed formulation constitutes a natural basis for the global projection within elastic predictor/plastic corrector algorithms.

1. Introduction

THERE IS a broad class of problems in the theory of plasticity which are nonconvex and/or nondifferentiable [8, 18, 36, 54, 58, 65, 73]. These problems are of great practical importance due to the demands of modern, high-developed industries to use new materials and structural elements that could work at severe loading and temperature regimes, e.g. fibre composites or perforated structural elements.

The deformation process of elastoplastic materials is a very complex phenomenon which can be analysed at different length scales. In practice some reasonable compromise must be found, hence the mathematical models being usually used are based on many assumptions and simplifications. Over the last three decades a lot of efforts have been made to describe the elastic-plastic deformation process more precisely. The volume of the literature is very extensive. We mention here only some representative examples of works which illustrate a variety of issues involved and approaches applied in modelling the behaviour of elastic-plastic materials. Many sophisticated concepts have been employed in developing constitutive models [2, 6, 13, 28, 32, 34, 38, 47, 48, 49, 60, 69] and new algorithms have been proposed for the numerical solution of the corresponding boundary value problems [51, 45, 53, 59, 66, 72].

In the flow theory of plasticity the concept of a yield (or loading) function is fundamental. Normally, one assumes that the yield function is convex. This assumption is very advantageous in the thermomechanical consideration of the process, and seems to be crucial for the numerical algorithms developed for plasticity problems [66]. In fact, for the generalized standard model developed by HALPHEN and NGUYEN [20], the assumption of a convex yield function and a convex potential function allows one to satisfy automatically the second principle of thermodynamics. But convexity of a yield function need not be assumed *a priori*, it should be rather regarded as an additional constitutive assumption, see GREEN and NAGHDI [17] or HILL [22]. Guided by the principles of thermodynamics, Green and Naghdi have shown that star-shaped yield surfaces in stress space are pos-

(*) On leave from the Technical University of Poznań, Poland. The work of M.S.K. was supported by the European Communities under the grant *ERB-CIPA-CT-922073*. This support is gratefully acknowledged.

sible. In this context it should be mentioned that the well-known and useful postulate of DRUCKER [12] and that of ILYUSHIN [25], which imply convexity of a yield surface under the assumption of small strains, are not unconditionally valid but rather can only provide for classification of material behaviour, as was shown by HILL and RICE, cf. [23], and restated by NEMAT-NASSER [50]; for an extension of Drucker's postulate, see also PANAGIOTOPOULOS [55]. It is also worthy to note that the general anisotropic yield condition proposed by HILL [21] "to account for the so-called anomalous behaviour of some materials" can be nonconvex for many combinations of the defining parameters [71]. Moreover, it may be noted that there is some ambiguity in the practical implementations of the notion of yield surface, e.g. PHILLIPS and SIERAKOWSKI [57] have distinguished between a yield surface and a loading surface, and also HILL [21] has differentiated between surfaces related to an elastic limit and to a plastic limit. This reflects to some extent the fact that the experimental determination of a yield surface for a given material is a complex task as it is subject to some unavoidable disturbances.

The behaviour of real materials subjected to complex loading histories is quite complicated as has been recently revealed in many computer-controlled experimental investigations, using improved and accurate experimental techniques [7, 8, 11, 18, 34]. The main difficulties arise due to plastic anisotropy which is a common feature of commercial metals or can be induced by a deformation process. Experimentally determined subsequent yield surfaces for metals exhibit translation and changes in size and shape, including non-affine distortion. However, it should be noted that the definition of the yield point strongly affects the experimental results on subsequent yield surfaces. In the literature, the generally adopted definitions are based on: (a) departure from linearity, (b) strain-offset and (c) backward extrapolation method. In many experimental investigations, especially on materials with sharp yield point, the offset method is used, although the drawn conclusions on the existence of nonconvex yield surfaces may be doubtful. A comprehensive survey of experimental results in plasticity was given by IKEGAMI [24], and by MICHNO and FINDLEY [44]. For additional references on plastic anisotropy, the conference proceedings edited by BOEHLER [4] and BESDO and STEIN [3], and the paper by SZCZEPIŃSKI [70] can be consulted.

Analysis of non-smooth multisurface plasticity was initiated by KOITER [29, 30] forty years ago, and further advanced by MANDEL [42]. MAIER, see e.g. [41], has applied the mathematical programming approach to elastoplasticity problems with piecewise linear yield surfaces, this approach was also used to the so-called slackened systems by GAWEŃKI [16]. An integration algorithm for a singular yield function was proposed by DE BORST [5]. SIMO *et al.* [67] have carried out a systematic analysis of the computational aspects of non-smooth multisurface plasticity and viscoplasticity and developed a closest-point-projection algorithm for this sort of problems.

The variational approach to many problems in solid mechanics provides the most natural framework that takes into account all specific features of the problem. Usually, the energy functionals encountered in mechanics are differentiable and convex. Convexity of a functional is a required property since it assures, in principle, the existence and uniqueness (for strict convexity) of a solution to the corresponding boundary value problem. Differentiability being a measure of smoothness of a function is another restrictive requirement which, from mechanical considerations of many practical problems, can be weakened drastically. Yet, there are many practical problems in mechanics, e.g. unilateral contact problems and problems in plasticity where one may consider only unilateral variations of

some quantities governing the problem. The unilateral problems can be efficiently dealt with by means of the theory of variational inequalities, as presented by DUBAUT and LIONS [14] and ODEN [52]. The theory of variational inequalities is, on the other hand, closely connected to the notion of subdifferential, introduced in the 1960's by MOREAU, see e.g. [46], and ROCKAFELLAR, cf. [64]. The mechanical notion of superpotential covers the case of generally nondifferentiable but convex energy functions. The requirement of convexity of the superpotential poses a restriction on subdifferential laws to be monotone. But in engineering practice, many constitutive laws are not monotone, e.g. the behaviour of granular media, or can be properly described by nonconvex models, e.g. the behaviour of composites or materials with phase transitions.

A general approach to nonconvex and nondifferentiable functions has been developed in the 1970's by CLARKE [9] and ROCKAFELLAR [63]. This approach hinges also on convexity, i.e. instead of local linearization of a function at a given point on its graph one looks for convexification at this point. Clarke showed how it can be done automatically. These mathematical ideas have been introduced into mechanics by PANAGIOTOPOULOS, see e.g. [56]. KIM and ODEN [26, 27] have studied nonconvex problems in finite elastoplasticity for the so-called materials of *Type N*, i.e. materials which obey the (generalized) normality rule.

Our aim in this paper is twofold: first, by way of motivation, to show some evidence of nonconvex problems in the theory of plasticity; and second, to provide a new variational inequality formulation for a class of problems of this type. The variational inequality is derived directly from the very basic requirement of the theory of plastic flow that

$$(1.1) \quad F \leq 0, \quad \dot{\lambda} \geq 0, \quad F \cdot \dot{\lambda} = 0.$$

For (a yield function) F being a function of $\dot{\lambda}$, $F = F(\dot{\lambda})$, Eqs. (1.1) constitute the so-called complementarity problem [10], which is in general nonlinear. In the particular case when F is an affine function of $\dot{\lambda}$, Eqs. (1.1) are called a *linear complementarity problem*. As will be shown later, conditions of type (1.1) are equivalent to a variational inequality. The formulation based on this observation was applied lately for a convex differentiable elastic-plastic problem by KUCZMA and WHITEMAN [31]. The layout of the paper is following. In the next section we shall briefly review problems in which nonconvex yield surfaces were obtained. In Sec. 3 we define a general mechanical model of the elastoplastic deformation process and develop the variational formulation. Some remarks close the paper. Selected concepts of nonlinear functional analysis that are useful in approaching the problem are summarized in an appendix.

2. Nonconvex problems in plasticity

In this section we shall briefly review both the available results of experimental tests and the results of theoretical considerations on micromechanical modelling of fibre composites in which nonconvex yield surfaces were obtained. Complete details are contained in the references cited below.

2.1. Experimental results

Plastic behaviour of initially anisotropic metals was experimentally investigated by SHIRATORI *et al.* in the 1970's, cf. [65]. The authors tested, among others, tubular speci-

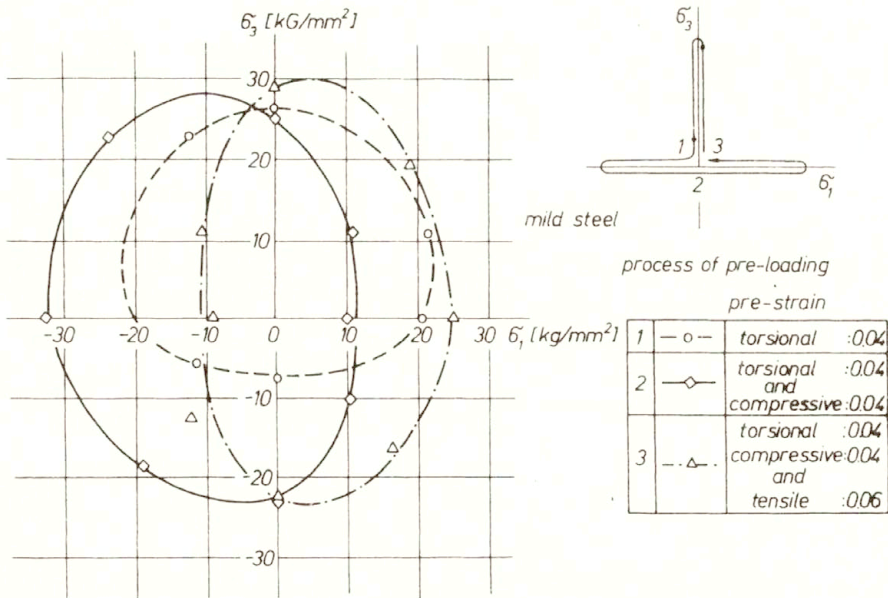


FIG. 1. Subsequent yield curves after prestraining along stress paths displayed in the figure, obtained by SHIRATORI *et al.* [65]. A concavity can be seen in the yield locus defined by (- Δ -) or (- ◊ -) points.

mens of mild steel by applying various prestraining and reloading paths, and taking the von Mises effective stress/effective strain relation. The yield surfaces was determined by the stress points corresponding to the offset strain of 0.0002. Figure 1 shows the results they obtained for a tubular specimen of mild steel in reloading under combined torsional and axial prestrainings. The results were approximated by convex curves, although some concavity of the yield locus can be seen in the zone opposite the last prestraining in the cases denoted with symbols (- Δ -) and (- ◊ -). ŻYCZKOWSKI and KURTYKA [74] represented these experimental results also by convex curves, using a geometrical description of anisotropic hardening, see Fig. 2. On developing the description the authors [74] employed Ilyushin's postulate of anisotropy and defined the subsequent yield surfaces in a generalized Ilyushin space. The general functions they arrived at for the distorted yield surfaces may be nonconvex; in the above example, a simplified (convex) version was applied.

In 1983 GUPTA and LAUERT [18] published the results of their experiments on subsequent yield surfaces of annealed mild steel, Ck-15. The experiments were performed on tubular specimens, using an automated machine with computer interface. The yield points were determined in all four quadrants of normal-shear stress plane according to a regular pattern of probing (16 points on each yield surface). The specimens were analysed in annealed condition and after having been prestrained by 10% in pure tension. The offset definition of yield-point was adopted. The subsequent yield surfaces they obtained for the prestrained specimen, when taking different values of offset, are shown in Fig. 3. For the values of offset equal to 1×10^{-4} and 2×10^{-4} , a vertex can be seen in the direction of prestraining, accompanied by a reentrant corner in the opposite direction, where the yield curve becomes nonconvex. LEHMANN [33] is seemed to be the first who attempted to explain and describe the phenomenon observed by Gupta and Lauert. He proposed

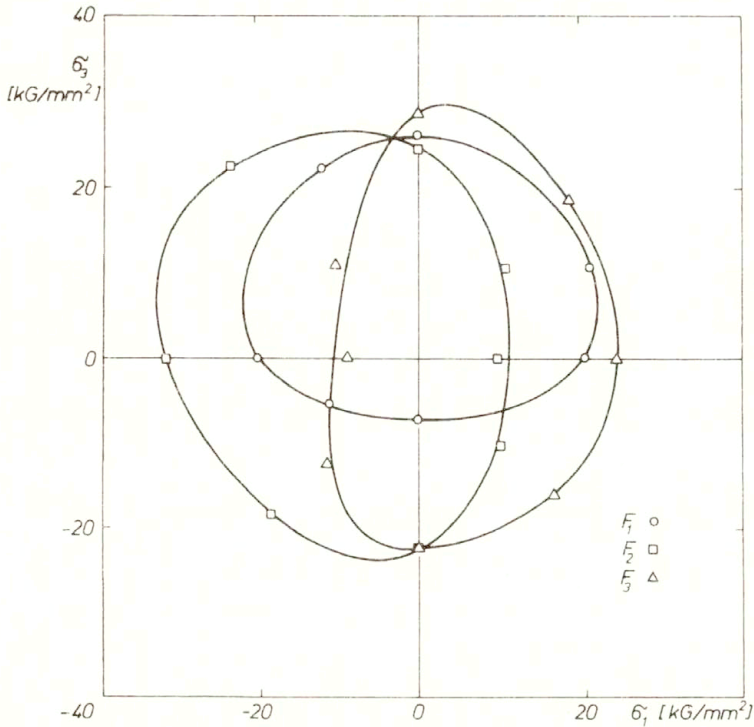


FIG. 2. ŻYCKOWSKI and KURTYKA'S [74] approximation of the experimental results of SHIRATORI *et al.* [65].

a constitutive law with two yield mechanisms that leads to a nonconvex resulting yield surface (cf. Fig. 4). A yield function that accounts for prestrain and is based on one yield mechanism was proposed by GUPTA and MEYERS [19]. The proposed relation is a function of second and third invariants of the shifted deviator stress tensor and can generate nonconvex functions, see MEYERS [43].

The similar material, i.e. an annealed mild steel with comparable composition, was earlier tested in a series of experiments by MICHNO and FINDLEY, cf. [44]. The yield surfaces they obtained were convex and smooth. Michno and Findley determined yield points adopting also the offset definition, but used a rather random sequence of probing, and constructed the resulting yield surface as an approximating curve of 30 to 40 probes. In the discussion paper [15], these authors have attempted to find out possible reasons for the differences between their results and the results of GUPTA and LAUERT [18]. As an explanation of the findings of GUPTA and LAUERT [18], FINDLEY and MICHNO [15] pointed out a possibility of reverse yielding on unloading to zero from the first 10% straining, followed by the ordered sequence of probing of local yield points. According to the authors' opinion, this resulted in that "each of the 16 probes represents only one point on 16 different subsequent yield surfaces caused by yielding under each "probing". A critical discussion about the existence of the vertices and concavities in Gupta and Lauert's experiments, and the explanations of FINDLEY and MICHNO [15] has been recently given by SUPRUN [68]. It was showed in [68] that also the experimental results of MICHNO and FINDLEY [15] represent a yield surface with the pointed vertex and cusp, like that of

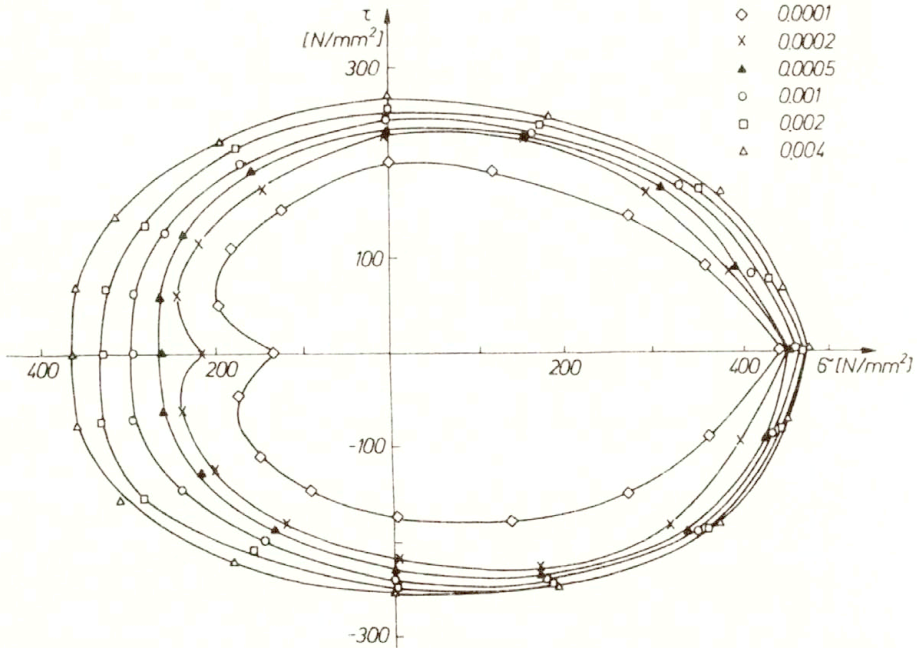


FIG. 3. Experimentally determined yield curves for the mild steel specimen prestrained of 10% in tension, due to GUPTA and LAUERT [18]. Different symbols stand for different values of strain offset given in inset.

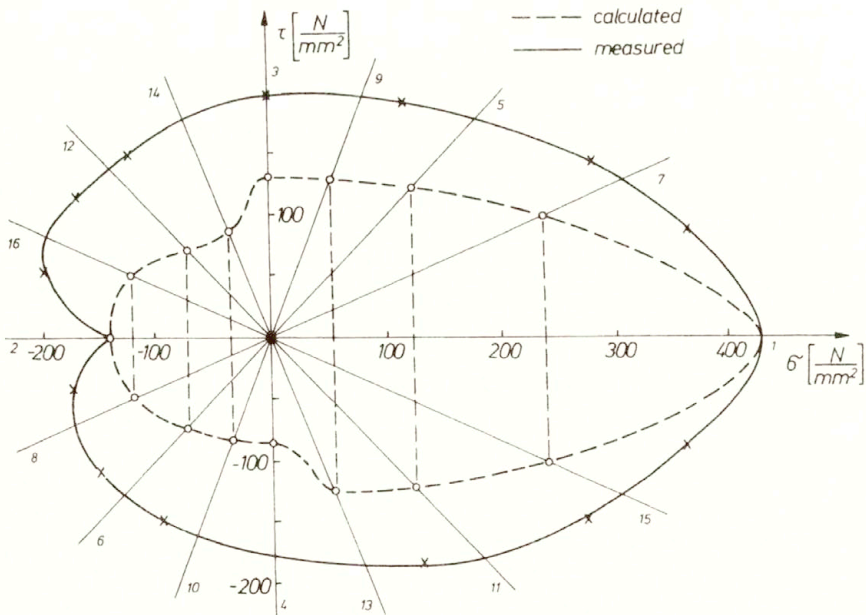


FIG. 4. Lehmann's nonconvex approximation of the experimental results of GUPTA and LAUERT [18], from LEHMANN [33]. $\varepsilon_{\text{off}} = |\varepsilon'_k|_{\text{max}} \times 10^{-4}$, $\zeta = 9.3 \cdot 10^5 \text{ N/mm}^2$, $\varkappa = 10 \cdot 10^{-6} \text{ mm/N}$, $l = 145 \text{ N/mm}^2$.

GUPTA and LAUERT [18], if the yield surface were defined only by the first 12 yield points. Suprun has emphasized the role of time effects in the deformation process and claimed, at some variance to FINDLEY and MICHINO [15], that the 16 points represent one point on 16 different yield surfaces, but this is mainly due to the process of recovery or return of the surface. According to his suggestion, the theory of viscoplasticity could be a remedy for the situation considered.

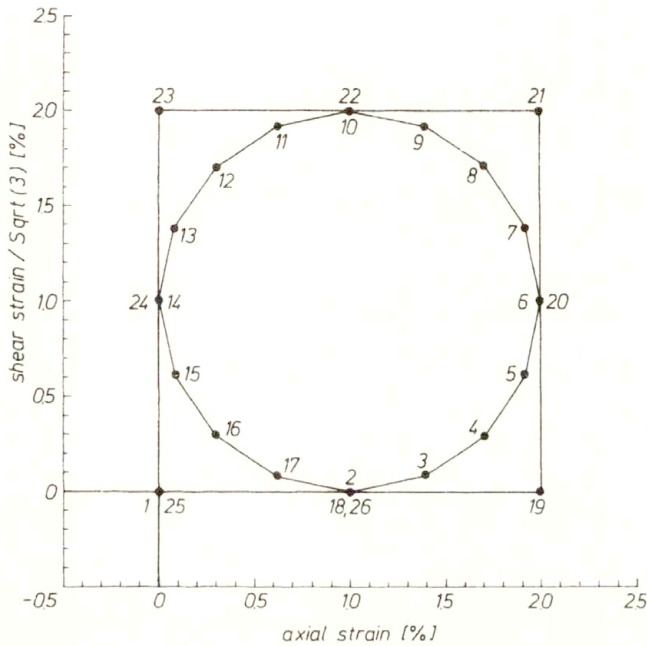


FIG. 5. Polygonal and square strain paths applied by CHENG and KREMPL [8]. The numbers indicate the stations or prestrain points from which yield surface probing can start.

CHENG and KREMPL [8] have recently reported interesting results of their detailed experimental studies on yield surfaces of an Al/Mg alloy. The experiments were conducted on tubular specimens, using a servohydraulic computer-controlled axial-torsion testing machine. In determining yield curves, the offset definition was used, with a plastic offset strain of 1×10^{-4} , and 16 probes radially emanating from a base point. Long and complex, nonproportional loading paths were examined, cf. Fig. 5. Yield surfaces in stress space as well as in strain space were determined. The yield surfaces experimentally determined by 16 yield points were then smoothed with cubic spline curves by the least square method. The whole experiment and data postprocessing were performed by the computer. The subsequent yield surfaces obtained by CHENG and KREMPL in [8] exhibit the characteristic features: translation, change in shape and size and a cross-effect. Figure 6 (Fig. 12 in [8]) illustrates the effect of prior history on the subsequent yield surfaces at the same prestrain point. The increase in size and the characteristic front part and the flattened rare part with a small concavity can be observed.

Finally, it should be noted that a pronounced concavity of the yield surface was reported a long time ago in experiments involving high hydrostatic pressure by BRIDGMAN (1955) and VERESHCHAGIN and SHAPOCHKIN (1960), cf. LEVITAS [35]. Following Levitas

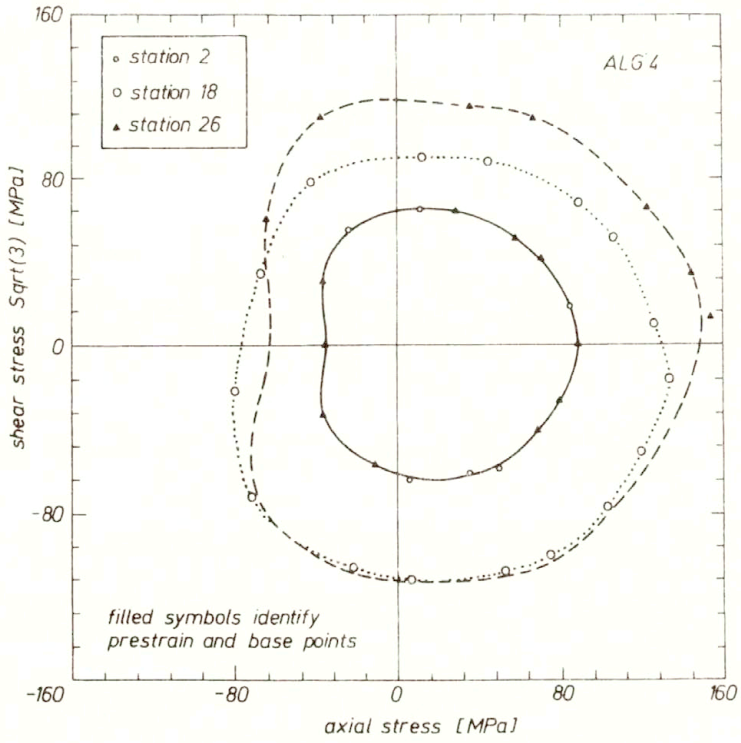


FIG. 6. From CHENG and KREML [8]. Smoothed yield surfaces of specimen ALG4 at the same point in strain space but with different prior history (cf. Fig. 5).

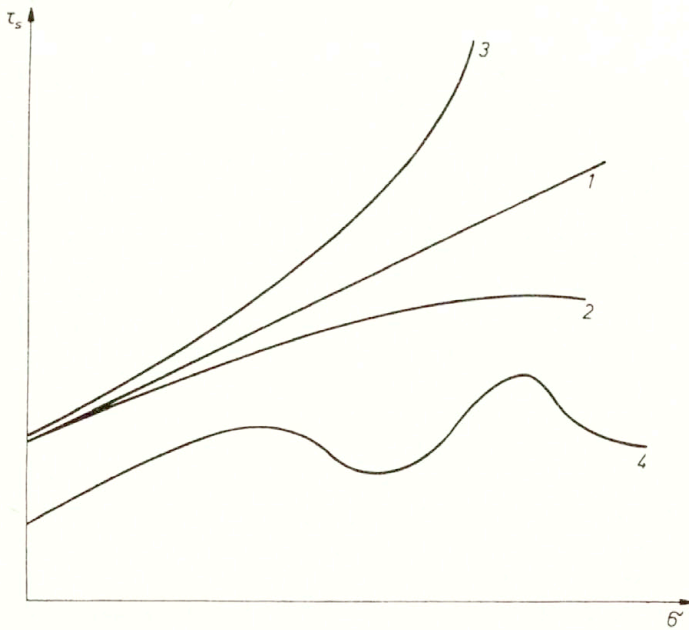


FIG. 7. Characteristic relations $\tau_s = \tau_s(\sigma_0)$ for four groups of materials, from LEVITAS [36].

[36] we display in Fig. 7 four typical relations $\tau_s = \tau_s(\sigma_0)$ between hydrostatic pressure σ_0 and ultimate shear strength τ_s , obtained for different groups of materials. The relations may be treated as a yield condition of Schleicher–Nádái type. To account for this phenomenon LEVITAS, cf. [35], developed a mechanical model with structural changes; for further extensions of the model, see Levitas [37].

In the next subsection we describe a mechanical model of a medium in which the loss of convexity of an initial yield surface is caused by the influence of plastic deformation on the elastic properties of the medium.

2.2. Micromechanics model of metal matrix composites [58]

PINDERA *et al.* [58] have reported recently interesting results concerning the elastic-plastic response of metal matrix composites. Some main points of their analysis are briefly presented below. The authors have investigated the initial yield surfaces of the graphite/aluminium composites in the presence of material nonlinearities of the fibre phase that exhibits a stiffening response along the fibre direction. By accounting for the stiffening effect in fibres the authors arrived at a material model which was already considered in a simpler form by PALMER *et al.* [54]. In the investigation [58] ABOUDI'S micromechanics model of fibre-reinforced composites was employed, for a description of the model see ABOUDI [1]. Here we only record that the model relies on the analysis of a repeating cell of a unidirectional fibrous matrix composite in which the fibres are distributed regularly in the matrix, cf. Fig. 8a. The representative cell, showed in Fig. 8b, consists of four subcells ($\beta, \gamma = 1, 2$), one of which is occupied by the fibre ($\beta = \gamma = 1$) and the other are occupied by the matrix ($\beta + \gamma \neq 2$). The micromechanics analysis of the representative cell is based on the assumption of a linear variation of the displacements in each subcell, and enforces the continuity of displacements and tractions at the interfaces between the subcells and between adjacent cells through an averaging process. This approximation leads finally to closed-form constitutive relations in terms of average stresses and strains, which describe the overall response of the composite.

In [58] the elastic response of the fibre phase was derived from a potential function and is defined by the following nonlinear stress-strain relation

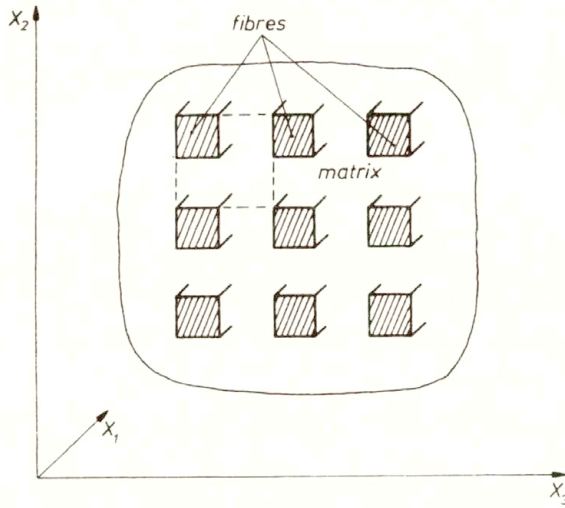
$$(2.1) \quad \varepsilon_i = A_{ij} \sigma_j + \frac{l_{ij} \sigma_j}{\sqrt{l_{mn} \sigma_m \sigma_n}} (1 - e^{-\alpha \sqrt{l_{mn} \sigma_m \sigma_n}}),$$

where the reduced notation is used, and A_{ij} and l_{ij} are positive definite and positive semidefinite fourth-order tensors, respectively, and α is a positive scalar. The elastic-plastic behaviour of the matrix is assumed to be linearly elastic with yielding governed by the Huber–von Mises condition:

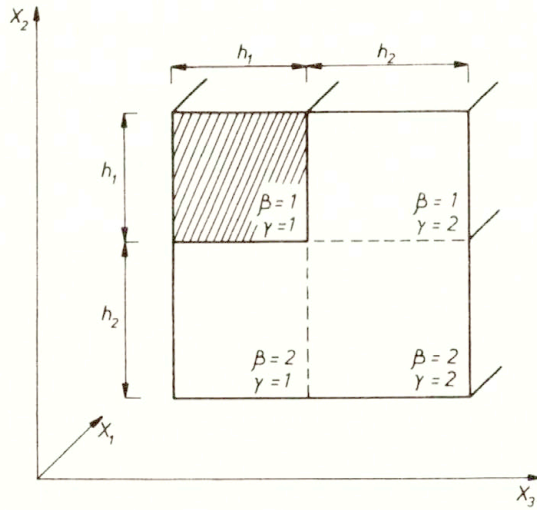
$$(2.2) \quad F^{(\beta\gamma)}(\widehat{\mathbf{S}}^{(\beta\gamma)}) - Y = 0, \quad \beta + \gamma \neq 2,$$

where Y is the yield stress of the matrix, and $\widehat{\mathbf{S}}^{(\beta\gamma)}$ are the matrix subcell stress deviators, whilst the stresses $\mathbf{S}^{(\beta\gamma)}$ developed in the matrix and fibre subcells are defined by

$$\mathbf{S}^{(\beta\gamma)} = \mathbf{B}^{(\beta\gamma)} \bar{\boldsymbol{\sigma}}$$



a) doubly periodic array



b) representative unit cell

FIG. 8. Repeating unit cell of ABOUDI'S model [1].

with $\bar{\sigma}$ being the external loading, and $\mathbf{B}^{(\beta\gamma)}$ is Hill's stress concentration matrix:

$$\mathbf{B}^{(\beta\gamma)} = \begin{bmatrix} B_{11} & B_{12} & B_{13} & 0 & 0 & 0 \\ B_{21} & B_{22} & B_{23} & 0 & 0 & 0 \\ B_{31} & B_{32} & B_{33} & 0 & 0 & 0 \\ 0 & 0 & 0 & B_{44} & 0 & 0 \\ 0 & 0 & 0 & 0 & B_{55} & 0 \\ 0 & 0 & 0 & 0 & 0 & B_{66} \end{bmatrix}^{(\beta\gamma)}$$

In this model, initial yielding takes place if the condition (2.2) is satisfied in any matrix subcell of the cell, whereas the yield surface of the composite is defined as the inner

envelope of the three yield surfaces of the individual matrix subcells. On demonstrating the loss of convexity, the authors considered the simplest case in which the nonlinear relation (2.1) was approximated, under longitudinal stress σ_1 , by a bilinear function

$$(2.3) \quad \varepsilon_1 = \frac{\sigma_1}{E_0} \quad \text{for } 0 < \sigma_1 \leq \sigma_1^*$$

$$(2.4) \quad \varepsilon_1 = \frac{\sigma_1}{E_\infty} + \varepsilon_1^* \quad \text{for } \sigma_1 \geq \sigma_1^*.$$

In (2.3) and (2.4), $E_0 = 1/(A_{11} + \alpha l_{11})$, $E_\infty = 1/A_{11}$ are the initial and final Young's moduli of the fibre, respectively, and $\varepsilon_1^* = \sqrt{l_{11}}$. In this case the yield condition (2.2) in the matrix subcells is defined by the following two expressions:

$$(2.5) \quad F^{(\beta\gamma)}(\mathbf{B}^{(\beta\gamma)}\bar{\sigma}) - Y = 0, \quad \beta + \gamma \neq 2, \quad \text{if } |S_{11}^{(11)}| \leq \sigma_1^*,$$

where $S_{11}^{(11)}$ is the longitudinal stress in the fibre, and

$$(2.6) \quad F^{*(\beta\gamma)}(\mathbf{B}^{*(\beta\gamma)}\bar{\sigma} + \mathbf{S}^{*(\beta\gamma)}) - Y = 0, \quad \beta + \gamma \neq 2, \quad \text{if } |S_{11}^{(11)}| \geq \sigma_1^*,$$

where

$$\mathbf{S}^{*(\beta\gamma)} = \mathbf{B}^{(\beta\gamma)}\bar{\sigma}^*$$

and the composites stresses $\bar{\sigma}^*$ correspond to the stress $S_{11}^{(11)}$ through the following equation

$$(2.7) \quad S_{11}^{(11)} = B_{11}^{(11)}\bar{\sigma}_{11}^* + B_{12}^{(11)}\bar{\sigma}_{22}^* + B_{13}^{(11)}\bar{\sigma}_{33}^* = \bar{\sigma}_{11}^*.$$

Equation (2.7) defines a plane in stress space that separates the two regions within which (2.5) and (2.6) are satisfied. Comparing the form of arguments in the yield conditions (2.5) and (2.6) it can be seen that due to the stiffening effect the yield surface (in each subcell) is translated and rotated. Such a situation is presented in Fig. 9, taken from PINDERA *et al.* [58], for loading in the $\bar{\sigma}_{11} - \bar{\sigma}_{22}$ space, where the resulting yield surface

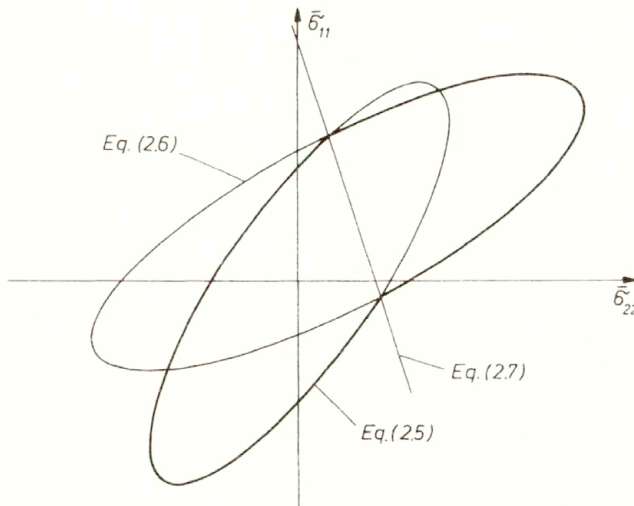


FIG. 9. Illustration of the loss of convexity of the initial yield surfaces of unidirectional composite with a bilinear fibre response in the $\bar{\sigma}_{11} - \bar{\sigma}_{22}$ stress space due to yielding in one matrix subcell, from PINDERA *et al.* [58].

is denoted by the bold line. The authors have noted that in the case of unidirectional graphite/aluminium and loading conditions considered in [58], the loss of convexity of the yield surfaces occurs when the ratio $R = E_\infty/E_0$ of asymptotic moduli is four and higher (the documented stiffening is much smaller, cf. [58]). But they claimed that in some laminated structures the loss of convexity may occur under specific combinations of loads for realistic values of R . The influence of temperature on convexity of the yield surfaces is also analysed in [58].

3. Variational formulation of the problem

In this section we are concerned with the elastic-plastic quasi-static deformation process of a solid body. The process is described by a mechanical model which is based on the assumption of (generalized) normal dissipation.

3.1. Mechanical model

Let the body occupy an open bounded domain $\Omega \subset R^3$ with sufficiently smooth boundary Γ . The quantities describing the elastic-plastic deformation process are functions of the space variable $\mathbf{x} \in \Omega$ and the scalar, time-like parameter $t \in [0, T]$, $T < \infty$, which determines the sequence of events as the process develops. The boundary Γ consists of two mutually disjoint parts Γ_u and Γ_σ , on which, respectively, the conditions for the displacement vector $\mathbf{u} = (u_1(\mathbf{x}, t), u_2(\mathbf{x}, t), u_3(\mathbf{x}, t))$ and the stress tensor $\boldsymbol{\sigma} = (\sigma_{ij}(\mathbf{x}, t))$, $1 \leq i, j \leq 3$, are prescribed. Let ∇ stand for the gradient operator. Confining ourselves to small deformations we may split the total strain tensor

$$(3.1) \quad \boldsymbol{\varepsilon} = \frac{1}{2}[\nabla \mathbf{u} + (\nabla \mathbf{u})^T]$$

into an elastic $\boldsymbol{\varepsilon}^e$ and a plastic $\boldsymbol{\varepsilon}^p$ part,

$$(3.2) \quad \boldsymbol{\varepsilon} = \boldsymbol{\varepsilon}^e + \boldsymbol{\varepsilon}^p$$

which can be expressed in rate form

$$(3.3) \quad \dot{\boldsymbol{\varepsilon}} = \dot{\boldsymbol{\varepsilon}}^e + \dot{\boldsymbol{\varepsilon}}^p.$$

Passing on to the constitutive relations we adopt the general assumption that the irreversible characteristics of the deformation process can be described by means of a suitable collection of internal state variables $\boldsymbol{\alpha}$. Let $\Sigma \subset R^6$ denote the space of stress values at a point $\mathbf{x} \in \Omega$ and time t and let $A \subset R^q$ be the space of values of the internal variables $\boldsymbol{\alpha}$.

When employing the concept of the yield function $F = F(\boldsymbol{\sigma}, \boldsymbol{\alpha})$ it is said that the state of stress is admissible if the following condition is satisfied

$$(3.4) \quad F(\boldsymbol{\sigma}, \boldsymbol{\alpha}) \leq 0.$$

The *elastic region* is defined by the strict inequality

$$(3.5) \quad F(\boldsymbol{\sigma}, \boldsymbol{\alpha}) < 0$$

and is supplemented with the condition of no progress in irreversibility

$$(3.6) \quad \dot{\boldsymbol{\varepsilon}}^p = 0, \quad \dot{\boldsymbol{\alpha}} = 0.$$

We further suppose that within the elastic region the relation between the stress rate tensor and the elastic strain rate tensor is given by a linear symmetric operator \mathbf{C} which may possibly depend on the actual state $(\boldsymbol{\sigma}, \boldsymbol{\alpha})$:

$$(3.7) \quad \dot{\boldsymbol{\varepsilon}}^e = \mathbf{C}(\boldsymbol{\sigma}, \boldsymbol{\alpha})\dot{\boldsymbol{\sigma}}.$$

The *plastic region* is defined by the equality

$$(3.8) \quad F(\boldsymbol{\sigma}, \boldsymbol{\alpha}) = 0$$

and is accompanied by increments of the irreversible quantities, so that

$$(3.9) \quad \dot{\boldsymbol{\varepsilon}} = \mathbf{C}(\boldsymbol{\sigma}, \boldsymbol{\alpha})\dot{\boldsymbol{\sigma}} + \dot{\boldsymbol{\varepsilon}}^p.$$

The flow rule and the hardening rule are, besides the yield function, the basic constituents of the flow theory of plasticity. In this paper we take the associative form of these rules and consider first the case in which the yield function is differentiable in the classical sense. Then the evolution of the irreversible variables involved in the process may be expressed by the following laws:

$$(3.10) \quad \begin{aligned} \dot{\boldsymbol{\varepsilon}}^p &= \dot{\lambda} \nabla_{\boldsymbol{\sigma}} F(\boldsymbol{\sigma}, \boldsymbol{\alpha}), \\ -\mathbf{H}(\boldsymbol{\sigma}, \boldsymbol{\alpha})\dot{\boldsymbol{\alpha}} &= \dot{\lambda} \nabla_{\boldsymbol{\alpha}} F(\boldsymbol{\sigma}, \boldsymbol{\alpha}) \quad \text{with} \quad \dot{\lambda} \geq 0, \end{aligned}$$

where $\dot{\lambda}$ is an unspecified scalar function called the *plastic multiplier*, whilst \mathbf{H} is an operator that defines the conjugate variable to $\boldsymbol{\alpha}$; see e.g. [67] for a discussion concerning \mathbf{H} and \mathbf{C} .

The introduction of internal variables $\boldsymbol{\alpha}$ in the description of material response accounts for specific microstructural rearrangements of the constituent parts of the material in the course of deformation. Using the internal variable framework, RICE [61, 62] has studied the form of macroscopic constitutive laws in metal plasticity as motivated by underlying microscale mechanisms of deformation. He showed that the macroscopic laws for a class of microstructural deformation mechanisms possess a plastic normality structure, which is similar to (3.10)₁. Moreover, in [61] the rates $\dot{\boldsymbol{\alpha}}$ were proposed to be governed by the consistency condition, i.e. $\dot{F} = 0$. LUBLINER [39, 40] has also analysed the general forms of rate equations for internal variables and derived some restrictions imposed on them by thermodynamics. The form (3.10)₂ is a specialization of the general local hardening law, in the isothermal case. Referring to LUBLINER [39], we suppose that there exists the operator \mathbf{H}^{-1} which can be expressed as

$$\mathbf{H}^{-1}(\boldsymbol{\sigma}, \boldsymbol{\alpha}) = \mathbf{h}(\boldsymbol{\sigma}, \boldsymbol{\alpha}) \cdot (\nabla_{\boldsymbol{\alpha}} F(\boldsymbol{\sigma}, \boldsymbol{\alpha}))^{-1}.$$

Then it follows that (3.10)₂ represents an evolution law which is similar to that assumed by LUBLINER (Eq. 17 in [39]). The presence of $\dot{\lambda}$ in (3.10)₂ is motivated — as generally known — by physical aspects of the process, and it is useful from the computational point of view. Furthermore, the permitted nonconvex yield function and the matrix operator \mathbf{H} may cover nonmonotone evolution laws for $\boldsymbol{\alpha}$, e.g. due to phase changes or damage processes in the material. Note that substituting $\dot{\lambda} > 0$ from (3.10)₁ into (3.10)₂ leads to a relation between the rates $\dot{\boldsymbol{\varepsilon}}^p$ and $\dot{\boldsymbol{\alpha}}$ which is similar to that derived by RICE (Eq. 25 in [61]). It may also be noted that convexity of the yield potential was proved by RICE [62] under some additional assumptions concerning monotonicity of the rates $\dot{\boldsymbol{\alpha}}$.

As can be easily seen at any point of the material the following possibilities may be distinguished:

$$(3.11) \quad \left. \begin{array}{ll} F < 0 & \text{then } \dot{\lambda} = 0 \quad \text{elastic state} \\ F = 0 & \text{and } \dot{\lambda} = 0 \quad \text{plastic state: neutral loading} \\ F = 0 & \text{and } \dot{\lambda} > 0 \quad \text{plastic state: plastic loading} \end{array} \right\} \begin{array}{l} \text{elastic process,} \\ \\ \text{plastic process.} \end{array}$$

Thus the process (or loading) is termed *plastic*, if it is accompanied by an increment of plastic strain together with a change of internal variables, otherwise it is *elastic*.

The relations (3.11) can be equivalently written in a more compact way as the complementarity conditions

$$(3.12) \quad F \leq 0, \quad \dot{\lambda} \geq 0, \quad F \cdot \dot{\lambda} = 0.$$

Now we wish to extend the presented constitutive relations to the case in which the elastic region is described by a yield function consisting of a number of segments. Following KOITER ([29]), we let the yield function to be defined as the maximum-type function

$$(3.13) \quad F(\boldsymbol{\sigma}, \boldsymbol{\alpha}) = \max_{1 \leq j \leq m} F^j(\boldsymbol{\sigma}, \boldsymbol{\alpha}).$$

We assume that the component yield functions F^j are differentiable, but they may intersect in a non-smooth manner and may be non-convex. The case in which F is defined by three differentiable and convex yield functions (Mises ellipses) has been considered by PINDERA *et al.*, cf. Fig. 2 in [58]. A non-convex, non-smooth yield function generated by two differentiable convex functions F^j is illustrated in Fig. 9, in which case an additional condition corresponding to (2.7) must be taken into account.

Note that in the case of the non-smooth yield function only the evolution laws (3.10) must be generalized due to the lack of classical differentiability at the vertices (conical points) of the set K ,

$$(3.14) \quad K = \{(\boldsymbol{\sigma}, \boldsymbol{\alpha}) \in \Sigma \times A \mid F(\boldsymbol{\sigma}, \boldsymbol{\alpha}) \leq 0\}.$$

As the plastic potential we take the indicator function of the set K ,

$$(3.15) \quad \psi_K(\boldsymbol{\sigma}, \boldsymbol{\alpha}) = \begin{cases} 0 & \text{if } (\boldsymbol{\sigma}, \boldsymbol{\alpha}) \in K, \\ \infty & \text{if } (\boldsymbol{\sigma}, \boldsymbol{\alpha}) \notin K. \end{cases}$$

In the case of nonconvex nonsmooth yield function we assume, as a generalization of (3.10), that the evolution of irreversible variables satisfy the following normality condition

$$(3.16) \quad (\dot{\boldsymbol{\epsilon}}^p, -\mathbf{H}(\boldsymbol{\sigma}, \boldsymbol{\alpha})\dot{\boldsymbol{\alpha}}) \in \bar{\partial}\psi_K(\boldsymbol{\sigma}, \boldsymbol{\alpha}) = N_K(\boldsymbol{\sigma}, \boldsymbol{\alpha}).$$

In (3.16) $\bar{\partial}$ denotes the generalized subdifferential operator, and N_K is the normal cone to the set K , as defined in the Appendix by (A.11) and (A.6), respectively; cf. also (A.14). A two dimensional case, i.e. $K \subset R^2$ is illustrated in Fig. 10, where both the normal cone and the tangent cone to K are shown.

Hence the elastic-plastic deformation process is characterized by the following relations

$$(3.17) \quad \begin{aligned} &(\boldsymbol{\sigma}, \boldsymbol{\alpha}) \in K, \\ &\dot{\boldsymbol{\epsilon}} = \mathbf{C}(\boldsymbol{\sigma}, \boldsymbol{\alpha})\dot{\boldsymbol{\sigma}} + \dot{\boldsymbol{\epsilon}}^p, \\ &(\dot{\boldsymbol{\epsilon}}^p, -\mathbf{H}(\boldsymbol{\sigma}, \boldsymbol{\alpha})\dot{\boldsymbol{\alpha}}) \in N_K(\boldsymbol{\sigma}, \boldsymbol{\alpha}). \end{aligned}$$

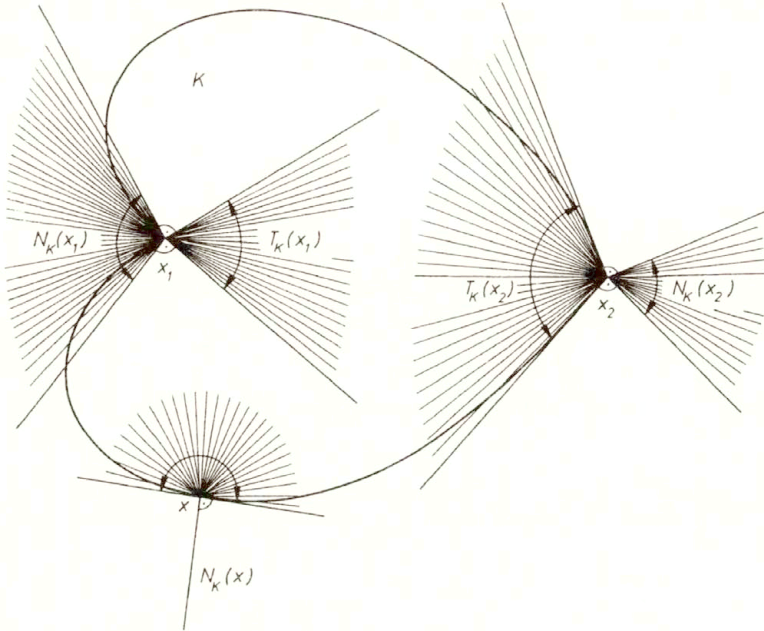


FIG. 10. Tangent and normal cones to a set $K \subset R^2$.

By virtue of (A.13) relation (3.16) implies the inequality

$$(3.18) \quad \langle \dot{\epsilon}^p \mid \sigma' \rangle_{\Sigma} + \langle -\mathbf{H}(\sigma, \alpha) \dot{\alpha} \mid \alpha' \rangle_A \leq \psi_K^{\perp}((\sigma, \alpha); (\sigma', \alpha')) \quad \forall (\sigma', \alpha') \in \Sigma \times A,$$

where $\langle \cdot \mid \cdot \rangle_{\Sigma}$ and $\langle \cdot \mid \cdot \rangle_A$ signify duality pairings on $\Sigma^* \times \Sigma$ and $A^* \times A$, respectively.

On the other hand, by making use of the definition of the normal cone to the set K , Eq. (A.6), we may write

$$(3.19) \quad \langle \dot{\epsilon}^p \mid \sigma' \rangle_{\Sigma} + \langle -\mathbf{H}(\sigma, \alpha) \dot{\alpha} \mid \alpha' \rangle_A \leq 0 \quad \forall (\sigma', \alpha') \in T_K(\sigma, \alpha).$$

When the set K is convex Eqs. (3.18) and (3.19) reduce to the known form, cf. (A.4),

$$(3.20) \quad \langle \dot{\epsilon}^p \mid \sigma' - \sigma \rangle_{\Sigma} + \langle -\mathbf{H}(\sigma, \alpha) \dot{\alpha} \mid \alpha' - \alpha \rangle_A \leq 0 \quad \forall (\sigma', \alpha') \in K.$$

Nonconvex nondifferentiable problems for finite elastoplasticity were studied in the framework of thermodynamics by KIM and ODEN [26, 27] who extended the normality condition to the (generalized) normal cone and introduced materials of *Type N*. These authors proposed generalized plastic potentials in the form suitable for computations by an interior penalty method. When the set K is convex, they recovered the generalized standard materials introduced by HALPHEN and NGUYEN [20].

In the next subsection we demonstrate a variational inequality formulation for the elastic-plastic process which is derived directly from the loading/unloading conditions as in (3.12).

3.2. Variational inequality formulation

The variational inequality formulation proposed here is based upon a lemma which states the equivalence between the so-called (generalized) complementarity problem and a class of variational inequalities.

Let $\mathbb{C} \subset U$ be a non-empty closed convex cone in a real Hilbert space U , and let $\mathbb{C}^* \subset U^*$ denote its polar cone in the dual space U^* . Moreover, let $P : K \rightarrow U^*$ stand for a continuous operator, and let $\langle \cdot | \cdot \rangle$ indicate duality pairing in $U^* \times U$.

The lemma is concerned with the following problems.

- The (generalized) complementarity problem (in short, CP):

Find $u \in \mathbb{C}$ such that

$$(3.21) \quad P(u) \in \mathbb{C}^*, \quad \langle P(u) | u \rangle = 0.$$

- The variational inequality (in short, VI)

$$(3.22) \quad u \in \mathbb{C}, \quad \langle P(u) | v - u \rangle \geq 0 \quad \forall v \in \mathbb{C}.$$

LEMMA. The complementarity problem (3.21) and the variational inequality (3.22) are equivalent.

The prove will be given in two steps. First it will be shown that VI (3.22) implies CP (3.21). If \mathbb{C} is a convex cone (with vertex at the origin), then $\eta u \in \mathbb{C}$ and $u + w \in \mathbb{C}$ for any $u, w \in \mathbb{C}$, $\eta \in [0, \infty)$. After substitution $v = 0$ and $v = 2u$ into (3.22), we obtain respectively

$$\langle P(u) | -u \rangle \geq 0 \quad \text{and} \quad \langle P(u) | u \rangle \geq 0$$

thus, for $u \in \mathbb{C}$,

$$\langle P(u) | u \rangle = 0.$$

Next, taking $v = u + w$ in (3.22), the latter is reduced to

$$\langle P(u) | w \rangle \geq 0 \quad \forall w \in \mathbb{C}$$

which means that $P(u) \in \mathbb{C}^*$.

In order to show the inverse implication we shall use the definition of the polar cone. If $u \in \mathbb{C}$ and $P(u) \in \mathbb{C}^*$, then

$$u \in \mathbb{C}, \quad \langle P(u) | v \rangle \geq 0 \quad \forall v \in \mathbb{C}.$$

Subtraction of the equality $\langle P(u) | u \rangle = 0$ from the above inequality gives VI (3.22), which completes the proof.

Returning to the multisurface yield function F we can see that the condition (3.13) implies that each component function satisfies

$$(3.23) \quad F^j(\boldsymbol{\sigma}, \boldsymbol{\alpha}) \leq 0, \quad \forall 1 \leq j \leq m.$$

Furthermore we note that, for any fixed $\mathbf{x} \in \Omega$ and time t , the function F is defined in finite-dimensional space R^n , with $n = 6 + q$ being the number of components of the pair $\mathbf{p} = (\boldsymbol{\sigma}, \boldsymbol{\alpha})$. The normal cone to the set K can be defined as a linear combination of the gradients of functions F^j :

$$(3.24) \quad N_K(\mathbf{p}) = \left\{ \mathbf{w} \in R^n \mid \mathbf{w} = \sum_{j=1}^m \xi^j \nabla F^j(\mathbf{p}), \xi^j \geq 0, \xi^j = 0 \text{ if } F^j(\mathbf{p}) < 0 \right\},$$

where

$$\nabla F^j(\mathbf{p}) \equiv \nabla F^j(\boldsymbol{\sigma}, \boldsymbol{\alpha}) = (\nabla_{\boldsymbol{\sigma}} F^j(\boldsymbol{\sigma}, \boldsymbol{\alpha}), \nabla_{\boldsymbol{\alpha}} F^j(\boldsymbol{\sigma}, \boldsymbol{\alpha})).$$

Eventually, in the light of (3.23) and (3.24), relations (3.17) can be written as follows

$$\begin{aligned} \dot{\epsilon} &= \mathbf{C}(\boldsymbol{\sigma}, \boldsymbol{\alpha})\dot{\boldsymbol{\sigma}} + \dot{\epsilon}^p, \\ (3.25) \quad (\dot{\epsilon}^p, -\mathbf{H}(\boldsymbol{\sigma}, \boldsymbol{\alpha})\dot{\boldsymbol{\alpha}}) &= \sum_{j=1}^m \dot{\lambda}^j \nabla F^j(\boldsymbol{\sigma}, \boldsymbol{\alpha}). \end{aligned}$$

$$F^j(\boldsymbol{\sigma}, \boldsymbol{\alpha}) \leq 0, \quad \dot{\lambda}^j \geq 0, \quad F^j(\boldsymbol{\sigma}, \boldsymbol{\alpha})\dot{\lambda}^j = 0 \quad \forall 1 \leq j \leq m.$$

Let $\langle \cdot | \cdot \rangle$ be now defined as the inner product in $(L_2(\Omega))^m$, i.e. for $\mathbf{r}, \mathbf{v} \in (L_2(\Omega))^m$

$$\langle \mathbf{r} | \mathbf{v} \rangle = \sum_{j=1}^m \int_{\Omega} r^j(\mathbf{x})v^j(\mathbf{x}) \, d\mathbf{x},$$

and let \mathbb{C} stand for the closed convex positive cone in $(L_2(\Omega))^m$,

$$\mathbb{C} = \{ \mathbf{r} \in (L_2(\Omega))^m \mid \langle \mathbf{r} | \mathbf{v} \rangle \geq 0 \quad \forall \mathbf{v} \geq \mathbf{0} \quad \text{in} \quad (L_2(\Omega))^m \}.$$

By $\dot{\boldsymbol{\lambda}}$ we denote the vector of plastic multipliers, $\dot{\boldsymbol{\lambda}} \in \mathbb{C}$.

From Eq. (3.25)_{1,2} one obtains the following formulae for the stress, plastic strain and internal variables at a given point $\mathbf{x} \in \Omega$ and time level $t \in [0, T]$:

$$\begin{aligned} (3.26) \quad \boldsymbol{\sigma}(t) &= \int_0^t \mathbf{C}^{-1}(\boldsymbol{\sigma}(\tau), \boldsymbol{\alpha}(\tau))\dot{\boldsymbol{\epsilon}}(\tau) \, d\tau \\ &\quad - \int_0^t \mathbf{C}^{-1}(\boldsymbol{\sigma}(\tau), \boldsymbol{\alpha}(\tau)) \sum_{j=1}^m \dot{\lambda}^j(\tau) \nabla_{\boldsymbol{\sigma}} F^j((\boldsymbol{\sigma}(\tau), \boldsymbol{\alpha}(\tau))) \, d\tau, \end{aligned}$$

$$(3.27) \quad \epsilon^p(t) = \int_0^t \sum_{j=1}^m \dot{\lambda}^j(\tau) \nabla_{\boldsymbol{\sigma}} F^j((\boldsymbol{\sigma}(\tau), \boldsymbol{\alpha}(\tau))) \, d\tau,$$

$$(3.28) \quad \boldsymbol{\alpha}(t) = \int_0^t -\mathbf{H}^{-1}(\boldsymbol{\sigma}(\tau), \boldsymbol{\alpha}(\tau)) \sum_{j=1}^m \dot{\lambda}^j(\tau) \nabla_{\boldsymbol{\alpha}} F^j((\boldsymbol{\sigma}(\tau), \boldsymbol{\alpha}(\tau))) \, d\tau.$$

When \mathbf{C} and \mathbf{H} are constant, (3.26) and (3.28) take the usual forms

$$\begin{aligned} \boldsymbol{\sigma}(t) &= \mathbf{C}^{-1}\boldsymbol{\epsilon}(t) - \mathbf{C}^{-1}\epsilon^p(t), \\ \boldsymbol{\alpha}(t) &= -\mathbf{H}^{-1}\boldsymbol{\omega}(t), \end{aligned}$$

with

$$\boldsymbol{\omega}(t) = \int_0^t \sum_{j=1}^m \dot{\lambda}^j(\tau) \nabla_{\boldsymbol{\alpha}} F^j((\boldsymbol{\sigma}(\tau), \boldsymbol{\alpha}(\tau))) \, d\tau.$$

Substitution of the pair $(\boldsymbol{\sigma}, \boldsymbol{\alpha})$ as defined by (3.26) and (3.28) to $\mathbf{F} = \{F^j\}$ leads to new yield functions which will be designated by $\mathbf{G} = \{G^j\}$, i.e.

$$(3.29) \quad G^j(\boldsymbol{\epsilon}, \epsilon^p, \boldsymbol{\alpha}) \equiv F^j(\boldsymbol{\sigma}(\boldsymbol{\epsilon}, \epsilon^p), \boldsymbol{\alpha}).$$

By taking advantage of the lemma, we can express the complementarity conditions (3.25)₃ in the weak form as the following variational inequality

$$(3.30) \quad \langle -\mathbf{G}(\boldsymbol{\epsilon}(\mathbf{u}), \epsilon^p(\dot{\boldsymbol{\lambda}}), \boldsymbol{\alpha}(\dot{\boldsymbol{\lambda}})) | \boldsymbol{\gamma} - \dot{\boldsymbol{\lambda}} \rangle \geq 0 \quad \forall \boldsymbol{\gamma} \in \mathbb{C}.$$

The system (3.30) describes completely the evolution of irreversibility during the deformation process under consideration. The variational inequality (3.30) is defined for the whole body Ω on two fields: the plastic multiplier $\dot{\lambda} \in \mathbb{C}$ and the displacement $\mathbf{u} \in V$, V being a set of kinematically admissible displacements of the body. The displacement \mathbf{u} can be determined through the equilibrium equation for the body and is treated, in this paper, as given. Bearing this in mind, consider the time integration of the variational inequality of evolution. To this end, the time interval $[0, T]$ is divided into finite subintervals by selecting on the time axis points $t_0 = 0, t_1, \dots, t_{\tau-1}, t_\tau, t_{\tau+1}, \dots, t_N = T$. The quantities at a fixed $t = t_\tau$ will be indicated with the subscript τ , thus e.g. $\mathbf{u}_\tau \equiv \mathbf{u}(t_\tau, \cdot)$ is a function only of the space variable \mathbf{x} , and let Δ stand for a finite increment.

A typical time-step $t_\tau \rightarrow t_{\tau+1}$ consists in the following updating:

- given the pair $(\mathbf{u}_\tau, \lambda_\tau)$ which defines the state of the process at time $t = t_\tau$, i.e.

$$\langle -\mathbf{G}(\varepsilon(\mathbf{u}_\tau), \varepsilon^p(\lambda_\tau), \alpha(\lambda_\tau)) \mid \gamma - \Delta\lambda_\tau \rangle \geq 0 \quad \forall \gamma \in \mathbb{C}.$$

- determine the increment $(\Delta\mathbf{u}_{\tau+1}, \Delta\lambda_{\tau+1})$ which will define the state of the process at time level $t = t_{\tau+1}$ through the pair

$$\begin{aligned} \mathbf{u}_{\tau+1} &= \mathbf{u}_\tau + \Delta\mathbf{u}_{\tau+1}, \\ \lambda_{\tau+1} &= \lambda_\tau + \Delta\lambda_{\tau+1}. \end{aligned}$$

This amounts to solving the problem (given $\Delta\mathbf{u}_{\tau+1}$):

find $\Delta\lambda_{\tau+1} \in \mathbb{C}$ such that

$$\langle -\mathbf{G}(\varepsilon(\mathbf{u}_\tau + \Delta\mathbf{u}_{\tau+1}), \varepsilon^p(\lambda_\tau + \Delta\lambda_{\tau+1}), \alpha(\lambda_\tau + \Delta\lambda_{\tau+1})) \mid \gamma - \Delta\lambda_{\tau+1} \rangle \geq 0 \quad \forall \gamma \in \mathbb{C}.$$

The proposed variational inequality formulation provides for the global projection step in the sense of *elastic predictor/plastic corrector* algorithms. This kind of numerical scheme was applied in KUCZMA and WHITEMAN [31] for an initial elastic-plastic boundary value problem with linear elastic behaviour and yielding governed by the Huber–von Mises criterion. After having been discretized by the finite element method, the variational inequality therein is solved as a sequence of linear complementarity problems.

4. Closing remarks

A variational formulation for a class of nonconvex problems in multisurface elastoplasticity was proposed. This represents a coupled system of variational inequalities that can be interpreted as a weak form of the loading/unloading conditions for the whole body under consideration. The formulation seems to be attractive from the computational standpoint, as it leads directly to an elastic predictor/plastic corrector algorithm within which the projection onto the yield surface is performed for the whole body under study. This formulation enables one to apply various finite element approximations of the field of plastic multiplier $\Delta\lambda$.

It is noted that nonconvex models arise in describing the elastic-plastic behaviour of materials with complicated substructure, e.g. composites, or when the influence of high pressure is taken into account (phase transitions). The existence of a nonconvex yield function for metals is a very controversial issue. It was not the purpose of the present paper to explain the causes of the observed concavity on experimentally determined yield surfaces of metal specimens. In the light of the presented results the following questions are still open: (a) what is the influence of these (local) anisotropic singularities of the yield surface, e.g. measured by offset tests, on the overall response of the body or in

other words, on the solution of the corresponding initial boundary value problem and, (b) what is the admissible extent to which the experimentally determined, nonconvex and nonsmooth yield surface can be approximated by a convex and smooth one so as not to lose the proper information about the material behaviour.

Appendix

We present here a brief summary of selected concepts of convex and nonconvex analysis; further details can be found in [63, 9, 26, 56]. Let \bar{R} be the extended real number system, i.e. $\bar{R} = R \cup \{\pm\infty\}$. Letting X indicate a real topological linear space and X^* its dual, we denote by $\langle \cdot | \cdot \rangle_X$ duality pairing on $X^* \times X$, i.e. if $x^* \in X^*$ and $x \in X$, then $x^*(x) = \langle x^* | x \rangle_X$.

A set $K \subset X$ is said to be convex if and only if for every pair of elements $x, y \in K$ the element $\theta x + (1 - \theta)y$ is in K for all $\theta \in [0, 1]$, i.e. K is convex iff the line segment connecting any two points $x, y \in K$ is entirely contained in the set K .

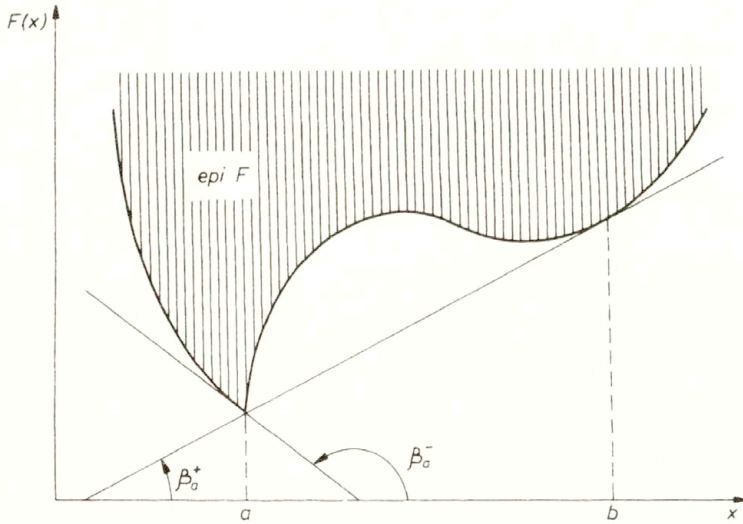


FIG. 11. Epigraph of a function F defined on R .

The epigraph of an extended real-valued function $F : X \rightarrow \bar{R}$, is the set (see Fig. 11)

$$\text{epi } F = \{(x, r) \in X \times \bar{R} \mid r \geq F(x)\}.$$

Let K be a convex subset of X . A function $F : K \rightarrow \bar{R}$ is said to be convex on K iff it satisfies the condition

$$F(\theta x + (1 - \theta)y) \leq \theta F(x) + (1 - \theta)F(y) \quad \forall x, y \in K, \quad \forall \theta \in [0, 1],$$

whenever the righthand side is defined; i.e. F is convex iff $\text{epi } F$ is a convex set (cf. Fig. 11).

A function $F : X \rightarrow \bar{R}$ is Gateaux-differentiable (G-differentiable) at a point $x \in X$ iff a unique continuous linear functional $F'(x) \in X^*$ exists such that

$$\lim_{\theta \rightarrow 0^+} \frac{1}{\theta} (F(x + \theta y) - F(y)) = \langle F'(x) \mid y \rangle_X \quad \forall y \in X.$$

If $F : X \rightarrow R$ is G-differentiable on X , then F is convex iff

$$(A.1) \quad F(y) - F(x) \geq \langle F'(x) \mid y - x \rangle_X \quad \forall x, y \in X.$$

The *subdifferential* of a function $F : X \rightarrow \bar{R}$ at $x \in X$ is the subset $\partial F(x) \subset X^*$, defined by

$$(A.2) \quad \partial F(x) = \{x^* \in X^* \mid F(y) - F(x) \geq \langle x^* \mid x - y \rangle_X \quad \forall y \in X\}.$$

The elements $x^* \in \partial F(x)$ are called *subgradients* of F at x . It is worth noting here that the condition in (A.2) must be satisfied for every direction $y \in X$, cf. also (A.1). The geometrical interpretation of the subdifferential of a continuous function $F : R \rightarrow \bar{R}$ is illustrated in Fig. 11, where e.g. $\partial F(a) = [\text{tg } \beta_a^-, \text{tg } \beta_a^+]$. The subdifferential $\partial F(x)$ may be an empty set, even in the cases where ordinary derivatives exist, e.g., $\partial F(x) = \emptyset$ for $a < x < b$ in Fig. 11.

Let K be a nonempty subset of X . The *indicator function* $\psi_K : X \rightarrow \bar{R}$ of the set K is defined by

$$(A.3) \quad \psi_K(x) = \begin{cases} 0 & \text{if } x \in K, \\ \infty & \text{if } x \notin K. \end{cases}$$

The indicator function ψ_K is l.s.c. iff K is closed. When K is a nonconvex set then ψ_K is nonconvex. If K is convex, then ψ_K is a convex function and its subdifferential

$$(A.4) \quad \begin{aligned} \partial \psi_K(x) &= \{x^* \in X^* \mid \psi_K(y) - \psi_K(x) \geq \langle x^* \mid y - x \rangle_X \quad \forall y \in X\} \\ &= \{x^* \in X^* \mid \langle x^* \mid y - x \rangle_X \leq 0 \quad \forall y \in K\}. \end{aligned}$$

The *tangent cone* to K at $x \in K$ is the set

$$(A.5) \quad T_K(x) = \liminf_{\substack{x' \rightarrow_K x \\ \theta \rightarrow 0^+}} \frac{1}{\theta} (K - x') = \bigcap_{A \in U(0)} \bigcup_{\substack{B \in U(x) \\ \alpha > 0}} \bigcap_{\substack{x' \in K \cap B \\ \theta \in (0, \alpha)}} \left(\frac{1}{\theta} (K - x') + A \right).$$

In the finite dimensional case, for $K \subset R^2$ cf. Fig. 12, (A.5) can be simplified:

$$T_K(\mathbf{x}) = \{ \mathbf{y} \in R^n \mid \forall \theta_k \rightarrow 0^+, \mathbf{x}^k \rightarrow \mathbf{x} \text{ with } \mathbf{x}^k \in K, \\ \exists \mathbf{y}^k \rightarrow \mathbf{y} \text{ such that } \mathbf{x}^k + \theta_k \mathbf{y}^k \in K \}.$$

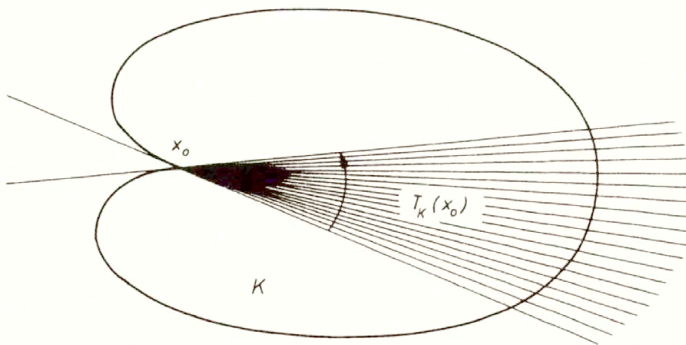


FIG. 12. Tangent cone to a set $K \subset R^2$ at x_0 .

In (A.5) the notation is used that

$$x' \dashv_K x \Leftrightarrow x' - x \quad \text{with} \quad x' \in K.$$

It should be remarked that $T_K(x)$ is a closed convex cone containing 0. If K is convex, then

$$T_K(\mathbf{x}) = \text{cl}\{y \in R^n \mid \exists \theta > 0 \mathbf{x} + \theta y \in K\}.$$

The *normal cone* to K at $x \in K$, denoted $N_K(x)$, is a subset of the dual space X^* and can be defined by polarity to the tangent cone $T_K(x)$,

$$(A.6) \quad N_K(x) = \{x^* \in X^* \mid \langle x^* \mid y \rangle \leq 0 \quad \forall y \in T_K(x)\}.$$

It is noted that $N_K(x)$ is a convex cone, and in two dimensions $N_K(x)$ consists of these vectors which make obtuse angles with vectors belonging to $T_K(x)$, cf. Fig. 10. If K is convex, then

$$(A.7) \quad N_K(x) = \{x^* \in X^* \mid \langle x^* \mid y - x \rangle \leq 0 \quad \forall y \in K\},$$

and in this case the normal cone $N_K(x)$ coincides with what has been called the normal cone in convex analysis. If $x \in \text{int } K$, i.e. x belongs to the interior of the set K , then $N_K(x) = 0$.

Let F be an extended real-valued function defined on X , $F : X \rightarrow \bar{R}$ and let $x \in X$ be any point where F is finite. The (Clarke–Rockafellar) *upper subderivative* of F at x in direction $y \in X$ is defined by the expression

$$(A.8) \quad F^\uparrow(x; y) = \limsup_{\substack{(x', \alpha') \downarrow_F x \\ \theta \rightarrow 0^+}} \inf_{y' \rightarrow y} \frac{F(x' + \theta y') - \alpha'}{\theta},$$

where, with $(x', \alpha') \in \text{epi } F$, the notation is used

$$(x', \alpha') \downarrow_F x \Leftrightarrow (x', \alpha') - (x, F(x)) \quad \text{with} \quad \alpha' \geq F(x').$$

If F is l.s.c. at x , then (A.8) can be reduced to the slightly simpler form

$$(A.9) \quad F^\uparrow(x; y) = \limsup_{\substack{x' \dashv_F x \\ \theta \rightarrow 0^+}} \inf_{y' \rightarrow y} \frac{F(x' + \theta y') - F(x')}{\theta},$$

with

$$x' \dashv_F x \Leftrightarrow x' - x \quad \text{and} \quad F(x') - F(x).$$

If F is locally Lipschitzian at a given point x , then $F^\uparrow(x; y)$ reduces to Clarke’s original, directional derivative

$$(A.10) \quad F^0(x; y) = \limsup_{\substack{x' \dashv_F x \\ \theta \rightarrow 0^+}} \frac{F(x' + \theta y) - F(x')}{\theta}.$$

Let F be an extended real-valued functional on X , $F : X \rightarrow R \cup \{\infty\}$, and let x be any point at which F is finite. The *generalized subdifferential* of F at x is defined as the set

$$(A.11) \quad \bar{\partial}F(x) = \{x^* \in X^* \mid \langle x^* \mid y \rangle \leq F^\uparrow(x; y) \quad \forall y \in X\},$$

or equivalently as

$$(A.12) \quad \bar{\partial}F(x) = \{x^* \in X^* \mid (x^*, -1) \in N_{\text{epi } F}(x, F(x))\}.$$

The following propositions may be proved. If F is differentiable at x , then its generalized subdifferential consists of only one element, the gradient of F at x , i.e. $\bar{\partial}F(x) = \{\nabla F(x)\}$. If $F^1(x; 0) = -\infty$, then $\bar{\partial}F(x)$ is empty, but otherwise $\partial F(x)$ is nonempty and

$$(A.13) \quad F^1(x; y) = \sup\{\langle x^* | y \rangle \mid x^* \in \bar{\partial}F(x) \quad \forall y \in X\}.$$

If F is the indicator function of a set K , i.e. $F(x) \equiv \psi_K(x)$, the latter being defined in (A.3), then

$$(A.14) \quad \begin{aligned} \bar{\partial}F(x) &= \{x^* \in X^* \mid \langle x^* | y \rangle \leq \psi^1(x; y) \quad \forall y \in X\} \\ &= N_K(x). \end{aligned}$$

If F is a convex function on X , then $\bar{\partial}F(x)$ is equivalent to the subdifferential in the sense of convex analysis, as defined in (A.2).

Acknowledgment

This work was done whilst M. S. KUCZMA visited the Institute for Structural and Numerical Mechanics of Hannover University, under financial support from the European Communities (grant ERB-CIPA-CT-922073). This author would like to express his gratitude for the support.

References

1. J. ABOUDI, *Micromechanical analysis of composites by the method of cells*, Appl. Mech. Rev., **42**, 193–221, 1989.
2. D. BESDO and M. MÜLLER, *The influence of texture development on the plastic behaviour of polycrystals*, [in:] D. BESDO and E. STEIN, [Eds.], *Finite Inelastic Deformations Theory and Applications*, pp. 135–144, Springer-Verlag, Hannover, 1992.
3. D. BESDO and E. STEIN, [Eds.], *Finite inelastic deformations. Theory and Applications*, IUTAM Symposium Hannover, Germany 1991, Springer-Verlag, Berlin, 1992.
4. J.-P. BOEHLER, [Ed.], *Yielding, damage and failure of anisotropic solids*, Mechanical Engineering Publications, London, 1990.
5. R. DE BORST, *Integration of plasticity equations for singular yield functions*, Computer and Structures, **26**, 823–829, 1987.
6. O.T. BRUHNS, *Neue Materialgleichungen der Plastomechanik*, ZAMM, **73**, T6–T19, 1993.
7. O.T. BRUHNS, T. LEHMANN, and A. POPE, *On the description of transient hardening behaviour of mild steel Ck15.*, Int. J. Plasticity, **8**, 331–359, 1992.
8. S. CHENG and E. KREMPL, *Experimental determination of strain-induced anisotropy during nonproportional straining of an Al/Mg alloy at room temperature*, Int. J. Plasticity, **7**, 827–846, 1991.
9. F.H. CLARKE, *Optimization and Nonsmooth Analysis*, John Wiley and Sons, New York, 1983.
10. R.W. COTTE, F. GIANNESI, and J.-L. LIONS, [Eds.], *Variational Inequalities and Complementarity Problems*, John Wiley and Sons, Chichester, 1980.
11. A. B. DOUCET and S. NATARAJAN, *Yield behaviour of prestrained interstitial-free steel and 70/30 brass*, Metall. Trans., **22A**, 393–401, 1991.
12. D. C. DRUCKER, *A definition of stable inelastic material*, Transaction of the ASME J. Appl. Mech., **26**, 1, 101–106, March 1959.
13. M. K. DUSZEK, P. PERZYNA and E. STEIN, *Adiabatic shear band localization in elastic-plastic damaged solids*, Int. J. Plasticity, **8**, 361–384, 1992.
14. G. DUVAUT and J.-L. LIONS, *Inequalities in Mechanics and Physics*, Springer-Verlag, Berlin, 1976.
15. W. N. FINDLEY and M. J. MICHNO, *Concerning cusps and vertices on the yield surface of annealed mild steel*, ZAMM, **67**, 309–312, 1987.

16. A. GAWEŃCKI, *Elasto-plasticity of slackened systems*, Arch. Mech., **44**, 363–390, 1992.
17. A. E. GREEN and P. M. NAGHDI, *A general theory of an elastic-plastic continuum*, Arch. Rat. Mech. Anal., **18**, 251–281, 1965.
18. N. K. GUPTA and H. A. LAUERT, *A study of yield surface upon reversal of loading under biaxial stress*, ZAMM, **63**, 497–504, 1983.
19. N. K. GUPTA and A. MEYERS, *Description of initial and subsequent yield surfaces*, ZAMM, **66**, 435–439, 1986.
20. B. HALPHEN and Q. S. NGUYEN, *Sur les matériaux standards généralisés*, J. Méc., **14**, 1, 39–63, 1975.
21. R. HILL, *Theoretical plasticity of textured aggregates*, Math. Proc. Camb. Phil. Soc., **85**, 179–191, 1979.
22. R. HILL, *Constitutive dual potentials in classical plasticity*, J. Mech. Phys. Solids, **3**, 23–33, 1987.
23. R. HILL and J. R. RICE, *Elastic potentials and structure of inelastic constitutive laws*, SIAM J. Appl. Math., **25**, 448–461, 1973.
24. K. IKEGAMI, *Experimental plasticity on the anisotropy of metals*, [in:] J. -P. BOEHLER [Ed.], *Mechanical Behavior of Anisotropic Solids*, pp. 201–242. Martinus Nijhoff Publishers, 1982.
25. A. A. ILYUSHIN, *On the postulate of plasticity* [in Russian], Prikl. Mat. Mech., **25**, 503–507, 1961.
26. S. J. KIM and J. T. ODEN, *Generalized potentials in finite elastoplasticity (Part I)*, Internat. J. Engng. Sci., **22**, 1235–1257, 1984.
27. S. J. KIM and J. T. ODEN, *Generalized potentials in finite elastoplasticity (Part II)*, Internat. J. Engng. Sci., **23**, 515–530, 1985.
28. U. F. KOCKS, *Constitutive behavior based on crystal plasticity*, [in:] A. K. MILLER [Ed.], *Unified Constitutive Equations for Creep and Plasticity*, pp. 1–88. Elsevier, 1987.
29. W.T. KOITER, *Stress-strain relations, uniqueness and variational theorems for elasto-plastic materials with a singular yield surface*, Quart. Appl. Math., **11**, 350–354, 1953.
30. W.T. KOITER, *General theorems for elastic-plastic solids*, [in:] I. N. SNEDDON and R. HILL [Eds.], *Mechanics of Engineering Materials*, Chapter 3, pp. 165–221, North-Holland, Amsterdam, June 1960.
31. M. S. KUCZMA and J. R. WHITEMAN, *Variational inequality formulation for flow theory plasticity*, Int. J. Engng. Sci. (in print).
32. R. B. LAMMERING, R. PECHERSKI and E. STEIN, *Theoretical and computational aspects of large plastic deformations involving strain-induced anisotropy and developing voids*, Arch. Mech., **42**, 347–375, 1990.
33. T. LEHMANN, *On a generalized law in thermo-plasticity, taking into account different yield mechanisms*, Acta Mech., **57**, 1–23, 1985.
34. J. LEMAITRE and J.-L. CHABOCHE, *Mechanics of solids materials*. Cambridge University Press, Cambridge, 1990.
35. V. LEVITAS, *Some models of inelastic deformation of materials*, Communications 1 & 2. Strength of materials, **12**, 1536–1552, 1980.
36. V. I. LEVITAS, *Large elastoplastic deformations at high pressure* [in Russian], Naukova Dumka, Kiev, 1987.
37. V. I. LEVITAS, *Large deformation of materials with complex rheological properties at normal and high pressure*, Nova Science Publishers, NY, 1993.
38. A. LITEWKA and A. SAWCZUK, *On a continuum approach to plastic anisotropy of perforated materials*, [in:] J. -P. BOEHLER, *Mechanical Behavior of Anisotropic Solids*, 803–818. Martinus Nijhoff Publishers, 1982.
39. J. LUBLINER, *On the thermodynamic foundations of non-linear solid mechanics*, Int. J. Non-Linear Mech., **7**, 237–254, 1972.
40. J. LUBLINER, *On the structure of the rate equations of materials with internal variables*, Acta Mech., **17**, 109–119, 1973.
41. G. MAIER, *Piecewise linearization of yield criteria in structural plasticity*, SM Arch., **1**, 239–281, 1976.
42. J. MANDEL, *Generalisation de la théorie de plasticité de W.T. Koiter*, Int. J. Solids Struct., **1**, 273–295, 1965.
43. A. MEYERS, *Certain considerations on yield surfaces*, 32nd ISTAM Congress, pp. 56–65.
44. M. J. MICHNO and W. N. FINDLEY, *A historical perspective of yield surface investigations for metals*, Int. J. Non-Linear Mech., **11**, 59–82, 1976.
45. C. MIEHE and E. STEIN, *A canonical model of multiplicative elasto-plasticity, formulation and aspects of the numerical implementation*, Eur. J. Mech. A/Solids, **11**, 25–43, 1992.
46. J. J. MOREAU, *On unilateral constraints, friction and plasticity* [in:] G. CAPRIZ and G. STAMPACCHIA [Eds.], *New Variational Techniques in Mathematical Physics*, pp. 171–322, Edizioni Cremonese, Roma 1974.
47. Z. MRÓZ, *On the description of anisotropic work hardening*, J. Mech. Phys. Solids, **15**, 163–175, 1967.

48. P. M. NAGHDI, *Stress-strain relations in plasticity and thermoplasticity*, [in:] E. H. LEE and P. S. SYMONDS [Eds.], *Plasticity*, pp. 121–169, Pergamon Press, Oxford, 1960.
49. P. M. NAGHDI and J. A. TRAPP, *The significance of formulating plasticity theory with reference to loading surface in strain space*, *Int. J. Engng. Sci.*, **13**, 785–797, 1975.
50. S. NEMAT-NASSER, *Phenomenological theories of elastoplasticity and localization at high strain rates*, *Appl. Mech. Rev.*, **45**, 3, S19–S45, 1992.
51. Q. S. NGUYEN, *On the elastic plastic initial-boundary value problem and its numerical integration*, *Int. J. Num. Meth. Engng.*, **11**, 817–832, 1977.
52. J. T. ODEN, *Qualitative Methods in Nonlinear Mechanics*, Prentice-Hall, Englewood Cliffs, NJ, 1986.
53. M. ORTIZ and E. P. POPOV, *Accuracy and stability of integration algorithms for elastoplastic constitutive relations*, *Int. J. Numer. Meth. Engng.*, **21**, 1561–1576, 1985.
54. A. C. PALMER, G. MAIER, and D. C. DRUCKER, *Normality relations and convexity of yield surfaces for unstable materials or structural elements*, *Transactions of the ASME J. Appl. Mech.*, pp. 464–470, June 1967.
55. P. D. PANAGIOTOPOULOS, *Non-convex energy functionals, application to non-convex elastoplasticity*, *Mech. Res. Comm.*, **9**, 23–29, 1982.
56. P. D. PANAGIOTOPOULOS, *Inequality problems in mechanics and applications. Convex and nonconvex energy functions*, Birkhäuser, Boston, 1985.
57. A. PHILLIPS and R. L. SIERAKOWSKI, *On the concept of the yield surface*, *Acta Mech.*, **1**, 29–35, 1965.
58. J. PINDERA, M. J. ABOUDI and J. BRAYSHAW, *Micromechanical investigation on the convexity of yield surfaces of metal matrix composites*, *Int. J. Plasticity*, **7**, 549–566, 1991.
59. L. PLANK, E. STEIN, and D. BISCHOFF, *Accuracy and adaptivity in the numerical analysis of thin-walled structures*, *Comp. Meth. Appl. Mech. Engng.*, **82**, 223–256, 1990.
60. B. RANIECKI, *Uniqueness criteria in solids with non-associated plastic flow laws at finite deformations*, *Bull. Acad. Pol. Sci., Serie Sci. Tech.*, **28**, 391–399, 1979.
61. J. R. RICE, *Inelastic constitutive relations for solids: An internal-variable theory and its application to metal plasticity*, *J. Mech. Phys. Solids*, **19**, 433–455, 1971.
62. J. R. RICE, *Continuum mechanics and thermodynamics of plasticity in relation to microscale deformation mechanisms*, [in:] A. S. ARGON, editor, *Constitutive Equations In Plasticity*, Chapter 2, pp. 23–79. The MIT Press, Cambridge, Massachusetts, and London, England, 1975.
63. R. T. ROCKAFELLAR, *Generalized directional derivatives and subgradients of nonconvex functions*, *Canad. J. Math.*, **32**, 257–280, 1980.
64. R. T. ROCKAFELLAR, *The theory of subgradients and its applications to problems of optimization. Convex and nonconvex functions*, Heldermann Verlag, Berlin 1981.
65. E. SHIRATORI, K. IKAGAMI and K. KANEKO, *Plastic behaviour of initially anisotropic metals after multi prestainings*, J. -P. BOEHLER [Ed.], *Mechanical Behavior of Anisotropic Solids*, pp. 257–271. Martinus Nijhoff Publishers, 1982.
66. J. C. SIMO, *Algorithms for static and dynamic multiplicative plasticity that preserve the classical return mapping of infinitesimal theory*, *Comput. Meth. Appl. Mech. Engng.*, **99**, 61–112, 1992.
67. J. C. SIMO, J. G. KENNEDY, and S. GOVINDJEE, *General return mapping algorithms for multisurface plasticity and viscoplasticity*, *Int. J. Numer. Meth. Engng.*, **26**, 2161–2185, 1988.
68. A. N. SUPRUN, *On the existence of conical points and concavities on the yield surface of metals*, *Mech. Solids*, **26**, 4, 175–180, 1991.
69. P.-M. SUQUET, *Local and global aspects in the mathematical theory of plasticity*, A. SAWCZUK and G. BIANCHI [Eds.], *Plasticity Today: Modelling, Methods and Applications*, pp. 279–310. Elsevier Applied Science Publishers, London 1985.
70. W. SZCZEPINSKI, *On deformation-induced plastic anisotropy of sheet metals*, *Arch. Mech.*, **45**, 3–38, 1993.
71. Y. ZHU, B. DODD, R. M. CADDEL, and W. F. HOSFORD, *Convexity restrictions on non-quadratic anisotropic yield criteria*, *Int. J. Mech. Sci.*, **29**, 10, 733–741, 1987.
72. O. C. ZIENKIEWICZ and R. L. TAYLOR, *The finite element method*, vol. 2, Mc-Graw-Hill, London, 1991.
73. M. ŻYCZKOWSKI, *Combined loadings in the theory of plasticity*, PWN–Polish Scientific Publishers, Warszawa, 1981.

74. M. ZYCKOWSKI and T. KURTYKA, *A description of distortional plastic hardening of anisotropic materials*, J.-P. Boehler [Ed.], *Yielding, Damage and Failure of Anisotropic Solids*, pp. 97–111, Mechanical Engineering Publications, London 1990.

INSTITUTE FOR STRUCTURAL AND NUMERICAL MECHANICS
UNIVERSITY OF HANNOVER, D-30167 HANNOVER, GERMANY.

Received February 23, 1994.

On Cosserat plasticity and plastic spin for isotropic materials

D. LACHNER, H. LIPPMANN (MÜNCHEN) and L.S. TÓTH (METZ)

DIFFERENT THEORETICAL approaches to the problem of the effect of grain rotations during plastic torsion are compared with experiments. On the theoretical side the concept of Cosserat plasticity includes a Cosserat continuum to calculate an independent macroscopic rotation — the plastic spin. Some crystal plasticity theories are applied to calculate the rotation of each individual grain. With the help of statistics, again a macroscopic rotation can be calculated. In experiments the rotations of a sample of grains in some Al-cylinders and rods of different geometries are measured with the v. Laue backreflection method. After statistical evaluation of the individual rotations, the averaged rotations are compared with the different theories.

Notations

- \mathbf{m} nonsymmetric tensor of couple stresses,
- m_c confidence interval,
- \mathbf{S} nonsymmetric stress tensor,
- Y uniaxial yield limit,
- α_L, β material constants,
- γ macroscopic rotation rate,
- σ symmetric part of \mathbf{S} ,
- τ antisymmetric part of \mathbf{S} ,
- $\lambda = \lambda_{xy}$ torsional shear rate,
- ω absolute rotation rate,
- Ω relative rotation rate (Cosserat rotation rate, plastic spin),
- Ω/λ normalized Cosserat rotation rate.

1. Introduction

THE SUBJECT of this paper is a comparison of experiments with the predictions of several different plasticity models that can describe more than just the deformation and stress state, usually accessible by the classical methods in plasticity.

A more detailed description may incorporate some internal parameters like hardening, damage or the development of a substructure that characterize the state of the material. The behaviour of the material then depends on these internal parameters. Often the rotation of the substructure of the material is regarded as an important parameter.

Numerous papers deal with the so-called “plastic spin” — in non-isotropic materials — and look for a constitutive law for this independent rotation, see for example [1] or [2]. According to these papers, the plastic spin vanishes in isotropic materials. Another approach to a detailed description of such rotational effects results from the crystal plasticity. It has to be noted here that the term “plastic spin” is defined as a macroscopic quantity in the continuum descriptions, while in crystal plasticity it has a different meaning under the same name, and originates from the crystallographic slip. Thus, with the help of some

theories of crystal slip, for example the Taylor theory [3], it is possible to calculate individual crystal rotations. Averaging these rotations over a number of crystals leads to a corresponding macroscopic quantity. A third possibility to calculate internal rotations has been presented in some papers of LIPPMANN [4] and BESDO [5]. In this latter approach the Cosserat-continuum based on extended yield conditions has been used. This approach is a generalization of the classical continuum plasticity in the sense of more degrees of freedom, where also the corresponding static quantities like couple stresses or antimetric shear stresses are incorporated.

The purpose of this paper is to compare the predictions of the Cosserat approach and some crystal plasticity approaches with each other and mainly with experiments, where the free rotations of the individual grains have been measured.

2. Experiments

Experiments have been carried out on cylindrical and tubular specimens made of pure aluminium Al 99.999. After a heat treatment this material is rather coarse-grained (Fig. 1) and its grain orientation distribution is nearly isotropic. The specimens were twisted up to a plastic shear deformation of about 10% under the condition of free end torsion (Fig. 2), and the rotations of about 60 to 100 randomly selected grains were measured. These grains lie on the outer surface of the specimen, and they have been marked in order to identify them before and after deformation. In this paper especially the experimental results obtained from two of the various specimens will be discussed as examples. Specimen DV2 is a full cylinder with 14 mm diameter, TB3 a tube with 39 mm outer and 22 mm inner diameter. For both specimens, the homogeneously deformed length amounts to 75 mm. The maximum torsional angle, imposed on this length, was about 45° (TB3) or 120° (DV2). This corresponds to a plastic shear of about 10%. This total deformation was achieved in three consecutive steps. In each step and for each grain, the rotation was calculated from the orientation change of the crystal. In order to get this orientation, the X-ray v. Laue-technique was employed. In order to measure the orientation of only one grain, the polychromatic X-ray beam must hit only one crystal in the polycrystalline material. For that reason the material must be coarse-grained. From the position of the reflection spots on the v. Laue photographs, the orientation of the crystal can be calculated in a given coordinate system. For more details the reader is referred to [6] and [7].

The values of the individual grain rotations can approximately be transformed into rotation rates by forming the differences between two subsequent rotational steps and dividing them by the time increment. In this way it is found that, up to the above-mentioned shear limit of 10%, the rotation rate of most grains remains nearly constant. For each grain, therefore, a constant angular velocity ω is assumed.

The macroscopic torsional shear rate λ and the macroscopic rate of rotation γ can be calculated from the symmetric and the antimetric part of the macroscopically homogeneous velocity gradient of the specimen. Thus, the relative rotation rate Ω for each grain can be obtained as

$$(2.1) \quad \Omega = \gamma - \omega.$$

Ω is also called the Cosserat rate of rotation, or the plastic spin (if, for large deformation, the elastic part is disregarded). To enable the comparison of different experiments (differ-

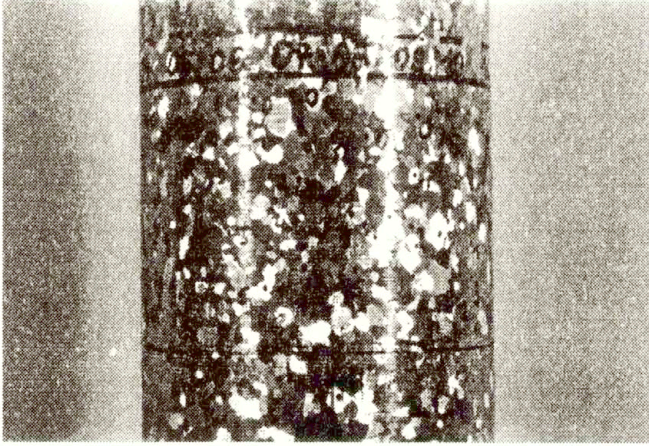


FIG. 1. Coarse-grained specimen of 99.999% purity Al (heat-treated and surface-etched, grain diameter about 1.5 mm).

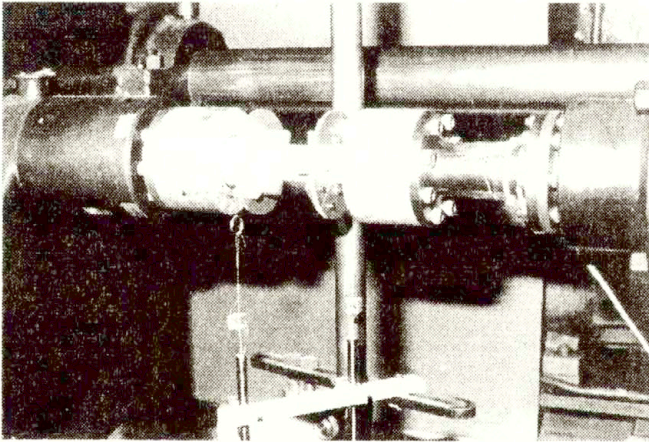


FIG. 2. Plastic torsion of cylindrical specimens.

ent specimen geometry or different twisting rates), Ω is normalized by the macroscopic shear rate $\lambda_{xy} = \lambda$. If the dimensionless quantity Ω/λ differs from zero, the individual grain rotation is larger or smaller than the macroscopic rotation rate related to the deformation field. In this way the distribution of the relative spin Ω/λ of the selected sample of all grains in each specimen can be obtained (Fig. 3), where the subscripts x , y or z refer to the axial, circumferential and radial direction, respectively, at the outer surfaces.

In the following these experimental results will be evaluated on a statistical basis. First of all a rather large scatter can be observed, especially for Ω_z/λ which is the rotation rate around the radial direction. A value of $\Omega_z/\lambda = 1$ means, because of $\gamma_z = \lambda_{xy}$ and (2.1), an absolute rotation rate $\omega_z = 0$. On the other hand, a value of $\Omega_z/\lambda = -1$ means an absolute rotation rate twice as large as the macroscopic rotation rate γ_z . These values ± 1 are reached for Ω_z/λ by a considerable number of grains; in the other two

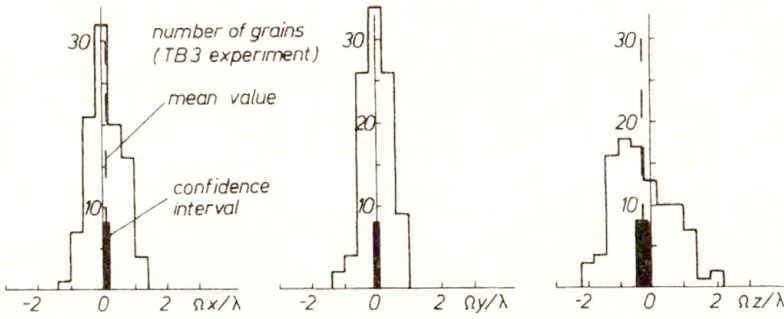


FIG. 3. Distribution of the experimental values of the relative spin Ω/λ for specimen TB3 x -axial, y -circumferential and z -radial direction.

directions at least by some grains. Therefore the individual grains show a very disperse rotational behaviour. This may depend on the initial orientation of the crystal lattice, the shape, the size and also the behaviour of the neighbouring grains. Besides it is interesting to notice that the angular velocity of a needle thrown into a fluid under simple shear λ_{xy} would also vary between the same limits, i.e., 0, if the needle is parallel to the stream lines, and $2\gamma_z$, if it is perpendicular. This implies that the needle in a shear flow constitutes the simplest model for the individual grain rotations, although it is not clear as yet whether or how the direction of the needle can be identified with the crystal lattice.

If one single parameter is looked for describing the rotation of the substructure of the material, it seems to be reasonable to choose the average value of all selected grains and to regard it as the mean rotation. The confidence interval m_c of this mean value is also calculated as

$$(2.2) \quad m_c = \frac{ts}{\sqrt{n}},$$

with the standard deviation s of the distribution, the number of grains n and a correction factor t (Student-distribution), that depends on the desired probability. This confidence interval is shown in Fig. 3 as an example. The real average spin of all grains of the specimen will lie inside the shown confidence intervals with a probability of 95%. Unfortunately, these confidence intervals are rather large in relation to the mean value of Ω/λ itself. The reason of it will be discussed later. The experimental confidence intervals compared to the theoretical predictions are also shown, for cylindrical or tubular specimens, in Figs. 5 and 6, respectively.

3. Cosserat plasticity

As mentioned in the introduction, it is possible to calculate the plastic spin by means of the application of a Cosserat continuum to plasticity ([4, 5, 6, 7]). The Cosserat brothers proposed, at the beginning of this century, a generalized continuum with three additional kinematic degrees of freedom, corresponding to the spin components around three (local Cartesian) axes. In a continuum they must represent local or spatial averages which will be compared with the average spin of the grains obtained from the experiments. Note that the continuum considered in the present paper is isotropic (within the technological limits), while the plastic spin as discussed in the contemporary literature (unaware of the

Cosserat approach) is related only to anisotropic, textured media in which the rotation of the texture may be interpreted a priori as an average grain rotation.

In the Cosserat continuum there are also additional static quantities related to the kinematic ones. The stress tensor \mathbf{S} , for example, may be nonsymmetric. Its antisymmetric part $\boldsymbol{\tau}$ is known to generate work against the spin components of $\boldsymbol{\Omega}$ ([4, 5]) — a property recently re-discovered by VAN DER GIESSEN [2]. Moreover, the non-symmetric tensor of couple stresses, \mathbf{m} , is introduced to generate work against the components of the so-called internal twist (i.e., local bending and torsion). Taking into account the complete set of all these static and kinematic quantities, generalized field equations can be set up comprising generalized equilibrium equations, compatibility equations and a constitutive law.

The constitutive law contains, as usual in plasticity, a yield condition and the flow rule. One yield condition for metals was proposed by LIPPMANN [4, 7]. It consists of two separate conditions, the first for the stresses, the second for the couple stresses, according to

$$(3.1) \quad \begin{aligned} f^1 &= \sqrt{\frac{3}{2}(\sigma_j^k \sigma_k^j + 2\beta^2 \tau_j \tau^j)} - Y = 0, \\ f^2 &= \sqrt{m_j^k m_k^j} - \frac{Y L}{\alpha_L} = 0, \end{aligned}$$

so that the simultaneous fulfilment of both equations corresponds to an edge in the generalized yield locus. Equation (3.1) is similar to the classical von Mises yield condition. Y describes the uniaxial yield limit which may depend on internal parameters like the equivalent strain. For this reason isotropic hardening is taken into account. L represents a characteristic length of the continuum to be identified with the mean grain diameter. α_L and β are material parameters to be identified experimentally with the help of one of the specimens only. This has been done in [6] with a specimen that was nearly identical to specimen DV2. These values for α_L and β are kept constant for the specimens regarded in this paper.

Complete Cosserat solutions for the case of free end torsion of full cylinders are presented in [6] and [7]. They have been extended in a straightforward manner also to tubular specimens [8].

4. Crystal plasticity theories

Another approach to plastic spin can be based on the theories of crystal plasticity. It gives us a possibility to calculate the behaviour of single crystals within a polycrystalline aggregate under plastic deformation. In crystal plasticity the initial orientation and the mechanical boundary conditions must be known in advance. Obviously, this latter information is not available for the individual grains, so it must be replaced by appropriate assumptions.

One crystal plasticity model employed in this paper is a Taylor-type viscoplastic model presented by TÓTH *et al.* [9] with various relaxed constraints conditions. In this model, several possibilities for the boundary conditions of the grains are available: If all components of the deformation gradient of the grain under consideration are prescribed, the classical Taylor theory is applied (in Fig. 5 and 6 entitled “Taylor”). If all components of the stress tensor are prescribed, the classical Sachs theory is modelled (in Figs.: “Sachs”).

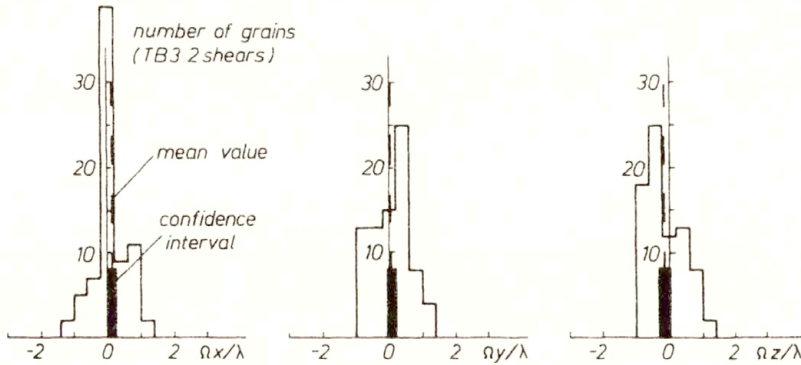


FIG. 4. Distribution of the predicted values of the relative spin Ω/λ . Specimen TB3, crystal plasticity model "2 shears", x , y , z as in Fig. 3.

Mixed boundary conditions are modelled if only one or two shear components of the deformation gradient are prescribed. (in Figs.: "1 shear" or "2 shears").

Other crystal plasticity models are also used in the present work: the minimum plastic spin theory of Fuh and Havner [10] ("Mi.pl.spi") and the self-consistent model of Molinari [11] ("Self cons."). For more details see ref. [12].

All these theories were applied to the grains measured in our specimens experimentally, using the v . Laue technique. With the initial orientation measured, the rotation was predicted by means of the different crystal plasticity models. The distribution of the nearly 100 spin values for each model (e.g. Fig. 4) was compared with the experimentally determined distribution (Fig. 3 as an example).

As a first result it was found that the calculated rotations for the individual grains as predicted by the different models show rather large deviations from the experimentally measured ones. Looking at the predictions of all theories, it is seen that some grain rotations agree well with one theory, others with another one, and some with none at all. This is understandable as the grain boundary conditions may vary very strongly from grain to grain, and can be very different from the assumed boundary conditions.

A statistical evaluation is also applied to these predictions. The mean value of the spin of all selected grains was determined together with the standard deviation and the confidence interval m_c (Eq. (2.1)) of the distribution. In this way, a comparison between the experimental results and the ones calculated by the different crystal plasticity theories could be done, not only with respect to their mean values, but also with respect to the widths of the distributions. The results are shown in Figs. 5 and 6 for the relative spin Ω/λ obtained at the outer surface of the specimen.

It is seen in Fig. 5 that the confidence intervals have all the same order of magnitude. This is due to a nearly equal standard deviation of the experimental and the predicted distributions, and it indicates that the large widths of the distributions of the relative spin Ω/λ must be a consequence of the distribution of the initial grain orientations. In our nearly isotropic specimens the initial grain orientations are rather homogeneously distributed. This obviously leads to a correspondingly wide distribution of the spin. As discussed in Sec. 2, the half-width may be comparable to the macroscopic rotation rate γ_z . In Fig. 3 or 4 this means a half-width 1 for Ω_z/λ . It is reached rather satisfactorily in the experiments as well as for the predictions based on crystal plasticity, so that the

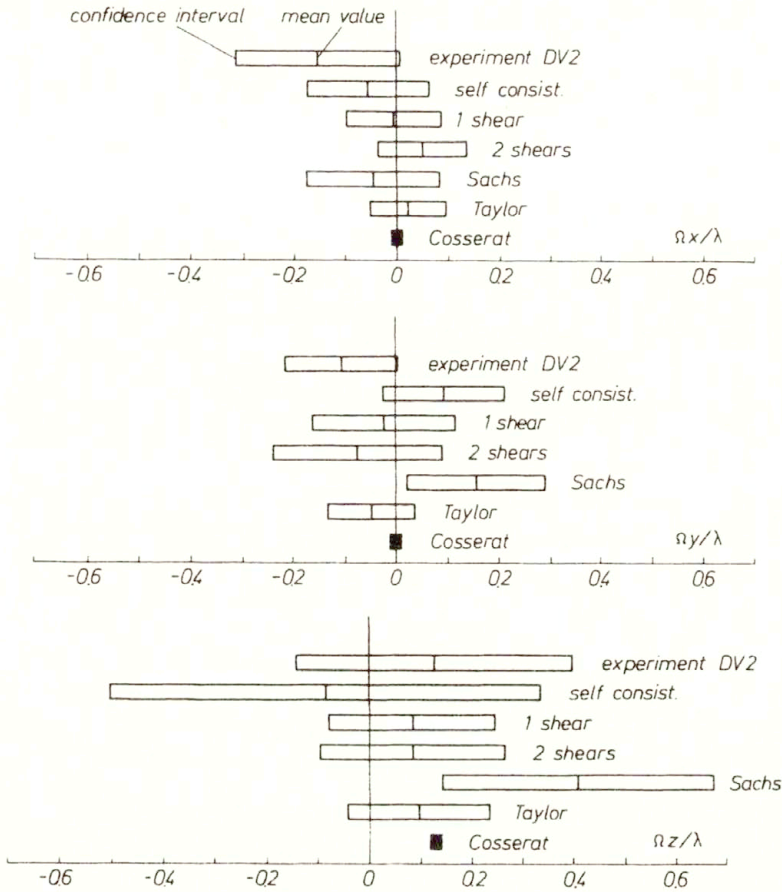


FIG. 5. Confidence intervals and mean values for the relative spin Ω/λ : experimental results and theoretical predictions, specimen DV2; x, y, z as in Fig. 3.

standard deviation or the adequate confidence interval of the distributions must actually be regarded to be specific for the initial state of the material. Note that the theoretical solution following the Cosserat plasticity yields only one value, so that there is no confidence interval.

Except for the theoretical results obtained from the Sachs-theory and from the self-consistent theory, both with respect to Ω_y/λ and to Ω_z/λ , the theoretical predictions do not differ very much from each other in Fig. 5 if the large width of the confidence intervals is taken into account. The experimental results agree also quite well with the theoretical ones, at least for Ω_y/λ and Ω_z/λ , the latter quantity being the most representative one. If the specimen was truly isotropic, $\Omega_x/\lambda = \Omega_y/\lambda = \Omega_z/\lambda = 0$ should hold as it is also reflected by the results of the Cosserat theory. However, the experiments as well as the other theories yield values different from 0 which are also different from each other. This must again be due to the initial distribution of the grain orientations showing obviously, despite the careful preparation of the specimen, some hidden anisotropy.

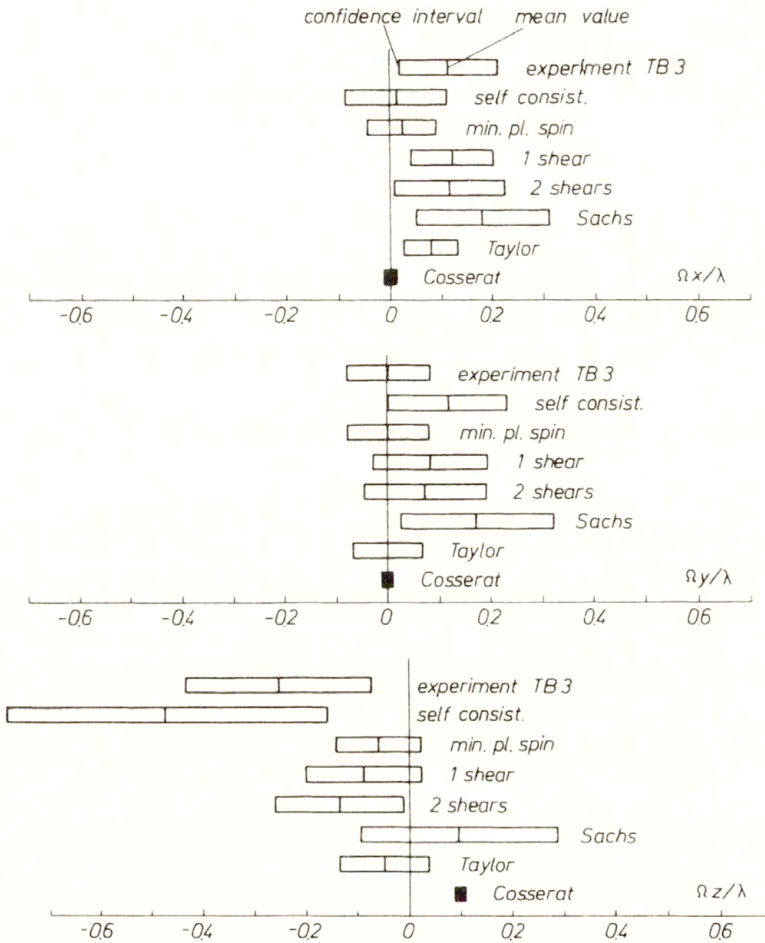


FIG. 6. Confidence intervals and mean values for the relative spin Ω/λ : experimental results and theoretical predictions, specimen TB3, x, y, z as in Fig. 3.

In specimen TB3 (Fig. 6) the differences are larger. In contrast to all the other specimens, the representative quantity, i.e. Ω_z/λ measured in the experiment, is not positive as it was predicted by the Cosserat theory (based on truly isotropic behaviour), and also measured experimentally on a different specimen with the same geometry (TB2, results not shown). The reason for this must be again a hidden texture, more pronounced in specimen TB3 than in the other ones.

5. Conclusions

In this investigation on the rotational behaviour of the metallic grains in isotropic non-textured aluminium specimens under torsion, experimental results were compared with theoretical predictions obtained from several different theories.

The Cosserat theory of plasticity as a macroscopic generalized continuum approach has the advantage that the individual inhomogeneous distribution of grain shapes and

crystal orientations are not required as an input. Thus the knowledge of the orientation distribution of the grains and the boundary conditions are not necessary for the calculation. The results obtained from this model are, nevertheless, not too far from the experiments. However, large deviations may occur if an initial texture can not be avoided, even if this texture is small due to a careful preparation of the specimens.

The crystal plasticity theories take the real distribution of the grain orientations into account, i.e., the initial texture of the material. Besides, also the mutual constraints of the grains are regarded by some assumed and simplified boundary conditions which vary from theory to theory. Nevertheless, the behaviour of individual grains shows a poor agreement with the experiments. Therefore statistical mean values of a number of grains are regarded, where the agreement with the experiments is better.

References

1. Y.F. DAFALLAS and H.W. CHO, *Verification of the plastic spin concept in viscoplasticity*, [in:] *Advances in Plasticity*, A.S. KHAN and M. TOKUDA [Eds.], 287–290, Pergamon Press, Oxford 1989.
2. E. VAN DER GIESSEN, *The plastic spin: micromechanical and thermodynamic aspects*, [in:] *Advances in Plasticity*, A.S. KHAN and M. TOKUDA [Eds.], 327–330, Pergamon Press, Oxford 1989.
3. G. I. TAYLOR, *Plastic strain in metals*, *J. Inst. Metals*, **62**, 307–324, 1938.
4. H. LIPPMANN, *Eine Cosserat-Theorie des plastischen Fließens*, *Acta Mechanica*, **8**, 255–284, 1969.
5. D. BESDO, *Ein Beitrag zur nichtlinearen Theorie des Cosserat-Kontinuums*, *Acta Mechanica*, **20**, 105–131, 1974.
6. W. DIEPOLDER, *Das Cosserat-Kontinuum als Strukturmodell für plastische Komdrehungen*, Dr.-Thesis, TU München 1989.
7. W. DIEPOLDER, V. MANNL and H. LIPPMANN, *The Cosserat-continuum, a model for grain rotation in metals?*, *Int. J. Plasticity*, **7**, 313–328, 1991.
8. D. LACHNER and H. LIPPMANN, *Plastisches Cosserat-Kontinuum*, Arbeitsbericht zum DFG-Forschungsvorhaben Li115/34-1, München 1993.
9. L.S. TÓTH, P. GILORMINI and J.J. JONAS, *Effect of rate sensitivity on the stability of torsion textures*, *Acta Metall.*, **36**, 3077–3091, 1988.
10. S. FUH and K.S. HAVNER, *A theory of minimum plastic spin in crystal mechanics*, *Proc. Roy. Soc. London A*, **422**, 193–239, 1989.
11. A. MOLINARI, G.R. CANOVA and S. AHZI, *A self-consistent approach of the large deformation polycrystal viscoplasticity*, *Acta Metall.*, **35**, 2983–2994, 1987.
12. L.S. TÓTH, H. LIPPMANN, D. LACHNER and W. DIEPOLDER, *Grain rotations in torsion*, *Proc. Fourth Int. Symp. on Plasticity and its Current Applications*, Baltimore, USA, July 19–23, 1993, in press.

LEHRSTUHL A FÜR MECHANIK
 TECHNISCHE UNIVERSITÄT, MÜNCHEN, GERMANY
 and
 LABORATOIRE DE PHYSIQUE ET MECANIQUE DES MATERIAUX
 UNIVERSITE DE METZ, METZ, FRANCE.

Received January 3, 1994.

Viscoplastic numerical analysis of dynamic plastic strain localization for a ductile material

T. LODYGOWSKI (POZNAŃ), P. PERZYNA (WARSZAWA)
M. LENGNICK and E. STEIN (HANNOVER)

THE THEORY of viscoplasticity was used to describe the plastic strain localization in a ductile material under dynamic loading, and serves as a tool for regularization of initial boundary value problem. The method of numerical integration of the constitutive equations is proposed and implemented into ABAQUS environment. During the presentation of the numerical results the problem of mesh dependence is discussed. Using a well-posed mathematical formulation one can avoid the so-called *Primary Mesh Dependence* which is defined in the paper.

1. Introduction

THE PHENOMENON called localization frequently accompanies inelastic deformation and consists in the formation of localized, relatively narrow, bands of intensive straining. For large variety of experiments the results expressed in load-displacement space exhibit a descending branch after the peak load has been obtained. In phenomenological approach, a simple mapping of such data onto stress-strain relations provides negative stiffnesses in the constitutive models. This introduces the so-called strain-softening models. It is known, and it was explored by many researchers, that in the classical frame of rate-independent continuum it can lead to the loss of well-posedness of the initial boundary value problem (IBVP).

The problem of well-posedness which is the fundamental one for the statement and the following numerical solution, has been studied by KATO [11] HUGHES, KATO, MARS-DEN [10], PERZYNA [25, 21], de BORST *et al.* [6], and recently also by KIBLER *et al.* [12].

The proper posedness of the BVP affects also, according to the study of LENGNICK *et al.* [14], the significant decreasing of the so-called *primary mesh dependence* (PMD) in finite element computations. By PMD we understand here the behaviour of the numerical solutions which is very sensitive to the finite element mesh and which directly is a result of ill-posedness of IBVP.

Application of rate-independent material models does not ensure the well-posedness in postcritical states. The classical papers of HILL [9], MANDEL [16], and RICE [27] stated that loss of material stability and, what follows, localization will not occur until at least one eigenvalue of the acoustic tensor is equal to zero. The Maxwell's or Hadamard's compatibility conditions used here decide that the localization is associated with a strain rate jump within a planar band, and it does not enforce any kinematic incompatibilities with the remaining material. According to the rate-independent model, the further study of evolution of the localization domain is not possible because of the change of type of the incremental governing operator. Instead of studying the abstract Cauchy problem to

discuss the posedness, it is easier to concentrate the attention on the acoustic tensor [12]. The interesting study on bifurcations in inelastic materials has been recently published by NEILSEN and SCHREYER [19].

For the static problems, when the system of governing equations changes from elliptic to hyperbolic (if one of the eigenvalues $\lambda = 0$ — to parabolic), we can not expect the results of the described physical phenomena in real space (ill-posedness).

Moreover, the bifurcation analysis mentioned above predicts only the localization line which basically is not fully confirmed in laboratory experiments. It appears, that always the localization zones have finite width, which depends upon material properties, but also very strongly on the boundary and initial conditions.

To regularize the system of equations (PDE) that drives the incremental process in post-localization states, one has to introduce a length scale parameter what leads to the specification of the width of localization. The comprehensive study was presented by SLUYS [28]. To enrich the softening continuum, the length scale parameter can be introduced to the formulation in a different way; for example: using nonlocal theories — BAŽANT and PIAUDIER-CABOT [2], the addition of higher order (second order) strain terms — BELYTCHKO [3], gradient model — DE BORST [5, 7], inclusion of micro-polar effects DE BORST [6], STEINMANN and WILLAM [29], or application of rate-dependent formulation — PERZYNA [25], NEEDLEMAN [18].

At last it is also possible to introduce the width of the localization zone (length scale parameter) explicitly into the formulation, as it was shown by PIETRUSZCZAK and MRÓZ [26], BELYTCHKO *et al.* [4], ORTIZ *et al.* [20] or ŁODYGOWSKI [15]. The only drawback of the rate-dependent formulation seems to be the necessity of full dynamical analysis of the process under consideration. In authors' opinion the rate-dependent model, specially for ductile metals, is physically well founded, and then it has a variety of advantages in comparison with the other models. Using such parameters like viscosity, particularly for fast mechanical processes, has a deep physical reason on the micromechanical level. For these reasons we will use viscoplasticity to describe the physical process, as a tool of mathematical regularization of softening behaviour.

In view of the achievements [14] for the viscoplastic (rate-dependent) formulation, the problem remains well-posed in each interval of time, so the unique solution in numerical calculations can be reached. Using dynamical formulation for two-dimensional cases, both failure modes (I-mode and II-mode) can be performed and also, because of the wave propagation phenomenon, no artificial imperfections are necessary in computations to be superposed to activate the process of localization. Approaching the calculations of localization phenomena, we are not going now to avoid all the variety of numerical subtleties which occur, for example, due to secondary mesh dependence SMD [14] or mesh alignment (cf. SLUYS [28]).

One of the aims of this presentation is to show numerically that proper mathematical formulation helps to avoid the serious mesh sensitivity called here PMD.

The study is reported as follows. First we will present the set of field equations which governs the described physical phenomena. Here the kinematics and the constitutive model will be formulated. Then 2-D plane strain case will be specified. Later, there are the remarks on the integration of the field equations. In the next section the results of numerical computations of two boundary value problems are presented and discussed.

These examples refer to the problem of biaxial impact loading, but with different initial conditions. The good agreement of the results for different finite element meshes

is shown, as well as a strong influence of initial boundary conditions on the results (the shape of localization zones). Final remarks close the paper.

2. Formulation

2.1. Kinematics

Following the notation of GURTIN [8] we assume two configurations: \mathcal{B}_τ at time $t = \tau$, for which the state is in equilibrium, and \mathcal{B}_t at time $t = \tau + \Delta t$ when the continuum is going to occupy the current configuration. Then the basic problem is to determine the equilibrium state of the body at each material point in \mathcal{B}_t based on the given constitutive law which is discussed in the next section. From the viewpoint of numerical formulation and computations, it is important to assure the consistency with the set of constitutive equations, numerical stability and objectivity; it means that the proposed algorithm should be invariant with respect to the rigid body motions. The summary of incrementally objective integration schemes was recently presented by ZABARAS and ARIF [32].

The requirements of objectivity starts from the definition of two motions $\Phi(\mathbf{X}, t)$ and $\Phi^*(\mathbf{X}, t)$. It can be stated that those motions are objectively equivalent if they fulfill

$$(2.1) \quad \Phi^*(\mathbf{X}, t) = \mathbf{Z}(t)(\Phi^*(\mathbf{X}, t) - \mathbf{o}) + \mathbf{c}(t),$$

where \mathbf{o} is a fixed point in space; $\mathbf{Z}(t)$ and $\mathbf{c}(t)$ are rotation and translation, purely time-dependent functions, respectively. Moreover, the rotation $\mathbf{Z}(t)$ satisfies the condition

$$(2.2) \quad \mathbf{Z}^T \mathbf{Z} = \mathbf{I} \quad \text{and} \quad \det \mathbf{Z} = 1.$$

As a consequence of the above assumption, the tensorial quantity is frame-independent if for any equivalent motion (2.1) we obtain the following tensor transformation laws for scalar s and tensors $\mathbf{a}, \mathbf{B}, \mathbf{C}$ of the first, second and fourth order, respectively;

$$(2.3) \quad \begin{aligned} s^* &= s, \\ \mathbf{a}^* &= \mathbf{Z}\mathbf{a}, \\ \mathbf{B}^* &= \mathbf{Z}\mathbf{B}\mathbf{Z}^T, \\ \mathbf{C}^* &= \mathbf{Z}[\mathbf{Z}\mathbf{C}\mathbf{Z}^T]\mathbf{Z}^T. \end{aligned}$$

2.2. Constitutive model

Assuming after LEE [13] the multiplicativity of the deformation gradient in the form $\mathbf{F} = \mathbf{F}^e \mathbf{F}^p$ (see Lee), it follows that the total deformation rate \mathbf{D} is simply a sum of its elastic \mathbf{D}^e and plastic \mathbf{D}^p parts. In GURTIN's [8] notation, one can write the evolution of the Cauchy stress tensor in the form:

$$(2.4) \quad \overset{\nabla}{\mathbf{T}} = \mathbf{C}^e [\mathbf{D} - \mathbf{D}^p],$$

where $\overset{\nabla}{\mathbf{T}}$ is Jaumann rate of Cauchy stress and $\mathbf{C}^e = 2G\mathbf{I} + (K - \frac{2}{3}G)\mathbf{I} \otimes \mathbf{I}$ is an elastic isotropic modulus. In the last formula, G and K are the known shear and bulk moduli, respectively, and \mathbf{I} and \mathbf{I} denote the fourth rank and second rank unit tensors.

To specify the essence of the plastic approach, one has to assume the fundamental definition of inelastic part of deformation rate, generally in the form:

$$(2.5) \quad \mathbf{D}^p = F(\mathbf{S}, \Theta, \mu),$$

where \mathbf{S} is the deviatoric stress tensor, Θ is the temperature, and μ represents the vector of internal state variables which can consist of scalar, vector or tensor components. The variety of models can be analysed and/or constructed using in general the following basic relations:

- a flow rule of tensorial character,
- the necessary evolution equations which describe the evolution of internal variables μ ,
- a kinetic equation (e.g. balance of energy) of scalar type that relates stresses, inelastic parts of strain rate and temperature.

We will restrict our attention to the isothermal processes and assume the *flow rule* in the form:

$$(2.6) \quad \mathbf{D}^p = \Lambda \tilde{\mathbf{n}},$$

where Λ denotes a scalar-valued function, and $\tilde{\mathbf{n}}$ represents a tensor of second rank.

2.2.1. Rate-independent plasticity. If we assume the flow rule in the form (2.6) and the definition of scalar function Λ as follows:

$$(2.7) \quad \Lambda = \begin{cases} \dot{\lambda} & \text{if } \phi = 0 \quad \text{and} \quad \tilde{\mathbf{n}} : \mathbb{C} : \bar{\mathbf{D}} > 0, \\ 0 & \text{if } \phi \leq 0 \quad \text{or} \quad \phi = 0 \quad \text{and} \quad \tilde{\mathbf{n}} : \mathbb{C} : \bar{\mathbf{D}} \leq 0, \end{cases}$$

where ϕ represents the yield condition, we arrive at the definition of rate-independent plasticity. For $\tilde{\mathbf{n}} = \partial g / \partial \mathbf{T}$ we specify the associative plasticity if $g = f$, or nonassociative one if $g \neq f$.

The parameter $\dot{\lambda}$ is derived from the consistency conditions.

2.2.2. Rate-dependent plasticity. If we assume that Λ is an isothermal function of the type $\Lambda(\tilde{\mathbf{S}}, \mu)$, we are starting to determine the rate-dependent law which has to be supplemented by the next two relations which were pointed out before. It means, that for the rate-dependent flow law we arrive at:

$$(2.8) \quad \mathbf{D}^p = \Lambda(\tilde{\mathbf{S}}, \mu) \tilde{\mathbf{n}}.$$

Additionally we have to define the evolution equations for the internal state variables. Among the variety of internal parameters μ , let us now restrict our attention to only two of them, namely: the scalar value which describes the yield limit s , which is responsible for isotropic hardening/softening, and tensorial value \mathbf{B} which is called back-stress (symmetric, traceless tensor) that defines the kinematic hardening effect, both expressed in stress units.

The *evolution of internal state variables* can be then proposed, for example in the following form:

$$(2.9) \quad \dot{s} = r\Lambda,$$

$$(2.10) \quad \dot{\mathbf{B}} = H\mathbf{D}^p - \Lambda\mathbf{C}\mathbf{B},$$

where r is the hardening/softening parameter, and H and C are parameters which are assumed to be functions of the list of variables μ .

A different function can be adopted to specify Λ what defines the type of rate-dependence.

Let us for example assume

$$(2.11) \quad \mathbf{D}^p = \sqrt{\frac{3}{2}} \dot{\epsilon}^p \tilde{\mathbf{n}}$$

and

$$(2.12) \quad \tilde{\mathbf{n}} = \sqrt{\frac{3}{2}} \frac{\mathbf{S}}{\tilde{S}},$$

where $\mathbf{S} = \mathbf{T}' = \mathbf{T} - \frac{1}{3} \text{tr}(\mathbf{T})\mathbf{I}$ is the deviatoric part of the Cauchy stress tensor, and

$$(2.13) \quad \tilde{S} = \sqrt{\frac{3}{2} \mathbf{S} : \mathbf{S}}$$

is the equivalent stress.

Additionally, plastic equivalent strain rate $\dot{\epsilon}^p = (\frac{2}{3} \mathbf{D}^p : \mathbf{D}^p)^{\frac{1}{2}}$ is prescribed as a function of current equivalent stress \tilde{S} and state variables μ ,

$$(2.14) \quad \dot{\epsilon}^p = f(\tilde{S}, \mu).$$

To complete the system of equations it is necessary to add the evolution equations:

$$(2.15) \quad \dot{\mu} = m(\tilde{S}, \mu),$$

where

$$(2.16) \quad m(\tilde{S}, \mu) = h(\mu) \dot{\epsilon}^p,$$

and $h(\mu)$ denotes the hardening/softening function.

The selection of functions $f(\tilde{S}, \mu)$ and $m(\tilde{S}, \mu)$ is based on phenomenological theories and should be strongly related to micromechanical observations and to the experimental results obtained in physics of solids.

For further numerical considerations, let us now restrict the class of functions $f(\tilde{S}, \mu)$ in such a way that μ will be represented only by a scalar value s . If we assume then the yield function in the form:

$$(2.17) \quad f(\tilde{S}, s) = \begin{cases} \eta \left(\frac{\tilde{S}}{s} - 1.0 \right)^n & \text{if } \tilde{S} \geq s, \\ 0 & \text{if } \tilde{S} < s. \end{cases}$$

we arrive at the restricted version of viscoplasticity originally introduced by PERZYNA [22, 23, 24], where η is the viscosity which is the reciprocal of the relaxation time of mechanical disturbances T_m , ($\eta = 1/T_m$).

If we assume the form

$$f(\tilde{S}, s) = \dot{\epsilon}_0 \left(\frac{\tilde{S}}{s} \right)^{\frac{1}{m}},$$

we define the known viscoplastic power law. There are also other possibilities of choosing $f(\tilde{S}, s)$ functions, which can be successfully applied in various particular cases.

2.2.3. Rotation-neutralized description. Following the discussion in [30, 31] we introduce rotational-neutralized form of our constitutive model. Bar form of the Cauchy stress tensor

$\bar{\mathbf{T}}$ is now expressed as,

$$(2.19) \quad \bar{\mathbf{T}} = \mathbf{Q}^T \mathbf{T} \mathbf{Q},$$

where the rotation tensor $\mathbf{Q}(t)$ was introduced as the solution of the following initial value problem:

$$(2.20) \quad \begin{aligned} \dot{\mathbf{Q}}(t) \mathbf{Q}^T(t) &= \mathbf{W}(t) \quad \text{for } t_n \leq t \leq t_{n+1}, \\ \mathbf{Q}(t_n) &= \mathbf{I}, \end{aligned}$$

in which the spin $\mathbf{W}(t)$ is defined as an nonsymmetric part of the velocity gradient \mathbf{L} . This significantly simplifies the equation (2.1), see also NAGTEGAAL [17], to the form:

$$(2.21) \quad \dot{\bar{\mathbf{T}}} = \mathbf{Q}^T \overset{\nabla}{\bar{\mathbf{T}}} \mathbf{Q} = \mathbb{C}[\bar{\mathbf{D}} - \bar{\mathbf{D}}^p].$$

Using this bar formulation we obtain the following system of equations that, together with Eq. (2.21), describes our rate-dependent model:

$$(2.22) \quad \bar{\mathbf{D}}^p = \sqrt{\frac{3}{2}} \dot{\varepsilon}^p \bar{\mathbf{n}}(\bar{\mathbf{S}}, \tilde{S}),$$

$$(2.23) \quad \bar{\mathbf{n}}(\bar{\mathbf{S}}, \tilde{S}) = \sqrt{\frac{3}{2}} \frac{\bar{\mathbf{S}}}{\tilde{S}},$$

$$(2.24) \quad \tilde{S} = \sqrt{\frac{3}{2} \bar{\mathbf{S}} : \bar{\mathbf{S}}},$$

$$(2.25) \quad \dot{\varepsilon}^p = f(\tilde{S}, s).$$

The evolution equation for the only one scalar value s is

$$(2.26) \quad \dot{s} = m(\tilde{S}, s) = h(s) \dot{\varepsilon}^p.$$

Then for different choice of functions $f(\tilde{S}, s)$ we can define the Perzyna's type viscoplasticity (2.17), or creep model (2.18). The integration of such a system (bar formulation) is computationally much more efficient.

3. Time integration procedure

The goal of this integration is to find the state represented by Cauchy stress tensor \mathbf{T} and the scalar independent variable s at time $t = \tau + \Delta t = t_{n+1}$, when the state (\mathbf{T}_n, s_n) at time $t = \tau = t_n$ is known. The values of the unknown can be obtained from the formula

$$(3.1) \quad \mathbf{T}_{n+1} = \mathbf{Q}_{n+1} \left(\mathbf{T}_n + \int_{t_n}^{t_{n+1}} \mathbb{C} \left[\mathbf{D} - \sqrt{\frac{3}{2}} \dot{\varepsilon}^p \bar{\mathbf{n}} \right] dt \right) \mathbf{Q}_{n+1}^T,$$

$$(3.2) \quad s_{n+1} = s_n + \int_{t_n}^{t_{n+1}} \dot{s} dt,$$

where \mathbf{Q}_{n+1} is the rotation tensor at time $t + 1$ corresponding to the configuration at t_n .

Using the following classical approximation:

$$(3.3) \quad s_{n+\beta} = s_n + \beta \dot{s}_{n+\beta} \Delta t,$$

$$(3.3) \quad \begin{aligned} \dot{s}_{n+\beta} &= m(\tilde{S}_{n+\beta}, s_{n+\beta}), \\ \text{[cont.]} \quad \bar{\mathbf{T}}_{n+\beta} &= (1 - \beta)\bar{\mathbf{T}}_n + \beta\bar{\mathbf{T}}_{n+1}, \end{aligned}$$

one can generate different integration schemes. We will use here for $\beta = 1$ the so-called full backward integration method. Then we arrive at

$$(3.4) \quad \bar{\mathbf{T}}_{n+1} = \mathbf{T}_{n+1}^{\text{pre}} - \sqrt{6G}\Delta t f(\tilde{S}_{n+1}, s_{n+1})\bar{\mathbf{n}}_{n+1},$$

$$(3.5) \quad s_{n+1} = s_n + \Delta t m(\tilde{S}_{n+1}, s_{n+1}),$$

where

$$(3.6) \quad \mathbf{T}_{n+1}^{\text{pre}} = \mathbf{Q}_{n+1}\bar{\mathbf{T}}_n\mathbf{Q}_{n+1}^T + \mathbb{C}[\Delta\mathbf{E}_{n+1}],$$

and the strain increment $\Delta\mathbf{E}_{n+1}$ is

$$\Delta\mathbf{E} = \mathbf{Q}_{n+1} \left(\int_{t_n}^{t_{n+1}} \bar{\mathbf{D}} dt \right) \mathbf{Q}_{n+1}^T.$$

Finally, the problem is reduced to determining the scalar values s_{n+1} and \tilde{S}_{n+1} from the pair of algebraic equations:

$$(3.8) \quad \begin{aligned} s_{n+1} - s_n - \Delta t m(\tilde{S}_{n+1}, s_{n+1}) &= 0, \\ \tilde{S}_{n+1} - \tilde{S}_{n+1}^{\text{pre}} + 3G\Delta t f(\tilde{S}_{n+1}, s_{n+1}) &= 0. \end{aligned}$$

Locally this system of equations has to be solved in each point of integration at each increment (iteration). Good convergence of the results and the power of the algorithm depends on the efficiency of the solver. The subroutine BROWN that was adopted for this purpose appears to be unailing in the variety of tests which were performed. After the solution of the system (3.8), one can easily predict the corrector step and update the stresses.

The scheme of integration of the global system of equations (for dynamics), implicit or explicit, is realized by the environment of the ABAQUS [1] program.

The summary of necessary steps to integrate the system of rate-dependent equations that consists of two classical steps (elastic predictor and plastic corrector) is finally presented in Box 1.

BOX 1

Summary of the constitutive algorithm	
1. Calculate the trial stress and normal mean pressure	$\bar{\mathbf{T}}_{n+1}^{\text{pre}} = \mathbf{T}_n + \mathbb{C}[\Delta\mathbf{E}_{n+1}], \quad p_{n+1}^{\text{pre}} = \frac{1}{3} \text{tr}(\bar{\mathbf{T}}_{n+1}^{\text{pre}}).$
2. Deviatoric trial and equivalent tensile stresses	$\bar{\mathbf{S}}_{n+1}^{\text{pre}} = \bar{\mathbf{T}}_{n+1}^{\text{pre}} + p_{n+1}^{\text{pre}}\mathbf{I}, \quad \tilde{S}_{n+1}^{\text{pre}} = \sqrt{\frac{3}{2}\bar{\mathbf{S}}_{n+1}^{\text{pre}} : \bar{\mathbf{S}}_{n+1}^{\text{pre}}}.$
3. If $\tilde{S}_{n+1}^{\text{pre}} \leq s_n$ then only elastic deformations occur	$s_{n+1} = s_n, \quad \mathbf{T}_{n+1} = \bar{\mathbf{T}}_{n+1}^{\text{pre}} = \mathbf{Q}_{n+1}\bar{\mathbf{T}}_{n+1}^{\text{pre}}\mathbf{Q}_{n+1}^T$
the constitutive algorithm is complete	
else \longleftarrow continue	

4. Solve the system of algebraic equations

$$\begin{aligned} s_{n+1} - s_n - \Delta t g(\tilde{S}_{n+1}, s_{n+1}) &= 0 \\ \tilde{S}_{n+1} - \tilde{S}_{n+1}^{\text{pre}} + 3G \Delta t f(\tilde{S}_{n+1}, s_{n+1}) &= 0 \end{aligned}$$

5. Calculate the radial return factor

$$\eta_{n+1} = \frac{\tilde{S}_{n+1}}{\tilde{S}_{n+1}^{\text{pre}}}$$

6. Update stresses

$$\begin{aligned} \mathbf{T}_{n+1} &= \eta_{n+1} \bar{\mathbf{S}}_{n+1}^{\text{pre}} + p_{n+1}^{\text{pre}} \mathbf{I} \\ \mathbf{T}_{n+1} &= \mathbf{Q}_{n+1} \bar{\mathbf{T}}_{n+1} \mathbf{Q}_{n+1}^T \end{aligned}$$

4. Numerical results

The numerical calculations were supported by using a commercial general purpose finite element program ABAQUS. Using the open architecture of the code, which allows the user to create his own constitutive relation, all the necessary parts of the program were introduced by a procedure called UMAT⁽¹⁾.

The UMAT procedure is called at each Gauss point on every iteration. Among other information introduced by this procedure, the most important are the definition of the actual Jacobian of stiffness matrix of the material and the way of integration of the constitutive relation on the local level. Because the integration of the constitutive law at the local level is basically reduced to solving the nonlinear algebraic system of equations, one can imagine how important it is to use practically reliable solver. This role is played by the adapted procedure BROWN which, due to sophisticated tests which were chosen to check its validity, proved its high efficiency and very fast convergence, even if the starting points for the iterations were picked up arbitrarily. In practical computations this important local part of the code never failed and, together with such a formulation of integration, the constitutive relation confirmed its high quality. The hardening function $h(s)$ is assumed to be constant in the presented examples.

4.1. Biaxial impact loading — force controlled process

The specimen of dimensions 60 mm × 120 mm (a plane strain case) shown in Fig. 1a was loaded dynamically at the top side in longitudinal direction by the force $F(t)$, and to break the symmetric behaviour — by the horizontal force $0.1F(t)$.

The force $F(t)$ changes in time as it is depicted in Fig. 1b, so that after the time period $t_d = 15 \times 10^{-6}$ s it reaches its maximal value and remains constant for the rest of the process. The whole duration of the physical process is $t_m = 1.65 \times 10^{-4}$ s. The material data used in the computations were as follows:

$$E = 11920.0 \text{ N/mm}^2, \quad \nu = 0.49, \quad \sigma_0 = 100.0 \text{ N/mm}^2, \quad n = 1.0, \quad \rho = 5.0 \text{ g/mm}^3.$$

⁽¹⁾ In the version 4.9 of ABAQUS which the authors used, contrary to the newest version 5.3, the access to the deformation gradient at the beginning and at the end of the increment is not possible. The kind help of Dr. D. HIBBITT of HKS Inc. is gratefully acknowledged.

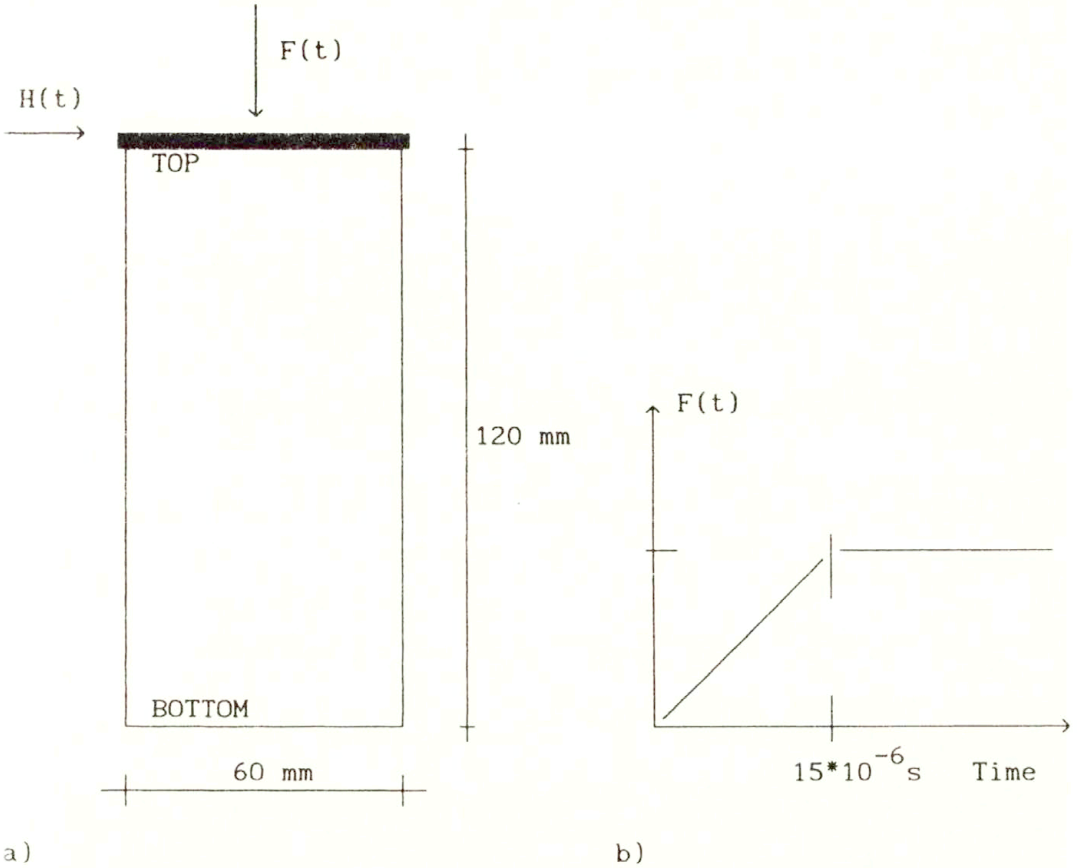


Fig. 1. Definition of the boundary value problem a) geometry of the specimen, b) loading history.

In spite of the fact that the authors have the experience with different spatial discretization (4-Node linear and bilinear and 8-Node quadratic elements), the results presented herein are restricted to those of 4-Node bilinear reduced integration elements. To study numerically the mesh sensitivity, three meshes 3×6 , 6×12 and 12×24 elements were used in the calculations.

The boundary conditions are formulated as follows:

- The bottom side of the specimen is fixed (the displacements of all the nodes that lie on this edge in both directions are zero),
- The top side can rotate as a rigid body, but the nodes remain on the same straight line (MPC — multipoint constrain option was used to declare this behaviour).

On the global level of the integration of nonlinear dynamical system of equations, the explicit method was used with the time step $\Delta t = 1.5 \times 10^{-6} s$ which ensures the stability of integration for the set of parameters defined above.

The whole process is realized in one step that declares simultaneous vertical and horizontal increment of loadings.

The process of creation of the zones of localized plastic strains is shown qualitatively in Fig. 2 a-h. The scale of indicated plastic equivalent strains which accompanies Fig. 2 a-h

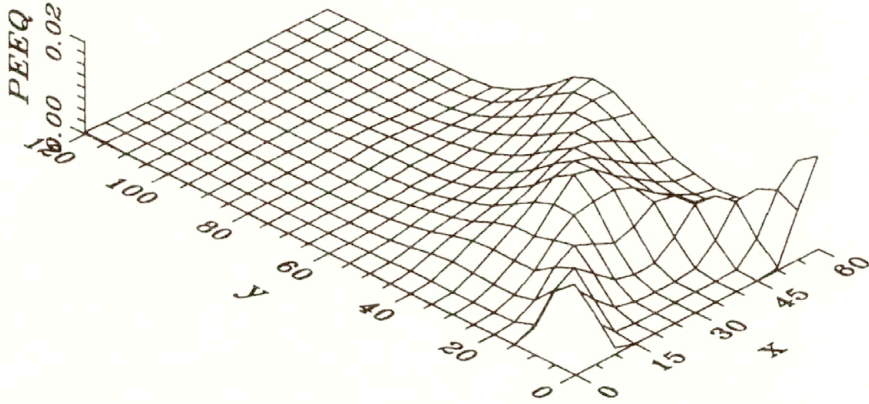


FIG. 3. Distribution of Plastic Equivalent Strains for $t = 1.65 \cdot 10^{-4} \text{ s}$ (3D plot).

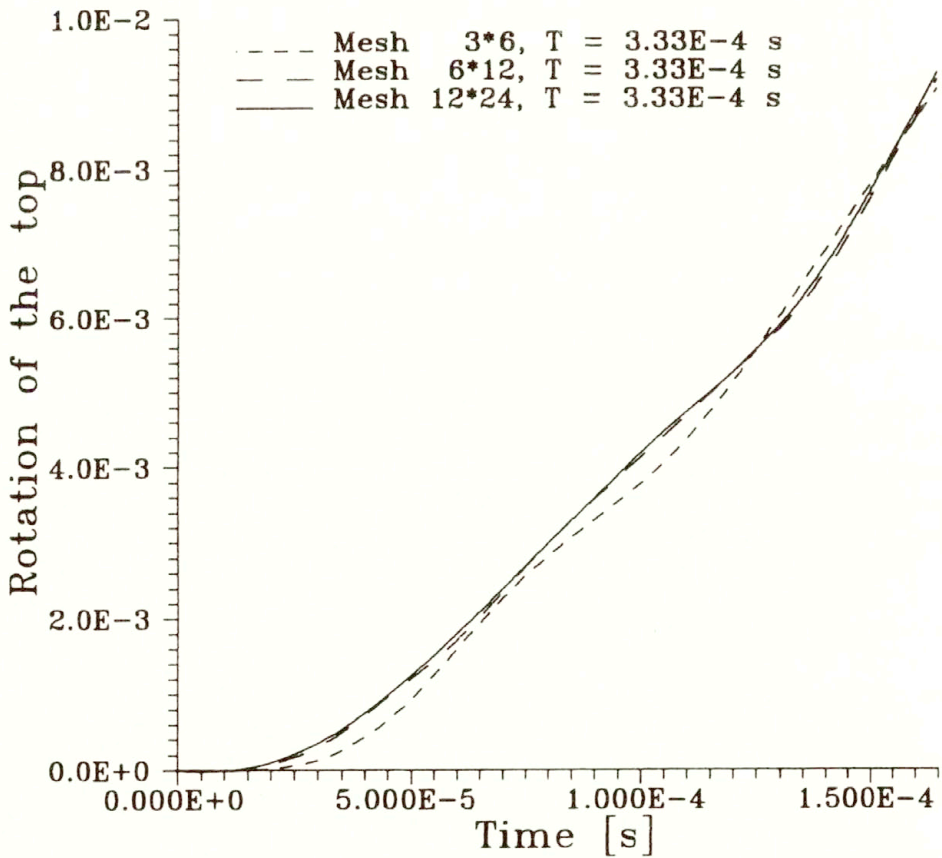
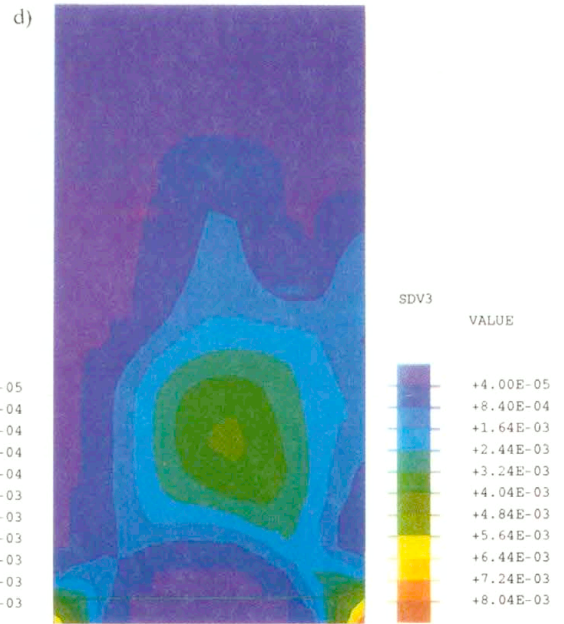
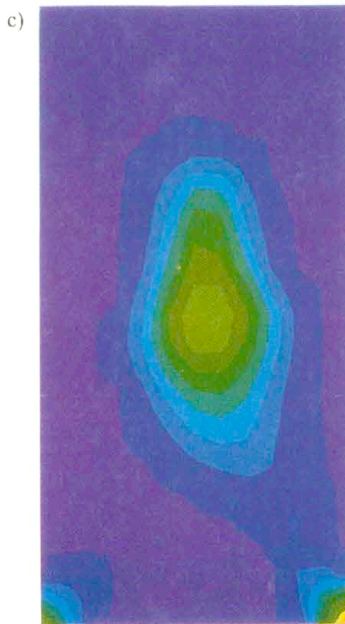
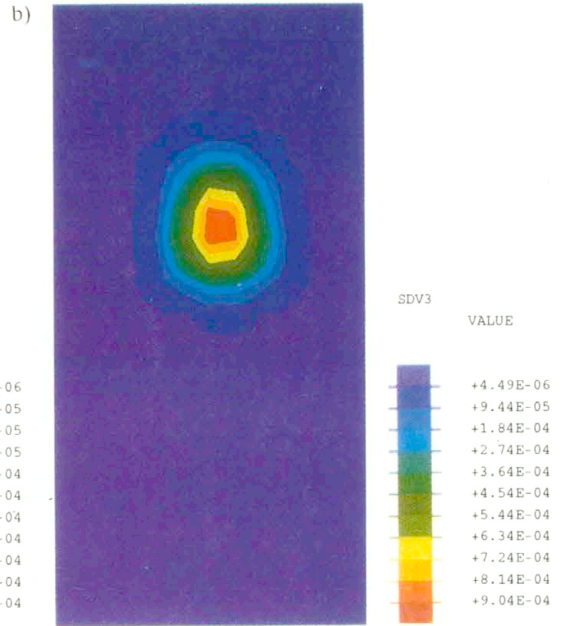
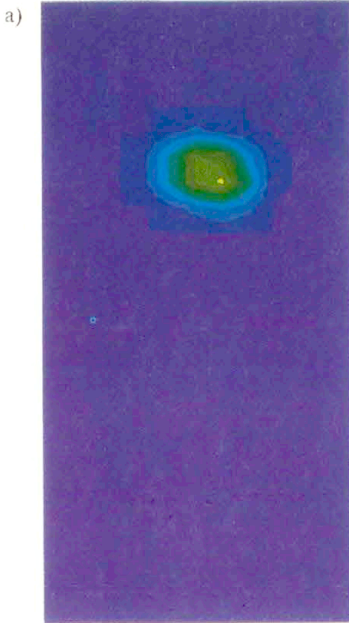


FIG. 4. Rotations of top side vs. time.



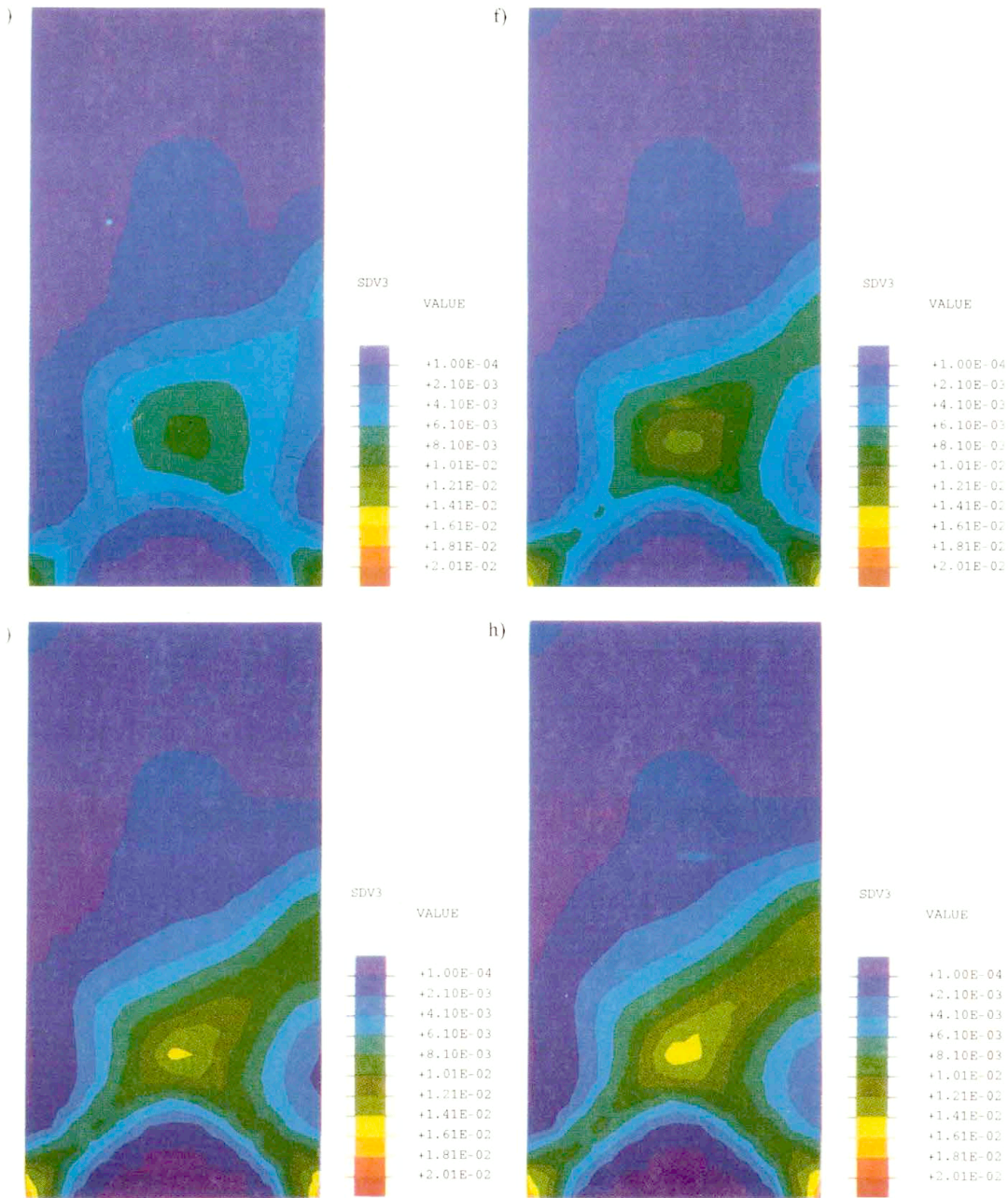


FIG. 2. Development of zones of plastic deformations (Plastic Equivalent Strains) for load-controlled dynamic analysis;

- a) $t = 6.00 * 10^{-5} s$, b) $t = 7.50 * 10^{-5} s$, c) $t = 9.00 * 10^{-5} s$, d) $t = 1.05 * 10^{-4} s$,
 e) $t = 1.20 * 10^{-4} s$, f) $t = 1.35 * 10^{-4} s$, g) $t = 1.50 * 10^{-4} s$, h) $t = 1.65 * 10^{-4} s$ (scale).

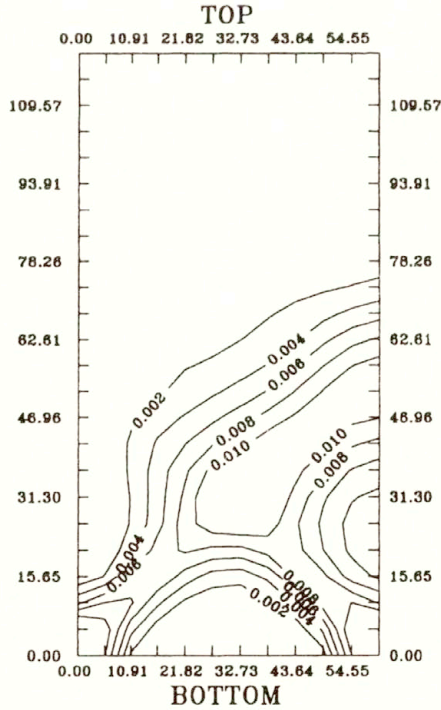
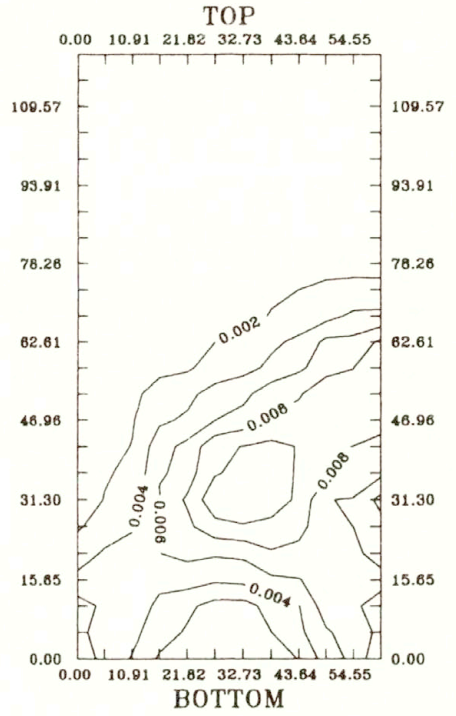
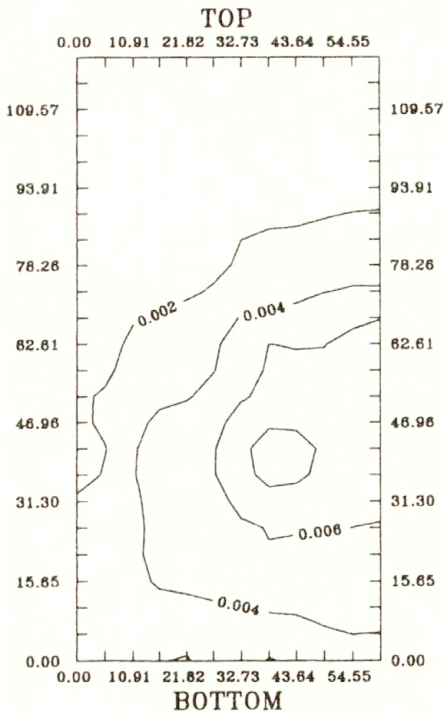


FIG. 5. Comparison of Plastic Equivalent Strains for $t = 1.65 \times 10^4$ s for different meshes.

is valid only for the final state $t = t_m = 1.65 \times 10^{-4}$ s. These results were obtained for the mesh of 12×24 elements. The stress relaxation time was of the order of $T_m = 10^{-4}$ s. The final state of the localization of plastic strain zones is shown in Fig. 3.

To compare the influence of mesh discretization on the results obtained, we propose the discussion on the integrated level of information by presenting the result in $P - \delta$ space and on the local level showing, for example, the distribution of plastic equivalent strains.

In Fig. 4 the rigid rotation of the top side against the time is depicted. One can observe very good agreement of the curves, in spite of the fact that the mesh 3×6 is very coarse. The important differences will be visible on the local level.

The contour plots of plastic equivalent strains are presented in Fig. 5 a-c for all the meshes under consideration. Of course, in this case the poor approximation obtained from the 3×6 mesh is evident, but the remaining meshes show the good agreement. This result is better visible in Fig. 6, which presents for all the meshes the distribution of the plastic equivalent strains along the line $x = 40.0$ mm in the specimen for time $t = t_m$.

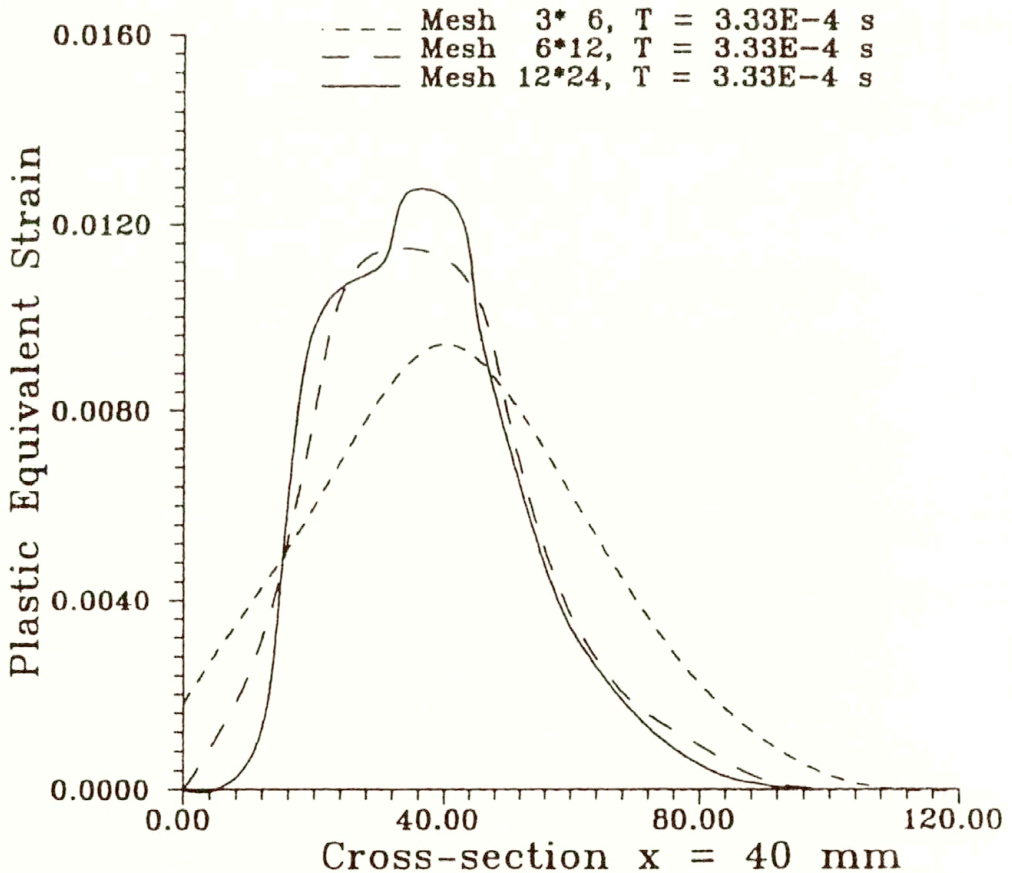


FIG. 6. Convergence of Plastic Equivalent Strains for $t = 1.65 \times 10^{-4}$ s in the cross-section $x = 40$ mm.

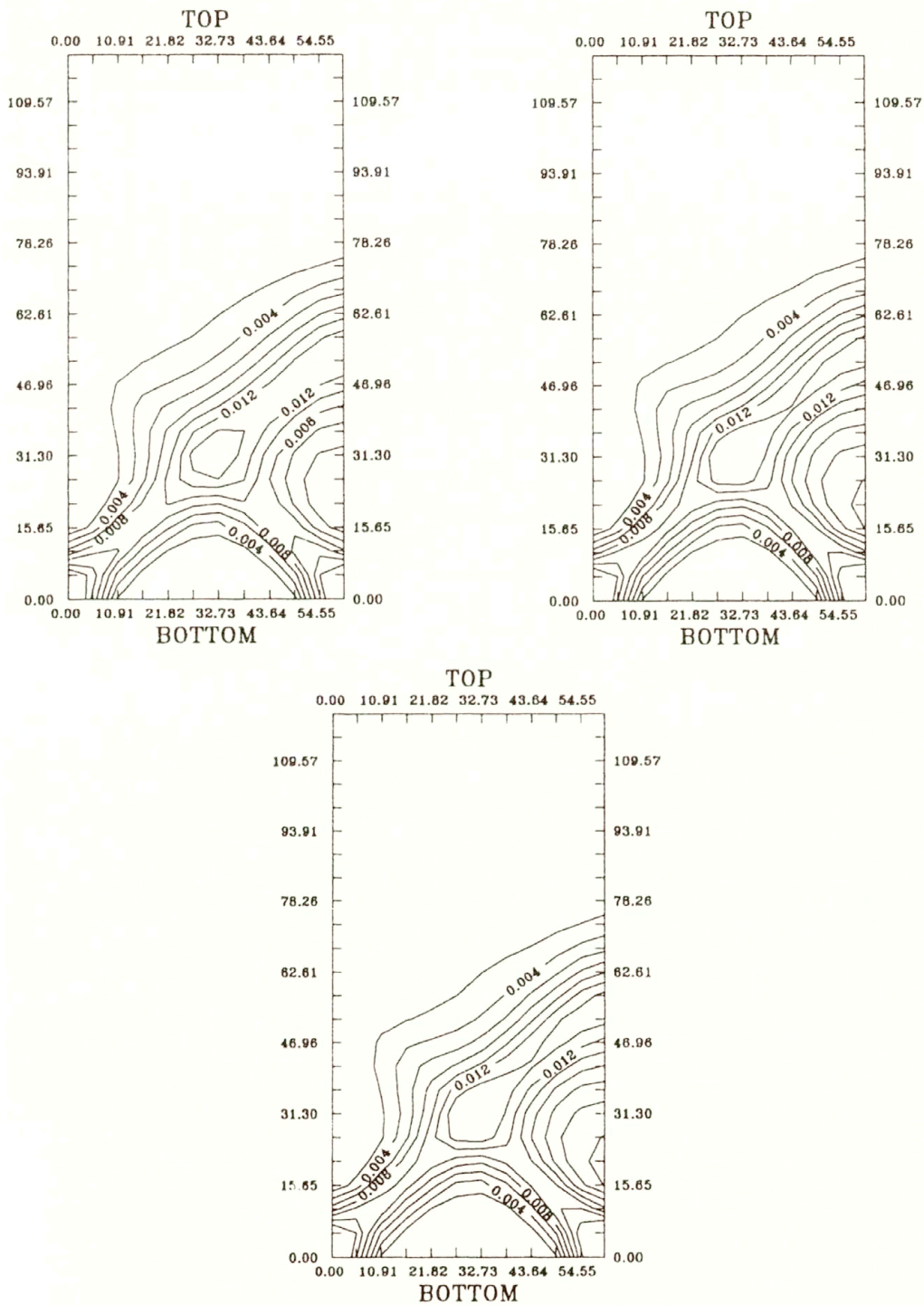


FIG. 7. Comparison of the distribution of Plastic Equivalent Strains for different relaxation times; a) $T_m = 10^{-4} s$, b) $T_m = 10^{-5} s$, c) $T_m = 10^{-6} s$.

The results presented in the last two figures computationally confirm that the rate-dependent formulation drives to the solutions which are free of spurious mesh dependence observed when the formulations of problems become ill-posed (for discussion see LENGNICK *et al.* [14]).

In the viscoplastic formulations the internal length scale is introduced implicitly by the relaxation time for stresses and the velocity of elastic wave propagation. Generally, it drives to the stronger localization for the shorter relaxation times. For the cases under consideration the different, but reasonable for the material parameters used, relaxation times that change between $T_m = 10^{-6} \div 10^{-4}$ s only slightly influence the distribution of plastic equivalent strains, see Fig. 7.

4.2. Biaxial impact loading — velocity-controlled process

Now for the specimen of the same dimensions as shown in Fig. 1a, the loading process is realized in two steps. The first one is static and kinematically driven. The rigid top edge of the specimen is horizontally moved (without rotation) by the distance of 2 mm. This introduces the initial state of stress for the second dynamical step. Then, on the top side of the specimen the ramp function of the velocity in the vertical direction is applied. The speed $v = 12121.212$ mm/s is such that after the time period $t = 3.3 \times 10^{-4}$ s the displacements of all the nodes which lie on this side are equal to 4 mm. In this case the displacements of the top side nodes in horizontal direction are not allowed.

The Fig. 8 a–f qualitatively show the process of nucleation and the development of the zones of plastic localized strains at different increments at the second dynamical step of the analysis.

In Figs. 9 one can observe the final position of the zones of localized plastic strains on the specimen area. Additionally, in Fig. 10 one can find the development of plastic equivalent strains along the line $x = 40$ mm for the three indicated time increments. The results shown in the last two figures confirm the localized character of the plastic strains distribution.

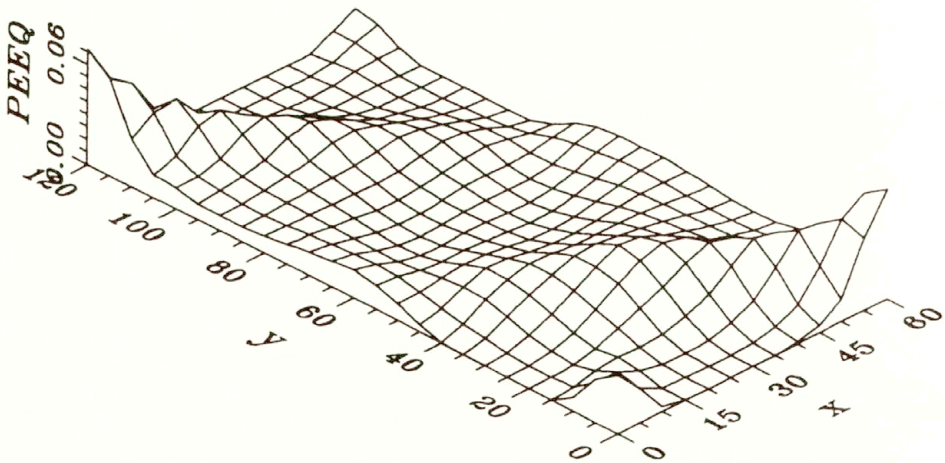
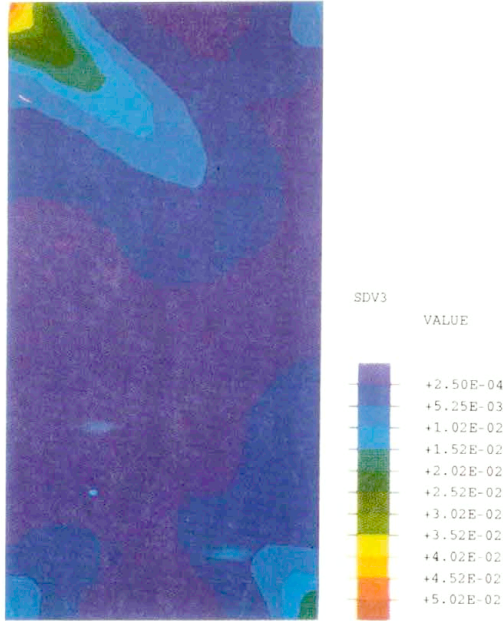
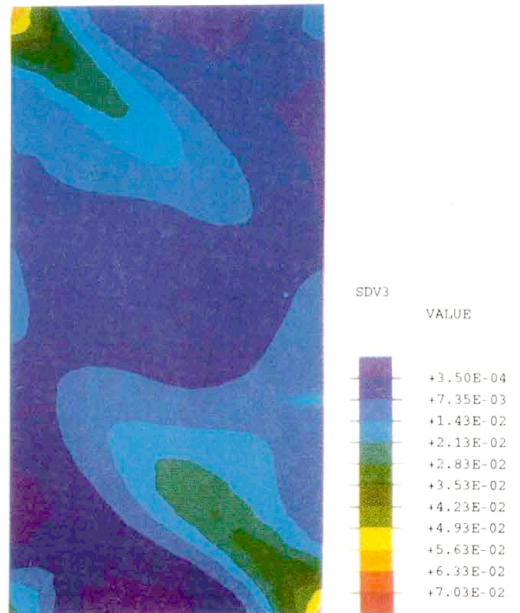


FIG. 9. Distribution of Plastic Equivalent Strains for $t = 3.3 \times 10^{-4}$ s (3D plot).

a)



c)



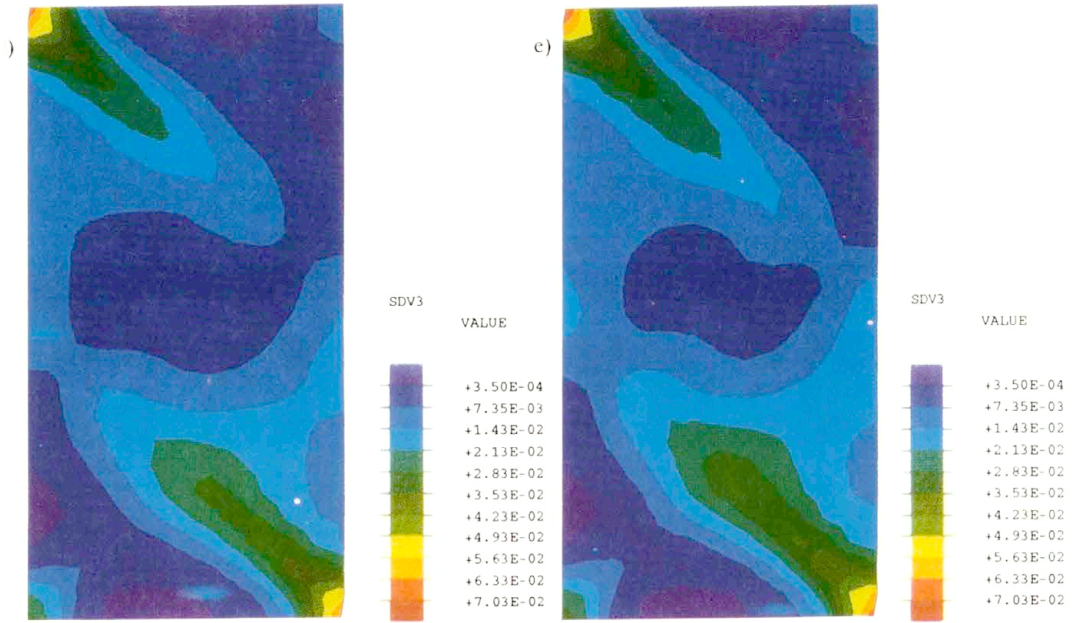


FIG. 8. Development of zones of plastic deformations (Plastic Equivalent Strains) in kinematically controlled process: first step statics, second step dynamics. Plots of the dynamic step only;

- a) $t = 6.0 \cdot 10^{-5} s$,
- b) $t = 1.2 \cdot 10^{-4} s$,
- c) $t = 1.8 \cdot 10^{-4} s$,
- d) $t = 2.4 \cdot 10^{-4} s$,
- e) $t = 3.0 \cdot 10^{-4} s$,
- f) $t = 3.3 \cdot 10^{-4} s$ (scale).

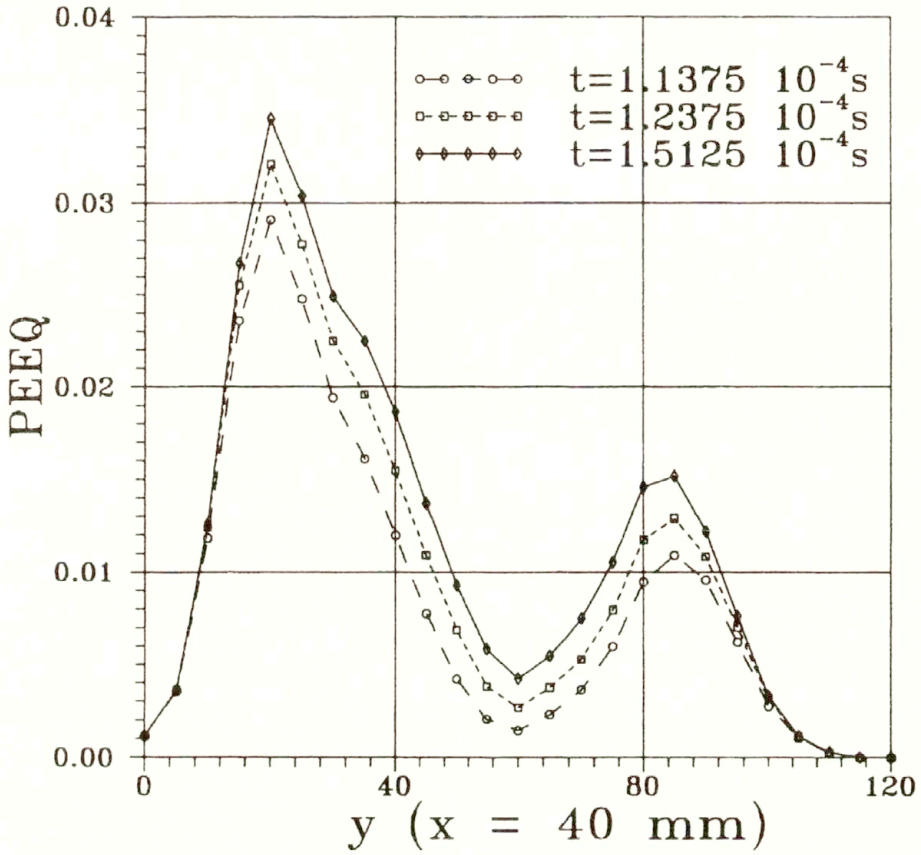


FIG. 10. Development of Plastic Equivalent Strains in time.

What is obvious, but still interesting to notice when comparing the results of the examples mentioned in Sections 4.1 and 4.2, is the observation how strongly the boundary conditions and initial conditions influence the distribution of localization zones.

All the results presented herein were obtained without introduction of any artificial local imperfections to start the localization process. This role is naturally played by dynamical formulation and the propagation of the wave in the solid body under analysis.

Conclusions

- The rate-dependent formulation is explored in the paper to study numerically the behaviour of a ductile material under dynamic loadings.
- The formulation presented preserves the well-posedness of the system of governing incremental equations and, in consequence, what is numerically shown in the examples, reduces significantly the severe mesh sensitivity on the final computation results.
- The material parameters which are used in this formulation have a good physical interpretation and these values can be easily obtained from the experiments. Especially for the case of ductile materials, introduction of the viscosity parameters (relaxation time

for stresses T_m) is physically justified and, moreover, as a parameter mathematically regularizes the system of PDE which incrementally describes the process.

- The constitutive model introduced into ABAQUS program can now serve to solve a class of problems important from the viewpoint of engineering applications.

Acknowledgment

The work was prepared during the stay of T. Łodygowski as an Alexander von Humboldt Fellow at the Hannover University. The support of AvH Foundation is gratefully acknowledged.

P. Perzyna and E. Stein acknowledge the support of DFG and KBN.

References

1. ABAQUS. Manuals for v. 4.9. Reports, Hibbitt, Karlsson and Sorensen, Inc., 1990.
2. Z. P. BAŽANT, J. PAN, and G. PIAUDIER-CABOT, *Softening in reinforced concrete beams and frames*.
3. T. BELYTSCHKO and D. LASRY, *A study of localization limiters for strain-softening in statics and in dynamics*, Comp. Struc. **33**, (3), 707–715, 1989.
4. T. BELYTSCHKO, X.-J. WANG, Z. P. BAŽANT and Y. HYUN, *Transient solutions for one-dimensional problems with strain softening*, J. Appl. Mech., **54**, 513–518, September 1987.
5. R. DE BORST, *Simulation of strain localization: A reappraisal of the Cosserat continuum*, Engng. Comp., **8**, 317–332, 1991.
6. R. DE BORST, H.-B. MUEHLHAUS, J. PAMIN and L. J. SLUYS, *Computational modelling of localisation of deformation*, [in:] Proc. Third Intern. Conference on Computational Plasticity, Fundamentals and Applications, Barcelona, April 6–10, 1992, D. R. J. OWEN, E. ONATE and E. HINTON [Eds.], pp. 483–508, Pineridge Press, Swansea, April 4–9, 1992.
7. R. DE BORST, *Gradient-dependent plasticity: Formulation and algorithmic aspects*, Int. J. Num. Meth. in Eng., **35**, 521–539, 1992.
8. M. E. GURTIN, *An Introduction to Continuum Mechanics*, Academic Press, 1981.
9. R. HILL, *Acceleration waves in solids*, J. Mech. Phys. of Solids, **10**, 1–16, 1962.
10. T. J. R. HUGHES, T. KATO and J. E. MARSDEN, *Well-posed quasi-linear second-order hyperbolic systems with applications to nonlinear elastodynamics and general relativity*, Arch. Rat. Mech. Anal., **63**, 273–294, 1977.
11. T. KATO, *The Cauchy problem for quasi-linear symmetric hyperbolic systems*, Arch. Rational Mech. Anal., **58**, 181–205, 1975.
12. K. KIBLER, M. LENGNICK and T. ŁODYGOWSKI, *Selected aspect of well-posedness of localized plastic flow processes*, [in preparation].
13. E. H. LEE, *Elastic-plastic deformations at finite strains*, J. Appl. Mech., **36**, 1969.
14. M. LENGNICK, T. ŁODYGOWSKI, P. PERZYNA and E. STEIN, *On regularization of plastic flow localization in a soil material*, Int. J. Num. Anal. Meth. Geomech. 1993 [submitted for publication].
15. T. ŁODYGOWSKI, *Mesh-independent beam elements for strain localization*, Comp. Meth. in Civil Eng., **3**, (3), 1993.
16. J. MANDEL, *Conditions de stabilite et postulat de Drucker*, [in:] Rheology and soil Mechanics, J. KRAV-TCHENKO and P. M. SIRIEYS [Eds.], pp. 58–68, Springer, Berlin 1966.
17. J. C. NAGIEGAAL, *On the implementation of inelastic constitutive equations with special reference to large deformation problems*, Comp. Meth. Appl. Mech. Eng., **33**, 469–486, 1982.
18. A. NEEDLEMAN, *Material rate dependence and mesh sensitivity in localization problems*, Comp. Meth. in Appl. Mech. Eng., **67**, 69–85, 1988.
19. M. K. NEILSEN and H. L. SCHREYER, *Bifurcation in elastic-plastic materials*, Int. J. Solids Structures, **30** 4, 521–544, 1993.
20. M. ORTIZ, Y. LEROY and A. NEEDLEMAN, *A finite element method for localized failure analysis*, Comp. Meth. in Appl. Mech. Eng., **61**, 1987.
21. P. PERZYNA, *Analysis of the fundamental equations describing thermoplastic flow process in solid body*, Arch. Mech.

22. P. PERZYNA, *The constitutive equations for rate-sensitive plastic materials*, Quart. Appl. Math., **20**, 321–332, 1963.
23. P. PERZYNA, *Fundamental problems in viscoplasticity*, [in:] Advances in Applied Mechanics, C.-S. YIH [Ed.], 9, pp. 243–377, Academic Press, 1966.
24. P. PERZYNA, *Thermodynamic theory of viscoplasticity*, [in:] Advances in Applied Mechanics, 11, pp. 313–354, Academic Press, 1971.
25. P. PERZYNA, *Constitutive equations of dynamic plasticity*, [in:] Computational Plasticity, Fundamentals and Applications, Barcelona, April 6–10, 1992; D. R. J. OWEN, E. ONATE and E. HINTON [Eds.], pp. 483–508, Pineridge Press, Swansea, April 4–9, 1992.
26. S. PIETRUSZCZAK and Z. MRÓZ, *Finite element analysis of deformation of strain-softening materials*, Int. J. Num. Meth. in Engng., **17**, 327–334, 1981.
27. J. R. RICE, *The localization of plastic deformation*, [in:] Theoretical and Applied Mechanics, W. T. Koiter [Ed.], pp. 207–220, North-Holland Publ. Comp., 1976.
28. L. J. SLUYS, J. BLOCK and R. DE BORST, *Wave propagation and localization in viscoplastic media*, [[in:] III Int. Conf. on Computational Plasticity, Fundamentals and Applications, COMPLAS III, Barcelona, Spain, April 4–9, 1992, E. HINTON, D. OWEN and E. ONATE [Eds.], pp. 539–550, 1992.
29. P. STEINMANN and K. WILLAM, *Localization within the framework of micropolar elasto—plasticity*, [in:] Advances in Continuum Mechanics, Springer, 1991.
30. G. WEBER and L. ANAND, *Finite deformation constitutive equations and a time integration procedure for isotropic, hyperelastic-viscoplastic solids*, Comp. Meth. in Appl. Mech. Engng., **79**, 173–202, 1990.
31. G. WEBER, A. M. LUSH, A. ZAVALANGOS and L. ANAND, *An objective time-integration procedure for isotropic rate-independent and rate-dependent elastic-plastic constitutive equations*, Int. J. Plasticity, **6**, 701–744, 1990.
32. N. ZABARAS and A. F. M. ARIF, *A family of integration algorithms for constitutive equations in finite deformation elasto-viscoplasticity*, Int. J. Num. Meth. in Eng., **33**, 59–84, 1992.

POZNAŃ UNIVERSITY OF TECHNOLOGY, POZNAŃ,
POLISH ACADEMY OF SCIENCES
INSTITUTE OF FUNDAMENTAL TECHNOLOGICAL RESEARCH
and
INSTITUT FÜR BAUMECHANIK UND NUMERISCHE MECHANIK
UNIVERSITÄT HANNOVER, HANNOVER, GERMANY.

Received January 5, 1994.

On yield surface interpolation of prestrained ductile materials

A. MEYERS (BOCHUM)

EXPERIMENTS SHOW that initial yield surfaces of ductile materials may show deviations from the von Mises representation. Moreover, after a prestrain yield surfaces are translated, rotated and distorted. In order to describe these effects, formulations have been presented in the past which considered functions of second and third invariants of the translated stress deviators. It could be shown that these formulations were able to interpolate efficiently the experimental yield surfaces, mostly in $\sigma_1 - \sigma_2$ and $\sigma - \tau$ planes. A special inconvenience, however, is the number of material and history-dependent parameters used in interpolation. A formulation is proposed, where this number seems to be quite restricted. The parameter variations are plotted as functions of the prestrain for a number of experimental yield surfaces taken from literature.

1. Introduction

PRECISE DETERMINATION of size and shape of initial and subsequent yield surfaces and their functional dependence on the hardening parameters is an important problem in plasticity. Initial yield surfaces are often well described by the von Mises yield criterion, i.e.

$$(1.1) \quad k^2 = J_2,$$

where

$$(1.2) \quad J_2 = \frac{1}{2} S_{ij} S_{ji}$$

is the second invariant of the stress deviator S .

In order to describe deviations from the von Mises description observed experimentally (see e.g. TAYLOR and QUINNEY [1]), PRAGER (reported by HILL [2]) and DRUCKER [3] introduced a relation of the form

$$(1.3) \quad k^2 = J_2 \left(1 + \alpha \frac{J_3^2}{J_2^3} \right),$$

where

$$(1.4) \quad J_3 = \frac{1}{3} S_{ij} S_{jk} S_{ki}$$

is the third invariant of the stress deviator and α is a material-dependent constant. Drucker proposed a relation of the form

$$(1.5) \quad k^6 = J_2^3 + \alpha J_3^2.$$

Both relations give better representation of the initial material behaviour, and they are closely connected. This may be seen when polar coordinates ρ, θ are used in the II -plane (Fig. 1). It may be found for the Prager relation (1.3)

$$(1.6) \quad k^2 = r^2 \left[1 - \frac{\alpha}{4} (1 - \cos 2\theta)(1 + 2 \cos 2\theta) \right],$$

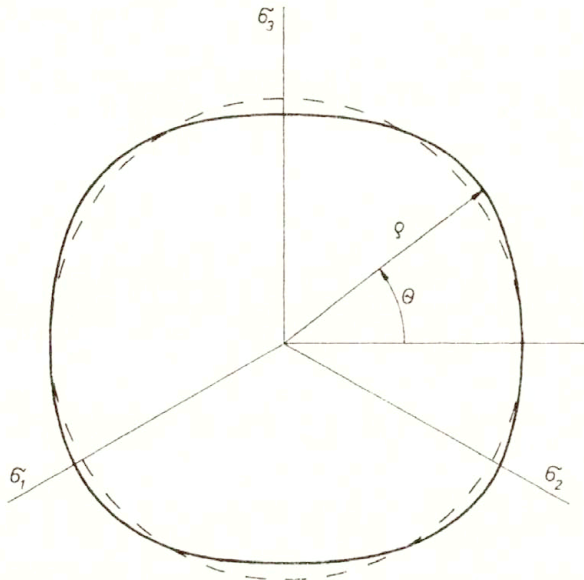


FIG. 1. Prager's yield function represented in the Π -plane.

and for the Drucker relation (1.5)

$$(1.7) \quad k^6 = r^6 \left[1 - \frac{\alpha}{4} (1 - \cos 2\theta)(1 + 2 \cos 2\theta) \right].$$

It may be noted that the terms in braces are identical.

Yield surfaces of predeformed materials are drastically changed in shape and size. A number of experiments have shown that a corner may appear in the direction of the preloading, whereas the surface tends to be flat in the direction opposite to it (see e.g. NAGHDI *et al.* [4], SHIRATORI *et al.* [5], GUPTA and LAUERT [6]). A function that represents such surfaces should also be able to describe the original material behaviour.

In order to take account of the described features, BETTEN [7] proposed the relation

$$(1.8) \quad k^2 = J_2 + \alpha J_3,$$

where α, k are material and history-dependent. This relation will reduce to the von Mises criterion in case of $\alpha = 0$. For the consideration of larger prestrain values, an extension of the formula was given by MAZILU and MEYERS [8]

$$(1.9) \quad k^2 = J_2^* + \alpha J_3^{**},$$

where the invariants

$$(1.10) \quad J_2^* = J_2(\sigma - \sigma^*), \quad J_3^{**} = J_3(\sigma - \sigma^{**})$$

are functions of material and history-dependent shifts (back stresses) σ^* and σ^{**} . Though this formula may represent yield surfaces well when there is a prestrain in direction of tension, it seems to fail in a general case. MAZILU and SKIADAS [9] extended Eqs. (1.10) to

$$(1.11) \quad k^2 \cdot \left[1 - \alpha_1 \cdot \left(1 - \sqrt{54} \frac{J_3^{**}}{J_2^{*3/2}} \right) - \alpha_2 \cdot \left(1 - 54 \frac{J_3^{**2}}{J_2^{*3}} \right) \right] = J_2^* + \alpha J_3^{**},$$

and found good representation for a couple of experimentally measured yield surfaces. REES [10] proposed a relation of translated stress deviators wherein the stress translation is a function of plastic strain-hardening. This relation, however, deviates from the experimental results when there is a corner or a rounded corner in the direction of preloading, and a flattening in the direction opposite to it. Further interpolation schemes proposed by DRUCKER, BETTEN and SAYIR [11] use tensors of the fourth or, respectively, of sixth order instead of scalar constant; BOEHLER and SAWCZUK [12] take functions of second and third invariants of translated and non-translated stress deviators. An overview and discussion of these formula is given by WEGENER [13]. ŻYCKOWSKI and KURTYKA [14] generalized a parametrical description of yield surfaces and showed the interpolation of experimental data in [15].

2. Proposed formula

1986 GUPTA and MEYERS [16] proposed the interpolation formula given by

$$(2.1) \quad 1 = \sum_{i=1}^n \left\{ a_i \cdot J_{2i} \cdot \left(1 + b_i \frac{J_{3i}}{J_{2i}^{3/2}} \right)^{m_i} \right\}.$$

Herein m_i are positive integers, a_i and b_i are material and history-dependent parameters. The stress deviator invariants J_{2i} and J_{3i} are functions and history-dependent stress shifts σ_i , i.e.

$$(2.2) \quad J_{2i} = J_2(\sigma - \sigma_i), \quad J_{3i} = J_3(\sigma - \sigma_i).$$

In the case of a single term ($n = 1$) and zero translations ($\sigma = \mathbf{0}$), Eq. (2.2) reduces to Prager's form (1.3).

The interpolation of experimental data, both for partial and full unloading, taken from the literature showed that a reasonably good interpolation can be achieved for $n = 3$ and m_i taking values of 1 and 2, respectively. The experimental yield surfaces were determined in the $\sigma - \tau$ plane with prestrain in the σ and τ directions, or in $\sigma_1 - \sigma_2$ plane with prestrain in σ_1 direction. The development of the various parameters involved have been plotted as functions of the prestrain (see GUPTA and MEYERS [17]).

Relation (2.2) may be simplified. The identity holds

$$(2.3) \quad \sum_{i=1}^n a_i J_{2i} = a J_2^* + K^2,$$

where

$$(2.4) \quad a = \sum_{i=1}^n a_i,$$

$$(2.5) \quad J_2^* = J_2(\sigma - \sigma^*),$$

$$(2.6) \quad \sigma^* = \frac{1}{a} \sum_{i=1}^n a_i \sigma_i$$

and K is a function of a_i and σ_i . Considering (2.3) and introducing further simplifications in the third invariant components, a revised yield function of the second and third invariants of translated stress deviators is proposed for describing the initial and subsequent

yield surfaces in the form

$$(2.7) \quad k^2 = J_2^* \left[1 + \sum_{i=1}^n c_i (J_{3i})^{m_i} \right],$$

c_i and k are material and history-dependent parameters. The first term on the right-hand side of (2.7) represents the translated von Mises surface, and deviations or distortions are given by the summation terms. Equation (2.7) cannot be reduced any more to Prager's form.

3. Comparison with experimental results

Experiments have mostly been conducted in $\sigma - \tau$ and $\sigma_1 - \sigma_2$ planes. In $\sigma - \tau$ plane the second and third invariants of the deviatoric stress tensor take the form

$$(3.1) \quad J_2^* = \frac{1}{3}(\sigma - \sigma^*)^2 + (\tau - \tau^*)^2,$$

$$(3.2) \quad J_{3i} = \frac{1}{3}(\sigma - \sigma_i) \left[\frac{2}{9}(\sigma - \sigma_i)^2 + (\tau - \tau_i)^2 \right];$$

in $\sigma_1 - \sigma_2$ plane one gets

$$(3.3) \quad J_2^* = \frac{1}{3}[(\sigma_1 - \sigma_1^*)^2 - (\sigma_1 - \sigma_1^*)(\sigma_2 - \sigma_2^*) + (\sigma_2 - \sigma_2^*)^2],$$

$$(3.4) \quad J_{3i} = -\frac{1}{27}(\sigma_1 - \sigma_{1i} + \sigma_2 - \sigma_{2i}) \cdot [\sigma_1 - \sigma_{1i} - 2(\sigma_2 - \sigma_{2i})][\sigma_2 - \sigma_{2i} - 2(\sigma_1 - \sigma_{1i})].$$

Several variously obtained initial and subsequent yield surfaces, taken from the literature, were interpolated with the proposed formulation (2.7), and their fittings were seen to be reasonably good, when one takes only one summation term and $m_1 = 2$, i.e.

$$(3.5) \quad k^2 = J_2^* [1 + c(J_3^{**})^2],$$

where J_{31} has been called J_3^{**} . The similarity to formula (1.10) may be noted.

In Fig. 2 the surface determined by IKEGAMI [18] in $\sigma - \tau$ plane for material prestrained in σ -direction after full unloading is shown. The prestraining values were 0%, 2%, 6%, 12%, 20% and 30%. As it may be observed, there is a corner in the direction of prestrained and a flattening in the direction opposite to it.

In Fig. 3 the parameter evolution is displayed. It may be noticed that the initial surface is best described with the third invariant included, i.e. $c \neq 0$. In the interpolation the shift σ_1 was zero.

For partial unloading and the same prestrains as above, the yield surfaces are leaving the stress-free state $\sigma = \tau = 0$. Figure 4 represents the yield surface by IKEGAMI [18] and interpolated through formula (3.5). The parameter evolution is displayed in Fig. 5, c was held constant to $1.03 \cdot 10^{-4}$. Due to experimental data, which differed already quite a bit from the positive to the negative side of τ (see e.g. the third curve from the left in Fig. 4), the parameter evolution is not very smooth. The shifts σ_0 and σ_1 are in the direction of prestrain.

Yield surfaces shown in Fig. 6 have been obtained by IVEY [19]; prestrains were in τ -direction and values of prestrain were 0%, 0.064%, 0.47% and 1.527%. The yield

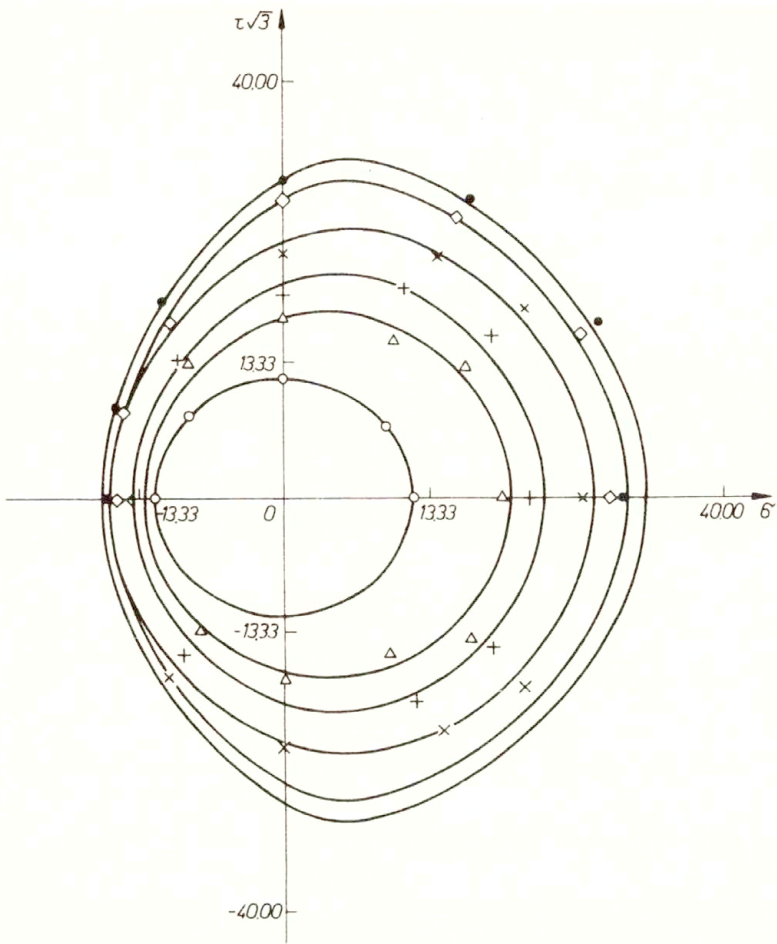


FIG. 2. Yield surface in $\sigma - \tau$ plane of Ikegami after full unloading and prestrains in σ -direction.

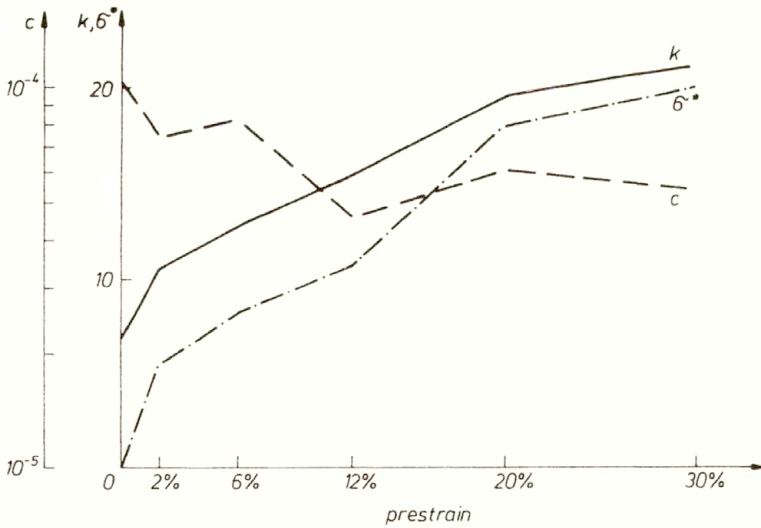


FIG. 3. Parameter evolution for yield surfaces in $\sigma - \tau$ plane of Ikegami after full unloading and prestrains in σ -direction.

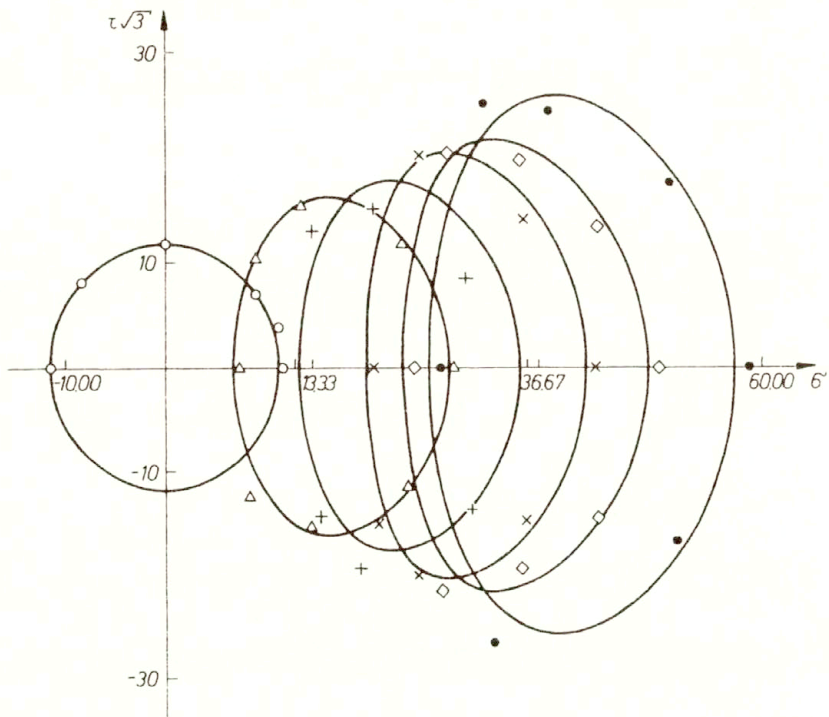


FIG. 4. Yield surfaces in $\sigma - \tau$ plane of Ikegami after partial unloading and prestrains in σ -direction.

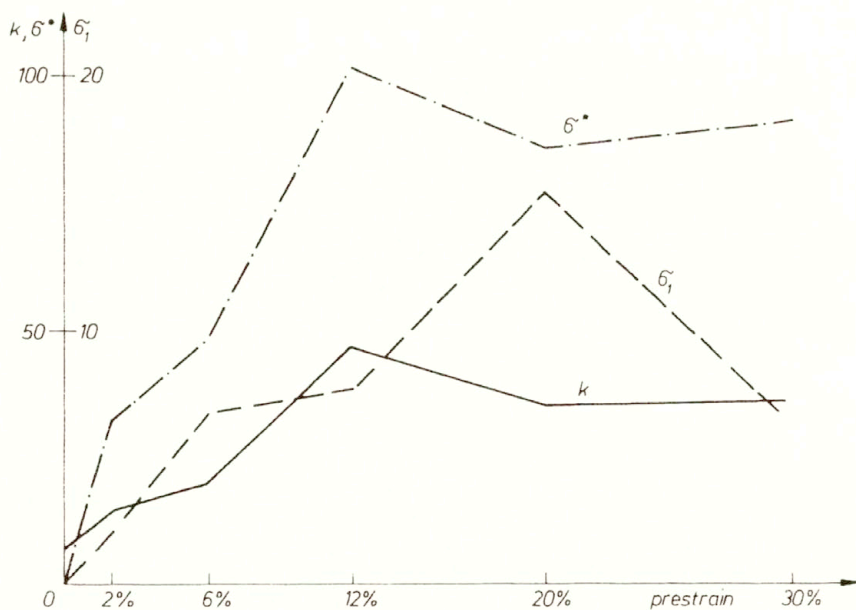


FIG. 5. Parameter evolution for yield surfaces in $\sigma - \tau$ plane of Ikegami after partial unloading and prestrains in σ -direction.

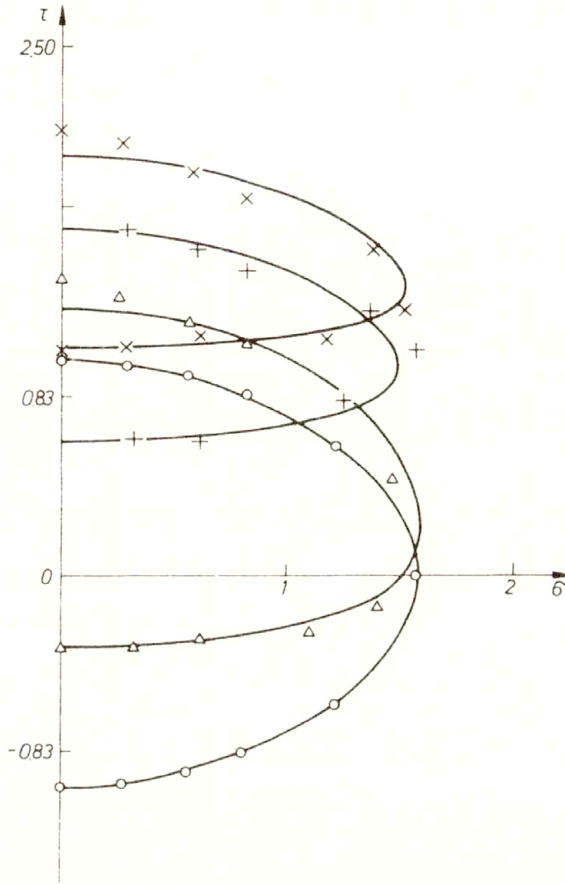


FIG. 6. Yield surfaces in $\sigma - \tau$ plane of Ivey after partial unloading and prestrains in τ -directions.

surfaces have been interpolated by formula (3.5), and parameter evolutions are shown in Fig. 7. The value of c_1 is varying from 2.11 for 0% prestrain to $-8.77 \cdot 10^{-4}$ for 1.527% prestrain. The shifts τ_0 and τ_1 are in the direction of prestrain.

For prestrains of 0%, 0.8%, 1.8%, 3.4% and 5.1% in the σ_1 -direction SHIRATORI *et al.* [20] measured the yield surfaces in the $\sigma_1 - \sigma_2$ -plane. Their interpolation through formula (3.5) is shown in Fig. 8 and the parameter variation in Fig. 9. In this case k remains almost constant; the shifts σ_{11}^* and σ_{11} are in the direction of prestrain.

SHIRATORI *et al.* [5] produced several yield surfaces for complex prestrain paths. In Fig. 10 prestrains were in the $(-\sigma_1, \sigma_2)$ -direction and had values of 0%, 0.8%, 1.8%, 3.4% and 5.1%. Although the material should be isotropic, the measured data reveal anisotropic behaviour. This leads us to consider a non-constant relation between σ_1^* and σ_2^* and, respectively, between σ_1^{**} and σ_2^{**} . In Fig. 11 the development of the parameter is displayed. In this case k seems to remain a constant value, whereas c_1 decreases to 1/10th of the starting value in the initial case. The shift directions are mainly, but not exclusively, in the prestrain direction; this may be due to the non-isotropic material behaviour in the initial state.

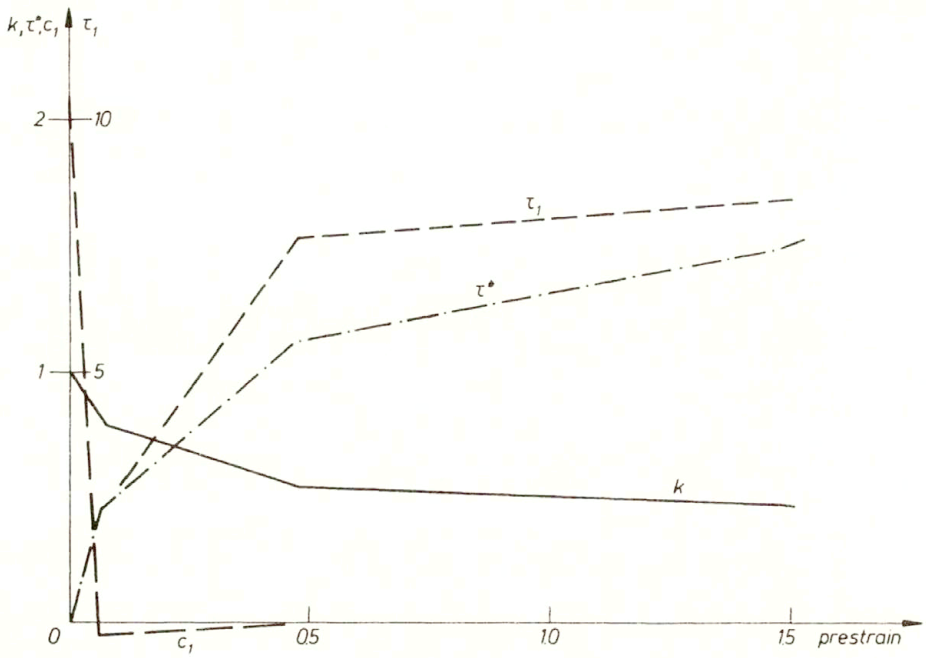


FIG. 7. Parameter evolution for yield surfaces in $\sigma - \tau$ plane of Ivey after partial unloading and prestrains in τ -direction.

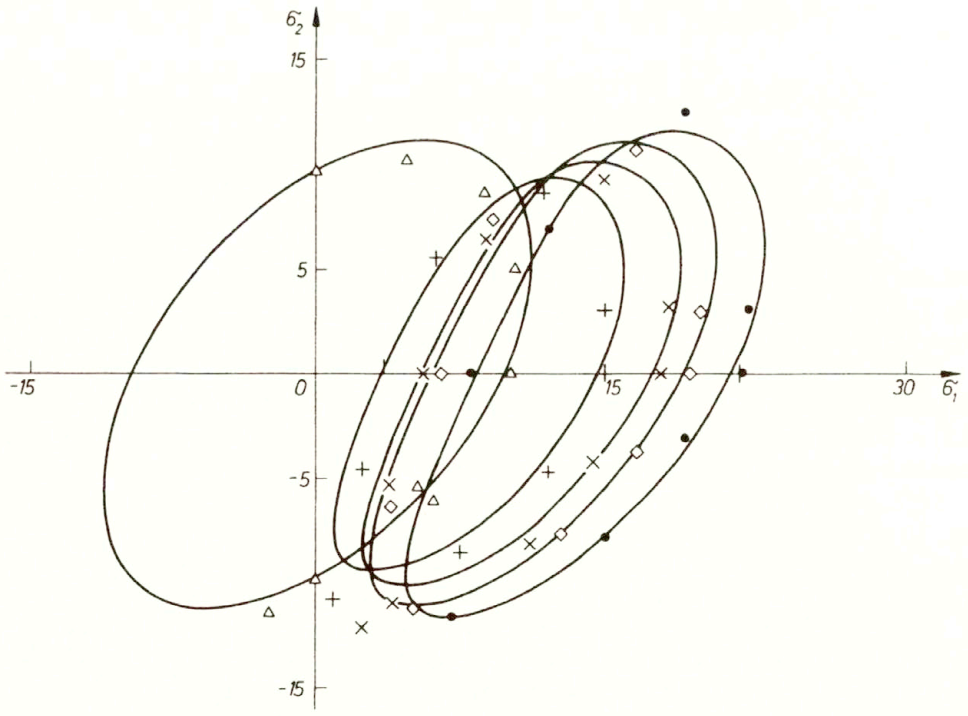


FIG. 8. Yield surfaces in $\sigma_1 - \sigma_2$ plane of Ikegami after partial unloading and prestrains in σ_1 -direction.

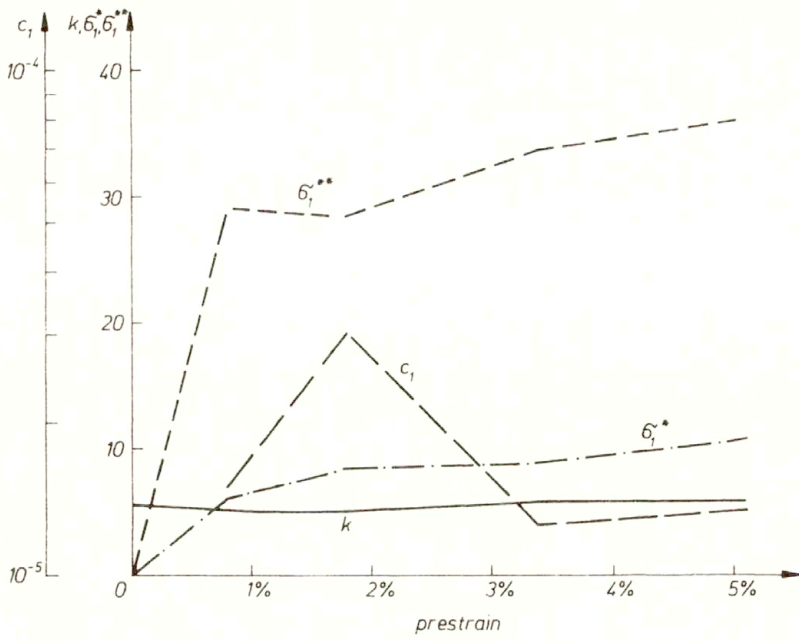


FIG. 9. Parameter evolution for yield surfaces in $\sigma_1 - \sigma_2$ plane of Ikegami after partial unloading and prestrains in σ_1 -direction.

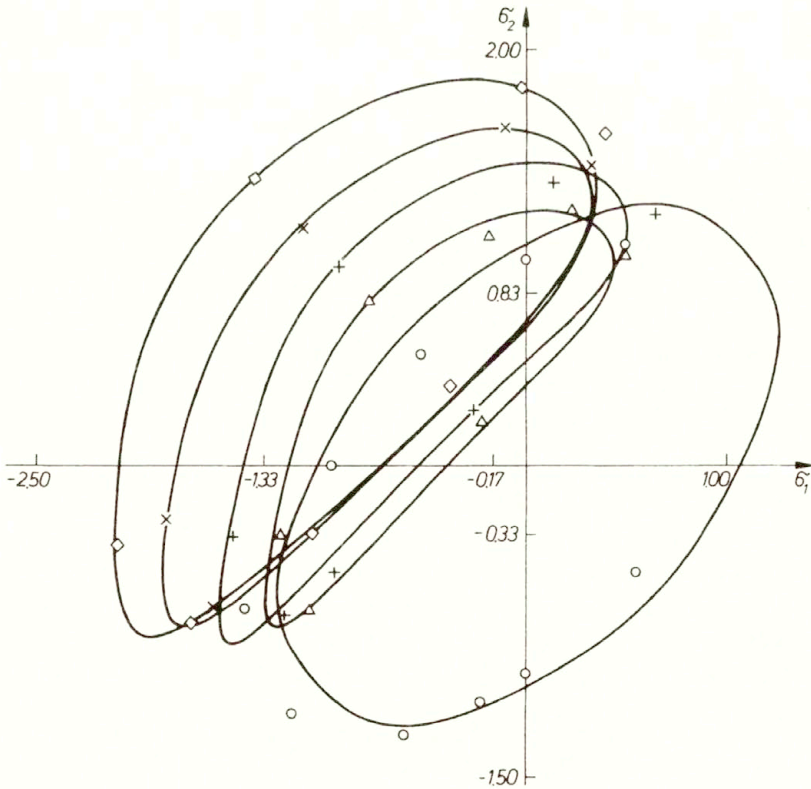


FIG. 10. Yield surfaces in $\sigma_1 - \sigma_2$ plane of SHIRATORI after partial unloading and prestrains in $(-\sigma_1)(\sigma_2)$ -direction.

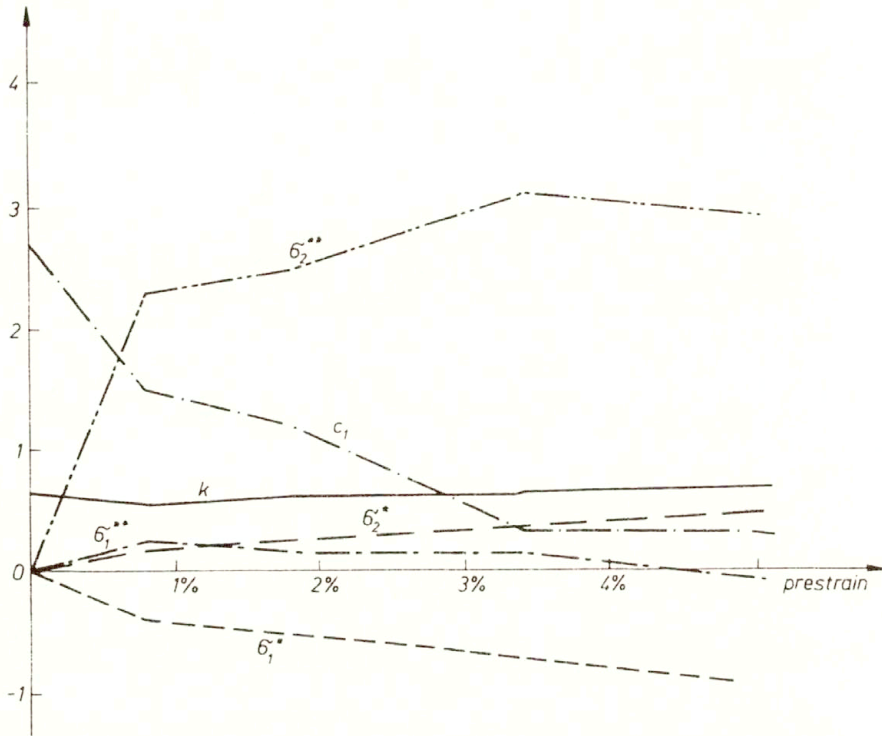


FIG. 11. Parameter evolution for yield surfaces in $\sigma_1 - \sigma_2$ plane of SHIRATORI after partial unloading and prestrains in $(-1 \cdot \sigma_1)(1 \cdot \sigma_2)$ -direction.

4. Numerical procedure

1. In the case of the required symmetry and when the number of experimental data was not sufficient on one side of the symmetry axis additional points on the other side were generated by reflection from the symmetry axis.

2. The first optimization procedure returns the center of the best von Mises ellipse where (see Fig. 12)

$$\sum_i^n (r_i - \rho_i)^2 = \min,$$

and ρ_i are the radii from the center of the ellipse to the experimental data, r_i are the parallel radii to the von Mises curve, and n is the number of experimental data.

3. The number of requested data points should be greater or equal to the number of free parameters. Often the number of experimental points supplied was not sufficient. In order to generate additional pseudo-experimental points, the following procedure was chosen:

a. Using the Akima spline algorithm adopted to periodical functions, the first curve was drawn through the experimental data (see Fig. 12).

b. $N = \max(20; 2n)$ equidistant radii were drawn to the spline curve. The intersection points of these radii and the spline curve generated a new set of data for which the interpolation was performed.

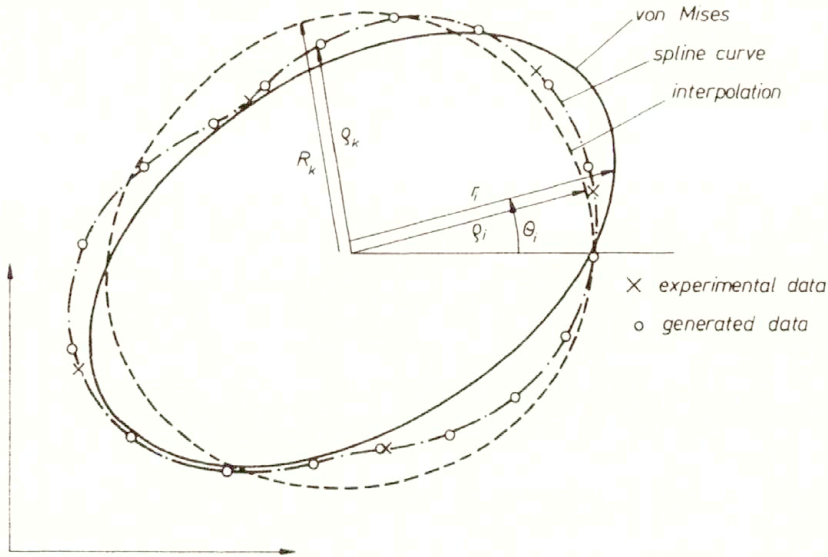


FIG. 12. Numerical procedure.

4. Finally, the variable metric optimization procedure was used to evaluate the free parameter for which (see Fig. 12)

$$\sum_{k=1}^N (R_k - \rho_k)^2 \rightarrow \min,$$

where ρ_k are the radii to the experimental data resp. to the generated data, and R_k are the parallel radii to the interpolating curve.

5. Conclusion

A revised formula is presented that enables us to interpolate the experimental yield surfaces taken from literature very well. This formula is a function of the second and third shifted deviatoric stresses. It is shown that the number of parameters taken into account may be restricted, and that the stress shifts are mainly in the direction of the prestrain. The formulation of evolution laws for the considered parameter, however, will require multiple sets of more precise experimental data.

References

1. G.I. TAYLOR and H. QINNEY, *The plastic distortion of metals*, Phil. Trans. of the Royal Society, **230A**, 232–362, 1931.
2. R. HILL, *The mathematical theory of plasticity*, Oxford Press, New York 1950.
3. D.C. DRUCKER, *Stress-strain relations for strain hardening materials; discussions and proposed experiments* [in:] American Mathematical Society, Proc. 1st Annual Symposium for Applied Mathematics, pp. 181–187, 1949.
4. P.M. NAGHDI, F. ESSENBURG and W. KORFF, *An experimental study of initial and subsequent yield surface in plasticity*, J. Applied Mech., **25**, 201–209, 1958.

5. E. SHIRATORI, H. IKEGAMI, K. KANEKO and T. SUGIBAYASHI, *Subsequent yield surfaces after large tensile or torsional prestrain*, Reprint of Japan Soc. Mech. Engng., **41**, 75.7.2, 1975.
6. N.K. GUPTA and H.-A. LAUERT, *A study of yield surface upon reversal of loading under biaxial stress*, ZAMM, **63**, 497–504, 1983.
7. J. BETTEN, *Über die Konvexität von Fließkörpern isotroper und anisotroper Stoffe*, Acta Mech., **33**, 233, 1979.
8. P. MAZILU and A. MEYERS, *Yield surface description of isotropic materials after cold prestrain*, Ing. Archiv, **55**, 213–220, 1985.
9. P. MAZILU and A. SKIADAS, *The description of yield surfaces for cold prestressed metals with the hypothesis of the isotropy centers translation* [in:] Modelling of Metal Forming Processes, J.L. CHENOT and E. OÑATE [Eds.], pp. 3–10, 1988.
10. D.W.A. REES, *The theory of scalar plastic deformation functions*, ZAMM, **63**, 217–228, 1983.
11. M. SAYIR, *Zur Fließbedingung der Plastizitätstheorie*, Ing. Archiv, **39**, 414–432, 1980.
12. J.P. BOEHLER and A. SAWCZUK, *Application of representation theorems to describe yielding of transversely isotropic solids*, Mech. Res. Comm., **3**, 277–283, 1975.
13. K. WEGENER, *Zur Berechnung grosser plastischer Deformationen mit einem Stoffgesetz vom Überspannungstyp*, [in:] Braunschweiger Schriften, vol. 2, p. 109, 1991.
14. T. KURTYKA and M. ŻYCZKOWSKI, *A geometric description of distortional plastic hardening of deviatoric materials*, Arch. Mech., **37**, 383–395, 1985.
15. T. KURTYKA, *Parameter identification of a distortional model of subsequent yield surfaces*, Arch. Mech., **40**, 433–454, 1988.
16. N.K. GUPTA and A. MEYERS, *Description of initial and subsequent yield surfaces*, ZAMM, **66**, 435–439, 1986.
17. N.K. GUPTA and A. MEYERS, *Considerations of translated stress deviators in describing yield surfaces*, Int. J. Plasticity, **8**, 761–772, 1992.
18. K. IKEGAMI, *Experimental plasticity; on the anisotropy of metals*, [in:] J.P. BOEHLER [Ed.], Proc. Euromech. Coll., volume 295, pp. 201–241, Villard-de Lans 1958.
19. H.J. IVEY, *Plastic stress strain relations and yield surfaces for aluminium alloys*, J. Mechanical Engng. Sci., **2**, 15–31, 1961.
20. E. SHIRATORI, K. IKEGAMI and K. KANEKO, *Subsequent yield surface determined in consideration of the Bauschinger effect*, [in:] Foundation of Plasticity, p. 477–489, Nordhoff Int. Publ., Leiden 1973.

RUHR UNIVERSITÄT BOCHUM
LEHRSTUHL FÜR TECHNISCHE MECHANIK, BOCHUM, GERMANY.

Received December 6, 1993.

Some remarks on modelling of semi-brittle ceramics by application of mesomechanics

T. SADOWSKI (LUBLIN)

THE PAPER PRESENTS an application of mesomechanics to the constitutive description of semi-brittle ceramics behaviour under external loading. Simple states of stress: uniaxial tension, uniaxial compression and pure shear were considered as examples of the deformation process.

1. Introduction

SEMI-BRITTLE, polycrystalline ceramics is a special kind of material which exhibits limited plastic flow during the deformation process. Plastic strain is of the order of the elastic one. Plastic flow is created by dislocation motion, mainly within the grains of polycrystalline structure. In general, the dislocations pile up at the grain boundaries which can resist their free sliding because of misorientation of crystalline axes at the border of the adjacent grains. In that way the grain boundaries play the most important role in the constitutive description of material behaviour. Namely, the activated dislocations pile up at the grain boundary and can initiate microcracks by Zener–Stroh’s mechanism. It is additionally motivated by the fact that mechanical parameters of the grain boundaries are much lower than those of pure crystals. Thus, microcracks spread mainly intergranularly, changing their direction of propagation (zig-zag cracks) and leading finally to the failure of the material.

In this paper we will discuss a possibility of application of mesomechanics to modelling the semi-brittle ceramics behaviour (MgO-type like in [1] and [2]) under complex loading.

2. Meso-macroscale transition in the description of material behaviour

Let us consider a polycrystalline specimen subjected to two-directional loading which increases quasi-statically.

To describe the deformation process of the material we apply a simple volume (area) averaging procedure over the unit cell. On the level of the unit cell (mesoscale), the solid is inhomogeneous and anisotropic because of different defects propagating in grains or at the grain boundaries. The state of the material is characterized by the local values of stress and strain (σ' , ϵ'). Averaging the influence of all these effects over the unit cell area A we obtain the material response in the macroscale, (σ , ϵ), as a continuum:

$$(2.1) \quad \sigma = \frac{1}{A} \int_A \sigma' dA,$$

$$(2.2) \quad \epsilon = \frac{1}{A} \int_A \epsilon' dA.$$

Having (2.1) and (2.2), one can postulate the following expression for constitutive relations [3]:

$$(2.3) \quad \varepsilon = \varepsilon(\sigma, \omega),$$

where ω is a tensor describing internal damage of the material. In case of a quasi-static load increase

$$(2.4) \quad \omega = \omega(\sigma),$$

and (2.3) takes the final form:

$$(2.5) \quad \varepsilon = \mathbf{S}(\sigma, \omega) : \sigma.$$

Here

$$(2.6) \quad \mathbf{S}(\sigma, \omega) = \mathbf{S}^0 + \mathbf{S}^*(\sigma, \omega),$$

where \mathbf{S}^0 is the compliance of the virgin material, and \mathbf{S}^* the compliance attributable to the propagation of all microdefects N_i inside the unit cell.

In the two-dimensional state of stress Eq. (2.5) can be rewritten as

$$(2.7) \quad \varepsilon_i = S'_{ij}(\sigma)\sigma_j, \quad i, j = 1, 2, 6,$$

in Voigt's notation.

3. Estimation of damage influence on the compliance tensor

During the deformation process of MgO ceramics the material passes through the following phases which reflect the changes of internal structure inside the unit cell:

- 1) dislocations nucleation and slip-band development phase,
- 2) initiation and propagation of straight mesocracks,
- 3) deflection of straight mesocracks (kinking process) and their elongation.

In other words, each phase of deformation is characterized by different components of the current state of the material damage.

It is worth noticing that the first phase is not recoverable during unloading of the material, whereas the second and third ones can be partly or totally recovered.

3.1. Slip phase

Experimental results show that, after a purely elastic phase, the dislocation sources are activated within grains (Fig. 1), creating the conjugate slip systems (100) $\langle 110 \rangle$. They pile up at the grain boundaries, but they cannot cross them, in general, because of a strong energetic barrier to easy glide. In that way surrounding grains resist free deformation of crystals with an activated slip system. According to [2], the following components of \mathbf{S}^* are different from zero:

$$(3.1) \quad S_{21}^{*(s)} = \frac{N_s}{\pi G_0(1-b_1)} \int_{D_m}^{D_M} \int_{\beta_1}^{\beta_2} \left[-\sin(\beta) \cos(\beta) - \frac{\tau_{s0}}{\sigma_1 + \sigma_2} \right] \alpha_{22}(\beta) p_2(D) d\beta dD,$$

$$(3.2) \quad S_{22}^{*(s)} = \frac{N_s}{\pi G_0(1-b_1)} \int_{D_m}^{D_M} \int_{\beta_1}^{\beta_2} \left[\sin(\beta) \cos(\beta) - \frac{\tau_{s0}}{\sigma_1 + \sigma_2} \right] \alpha_{22}(\beta) p_2(D) d\beta dD.$$

$$(3.3) \quad S_{11}^{*(s)} = -S_{21}^{*(s)}, \quad S_{12}^{*(s)} = -S_{22}^{*(s)},$$

where N_s is the number of grains with conjugate slip system inside the unit cell, τ_{s0} is the lattice resistance to dislocation glide, $p_2(D)$ — grain size distribution function, D_m and D_M — the smallest and largest grain sizes, G_0 is the Kirchhoff modulus of the virgin material, b_1 is the coefficient connected with the shape of grains. β is the angle of the slip band inclination to the axis x_1 , whereas $\beta_1 < \beta < \beta_2$ denotes the fan of N_s grains.

3.2. Mesocracks influence on the compliance tensor

The initiated dislocations slide to the grain boundaries under shear stress acting along the slip lines, Fig. 1. They are blocked at the grain boundaries and create tensile stress in that part of the material. When the critical value of the shear stress is exceeded, the Zener–Stroh microcracks can initiate. In general, such microcracks develop as an open or closed ones, depending on the sign of the normal stress to their faces. In case of a positive sign — microcracks grow to become mesocracks under mixed mode, whereas for negative one — under Mode II.

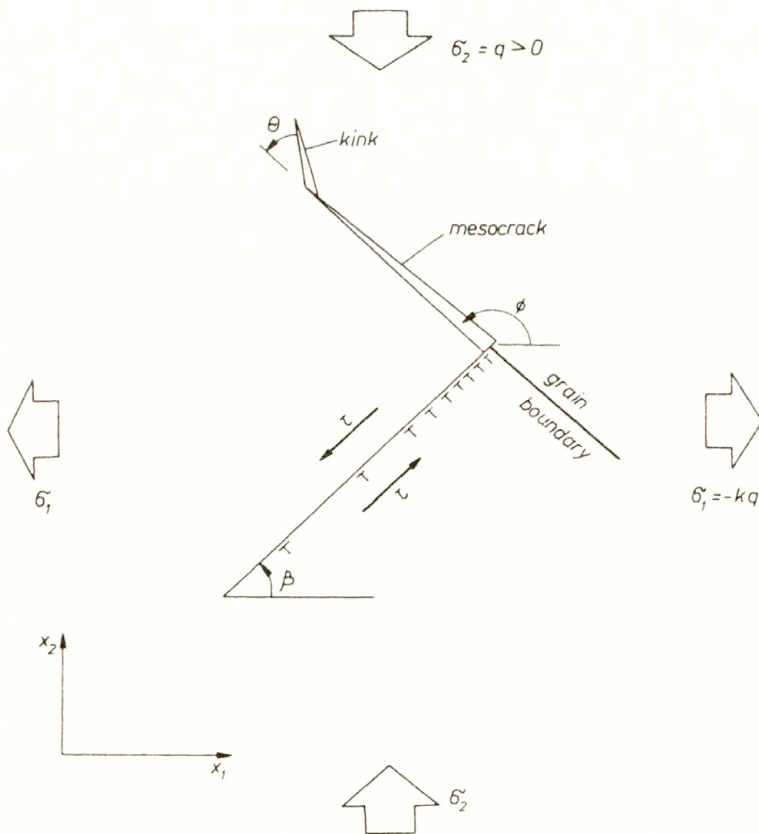


FIG. 1. The Zener–Stroh cracks nucleation mechanism.

Table 1. Components of the matrix $M_{ij}^{(0)}$.

$i \setminus j$	1	2	6
1	$\sin^2 \phi (2 - 3 \cos^2 \phi)$	$3 \sin^2 \phi \cos \phi$	0
2	$\cos^2 \phi (1 - \cos^2 \phi)$	$\cos^2 \phi (1 + \cos^2 \phi)$	0
6	$-\frac{1}{2} \sin 2\phi (1 + 2 \sin^2 \phi)$	$-\frac{1}{2} \sin 2\phi (1 + 2 \cos^2 \phi)$	0

Table 2. Components of the matrix $M_{ij}^{(c)}$.

$i \setminus j$	1	2	6
1	$-\frac{1}{4} \sin^2 2\phi + \mu \sin^3 \phi \cos \phi$	$\frac{1}{4} \sin^2 2\phi - \mu \sin \phi \cos^3 \phi$	0
2	$\frac{1}{4} \sin^2 2\phi + \mu \sin^3 \phi \cos \phi$	$-\frac{1}{4} \sin^2 2\phi + \mu \sin \phi \cos^3 \phi$	0
6	$\frac{1}{4} \sin 4\phi + \mu \sin^2 \phi \cos 2\phi$	$-\frac{1}{4} \sin 4\phi + \mu \cos^2 \phi \cos 2\phi$	0

Assuming that the mesocracks occupy a straight segment of the grain boundaries, one can simply estimate the compliance tensor components, [3]

$$(3.4) \quad S_{ij}^* = \frac{2\pi}{AE_0} \left\{ \begin{matrix} N_m^{(0)} \\ N_m^{(c)} \end{matrix} \right\} \int_{\phi_{c1}}^{\phi_{c2}} \int_{D_m}^{D_M} \left\{ \begin{matrix} M_{ij}^{(0)} \\ M_{ij}^{(c)} \end{matrix} \right\} \frac{D^2}{4} p_1(\phi) p_2(D) dD d\phi,$$

where $N_m^{(0)}$ and $N_m^{(c)}$ are numbers of open and closed mesocracks, respectively; $p_1(\phi)$, $p_2(D)$ are the inclinations of mesocracks and grain size distribution functions. $M_{ij}^{(0)}$ and $M_{ij}^{(c)}$ are the two-dimensional matrices, (see Table 1 and Table 2). $\phi_{c1} < \phi < \phi_{c2}$ denotes the fan of N_m cracks, and

$$(3.5) \quad N_m = N_m^{(0)} + N_m^{(c)}.$$

Integration in (3.4) must be performed separately for open cracks, $N_m^{(0)}$, and closed ones, $N_m^{(c)}$ for appropriate angles of inclination. In Table 2 symbol μ denotes the friction sliding coefficient.

3.3. Influence of the mesocracks deflection on the compliance tensor

Experimental evidences [4] show that mesocracks propagate mainly intergranularly, although transgranular mode is also possible. It is due to the fact that the surface energy of grain boundaries γ_{gb} is substantially less than the surface energy of pure crystals γ_g . Thus, the change of the mesocrack direction causes toughening of the ceramic materials.

Tension cracks (kinks) appearing at the end of main mesocracks inclined to it at the angle θ , propagate under mixed mode initially, but tend to become the Mode I cracks as l increases. The stress intensity factors at the kink tips can be approximated according to the formulae

$$(3.6) \quad k_I = -\frac{D}{2} \left\{ \begin{matrix} \tau_s \sin(\theta) \\ \tau_s \sin(\theta) + \sigma_2' \cos(\theta) \end{matrix} \right\} / [\pi(l + l^*)]^{1/2} - (\pi l)^{1/2} \frac{1}{2} [\sigma_2 + \sigma_1 + (\sigma_1 - \sigma_2) \cos 2(\theta + \phi)],$$

$$(3.7) \quad k_{II} = \frac{D}{2} \left\{ \begin{matrix} \tau_s \cos(\theta) \\ \tau_s \cos(\theta) + \sigma_2' \sin(\theta) \end{matrix} \right\} / [\pi(l + l^*)]^{1/2} - (\pi l)^{1/2} \frac{1}{2} [(\sigma_1 - \sigma_2) \sin 2(\theta + \phi)].$$

The upper expressions in the braces are related to the closed mesocracks like in [5], whereas the lower ones — to opened cracks. The second parts of (3.6) and (3.7) present an influence of external load. $l + l^*$ is the equivalent kink length, as in [5]. Here $\tau_s = \sigma'_6 + \mu\sigma'_2$ is the component of the shear stress.

With these assumptions, the influence of existence of the kinks on the compliance tensor can be described by

$$(3.8) \quad \widehat{S}_{ij}^* = \frac{\pi}{E_0} \left\{ \begin{matrix} \widehat{N}_m^{(0)} \\ \widehat{N}_m^{(c)} \end{matrix} \right\} \int_{\bar{l}_{k_1}}^{\bar{l}_{k_2}} p_{k_1}(\bar{l}) \int_{\theta_{k_1} + \phi_{k_1}}^{\theta_{k_2} + \phi_{k_2}} \left\{ \begin{matrix} \widehat{M}_{ij}^{(0)} \\ \widehat{M}_{ij}^{(c)} \end{matrix} \right\} p_{k_2}(\theta + \phi) \bar{l} d\bar{l} d(\theta + \phi),$$

where $\widehat{N}_m^{(0)}$ and $\widehat{N}_m^{(c)}$ are numbers of open and closed mesocracks strong enough to produce kinks, $\widehat{M}_{ij}^{(0)}$ and $\widehat{M}_{ij}^{(c)}$ are two-dimensional matrices (see Table 3 and Table 4). p_{k_1} and p_{k_2} are distribution functions of the tension crack lengths and their inclination angles, respectively. $\bar{l}_{k_1} \leq \bar{l} \leq \bar{l}_{k_2}$ characterizes the fan of the kink lengths, whereas $\theta_{k_1} + \phi_{k_1} \leq \theta + \phi \leq \theta_{k_2} + \phi_{k_2}$ the fan of kinked crack inclination. Integration in (3.8) must be performed separately for open crack $\widehat{N}_m^{(0)}$, and the closed ones, $\widehat{N}_m^{(c)}$, for appropriate angles of inclination.

Table 3. Components of the matrix $\widehat{M}_{ij}^{(0)}$.

$i \setminus j$	1	2	6
1	$\sin \phi \cos(2\theta) \sin(\theta + \phi)$	$\cos \phi \sin(2\theta) \sin(\theta + \phi)$	0
2	$-\sin \phi \sin(2\theta) \cos(\theta + \phi)$	$\cos \phi \cos(2\theta) \cos(\theta + \phi)$	0
6	$-\sin \phi \cos(3\theta + \phi)$	$-\cos \phi \sin(3\theta + \phi)$	0

Table 4. Components of the matrix $\widehat{M}_{ij}^{(c)}$.

$i \setminus j$	1	2	6
1	$\sin^2 \phi \cos \phi \sin(\theta + \phi)[\text{ctg } \phi - \mu]$	$\cos^3 \phi \sin(\theta + \phi)[\text{tg } \phi - \mu]$	0
2	$-\sin^3 \phi \cos(\theta + \phi)(\text{ctg } \phi - \mu)$	$\sin \phi \cos^2 \phi \cos(\theta + \phi)[\text{tg } \phi - \mu]$	0
6	$-\sin^2 \phi \cos(\theta + 2\phi)[\text{ctg } \phi - \mu]$	$\cos^2 \phi \cos(\theta + 2\phi)[\text{tg } \phi - \mu]$	0

The compliance \widehat{S}_{ij}^* , Eq. (3.8), is related to the opening effect of tension cracks due to slip of the main mesocrack faces. Another effect influencing total compliance of the material response is the closure or opening of kinks under external loading. The amount of changes can be estimated by the following expression:

$$(3.9) \quad \bar{S}_{ij}^* = \frac{\pi D^2}{16AE_0} \left[\left\{ \begin{matrix} \widehat{N}_m^{(0)} \\ \widehat{N}_m^{(c)} \end{matrix} \right\} \int_{\bar{l}_{k_1}}^{\bar{l}_{k_2}} p_{k_1}(\bar{l}) \int_{\theta_{k_1} + \phi_{k_1}}^{\theta_{k_2} + \phi_{k_2}} \bar{M}_{ij} p_{k_2}(\theta + \phi) \bar{l}^2 d\bar{l} d(\theta + \phi) \right],$$

where components of the matrix \bar{M}_{ij} are specified in Table 5.

Table 5. Components of the matrix $\bar{M}_{ij}^{(0)}$.

$i \setminus j$	1	2	6
1	$\sin^2(\theta + \phi)$	0	0
2	0	$\cos^2(\theta + \phi)$	0
6	$-\frac{1}{2} \sin 2(\theta + \phi)$	$-\frac{1}{2} \sin 2(\theta + \phi)$	0

3.4. Overall response compliance tensor

Summarizing our discussion of the preceding sections, the total response of the material (2.6) will be calculated by superposition of Eqs. (3.1)–(3.4), (3.8) and (3.9):

$$(3.10) \quad S_{ij}(\sigma) = S_{ij}^{(0)} + S_{ij}^{*(s)} + S_{ij}^* + \widehat{S}_{ij}^* + \overline{S}_{ij}^*.$$

The expression (3.10) shows a rather complicated structure of the compliance tensor, postulated for the Taylor model (no crack interaction). It strongly depends on the inclination fans of the existing mesocracks, and on the propagation mode of the secondary cracks. They are directly related to the actual state of stress σ .

4. Numerical examples of MgO ceramic deformation process

To illustrate the possibilities of the model, let us consider MgO ceramics characterized by the following constants [4]:

- Young's modulus $E_0 = 316.4$ GPa,
- Poisson's coefficient $\nu_0 = 0.272$,
- Kirchhoff's modulus $G_0 = 121.9$ GPa,
- the surface energy of grains $\gamma_g = 1.0$ N/m,
- the shear stress resistance for uniaxial compression $\tau_{s0}^c = 75$ MPa,
- the shear stress resistance for uniaxial tension $\tau_{s0}^t = 25$ MPa,

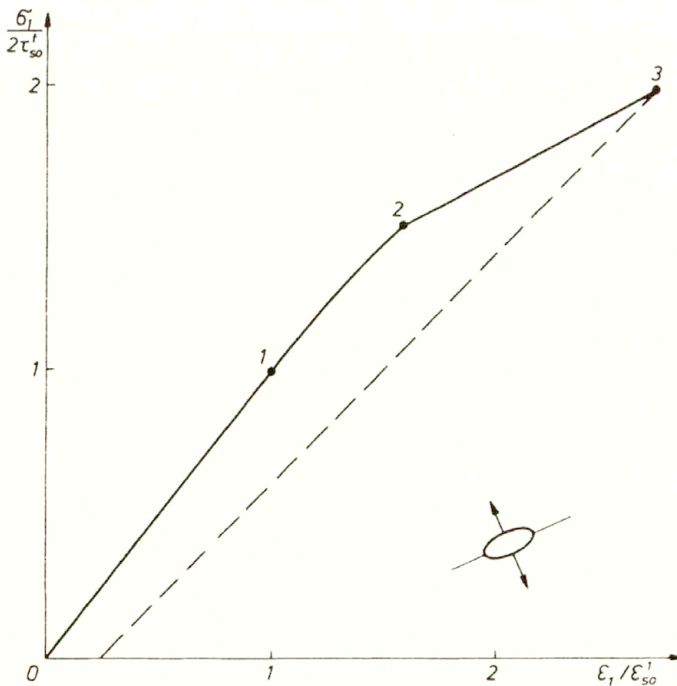


FIG. 2. Uniaxial tension.

We assume that the surface energy of grain boundaries is $\gamma_{gb} = 0.5\gamma_g$ and the mean grain diameter in the unit cell is $\bar{D} = 45\mu\text{m}$. It is also assumed that grains are hexagonal in shape ($\theta = 60^\circ$).

Figure 2 presents the deformation process of MgO semi-brittle ceramics subjected to simple tension. Only open mesocracks ($N_m^{(t)} > 0$) develop within the material. Segment 0-1 reflects a purely linear elastic response of the MgO ceramics. At point 1 (limit of the purely elastic phase, characterized by the stress $2\tau_{s0}^t$ and the strain ε_{s0}^t), the first conjugate slip systems are created inside the grains. They are potent enough to nucleate the first mesocrack at point 2. Segment 2-3 represents the nucleation and development of mesocracks. At point 3 the saturation state is reached and the "worst" mesocrack is capable of kinking and spreading along the grain boundaries causing final failure. It should be stressed that there is no continuity of the tangent in 2 due to the fact of intensive mesocracks initiation at the beginning of the fissuration process.

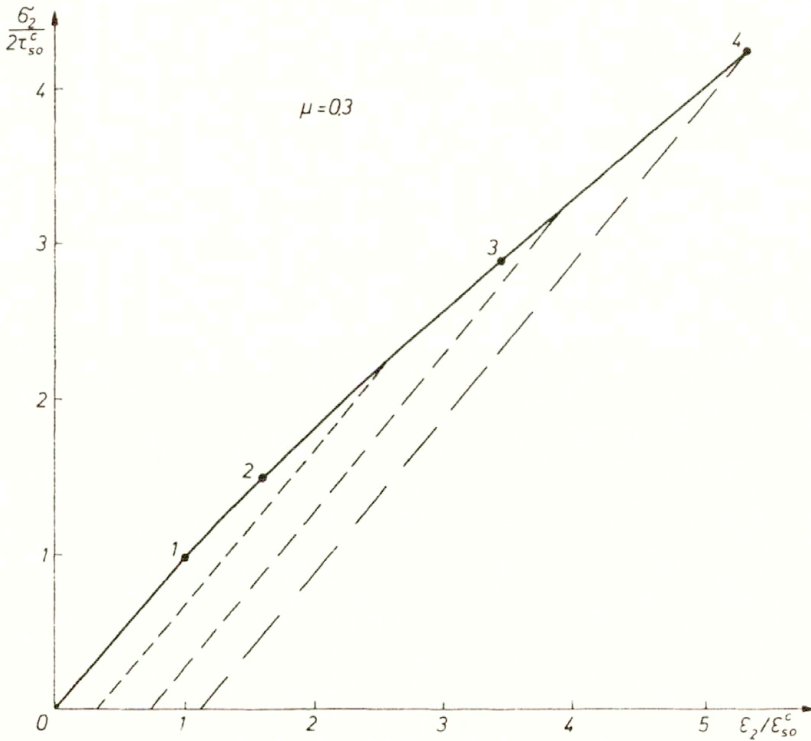


FIG. 3. Uniaxial compression.

Figure 3 shows the deformation process of MgO semi-brittle ceramic subjected to simple compression. Contrary to simple tension, only closed mesocracks appear, $N_m^{(c)} > 0$. Numerical calculations were performed for $\mu = 0.3$. Segment 0-1 reflects purely linear elastic response of the material. At point 1 (limit of the pure elasticity, characterized by the stress $2\tau_{s0}^c$ and the strain ε_{s0}^c) the slip line phase initiates. Nucleation of Zener–Stroh microcracks begins at point 2. Segment 2-3 obeys the nucleation and development of laws of mesocracks. The frictional sliding of some suitably oriented mesocracks initiates tension

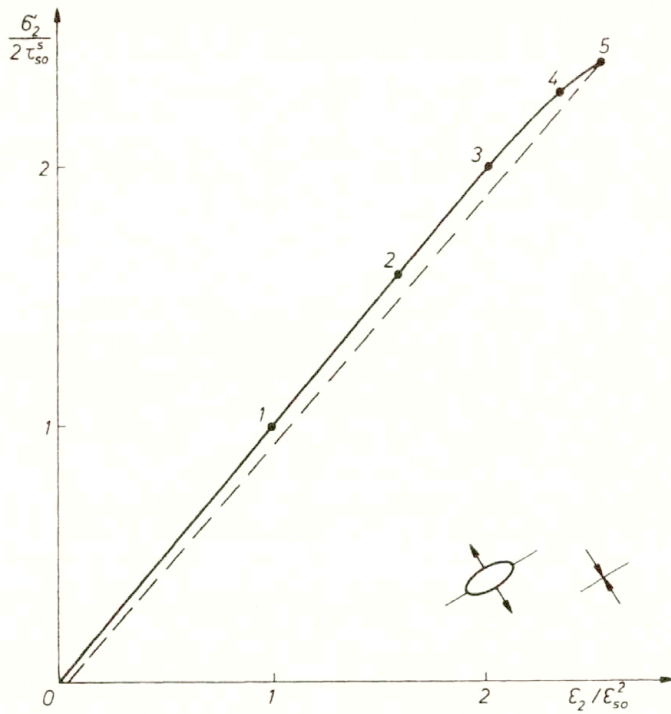


FIG. 4. Pure shear — $\sigma_2(\epsilon_2)$.

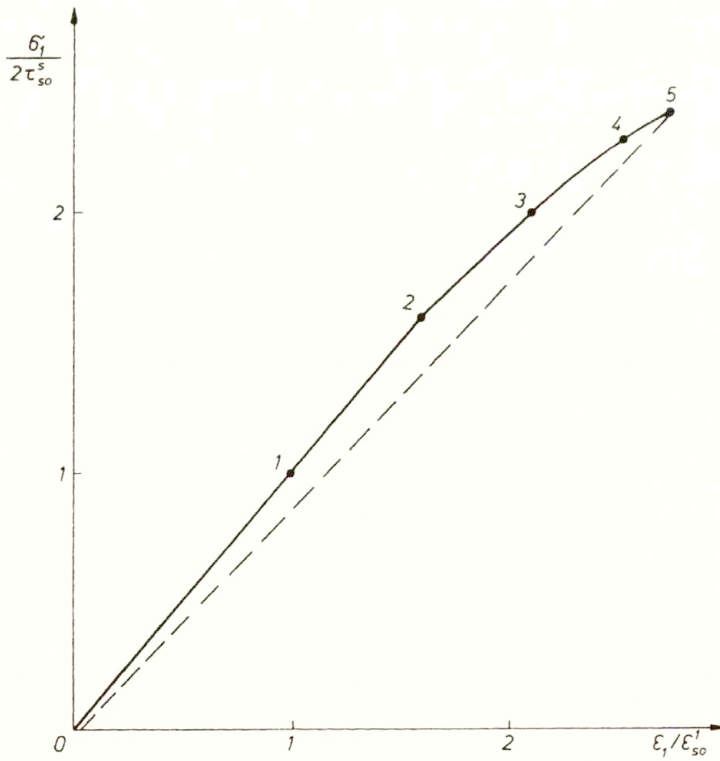


FIG. 5. Pure shear — $\sigma_1(\epsilon_1)$.

cracks at their ends. Further loading (3-4) causes the growth of the tension cracks and spreading along the sequential segments of the grains. At point 4 some tension cracks produce kinks again or spread through the adjacent crystal.

Under pure shear both the open and closed mesocracks appear inside the material ($N_m^{(0)} > 0; N_m^{(c)} > 0$). In numerical calculations it was assumed that friction sliding coefficient $\mu = 0.3$. Figure 4 presents the correlation $\sigma_2(\varepsilon_2)$, whereas Fig. 5 — $\sigma_1(\varepsilon_1)$, respectively. Segment 0-1 reflects purely linear elastic response. At point 1 (characterized by the stress $2\tau_{s0}^s$ and the state of strain $\varepsilon_{s0}^1, \varepsilon_{s0}^2$), the first conjugate slip systems are created inside the grains. They are able to produce the first mesocrack at point 2. Segment 2-3 represents the nucleation and development of mesocracks. Like in uniaxial tension, the function $\sigma_1(\varepsilon_1)$ has the characteristic shape with the small inflection, whereas $\sigma_2(\varepsilon_2)$ is smooth. At point 3 the first opened mesocrack produces kinks and spreads in a stable manner. The first compressed mesocrack changes its direction at the load level corresponding to point 4. Final failure is associated with unstable unconstrained propagation of compressed mesocracks.

In all the figures unloading of the material was marked by dashed lines.

4. Conclusions

The deformation process of semi-brittle materials is characterized by many different phenomena developing within the material. The most important ones are taken into account by application of the appropriate averaging procedure.

In mesomechanical modelling we do not introduce any internal parameter describing the damage process, contrary to the phenomenological description. However, many reasonable assumptions concerning geometry of the grain size, distribution of the crack lengths etc. must be done to obtain an effective constitutive model.

In the present paper the model was applied to the case of the so-called proportional loading by the two-dimensional stress. Unloading was described in [3]. It seems to be applicable also to nonproportional loading path as well as to cyclic loading, though it can entail more complex numerical calculations. The problem will be investigated in the nearest future.

However, because of its simplicity and deep physical foundations, the proposed model seems to be a very convenient tool for engineering applications concerning the analysis of deformation processes occurring in advanced materials and structures.

Acknowledgement

The author gratefully acknowledges the support rendered by the Research Committee, Poland, KBN Project No.3 1014 91 01 on thermomechanics of damage development and phase transformation in materials.

References

1. A. STOIMIROVIC, D. KRAJICINOVIC and T. SADOWSKI, *Constitutive model for polycrystalline MgO ceramics*, [in:] *Constitutive Modelling for Nontraditional Materials*, V. STOKES and D. KRAJICINOVIC [Eds.], ASME Publ., AMD-Vol. 85, pp.175–184, 1987.
2. T. SADOWSKI, *Modelling of semi-brittle MgO ceramic behaviour under compression*, *Mech. Mater.*, **18**, pp. 1–16, 1994.

3. T. SADOWSKI, *Mechanical response of semi-brittle ceramics subjected to tension-compression state. Part I. Theoretical modelling*, [to appear in *Int. J. Damage Mech.*, 1994].
4. W. DAVIDGE, *Mechanical behaviour of ceramics*, Cambridge University Press, Cambridge U.K. 1979.
5. H. HORII and S. NEMAT-NASSER, *Brittle failure in compression: splitting, faulting and brittle-ductile transition*, *Phil. Trans. Roy. Soc. London*, vol. 319, No 1594, pp. 337-374, 1986.

LUBLIN UNIVERSITY OF TECHNOLOGY
FACULTY OF CIVIL AND SANITARY ENGINEERING, LUBLIN.

Received February 14, 1994

Concept of a singular surface in contact mechanics

G. SZEFER, D. JASIŃSKA and J.W. SALAMON (KRAKÓW)

THE PAPER DEALS with an application of the notion of material singular surface to the description of contact problems in elastic continua. Two kinds of contact problems are considered: 1. Dynamic contact with friction in terms of large deformations, and 2. Static contact between reinforced media. In the first problem — the singular surface has been used to model the frictional contact; in the second one — the singular surface describes the reinforcement. Variational formulation and numerical results for both these problems are given.

1. Introduction

IN THE PAPER two classes of contact problems will be considered: 1. Dynamic analysis of frictional contact in terms of large deformations, 2. Frictional interaction between reinforcement and the layer in elastic, multilayered media. In both problems a unified approach based on the concept of a material singular surface in continua has been used: in the first case to describe the frictional interface response in the contact zone, in the second one — to describe the structural properties of the reinforcement.

The model of a continuum B with a singular surface Γ which divides the body into two parts $B^+ \cup B^- \cup \Gamma = B$ is known in continuum mechanics [4, 6, 9] and was used to describe several surface phenomena like transition, surface tension etc. The theory of continua with material singular surface is based on the assumption, that any thermodynamical quantity Ψ has the representation

$$\Psi = \int_{B-\Gamma} \psi d\nu + \int_{\Gamma} \psi_s da.$$

It means that, beside of the usual field density ψ , an additional independent field ψ_s on Γ is defined. Hence, using the standard procedure for balance equations and taking into account the Green–Gauss theorem for discontinuous fields, the system of equations of motion has the local form [9]

$$\begin{aligned} B \setminus \Gamma : \quad \operatorname{div} \sigma + \rho \mathbf{b} &= \rho \ddot{\mathbf{u}}, \\ \Gamma : \quad \operatorname{div}_s \sigma_s + \rho_s \mathbf{b}_s - \llbracket \sigma \rrbracket \mathbf{n} &= \rho_s \ddot{\mathbf{u}}_s, \end{aligned}$$

where

$\rho, \mathbf{b}, \mathbf{u}, \sigma$ mass density, body force, displacement and stress tensor of the body B ,
 $\rho_s, \mathbf{b}_s, \mathbf{u}_s, \sigma_s$ independent mass density, body force, displacement and stress tensor of the surface Γ particle, respectively,

$$\begin{aligned} \llbracket (\dots) \rrbracket &= (\dots)^- - (\dots)^+ \text{ discontinuity on } \Gamma, \\ \mathbf{n} &\text{ vector normal to the surface } \Gamma \text{ (Fig. 1).} \end{aligned}$$

These relations, together with the kinematical equations for the strain tensors \mathbf{e}, \mathbf{e}_s (of the body, and of the surface, respectively) and with the constitutive equations for the stresses σ and σ_s , constitute the closed system of the continuous body containing a material surface Γ .

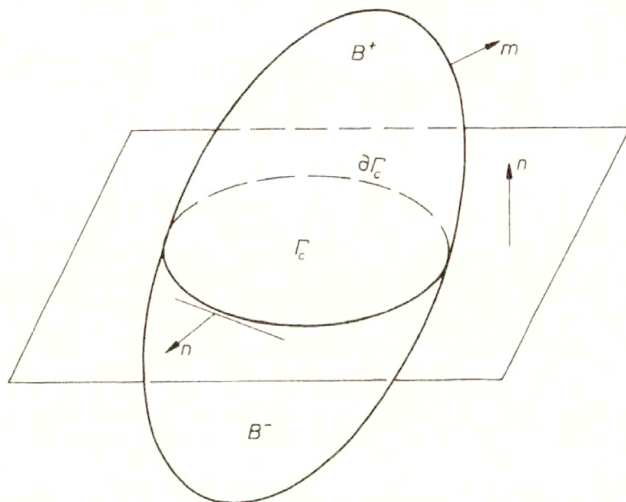


FIG. 1.

2. Dynamic contact problem with friction

2.1. Statement of the problem

Let us assume an elastic body B^+ (contactor) which may be in contact with another elastic body B^- (target or reference body) (Fig. 2b). Assume that the contact surface Γ_c is rough. To describe the frictional phenomena, the idea of a material singular surface will be used. It means, that the material particles of a contact zone Γ_c have physical properties different from the contacting bodies B^+ and B^- . The concept of singular surface in description of a rough contact is based on three fundamental, physically motivated postulates [15, 16]:

I. The contact zone Γ_c is a two-dimensional manifold, with material which has properties different from the contacting bodies (the concept of the "third body" [5, 20]).

II. The constitutive equations of this manifold should take into account the influence of asperities of the surface.

III. The process of friction has a "fractal" character.

From axiom I it results, that each frictional contact boundary value problem should consider the system of equations mentioned above with the additional unknown surface stress tensor σ_s defined on Γ_c .

Axiom II provides the constitutive law for the material of Γ_c . It should be of the type

$$\sigma_s = \mathcal{F}(a, \mathbf{e}_s),$$

where a means the approach or penetration (the definition will be given later).

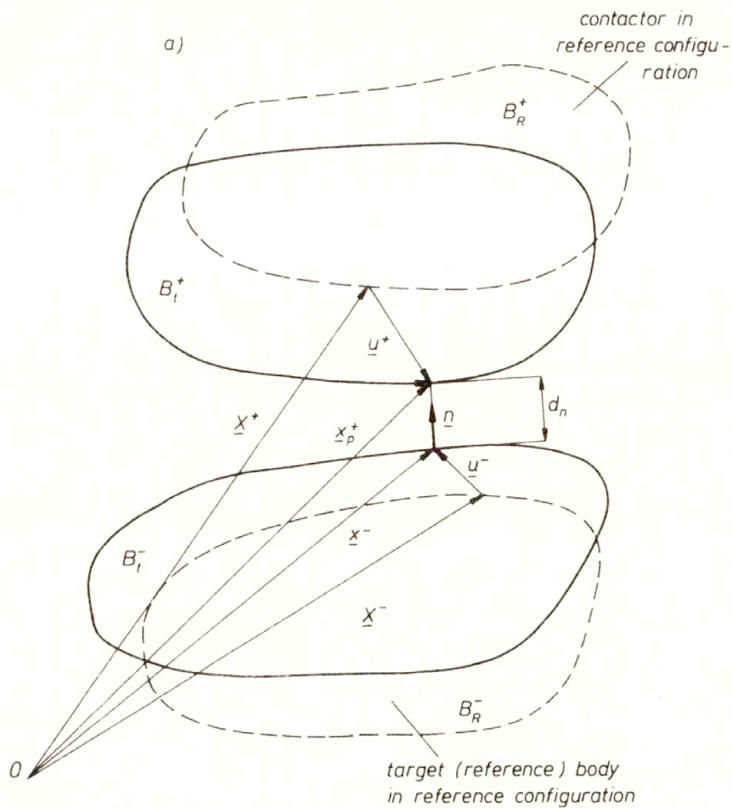
Axiom III leads to the criterion of friction (stick-slip condition). Here two kinds of formulation are possible:

i) A classical condition $f(t_T, t_N) = 0$,

t_T, t_N — tangential and normal contact stresses in bodies B^\pm ;

ii) A new condition of the type

$$\max |\mathbf{t}_s| = \max |\sigma_s \tilde{\mathbf{n}}| < S_{cr} \Rightarrow \text{stick},$$



b)

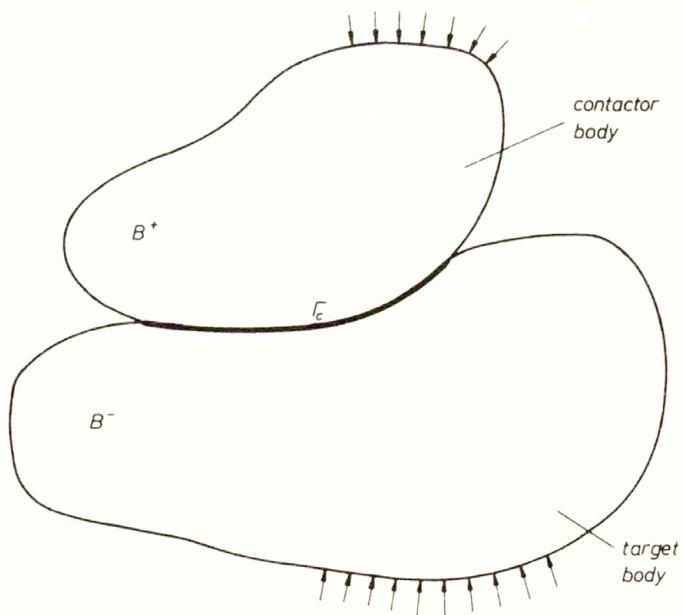


FIG. 2

$$\max |\sigma_s \tilde{\mathbf{n}}| = S_{cr} \Rightarrow \text{slip},$$

where \mathbf{t}_s — stress vector of the manifold Γ_c , $\tilde{\mathbf{n}}$ — vector normal to the cross-section in Γ_c (see Fig. 1), S_{cr} — critical value depending on the micro-structure of Γ_c and on the sliding velocity.

In the present paper, a dynamic contact problem of an elastic body with the above proposed model of friction will be formulated. The stick-slip condition in the classical version has been used. It means, that the material singular surface models the structure of the contact manifold in the form of a kind of “hardening” or “loosening” of the contact material. The break of cohesion is induced by the critical value of the tangential stresses t_T (according to the Coulomb law or to other formulas like those given by ODEN [11], GROSCH, or THIRION–DENNY [13, 14]).

The new criterion (ii) needs further experimental investigations on micro- and macro-structural level, and will be the aim of separate papers.

So, assuming large deformations, the system of equations in the natural Eulerian description contains:

equations of motion

$$(2.1) \quad \begin{aligned} B^+ : \quad & \sigma_{ij,j}^+ + \rho^+ \cdot b_i^+ = \rho^+ \cdot \ddot{u}_i^+, \\ \Gamma_c : \quad & \sigma_{i\alpha;\alpha}^s - \llbracket \sigma_{ij} \rrbracket \cdot n_j + \rho^s \cdot b_i^s = \rho^s \cdot \ddot{u}_i^s, \\ B^- : \quad & \sigma_{ij,j}^- + \rho^- \cdot b_i^- = \rho^- \cdot \ddot{u}_i^-, \end{aligned}$$

kinematical relations

$$(2.2) \quad \begin{aligned} B^+ : \quad & e_{ij}^+ = \frac{1}{2}(u_{i,j}^+ + u_{j,i}^+ - u_{k,i}^+ \cdot u_{k,j}^+), \\ \Gamma_c : \quad & e_{\alpha\beta}^s = \frac{1}{2}(u_{\alpha,\beta}^s + u_{\beta,\alpha}^s - u_{\gamma,\alpha}^s \cdot u_{\gamma,\beta}^s), \\ B^- : \quad & e_{ij}^- = \frac{1}{2}(u_{i,j}^- + u_{j,i}^- - u_{k,i}^- \cdot u_{k,j}^-), \end{aligned}$$

constitutive equations

$$(2.3) \quad \begin{aligned} \sigma_{ij}^+ &= \mathcal{F}_{ij}^+(\mathbf{e}^+), \\ \sigma_{\alpha\beta}^s &= \mathcal{F}_{\alpha\beta}^s(\mathbf{e}^s, a), \\ \sigma_{ij}^- &= \mathcal{F}_{ij}^-(\mathbf{e}^-). \end{aligned}$$

Here are: $\mathbf{u}^\pm, \mathbf{e}^\pm, \sigma^\pm$ — displacement vectors, Almansi–Hammel strain tensors, Cauchy stress tensors of the contactor and target body, respectively; $\mathbf{u}^s, \mathbf{e}^s, \sigma^s$ — displacements, strains and stresses of the surface Γ_c ; $\{x^i\}, i, j = 1, 2, 3; \{\theta^{\alpha\gamma}\}, \alpha, \beta = 1, 2$ — Eulerian coordinates defined in space and on the surface Γ_c , respectively; $(\dots)_{;\alpha}$ — means covariant differentiation, a — penetration (as mentioned by Axiom II);

the following transformation formulas should be taken into account:

$$\sigma_{i\alpha}^s = \sigma_{\alpha\beta}^s x_{,\beta}^i, \quad b_i^s = b_{\alpha}^s x_{,\alpha}^i, \quad u_i^s = u_{\alpha}^s x_{,\alpha}^i.$$

The systems (2.1)–(2.3) must be completed by

1. Boundary conditions

$$(2.4) \quad \begin{aligned} \sigma_{ij}^\pm \cdot m_j^\pm &= p_i^\pm(\mathbf{x}, t) \quad \text{on } \Gamma_\sigma^\pm, \\ u_i^\pm &= g_i^\pm(\mathbf{x}, t) \quad \text{on } \Gamma_u^\pm, \end{aligned}$$

$$(2.4) \quad \sigma_{\alpha\beta}^s \cdot \tilde{n}_\beta = p_\alpha^s(\mathbf{x}, t) \quad \text{on } \partial\Gamma_c.$$

[cont.]

2. Initial conditions

$$(2.5) \quad \begin{aligned} u_i^\pm(\mathbf{x}, t_0) &= {}^\pm u_i^0(\mathbf{x}), & \dot{u}_i^\pm(\mathbf{x}, t_0) &= {}^\pm v_i^0(\mathbf{x}), & \mathbf{x} &\in B^\pm, \\ u_i^s(\mathbf{x}, t_0) &= u_i^{0s}(\mathbf{x}), & \dot{u}_i^s(\mathbf{x}, t_0) &= v_i^{0s}(\mathbf{x}), & \mathbf{x} &\in \Gamma_c. \end{aligned}$$

3. Compatibility between the body B^+ and the singular surface Γ_c

$$(2.6) \quad \mathbf{u}^+ = \mathbf{u}^s$$

(generally not necessary but here assumed for simplicity).

4. Contact conditions describing the normal interface response. The unilateral contact in terms of large deformations is described by using the contact distance function defined as follows (see Fig. 2a):

$$(2.7) \quad d_n = (\mathbf{x}_p^+ - \mathbf{x}^-) \cdot \mathbf{n}^- = [(\mathbf{X}^+ + \mathbf{u}^+)_p - (\mathbf{X}^- + \mathbf{u}^-)] \cdot \mathbf{n}^- = d_n(\mathbf{x}^-, \mathbf{x}_p^+).$$

Here

$$\mathbf{x}_p^+ = \mathbf{x}_p^+(\mathbf{x}^-, \Gamma_c^+) = \text{proj}_{\Gamma_c^+} \mathbf{x}^-$$

is the projection of \mathbf{x}^- on the deformed potential target surface Γ_c^+ (candidate contact surface of B^+), cf. [19]. The unilateral contact law has then the form

$$(2.8) \quad \begin{aligned} d_n > 0 &\Rightarrow t_n = 0, & d_n = 0 &\Rightarrow t_n \leq 0, \\ t_n \cdot d_n &= 0, & t_n &= \sigma_{ij} \cdot n_i \cdot n_j. \end{aligned}$$

To avoid the Signorini unilateral conditions, one can use the so-called normal compliance law [11]

$$(2.9) \quad \begin{aligned} t_n = C_n \cdot a_+^{m_n}, & \quad a_+ = \begin{cases} 0 & \text{for } a < 0, \\ a & \text{for } a \geq 0. \end{cases} \\ a = -d_n & \quad \text{defines penetration} \end{aligned}$$

(note, that d_n is well defined even if the bodies penetrate each other, it means for $d_n < 0$).

5. Friction conditions

Taking into account the previous remark, the classical formulation of the friction condition will be used. Then we have

$$(2.10) \quad \begin{aligned} f(t_T, t_n) &\leq 0 \quad \text{on } \Gamma_c, \\ f(t_T, t_n) &< 0 \Rightarrow \dot{\mathbf{u}}_T^w = 0, \\ f(t_T, t_n) &= 0 \Rightarrow \exists \lambda \geq 0; \quad \dot{\mathbf{u}}_T^w = -\lambda \cdot \mathbf{t}_T, \end{aligned}$$

where

$$(2.11) \quad \begin{aligned} \dot{\mathbf{u}}_T^w &= \dot{\mathbf{u}}_T^+ - \dot{\mathbf{u}}_T^- \quad \text{— sliding velocity,} \\ t_T = |\mathbf{t}_T| &= (t_{T^i} \cdot t_{T^i})^{\frac{1}{2}}, & t_{T^i} &= \sigma_{ij} \cdot n_j - t_n \cdot n_i \\ & \begin{cases} t_T - \mu \cdot t_n & \text{for the Coulomb law,} \\ t_T - \frac{1}{A + B \cdot t_n} \cdot t_n & \text{for the Thirion–Denny model,} \\ t_T - \mu_0 \cdot \left(\frac{t_n}{E}\right)^{-\frac{1}{3}} \cdot t_n & \text{for the Gresh–Schallamach model,} \\ t_T - \frac{C_T}{C_n^{\frac{m_T}{m_n}}} \cdot t_n \frac{m_T}{m_n} & \text{for the normal compliance law.} \end{cases} \end{aligned}$$

The systems (2.1)–(2.3) with conditions (1)–(5) constitute a consistent system of relations for the boundary value problem of the frictional contact in local, Eulerian formulation. Contrary to the existing models of friction, additional terms \mathbf{u}^s , \mathbf{e}^s , σ^s describing the intrinsic frictional phenomena in form of a singular surface Γ_c are introduced.

2.2. Variational formulations

To solve the nonlinear boundary value problem (2.1)–(2.9), the variational formulation of the problem will be stated.

Defining the set of kinematically admissible velocities

$$(2.12) \quad \begin{aligned} V^+ &= \{ \mathbf{v}^+ = \dot{\mathbf{w}}^+; \mathbf{v}^+ = 0 \text{ on } \Gamma_u^+ \}, \\ V^- &= \{ \mathbf{v}^- = \dot{\mathbf{w}}^-; \mathbf{v}^- = 0 \text{ on } \Gamma_u^- \}, \end{aligned}$$

and applying the standard procedure for derivation of the virtual power principle, the variational formulation in Eulerian description takes the form

$$(2.13) \quad \begin{aligned} &\int_{\Omega_+} \sigma_{ij}(\mathbf{u}^+) \varepsilon_{ij}(\mathbf{v}^+) dV^+ + \int_{\Omega_-} \sigma_{ij}(\mathbf{u}^-) \varepsilon_{ij}(\mathbf{v}^-) dV^- + \int_{\Gamma_c} \sigma_{\alpha\beta}^s(\mathbf{u}^s) \varepsilon_{\alpha\beta}(\mathbf{v}^s) d\Gamma \\ &\quad + \int_{\Omega_+} \varrho^+ \ddot{u}_i^+ v_i^+ dV^+ + \int_{\Omega_-} \varrho^- \ddot{u}_i^- v_i^- dV^- + \int_{\Gamma_c} \varrho^s \ddot{u}_i^s v_i^s d\Gamma \\ &= \int_{\Omega_+} \varrho^+ \cdot b_i^+ v_i^+ dV^+ + \int_{\Omega_-} \varrho^- \cdot b_i^- v_i^- dV^- + \int_{\Gamma_c} \varrho^s \cdot b_i^s v_i^s d\Gamma \\ &\quad + \int_{\Gamma_f^+} p_i^+ \cdot v_i^+ d\Gamma + \int_{\Gamma_f^-} p_i^- \cdot v_i^- d\Gamma + \int_{\partial\Gamma_c} p_i^s \cdot v_i^s dS \\ &\quad + \int_{\Gamma_c} [\sigma_{ij}^- n_j^- (v_i^- - v_i^s) + \sigma_{ij}^+ n_j^+ (v_i^+ - v_i^s)] d\Gamma \quad \forall (\mathbf{v}^+, \mathbf{v}^-) \in V^\pm, \end{aligned}$$

where

$$\varepsilon_{ij}(\mathbf{v}) = \frac{1}{2}(v_{i,j} + v_{j,i}), \quad \varepsilon_{\alpha\beta}(\mathbf{v}^s) = \frac{1}{2}(v_{\alpha;\beta}^s + v_{\beta;\alpha}^s), \quad \mathbf{v}^s = \mathbf{v}^+ \quad \text{on } \Gamma_c,$$

and the following equalities

$$\sigma_{i\alpha}^s v_{i;\alpha}^s = \sigma_{ij}^s \varepsilon_{ij}^s = \sigma_{\alpha\beta}^s \varepsilon_{\alpha\beta}^s$$

have been used to describe the power of the surface stresses.

The last integral in (2.13) can be written in the form

$$\begin{aligned} J_c &= \int_{\Gamma_c} [\sigma_{ij}^- n_j^- (v_i^- - v_i^s) + \sigma_{ij}^+ n_j^+ (v_i^+ - v_i^s)] d\Gamma \\ &= \int_{\Gamma_c} [t_i^- (v_i^- - v_i^s) + t_i^+ (v_i^+ - v_i^s)] d\Gamma \\ &= \int_{\Gamma_c} [t_n^- (v_n^- - v_n^s) + t_{Ti}^- (v_{Ti}^- - v_{Ti}^s)] d\Gamma + \int_{\Gamma_c} [t_n^+ (v_n^+ - v_n^s) + t_{Ti}^+ (v_{Ti}^+ - v_{Ti}^s)] d\Gamma, \end{aligned}$$

where v_n^\pm and v_{Ti}^\pm denote the normal and tangential components of the vectors \mathbf{v}^\pm .

Taking into account the condition (2.6) and using the notation

$$(2.14) \quad v_n^w = v_n^- - v_n^s, \quad v_{Ti}^w = v_{Ti}^- - v_{Ti}^s,$$

it will be finally

$$(2.15) \quad J_c = \int_{\Gamma_c} t_n^- v_n^w d\Gamma + \int_{\Gamma_c} t_{Ti}^- v_{Ti}^w d\Gamma.$$

The variational statement (2.13) of the dynamic boundary value contact problem (2.1)-(2.9) needs additional remark. Since the kinematical admissible sets (2.12) are defined for velocities (and not for displacements), it is necessary to complete (2.13) by additional variational inequality

$$\int_{\Gamma_c} t_n(\mathbf{u}) [d_n(\mathbf{y}^-, \mathbf{y}_p^+) - d_n(\mathbf{x}^-, \mathbf{x}_p^+)] d\Gamma \geq 0$$

$$\forall \mathbf{y}^- \in K_1 = \{ \mathbf{y}^- : d_n(\mathbf{y}^-, \mathbf{y}_p^+) \geq 0 \text{ on } \Gamma_c \},$$

which is equivalent to the unilateral contact condition (2.8) (it vanishes of course, in the case of the normal compliance model (2.9)).

In numerical calculations, the current contact zone Γ_c is determined iteratively, so one can treat at each state (step) the actual configuration of Γ_c as known. In that case (2.8) will be fulfilled automatically and therefore formulation (2.13) needs no additional conditions. Another remark concerns the fact of creation and annihilation of the material surface Γ_c (third body), and hence the change of all balances (mass, momentum, energy). This situation will not be considered in the paper, since we assume that the contact zone exists all the time and wear is not taken into account.

From the numerical point of view it is also convenient to write all terms in (2.13) (except the contact integrals) in the material description.

Therefore, after introducing the II. Piola–Kirchhoff stress tensor for the bodies B^\pm

$$(2.16) \quad S_{KL}^\pm = J \cdot \sigma_{ij}^\pm \cdot X_{,i}^K \cdot X_{,j}^L,$$

$$J = \det(x_{,i}^j) > 0,$$

the equations of motion in the reference configuration Ω_R^\pm will have the form

$$B^\pm : (S_{KL}^\pm \cdot x_{i,K}^\pm)_{,L} + \varrho_0^\pm \cdot b_i^\pm = \varrho_0^\pm \cdot \ddot{u}_i^\pm.$$

Assuming that the common part of the boundaries which are in contact or the candidates of the contact zones Γ_{cR} are known in the reference configuration, it is emphasized that all kinematically admissible quantities (velocities and displacements) remain well defined in domains Ω_R^\pm and their boundaries. So, repeating again the usual procedure for the virtual power formulation, it will be

$$(2.17) \quad \int_{\Omega_R^+} S_{KL}(\mathbf{u}^+) \cdot x_{i,K}^+ \cdot v_{i,L}^+ dV_R + \int_{\Omega_R^-} S_{KL}(\mathbf{u}^-) \cdot x_{i,K}^- \cdot v_{i,L}^- dV_R$$

$$+ \int_{\Omega_R^+} \varrho_R^+ \ddot{u}_i^+ \cdot v_i^+ dV_R + \int_{\Omega_R^-} \varrho_R^- \ddot{u}_i^- \cdot v_i^- dV_R$$

$$\begin{aligned}
 (2.17) \quad &= \int_{\Omega_R^+} \varrho_R^+ \cdot b_i^+ \cdot v_i^+ dV_R + \int_{\Omega_R^-} \varrho_R^- \cdot b_i^- \cdot v_i^- dV^R + \int_{\Gamma_{fR}^+} p_{Ri}^+ \cdot v_i^+ d\Gamma_R^+ \\
 \text{[cont.]} \quad &+ \int_{\Gamma_{fR}^-} p_{Ri}^- \cdot v_i^- d\Gamma_R^- + \int_{\Gamma_{cR}^+} S_{KL}(\mathbf{u}^+) \cdot x_{i,K}^+ \cdot v_i^+ \cdot N_L^+ d\Gamma_{cR}^+ \\
 &+ \int_{\Gamma_{cR}^-} S_{KL}(\mathbf{u}^-) \cdot x_{i,K}^- \cdot v_i^- \cdot N_L^- d\Gamma_{cR}^- \quad \forall (\mathbf{v}^+, \mathbf{v}^-) \in V^\pm.
 \end{aligned}$$

After applying the formulas

$$\begin{aligned}
 \sigma_{ij}^\pm &= (J^\pm)^{-1} \cdot S_{KL}^\pm \cdot x_{i,K}^\pm \cdot x_{j,L}^\pm, \\
 N_J^\pm &= n_i^\pm \cdot \frac{da}{dA^\pm} \cdot (J^\pm)^{-1} \cdot x_{i,J}^\pm, \\
 \frac{da}{dA^\pm} &= \frac{d\Gamma_c}{d\Gamma_{cR}^\pm} \quad (da, dA \text{ are the area elements in the current} \\
 &\hspace{15em} \text{and reference configurations}),
 \end{aligned}$$

$$\mathbf{n}^+ = -\mathbf{n}^-$$

to the last two integrals, we obtain

$$\begin{aligned}
 I_c &= \int_{\Gamma_{cR}^+} S_{KL}(\mathbf{u}^+) \cdot x_{i,K}^+ \cdot v_i^+ \cdot N_L^+ d\Gamma_{cR}^+ + \int_{\Gamma_{cR}^-} S_{KL}(\mathbf{u}^-) \cdot x_{i,K}^- \cdot v_i^- \cdot N_L^- d\Gamma_{cR}^- \\
 &= \int_{\Gamma_c^+} \sigma_{ij}(\mathbf{u}^+) \cdot n_j^+ v_i^+ d\Gamma_c + \int_{\Gamma_c^-} \sigma_{ij}(\mathbf{u}^-) \cdot n_j^- \cdot v_i^- d\Gamma_c.
 \end{aligned}$$

Here $\Gamma_c^\pm = \Gamma_c \cup \Gamma_{cf}^\pm$ — means the mapping of Γ_{cR}^\pm in the current configuration, Γ_c — is the proper (common) contact zone, Γ_{cf}^\pm — denote these parts of Γ_c^\pm on which $d_n > 0$ (and hence the boundary traction vanishes).

Using the above mentioned meaning of the mapping zones and taking into account the equation (2.1)₂, we obtain

$$\begin{aligned}
 I_c &= \int_{\Gamma_c} \sigma_{ij}(\mathbf{u}^+) \cdot n_j^+ v_i^+ d\Gamma_c + \int_{\Gamma_c} \sigma_{ij}(\mathbf{u}^-) \cdot n_j^- \cdot v_i^- d\Gamma_c \\
 &= \int_{\Gamma_c} \|\sigma_{ij}\| \cdot n_j^+ v_i^+ d\Gamma_c + \int_{\Gamma_c} \sigma_{ij}(\mathbf{u}^-) \cdot n_j^+ \cdot (v_i^+ - v_i^-) d\Gamma_c \\
 &= \int_{\Gamma_c} (\sigma_{i\alpha,\alpha}^s(\mathbf{u}^s) + \varrho^s b_i^s - \varrho^s \ddot{u}_i^s) \cdot v_i^+ d\Gamma_c + \int_{\Gamma_c} t_n \cdot v_n^w + t_{Ti} \cdot v_{Ti}^w d\Gamma_c.
 \end{aligned}$$

Finally, the mixed variational formulation takes the form

$$(2.18) \quad \int_{\Omega_R^+} S_{KL}(\mathbf{u}^+) \cdot x_{i,K}^+ \cdot v_{i,L}^+ dV_R + \int_{\Omega_R^-} S_{KL}(\mathbf{u}^-) \cdot x_{i,K}^- \cdot v_{i,L}^- dV_R$$

$$\begin{aligned}
 (2.18) \quad & + \int_{\Gamma_c} \sigma_{\alpha\beta}^s(\mathbf{u}^s) \cdot \varepsilon_{\alpha\beta}^s(\mathbf{v}^c) d\Gamma \\
 & + \int_{\Omega_R^+} \varrho_R^+ \ddot{u}_i^+ \cdot v_i^+ dV_R^+ + \int_{\Omega_R^-} \varrho_R^- \ddot{u}_i^- \cdot v_i^- dV_R^- + \int_{\Gamma_c} \varrho^s \ddot{u}_i^s \cdot v_i^s d\Gamma \\
 = & \int_{\Omega_R^+} \varrho_R^+ \cdot b_i^+ \cdot v_i^+ dV_R + \int_{\Omega_R^-} \varrho_R^- \cdot b_i^- \cdot v_i^- dV_R + \int_{\Gamma_c} \varrho^s \cdot b_i^s \cdot v_i^s d\Gamma \\
 & + \int_{\Gamma_{fR}^+} p_{Ri}^+ \cdot v_i^+ d\Gamma_R^+ + \int_{\Gamma_{fR}^-} p_{Ri}^- \cdot v_i^- d\Gamma_R^- + \int_{\partial\Gamma_c} p_i^s \cdot v_i^s dS \\
 & + \int_{\Gamma_c} t_n \cdot v_n^w d\Gamma + \int_{\Gamma_c} t_{Ti} \cdot v_{Ti}^w d\Gamma \quad \forall (\mathbf{v}^+, \mathbf{v}^-) \in V^\pm.
 \end{aligned}$$

This equation constitutes the basis of our further considerations.

The last two terms which follow from the integral I_c lead to serious mathematical difficulties since the Signorini conditions (2.8) as well as the friction conditions (2.10), are multivalued and nondifferentiable. To omit these difficulties, the usual regularization procedure will be applied. Therefore, after introducing the regularization formulas

$$\begin{aligned}
 (2.19) \quad & t_{n\varepsilon 1}(\mathbf{u}^w) = -\frac{1}{\varepsilon 1} \cdot |d_n(\mathbf{x}^-, \mathbf{x}_\rho^+)| \quad \text{for } d_n < 0 \text{ only,} \\
 & t_{Ti\varepsilon} = -\mu(t_n, \dot{\mathbf{u}}^w) \cdot t_n \cdot \begin{cases} \frac{\dot{u}_{Ti}^w}{|\dot{\mathbf{u}}_{Ti}^w|} & \text{for } |\dot{\mathbf{u}}_{Ti}^w| > \varepsilon, \\ \frac{\dot{u}_{Ti}^w}{\varepsilon} & \text{for } |\dot{\mathbf{u}}_{Ti}^w| \leq \varepsilon \end{cases}
 \end{aligned}$$

the contact integrals mentioned should be understood in the sense of their regularization. To solve the nonlinear contact problem, the incremental approach has been used.

Applying the standard expressions [3]

$$\begin{aligned}
 \mathbf{u}^{t+\Delta t} &= \mathbf{u}^t + \Delta \mathbf{u} && \text{for displacements,} \\
 \mathbf{F}^{t+\Delta t} &= \mathbf{F}^t + \nabla \Delta \mathbf{u} && \text{for the deformation gradient,} \\
 \mathbf{S}^{t+\Delta t} &= \mathbf{S}^t + \Delta \mathbf{S}, \quad \Delta \mathbf{S} = \mathbf{C} \cdot \mathbf{e}(\Delta \mathbf{u}) && \text{for stresses,}
 \end{aligned}$$

$$\begin{aligned}
 e_{KL} &= \frac{1}{2}(\Delta u_{K,L} + \Delta u_{L,K} + u_{N,K}^t \cdot \Delta u_{N,L} \\
 & \quad + u_{N,L}^t \cdot \Delta u_{N,K}) \quad \text{for strains,}
 \end{aligned}$$

$$\sigma_{ij}^{s,t+\Delta t} = \sigma_{ij}^{s,t} + \Delta \sigma_{ij}^s, \quad \Delta \sigma^s = \mathbf{C}^s(\varepsilon) \cdot \varepsilon(\Delta \mathbf{u}^s) \quad \text{for the surface stresses,}$$

and using the substitution (2.19), one obtains (2.18) in the incremental form

$$\begin{aligned}
 (2.20) \quad & \int_{\Omega_R^+} C_{KLMN}^+ \cdot \epsilon_{KL}^+ \cdot F_{iM}^{t,+} \cdot v_{i,N} dV_R + \int_{\Omega_R^-} C_{KLMN}^- \cdot \epsilon_{KL}^- \cdot F_{iM}^{t,-} \cdot v_{i,N} dV_R \\
 & + \int_{\Gamma_c} C_{klmn}^s(\varepsilon(\mathbf{u}^{t,s})) \cdot \varepsilon_{kl}(\Delta \mathbf{u}^s) \cdot \varepsilon_{mn}(\mathbf{v}) d\Gamma + \int_{\Omega_R^+} S_{KL}^{t,+} \cdot \Delta u_{i,K}^+ \cdot v_{i,L} dV_R
 \end{aligned}$$

(2.20)
[cont.]

$$\begin{aligned}
 & + \int_{\Omega_R^-} S_{KL}^{t-} \cdot \Delta u_{i,K}^- \cdot v_{i,L} dV_R \\
 & + \int_{\Omega_R^+} \varrho_R^+ \ddot{u}_i^+ \cdot v_i dV_R + \int_{\Omega_R^-} \varrho_R^- \ddot{u}_i^- \cdot v_i dV_R + \int_{\Gamma_c} \varrho^s \ddot{u}_i^s \cdot v_i d\Gamma \\
 & + \int_{\Gamma_c} \left[\frac{\partial t_{Ti\varepsilon}}{\partial u_n} \cdot \Delta u_n^w + \frac{\partial t_{Ti\varepsilon}}{\partial \dot{\mathbf{u}}_T} \Delta \dot{\mathbf{u}}_T^w \right] v_i^w d\Gamma + \int_{\Gamma_c} \frac{\partial t_{n\varepsilon 1}}{\partial u_n} \Delta u_n^w \cdot v_n^w d\Gamma \\
 & = \int_{\Omega_R^+} \varrho_R^+ \cdot b_K^+ v_K dV_R + \int_{\Omega_R^-} \varrho_R^- \cdot b_K^- v_K dV_R + \int_{\Gamma_c} \varrho_R^s \cdot b_i^s v_i d\Gamma \\
 & + \int_{\Gamma_{JR}^+} p_K^{t+\Delta t,+} \cdot v_K d\Gamma_R + \int_{\Gamma_{JR}^-} p_K^{t+\Delta t,-} \cdot v_K d\Gamma_R + \int_{\partial\Gamma_c} p_i^{t+\Delta t,s} v_i dS \\
 & - \int_{\Omega_R^+} S_{KL}^{t,+} F_{iK}^t \cdot v_{i,L} dV_R - \int_{\Omega_R^-} S_{KL}^{t,-} F_{iK}^t \cdot v_{i,L} dV_R - \int_{\Gamma_c} \sigma_{ij}^{t,s} \cdot \varepsilon_{ij}(\mathbf{v}) d\Gamma \\
 & - \int_{\Gamma_c} t_{n\varepsilon 1}^t \cdot v_n^w d\Gamma - \int_{\Gamma_c} t_{Ti\varepsilon}^t \cdot v_{Ti}^w d\Gamma.
 \end{aligned}$$

The integral containing the term $\partial t_{n\varepsilon 1} / \partial u_n$ needs some explanation. It is important to note that $t_{n\varepsilon 1}$ is nondifferentiable (see (2.19)). Nevertheless, for small displacements (following from small increments) it will be $\mathbf{d}_n = \mathbf{g} - \mathbf{u}_n$ (where \mathbf{g} is the gap between the bodies). Hence the mentioned integral is well defined on Γ_c .

Finite element space discretization and the Newmark procedure for time integration were applied to solve the problem numerically.

Expressing the increments of the unknown displacement vector in the usual form

$$\Delta \mathbf{u}(\mathbf{X}, t) = \mathbf{H}(\mathbf{X}) \cdot \Delta \hat{\mathbf{u}}(t), \quad \Delta \mathbf{u}^s(\mathbf{X}, t) = \mathbf{H}_s(\mathbf{X}) \cdot \Delta \hat{\mathbf{u}}_s(t),$$

where \mathbf{H} is the shape function matrix, $\hat{\mathbf{u}}$ is the nodal displacement vector,

$$\begin{aligned}
 [\Delta \mathbf{u}_N, \Delta \mathbf{u}_T]^T &= [\mathbf{H}_N, \mathbf{H}_T]^T \cdot \Delta \hat{\mathbf{u}}, \\
 \mathbf{e} &= \mathbf{B}(\mathbf{X}, \mathbf{u}^t) \cdot \Delta \hat{\mathbf{u}}(t), \\
 \mathbf{F}(\mathbf{u}) &= \mathbf{B}_1 \cdot \hat{\mathbf{u}}, \\
 \varepsilon^s(\mathbf{u}) &= \mathbf{B}^s(\mathbf{X}) \cdot \hat{\mathbf{u}}(t), \\
 \Delta \mathbf{S} &= \mathbf{C} \cdot \mathbf{B} \Delta \hat{\mathbf{u}}, \quad \Delta \sigma^s = \mathbf{C}^s \cdot \mathbf{B}^s \Delta \hat{\mathbf{u}}
 \end{aligned}$$

one obtains from (2.20) the matrix equation

$$\mathbf{M} \cdot \ddot{\hat{\mathbf{u}}}^{t+\Delta t} + \mathbf{K}_T^t \cdot \Delta \dot{\hat{\mathbf{u}}} + [\mathbf{K}^t + \mathbf{K}_N^t + \mathbf{K}_{TN}^t] \cdot \Delta \hat{\mathbf{u}} = \mathbf{f}^{t+\Delta t} - \mathbf{f}_N^t - \mathbf{f}_T^t - \mathbf{R}^t,$$

where

$$\mathbf{M} = \int_{\Omega_{R\pm}} \varrho_R^\pm \cdot \mathbf{H}_\pm^T \cdot \mathbf{H}_\pm dV_R + \int_{\Gamma_c} \varrho^s \cdot (\mathbf{H}^s)^T \cdot \mathbf{H}^s d\Gamma,$$

$$\begin{aligned}
 \mathbf{K}^t &= \int_{\Omega_{R\pm}} (\mathbf{B}_{\pm})^T \cdot \mathbf{C}_{\pm} \cdot \mathbf{B}_{\pm} dV_R + \int_{\Gamma_c} (\mathbf{B}^s)^T \cdot \mathbf{C}^s \cdot \mathbf{B}^s d\Gamma_R \\
 &\quad + \int_{\Omega_{R\pm}} (\mathbf{B}_{I\pm})^T \cdot \mathbf{S}_{\pm}^t \cdot \mathbf{B}_{I\pm} dV_R, \\
 \mathbf{K}_T^t &= \int_{\Gamma_c} \frac{\partial \mathbf{t}_{T\varepsilon}^t}{\partial \dot{u}_T} (\mathbf{H}_T)^T \cdot \mathbf{H}_T d\Gamma, \\
 \mathbf{K}_{NT}^t &= \int_{\Gamma_c} \frac{\partial \mathbf{t}_{T\varepsilon}^t}{\partial u_n} \cdot (\mathbf{H}_N)^T \cdot \mathbf{H}_T d\Gamma, \\
 \mathbf{K}_N^t &= \begin{cases} \int_{\Gamma_c} \frac{1}{\varepsilon_1} \cdot \frac{(u_n^t - g)_+}{u_n^t - g} (\mathbf{H}_N)^T \cdot \mathbf{H}_N d\Gamma & \text{for the classical models,} \\ \int_{\Gamma_c} m_n \cdot C_n \cdot (u_n^t - g^t)_+^{m_n - 1} (\mathbf{H}_N)^T \cdot \mathbf{H}_N d\Gamma & \text{for the normal compliance} \\ & \text{model,} \end{cases} \\
 \mathbf{f}^{t+\Delta t} &= \int_{\Omega_{R\pm}} \varrho_{R\pm} \cdot b_{\pm}^{t+\Delta t} \cdot \mathbf{H}_{\pm} d\Omega_R + \int_{\Gamma_c} \varrho_s \cdot b_s^{t+\Delta t} \cdot \mathbf{H}^s d\Gamma \\
 &\quad + \int_{\Gamma_{fR\pm}} p_{\pm}^{t+\Delta t} \mathbf{H}_{\pm} d\Gamma_R + \int_{\partial\Gamma_c} p_s^{t+\Delta t} \mathbf{H}^s dS, \\
 \mathbf{f}_N^t &= \int_{\Gamma_c} t_n^t \cdot \mathbf{H}_N d\Gamma, \quad \mathbf{f}_T^t = \int_{\Gamma_c} t_t^t \cdot \mathbf{H}_T d\Gamma, \\
 \mathbf{R}^t &= \int_{\Omega_{R\pm}} \mathbf{B}_{\pm}^T \cdot \mathbf{S}_{\pm}^t dV_R + \int_{\Gamma_c} (\mathbf{B}^s)^T \cdot \mathbf{S}_s^t d\Gamma.
 \end{aligned}$$

The solution procedure is realized by an iterative process in which we calculate:

- the normal pressure and contact zone under the assumption that the friction stresses are known;
- the friction stresses with known normal pressures and known contact zone.

The algorithm starts with the assumed friction stresses $t_{Ti} = 0$, and ends when the norms of the errors are small enough.

2.3. Numerical example

Consider a rubber cube $B^+ : a \times b = 0.48 \times 0.5$ m in a plane state of strain, resting on a rigid half-space B^- (Fig. 3). The following data are introduced:

rubber

$$E = 5 \cdot 10^3 \text{ kN/m}^2, \quad \nu = 0.45, \quad \rho = 1.7 \cdot 10^3 \text{ (kg/m}^3\text{)}.$$

Singular surface

- 1) linear elastic $E_s = 10$ kN/m
- 2) linear elastic $E_s = -10$ kN/m (for testing only),
- 3) nonlinear elastic like in Fig. 4.

Boundary conditions

$$u_0 = 0.05 \text{ m}, \quad v = 1 \text{ m/s}.$$

Initial conditions

$$\mathbf{u} = \text{static solution for } u_0, \quad \dot{\mathbf{u}} = 0.$$

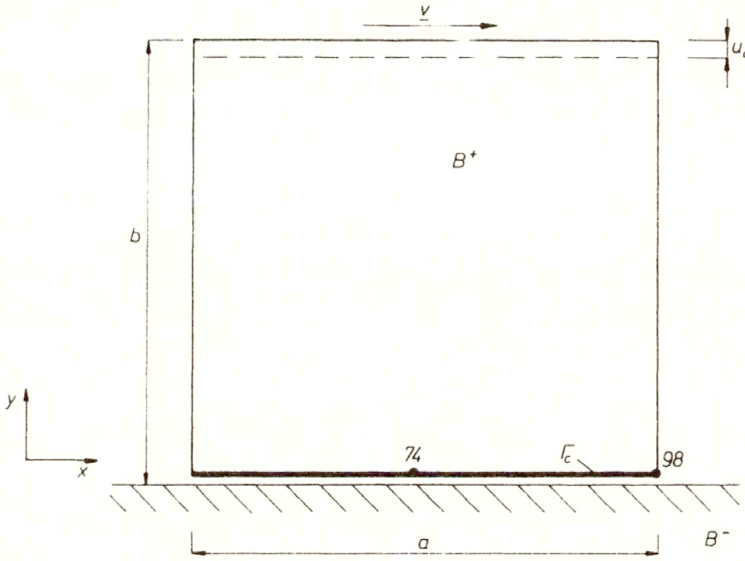


FIG. 3.

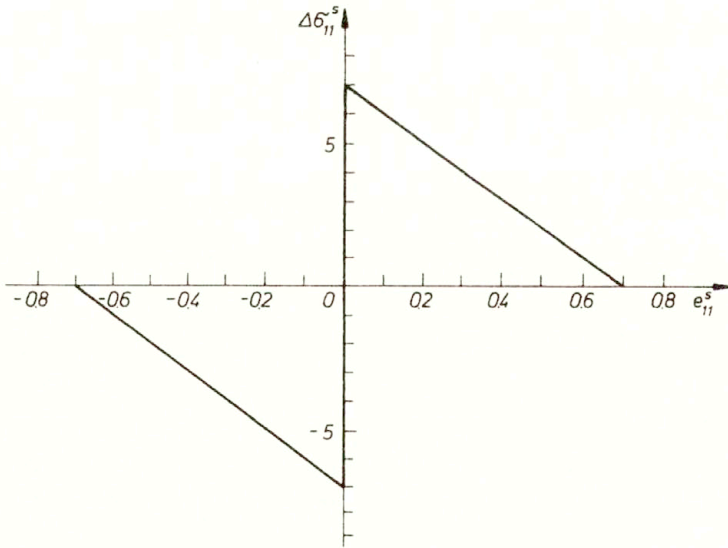


FIG. 4.

Space discretization: 348 four-node elements +48 two-node elements for the singular surface +48 four-node contact elements.

Time discretization — $\max \Delta t = 1.10^{-4}$.

Newmark's parameters $\alpha = 0.5$; $\beta = 0.25$.

Friction condition — for Odens model $m_N = 3$, $m_T = 8/3$, $c_N = 10^{12}$, $c_T = c_N^{8/9} E^{1/9}$.

Some of the obtained results are presented in Figs. 5–9.

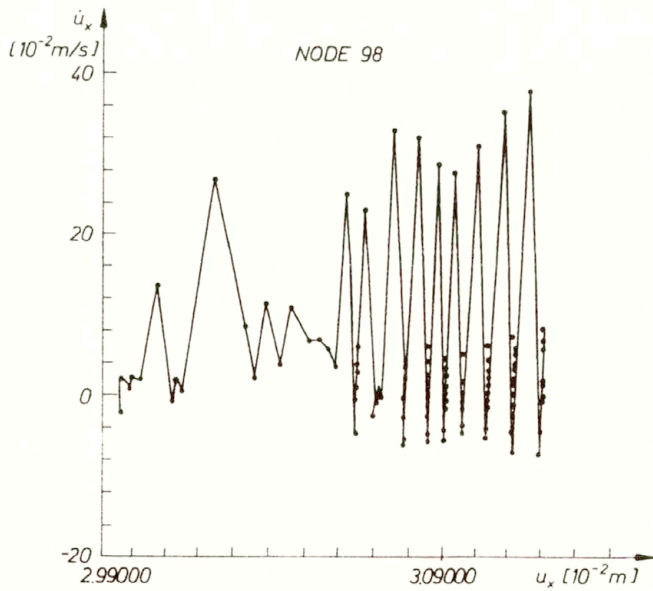
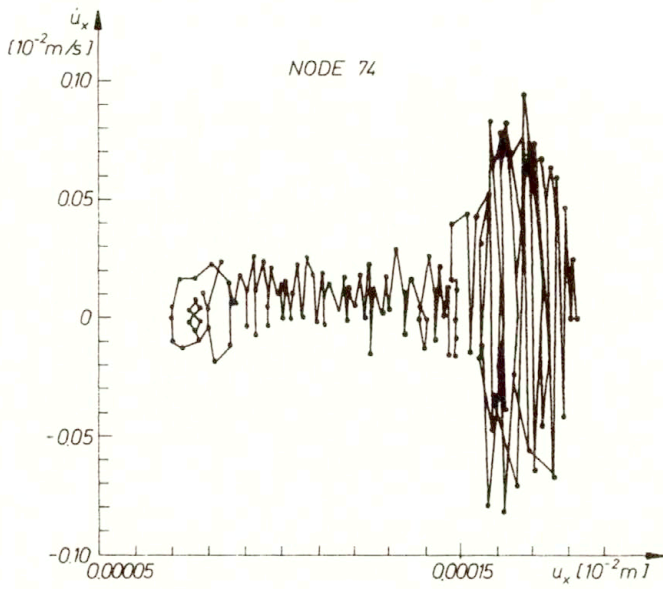


FIG. 5. Phase space in nodes 74 and 98 for $E_s > 0$.

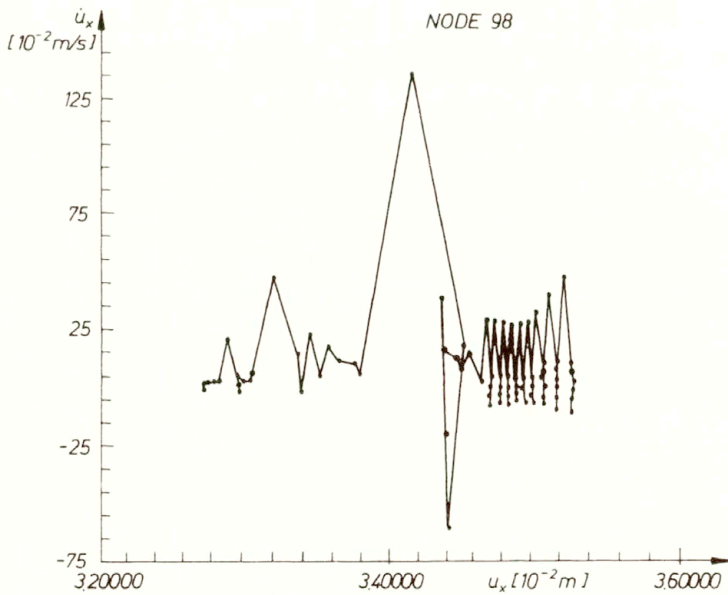
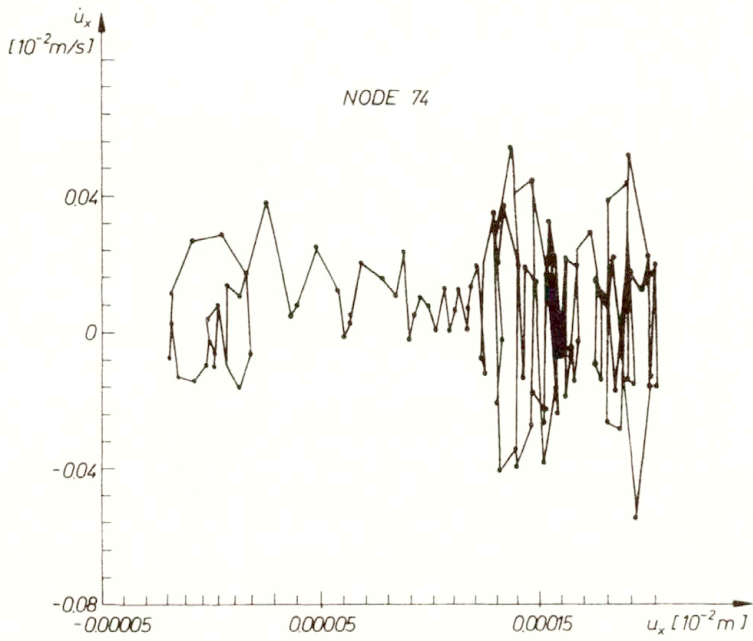


FIG. 6. Phase space in nodes 74 and 98 for $E_d < 0$.

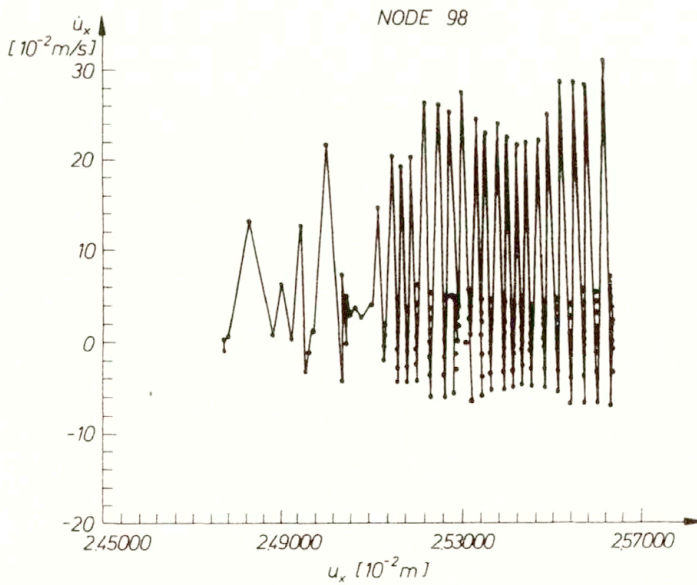
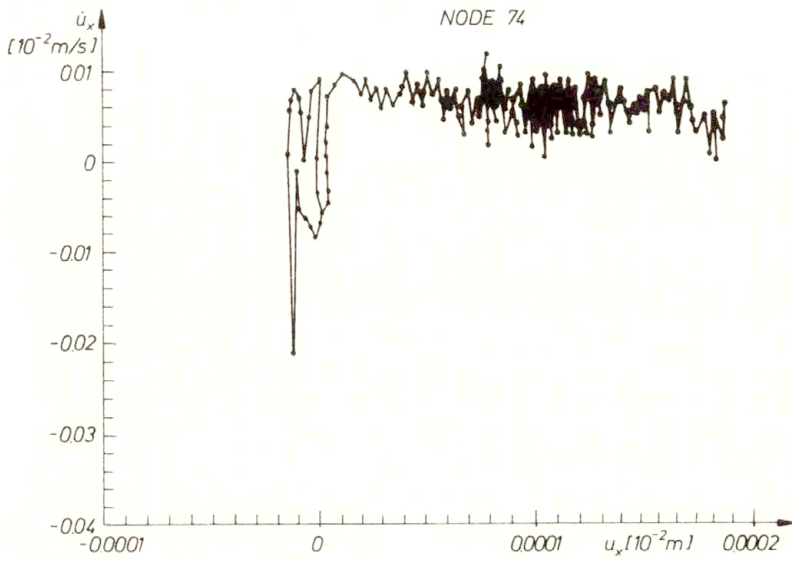


FIG. 7. Phase space in nodes 74 and 98 for singular surface with nonlinear constitutive relation.

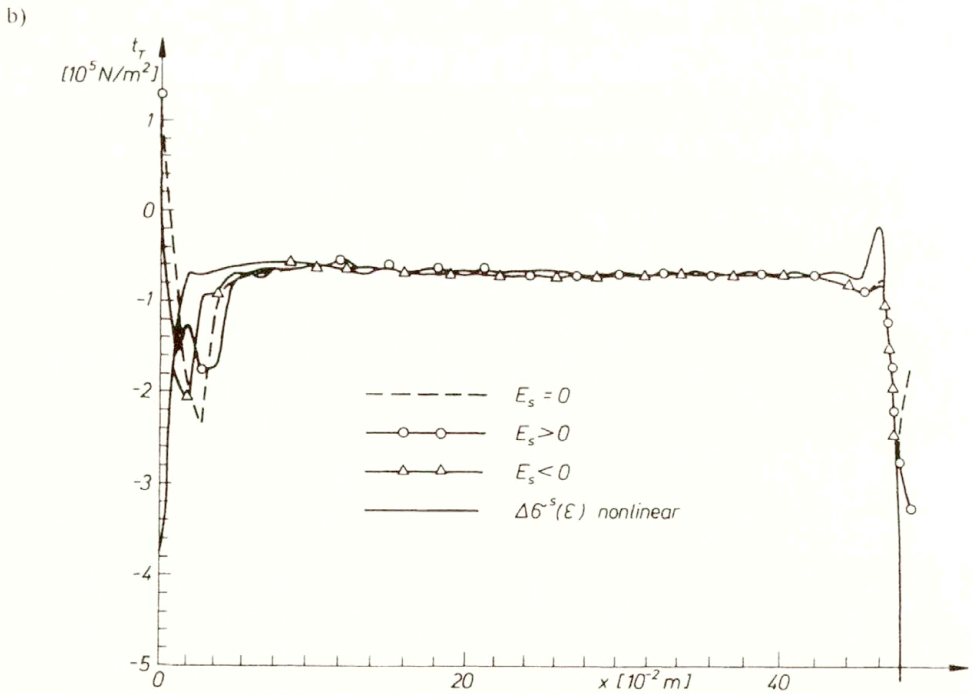
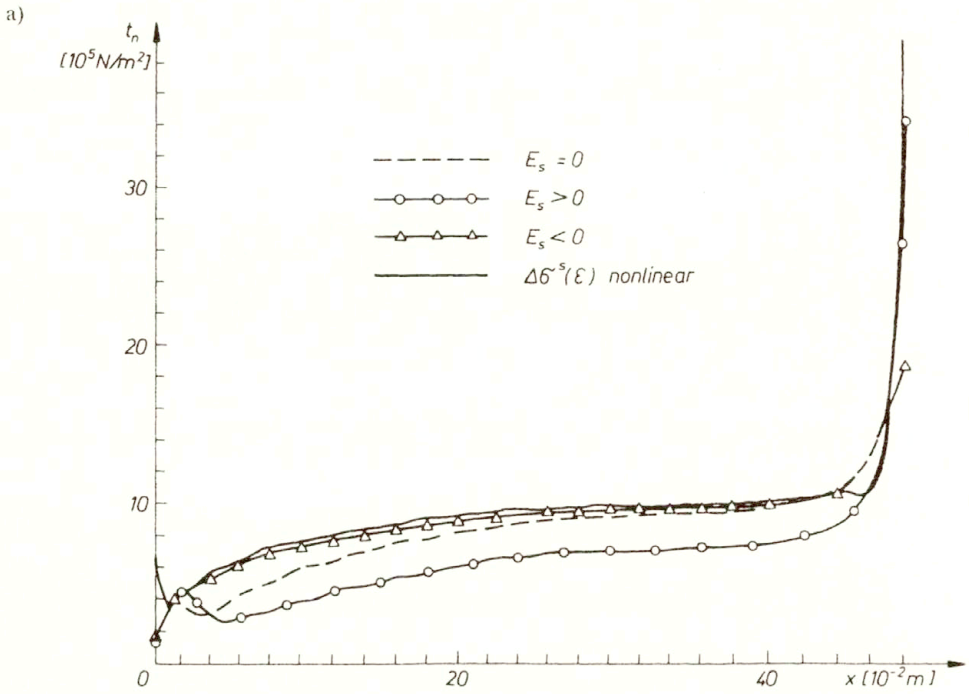


FIG. 8. a. Normal stresses along contact surface at time $t = 0.004$ s.
 b. Tangential stresses along contact surface at time $t = 0.004$ s.

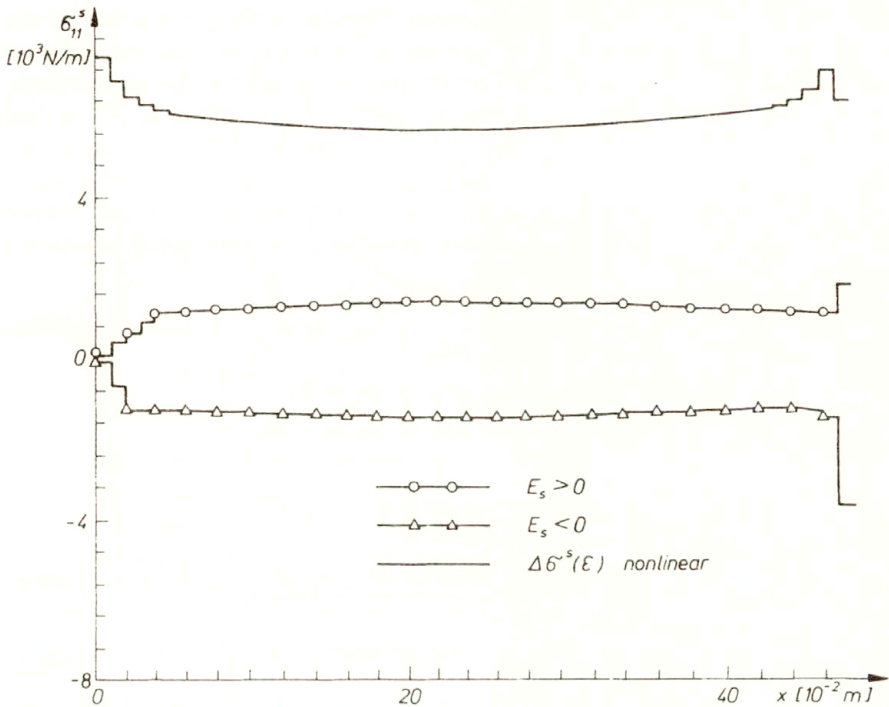


FIG. 9. Stresses in singular surface at time $t = 0.004 \text{ s}$.

3. Static contact in elastic, multilayered reinforced medium

Let us consider a multilayered halfspace like that in Fig.10. Such a system models the structure of road pavement reinforced by geosynthetics (dense geogrids or geotextiles). The layers are treated as linear elastic, the material of the reinforcement transmits tension only. We assume perfect glueing (adhesion) between the reinforcement and the upper layer B^+ ($\mathbf{u}^+ = \mathbf{u}^s$) which follows from technological conditions. Several contact conditions (adhesion, decohesion, friction, unilateral contact) between the reinforcement

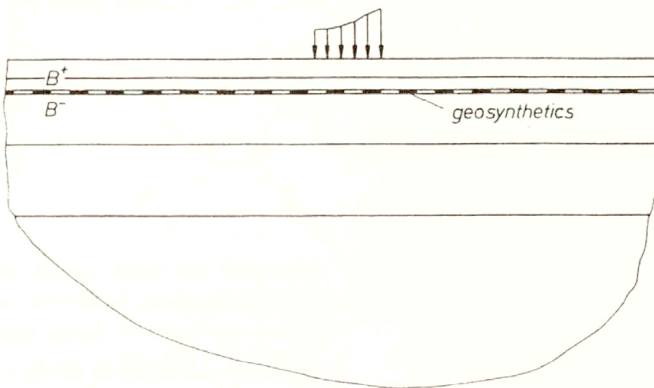


FIG. 10.

and the bottom layer B^- are taken into account. Singular surface as a model of the reinforcement has been used. Then, such a material structure will be described by equations (2.1)–(2.3) where, instead of $(2.3)_2$, the constitutive relations for the geosynthetic reinforcement should be used. Friction between the surface Γ and the layer B^- is described by means of the Coulomb law. Since the problem now concerns the static case, the variational principle is based on kinematically admissible displacements (instead of velocities). Neglecting the inertial terms and taking into account the unilateral contact between the reinforcement and the layer B^- (decohesion possible), the variational equation (2.13) can be used.

The friction conditions are of the type

$$\begin{aligned} d_n = 0 &\Rightarrow t_T \leq \mu t_n, \\ t_T < \mu t_n &\Rightarrow \mathbf{w}_T = 0, \\ t_T = \mu t_n &\Rightarrow \mathbf{w}_T = -\lambda \mathbf{t}_T. \end{aligned}$$

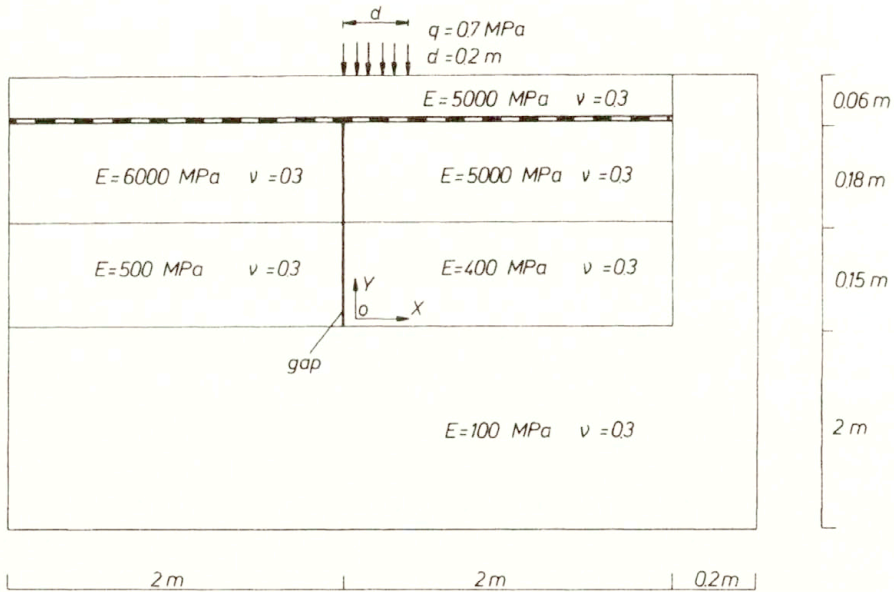


FIG. 11.

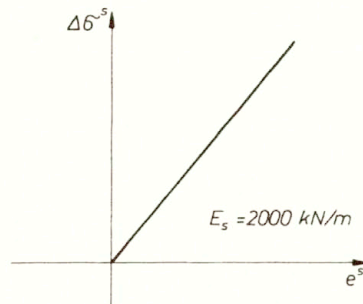


FIG. 12.

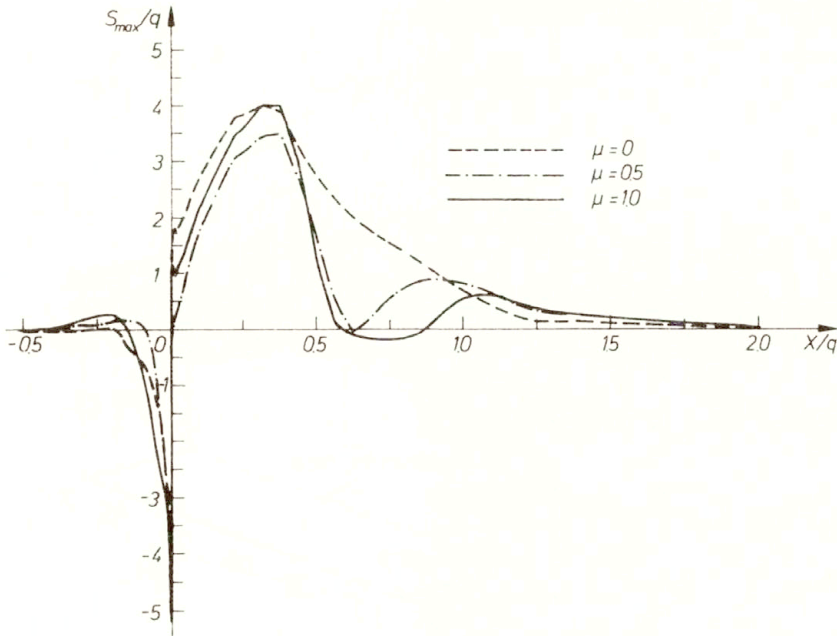


FIG. 13.

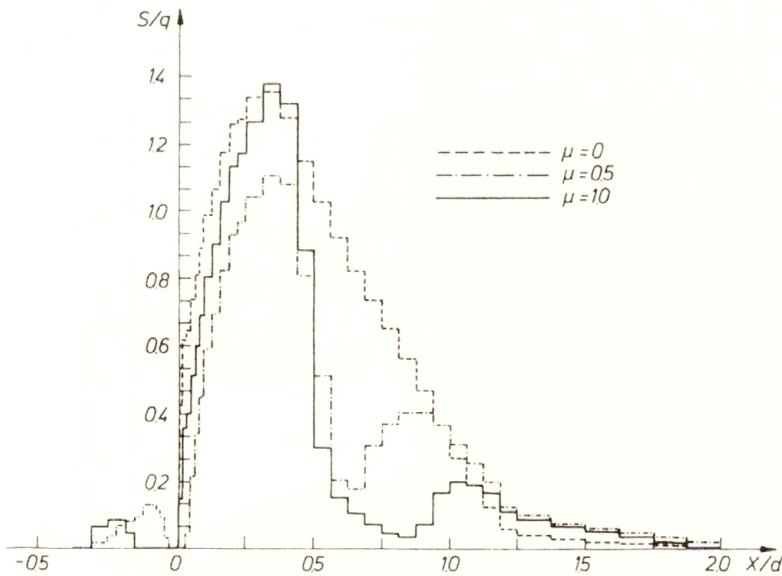


FIG. 14.

The quantity w_T means here the fictitious “velocity” (describing slip) which results from the incremental action of loads. This incremental procedure in updated Lagrangean description has been used to solve the problem.

For the data given in Figs. 11, 12 and for several values of friction coefficient, a series of numerical calculations was performed. Results for stress distributions are shown in Figs. 13–18.

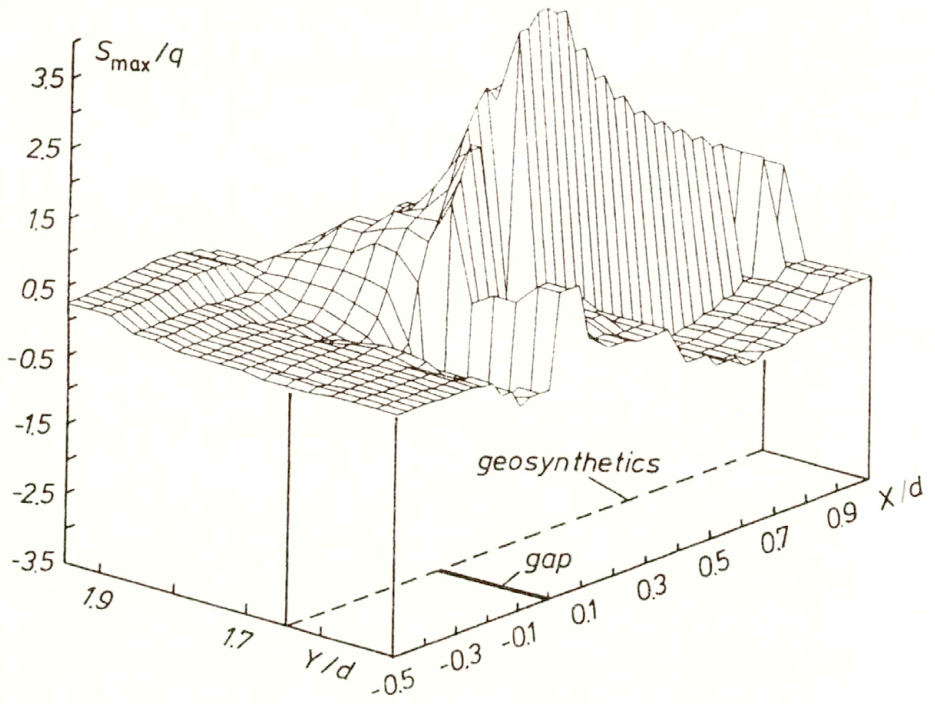


FIG. 15.

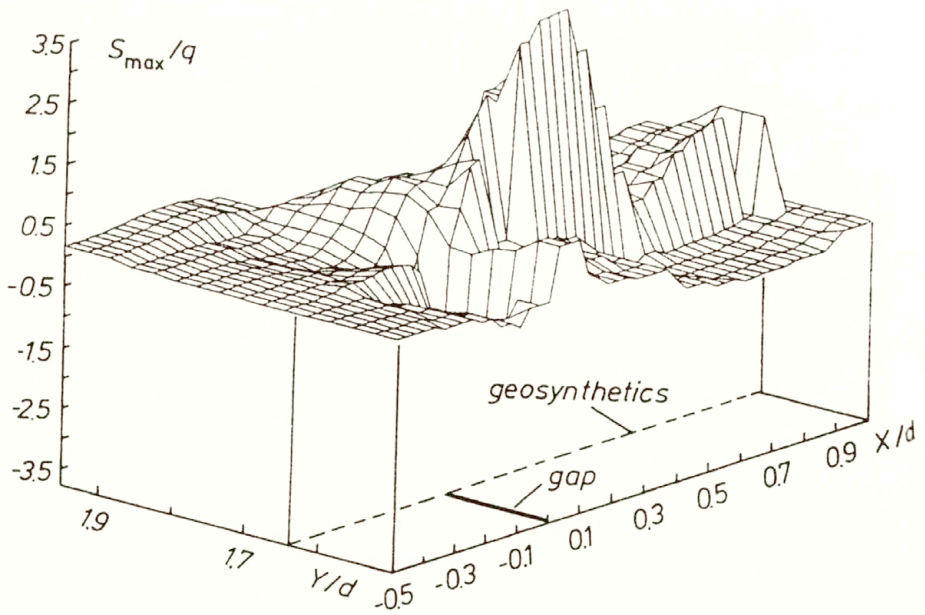


FIG. 16.

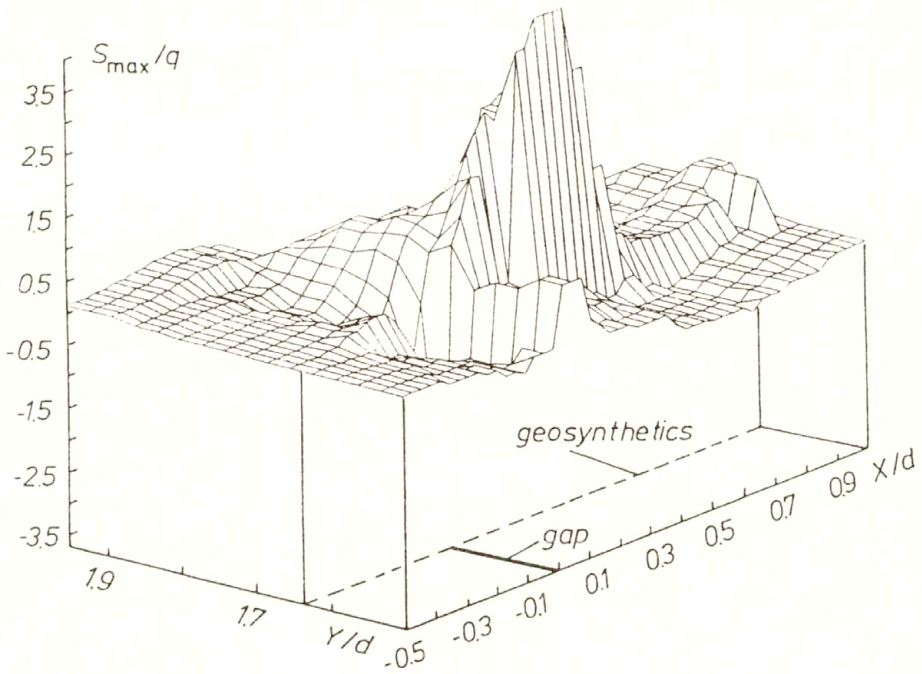


FIG. 17. Maximum principal stresses for $\mu = 1.0$.

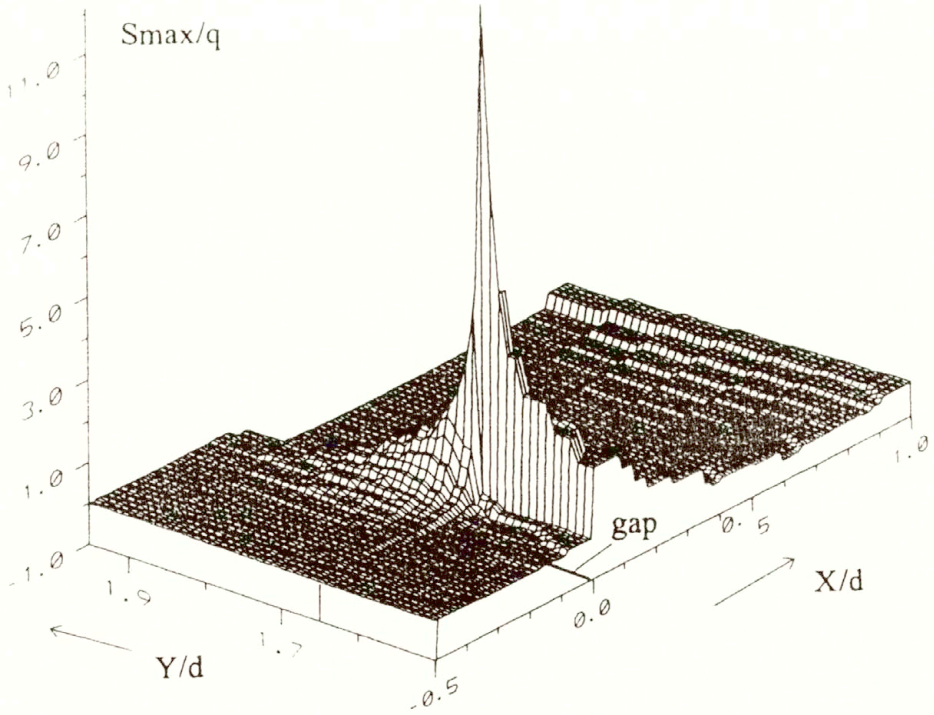


FIG. 18. Maximum principal stresses for full adhesion.

4. Conclusions

In Sec. 2 the notion of a singular surface to describe frictional phenomena has been presented. To formulate the constitutive equations for the real “third body” (contact zone) as well as for the friction criteria (stick-slip condition), further investigations and experiments in micro- and nanoscale are necessary. Nevertheless, the presented approach gives an effective formalism to describe such surface phenomena like friction, lubrication, wear etc. The numerical results show that high frequency vibrations occur in the contact zone, what is in agreement with experimental observations (e.g. for tires).

In Sec. 3, the state of stresses and deformation in layered, reinforced media is analyzed. Different contact conditions between the layer and the reinforcement are considered. The obtained results show the stresses in the reinforcement and the influence of the contact conditions on the stress distribution in the layer. Such an analysis can be important for the explanation of the influence of reinforcement on the initiation of the reflecting cracks in road pavements.

Further research for inelastic properties of the contact zone, as well as for the layered material, is necessary and will be presented in the future.

As one can see from the above considerations, the notion of singular material surface constitutes a useful formal tool for description and analysis of complex reinforced structures and interacting continua.

References

1. K.J. BATHE, *Finite element procedures in engineering analysis*, Prentice-Hall, Inc., Englewood Cliffs, N.J. 1982.
2. K.J. BATHE, S. MJAILOVICH, *Finite element analysis of frictional contact problems*, J. Theoretical and Applied Mech., **7**, 1988.
3. K.J. BATHE, A. RAMM and B. WILSON, *Finite element fomulation for large deformation dynamic analysis*, Int. J. Num. Mech. Engng., **9**, 1975.
4. A.C. ERINGEN, *Continuum physics*, Acad. Press, 1975.
5. M. GODET, *The third body approach. A mechanical view of wear*, Wear, **100**, 437-452, 1984.
6. M. GURTIN, A. MURDOCH, *A continuum theory of elastic material surface*, ARMA, **57**, 1975.
7. N. KIKUCHI, *A smoothing technique for reduced integration penalty methods in contact problems*, Int. J. Num. Meth. Engng., **18**, 1982.
8. N. KIKUCHI, J.T. ODEN, *Contact problems in elasticity: A study of variational inequalities and finite element methods*, SIAM, Philadelphia 1988.
9. W. KOSIŃSKI, *Introduction to the theory of singularities of the field and wave analysis* [in Polish], PWN, Warszawa-Poznań 1981.
10. J.T. ODEN, N. KIKUCHI, *Finite element methods for constrained problems in elasticity*, Int. J. Num. Mech. Engng., **18**, 1982.
11. J.T. ODEN, J.A.C. MARTINS, *Models and computational methods for dynamic friction phenomena*, Comp. Meth. Appl. Mech. Engng., **52**, 1985.
12. E.B. PIRES, J.T. ODEN, *Analysis of contact problems with friction under oscillating loads*, Comp. Meth. Appl. Mech. Engng., **39**, 1983.
13. A. SCHALLAMACH, *Recent advances in knowledge of rubber friction and tire wear*, Rubber Chem. and Technology, **41**, 1968.
14. A. SCHALLAMACH, *Zur Physik der Kautschukreibung*, Kolloid-Zeitschrift, Band 141, Heft 3, 1955.
15. G. SZEFER, *Rauher Kontakt deformierbarer Körper*, Report SFB 181, TU, Berlin 1991.
16. G. SZEFER, *Mesostructural modelling of friction based on the conception of a singular surface*, Proc. 2-th Int. Conf. Nonlin. Mech., Beijing, 195, 1993.

17. G. SZEFER, D. JASIŃSKA, *Dynamic contact analysis for a new model of friction*, ZAMM, 1994 [to appear].
18. G. SZEFER, J.W. SALAMON, *A new model of the reinforced, layered media*, ZAMM, 1994 [to appear].
19. A. CURNIER, HE QI-CHANG and J. TELEGA, *Formulation of unilateral contact between two elastic bodies undergoing finite deformations*, C.R. Acad. Sci. Paris, **314**, Serie II, pp. 1-6, 1992.
20. A. ZMITROWICZ, *A thermodynamical model of contact friction and wear*, I, II, III, Wear, 114, 1987.

CRACOW UNIVERSITY OF TECHNOLOGY
INSTITUTE OF STRUCTURAL MECHANICS, KRAKÓW

Received January 26, 1994.

PRELIMINARY PROGRAMME 1995

Courses

New Design Concepts for High Speed Air Transport Coordinator: H. Sobieczky (Göttingen)	June 5 - 9, 1995
Bone Cell and Tissue Mechanics Coordinator: S.C. Cowin (New York)	July 10 - 14, 1995
Liquid Bridge Theory and Applications Coordinator: J. Meseguer (Madrid)	July 17- 21, 1995
Mathematical Modelling for Arch Dam design and Safety Control Coordinators: M. E.R. de Arantes e Oliveira, J.O. Pedro (Lisboa)	Sept. 4 - 8, 1995
Mechanics of Solids with Phase Changes Coordinators: M. Berveiller (Metz), F.D. Fischer (Leoben)	Sept. 11 - 15, 1995
Modelling and Simulation of Hypersonic Flows for Spatial Flights Coordinator: R. Brun (Marseille)	Sept. 18 - 22, 1995
Control of Flow Instabilities and Unsteady Flows Coordinators: G.E.A. Meier (Göttingen), G.H. Schnerr (Karlsruhe)	Sept. 18 - 22, 1995
Advanced Methods of Tunnelling Coordinator: K. Kovari (Zürich)	Sept. 25 - 29, 1995
Earthquake Resistant Design Coordinator: R.T. Duarte (Lisboa)	Oct. 2 - 6, 1995
The Flow of Particles in Suspension Coordinator: G. Cognet (Grenoble)	Oct. 9 - 13, 1995

Meetings Hosted by CISM

Workshop on "Multimedia GIS Data" International Society for Photogrammetry and Remote Sensing – Commission I Coordinators: R. Galetto (Pavia), F. Crosilla (Udine)	June 12 - 16, 1995
10th International Conference on Artificial Intelligence in Engineering Chairmen: C.A. Brebbia (Southampton), C. Tasso (Udine)	July 4 - 6, 1995

Additional and more detailed information will be available in November 1994

I-33100 Udine (Italy), Palazzo del Torso, Piazza Garibaldi, 18
Tel: + 39 0432 - Secretariat 294989 or 508251 - Administration 294795 - Printing Office 45533 - Fax 501523
Partita I.V.A. 00401650304

Computer Assisted Mechanics and Engineering Sciences (CAMES)

to be published quarterly starting in 1994

Editor: M. Kleiber, Warsaw

Associate Editor: H.A. Mang, Vienna

Scope of the Journal

Computer Assisted Mechanics and Engineering Sciences (CAMES) is a referred international journal, published quarterly, providing an international forum and an authoritative source of information in the field of computational mechanics and related problems of applied science and engineering.

The specific objective of the journal is to support researchers and practitioners based in Central Europe by offering them a means facilitating (a) access to newest research results by leading experts in the field (b) publishing their own contributions and (c) dissemination of information relevant to the scope of the journal.

Papers published in the journal will fall largely into three main categories. The first will contain state-of-the-art reviews with the emphasis on providing the Central European readership with a guidance on important research directions as observed in the current world literature on computer assisted mechanics and engineering sciences.

The second category will contain contribution presenting new developments in the broadly understood field of computational mechanics including solid and structural mechanics, multi-body system dynamics, fluid dynamics, constitutive modeling, structural control and optimization, transport phenomena, heat transfer, etc. Variational formulations and numerical algorithms related to implementation of the finite and boundary element methods, finite difference method, hybrid numerical methods and other methodologies of computational mechanics will clearly be the core areas covered by the journal.

The third category will contain articles describing novel applications of computational techniques in engineering practice; areas of interest will include mechanical, aerospace, civil, naval, chemical and architectural engineering as well as software development.

The journal will also publish book reviews and information on activities of the Central European Association of Computational Mechanics.

Subscription and sale of single issues is managed by the Editorial Office.

Price of single issue: 25 USD (in Poland: 40 000 zł)

Address: Editorial Office, CAMES

Polish Academy of Sciences

Institute of Fundamental Technological Research

ul. Świątokrzyska 21, PL 00-049 Warsaw, Poland

Our Bankers: IV Oddz. Pekao SA Warszawa 501132-40054492-3111

INSTITUTE OF FUNDAMENTAL TECHNOLOGICAL RESEARCH
is publishing the following periodicals:

ARCHIVES OF MECHANICS — bimonthly (in English)
JOURNAL OF TECHNICAL PHYSICS — quarterly (in English)
ARCHIVES OF ACOUSTICS — quarterly (in English)
ENGINEERING TRANSACTION — quarterly (in English)
ADVANCES IN MECHANICS — quarterly (in English)
ARCHIVES OF CIVIL ENGINEERING — quarterly (in English)

Subscription orders for all the magazines published in Poland available through the local press distributors or directly through the *Foreign Enterprise ARS POLONA*, Krakowskie Przedmieście 7, 00-068 Warszawa, Poland.

Address of the Editorial Office:

Institute of Fundamental Technological Research,
Świętokrzyska 21, p. 508,
00-049 WARSZAWA, Poland.

DIRECTIONS FOR THE AUTHORS

The periodical *ARCHIVES OF MECHANICS (ARCHIWUM MECHANIKI STOSOWANEJ)* deals with the printing of original papers which should not appear in any other publications. The authors may publish in the Bull. Acad. Polon. Sci. short papers only, announcing the solutions of any problems as well as informing that the full text will be inserted in the columns of the *ARCHIVES OF MECHANICS (ARCHIWUM MECHANIKI STOSOWANEJ)*.

As a rule, the volume of a paper should not exceed 40 000 typographic signs, that is about 20 type-written pages, format: 210 × 297 mm, leaded. The papers should be submitted in two copies. They must be set in accordance with the norms established by the Editorial Office. Special importance is attached to the following directions:

1. The title of the paper should be as short as possible.
2. The text should be preceded by a brief introduction; it is also desirable that a list of notations used in the paper be given.
3. Short papers should be divided into sections and subsections, long papers into sections, subsections and points. Each section, subsection or point must bear a title.
4. The formula number consists of two figures: the first represents the section number and the other the formula number under that section. Thus the division into subsections does not influence the numbering of formulae. Only such formulae should be numbered to which the author refers throughout the paper, also the resulting formulae. The formula number should be written on the left-hand side of the formula; brackets are to be only to avoid any misunderstanding. For instance, if the author refers to formula 3 of the set (2.1), a subscript should be added to denote the set of formula, viz. (2.1)₃.
5. All the notations should be written very distinctly. Special care must be taken to write small and capital letters as precisely as possible. Semi-bold type must be underlined in black pencil. Explanations should be given on the margin of the manuscript in case of special type face.
6. It has been established to denote vectors semi-bold type, transforms of the corresponding functions by tilded symbols. Trigonometric functions are denoted by sin, cos, tg and ctg, inverse functions – by arc sin, arc cos, arc tg and arc ctg; hyperbolic functions are denoted by sh, ch, th and cth, inverse functions – by Arsh, Arch, Arth and Arcth.
7. Figures in brackets denote reference titles. Items appearing in the reference list should include the initials of the Christian name of the author and his surname, also the full title of the paper (in the language of the original paper); moreover:
 - a) in the case of books, the publisher's name, the place and year of publication should be given, e.g.,
S. S. Ziemia, *Vibration analysis*, PWN, Warszawa 1970;
 - b) in the case of a periodical, the full title of the periodical, consecutive volume number, current issue number, pp. from ... to ..., year of publication should be mentioned; the annual volume number must be marked in black pencil so as to distinguish it from the current issue number, e.g.,
M. Sokołowski, *A thermoelastic problem for a strip with discontinuous boundary conditions*, Arch. Mech., 13, 3, 337–354, 1961.
8. The authors should enclose a summary of the paper. The volume of the summary is to be about 100 words.
9. If the paper is to be translated into another language than that of the manuscript, the author is requested to include a glossary of special terms.

Upon receipt of the paper, the Editorial Office forwards it to the reviewer. His opinion is the basis for the Editorial Committee to determine whether the paper can be accepted for publication or not.

The printing of the paper completed, the author receives 25 copies of reprints free of charge. The authors wishing to get more copies should advise the Editorial Office accordingly, not later than the date of obtaining the galley proofs.

The papers submitted for publication in the journal should be written in English. No royalty are paid to the authors.

If possible, please send us, in addition to the typescript, the same text prepared on a diskette (floppy disk) 3 1/2" or 5 1/4".

EDITORIAL COMMITTEE
ARCHIVES OF MECHANICS
(ARCHIWUM MECHANIKI STOSOWANEJ)